Syntheses of urea-based supramolecular polymers for nanocylinders assemblies in solution and on surface

Mingsheng Ji

Sorbonne Université

École doctorale de Physique et Chimie des Matériaux (ED 397)

Institut Parisien de Chimie Moléculaire / Équipe de Chimie des Polymères (UMR 8232)

Syntheses of urea-based supramolecular polymers for nanocylinders assemblies in solution and on surface

Par **Mingsheng JI**

Thèse de doctorat de Physique et Chimie des Matériaux

Dirigée par Laurent BOUTEILLER

Présentée et soutenue publiquement le 06 Octobre 2025

Devant un jury composé de :

Mme Min-Hui LI	Directeur de Recherche Chimie ParisTech	Rapporteure
M. Julien BERNARD	Directeur de Recherche Université de Lyon	Rapporteur
M. Philippe ROGER	Professeur Université Paris-Saclay	Examinateur
M. Laurent BOUTEILLER	Directeur de Recherche Sorbonne Université	Directeur de thèse
Mme Jutta RIEGER	Directeur de Recherche Sorbonne Université	Invitée
Mme Sandrine PENSEC	Maître de Conférence Sorbonne Université	Invitée

“There is no royal road to science, and only those who do not dread the fatiguing climb of its steep paths have a chance of gaining its luminous summits.”

Karl Marx

Acknowledgements

I would like to express my sincerest acknowledgement to my supervisor, Dr. Laurent Bouteiller, for his supervision, encouragement and support of the research I did in the last four years. He is always kind, patient and pleasant to discuss research even though sometimes he may be not quite available when every time I knock the door of his office. Laurent is knowledgeable in many fields and I really appreciate his knowledge I learned a little from him. In addition to his expertise, his wisdom has deeply affected me in doing research, and surely, will help me get better in future career. Of course, I am grateful to him giving me much freedom in designing new projects, and in going to Le Mans and Orléans conducting some experiments. Such a nice supervisor I met is really my good fortune in my life.

Special thanks must go to Dr. Jutta Rieger and Dr. Sandrine Pensec, who not only correct some chapters of my thesis but also accompany and witness my growth in the last four years. I would like to thank Jutta for her selfless dedication in my projects, as well as productive discussions she had with me. When discussing with her, academics is more colorful and interesting. Also, I really appreciate supports and encouragements she gave me when I was in trouble in academics and in life. Meanwhile, I would like to express my gratitude to Sandrine for her participation of JASUR project which she spent much time in with me. For sure, without her good analyses of NMR spectra, my projects and thesis could not be performed smoothly.

I would like to thank Dr. Olivier Colombani for his active involvement in the projects of chapter II and chapter IV. I really appreciate his many helps in light scattering and neutron scattering. I enjoyed several days of stay in Le Mans with him and thanked the help he offered me there. I am also grateful to other collaborators in Le Mans, Dr. Erwan Nicol, Frédérick Niepceron, Dr. Sandra Kalem, and Ms. Rihab Zguir for their constructive discussions in many online meetings to better understand and learn supramolecular coassembly behavior in solution.

I am so thankful for Dr. Christophe Sinturel's offer for performing surface nanopatterning experiments that I am interested in. Due to his well organizations of the apartment and experiments in Orléans, there were no worries for many things. Surely, I would like to express my deep appreciation to Ms. Bochra Seaali for her kind and dedicated assistance of AFM in one week. At the same time, I am grateful to Dr. Marylène Vayer for valuable suggestions of AFM experiments.

I would like to thank my CST members, Dr. Olivier Colombani, Dr. Matthieu Raynal, Dr. Fanny Coumes, and Dr. Thibaud Coradin for their participations and helpful comments of my projects.

I would like to thank Dr. Matthieu Raynal again for treating with many trivial matters in the lab I worked in. I am so grateful for SAXS aid from Dr. Cécile Huin, cyro-TEM support from Jean-Michel Guigner, SEC assistance from Dr. Gaëlle Pembouong, and NMR help from Régina Maruchenko, and Claire Troufflard.

I would like to thank my group members whom former and current I work with, in particular, Dr. Patrice Castignolles, Dr. Sergei Kostjuk, Dr. Benjamin Isare, Dr. Jamal Moussa, Dr. David Siefker, Dr. Irene Antignano, Dr. Clément Debrie, Dr. Dimitrios Katsigiannopoulos, Dr. Daniel Aguilera, Dr. Ran Chen, Dr. Huanjun Kong, Dr. Antoine Perennes, Dr. Emma Mongkhoun, Dr. Solène Le Roux, Dr. Simon Peyras, Dr. Kelvin Mall Haidaraly, Ms. Rouguy Sognane, Ms. Diana Deaibess, Mr. Sébastian Berruee, Mr. Florent Mohimont, Mr. Chao Wu, Mr. Yang Yu, Ms. Wencui Zhang, Mr. Yongxiang Qu, Ms. Hongqing Fu, Mr. Chengjun Wu, Mr. Mikael Helali, Mr. Morgan Raguideau, Ms. Marine Durand and Mr. Ricardo Ayala Guzman for working closely with me on related research topics and for all of the inspiring discussions in academics or in life.

I am very grateful to the China Scholarship Council (CSC) for the funding during my PhD. Without it, I could not continue and finish my PhD.

Last but no least, I would like to express my deep appreciation to my parents, my brother and my sister. Their love and supports encourage me to become a better person.

Abbreviations

AFM	Atomic force microscopy
AIBN	2,2′-Azobis(isobutyronitrile)
BCPs	Block copolymers
Boc_2O	Di-tert-butyl dicarbonate
$CHCl_3$	Chloroform
Cryo-TEM	Cryogenic transmission electron microscopy
CTA	Chain transfer agent
CuCl	Copper(I) chloride
DCC	*N,N′*-Dicyclohexylcarbodiimide
DCM	Dichloromethane
DHS	Dihydroxystyrene
DIPFO	1,8-Diiodoperfluorooctane
DMAc	*N,N*-Dimethylacrylamide
DMAP	4-Dimethylaminopyridine
DMF	*N,N*-Dimethylformamide
DMSO	Dimethyl sulfoxide
DP_n	Number-average degree of polymerization
DSA	Directed self-assembly
EUV	Extreme ultraviolet
Et_2O	Diethyl ether
f	Volume fraction
FMA	Ferrocenemethyl acrylate
FTIR	Fourier transform infrared spectroscopy
HABA	2,4-Hydroxybenzeneazo benzoic acid
HCl	Hydrochloric acid
i-PrOH	Isopropyl alcohol
χ	Flory-Huggins interaction parameter
k_p	Propagation constant
L_o	Period domain size
LER	Line edge roughness
LiOTf	Lithium triflate

Me_6TREN	Tris[2-(dimethylamino)ethyl]amine
MeOH	Methanol
MH	Maltoheptaose
M_n	Number-average molar mass
$M_{n,\ NMR}$	Number-average observed NMR molar mass
$M_{n,\ SEC}$	Number-average observed SEC molar mass
$M_{n,\ th}$	Theoretical number-average molar mass
MT	Maltotriose
N	The overall degree of polymerization
NAM	*N*-acryloylmorpholine
NaOD	Sodium deuteroxide
NaOH	Sodium hydroxide
Napy	1,7-Diamidonaphthyridine
NMR	Nuclear magnetic resonance
ODT	Order-disorder transition
OEG	Oligo ethylene glycol
ONB	*o*-Nitrobenzyl
OsO_4	Osmium tetroxide
p	Packing parameter
P3HT	Poly(3-hexylthiophene)
P4VP	Poly(4-vinylpyridine)
PAA	Poly(acrylic acid)
P(AOEAmI-Br)	Poly(1-((2-acryloyloxy)ethyl)-3-alkylimidazolium bromide)
PB	Polybutadiene
PDEA	Poly((2-diethylamino) ethyl methacrylate)
PDHS	Poly(3,4-dihydroxystyrene)
PDMA	Poly((2-dimethylamino) ethyl methacrylate)
PDMAc	Poly(*N,N*-dimethylacrylamide)
PDMS	Polydimethylsiloxane
PDPA	Poly((2-diisopropylamino) ethyl methacrylate)
PEO	Poly(ethylene oxide)
PFMA	Poly(ferrocenemethyl acrylate)
PGM	Poly(glycerol monomethacrylate)

PHEA	Poly(2-hydroxyethyl acrylate)
PHFBMA	Poly(heptafluorobutyl methacrylate)
PHS	Poly(4-hydroxystyrene)
PLA	Poly(lactic acid)
PMAA	Poly(methacrylic acid)
PMMA	Poly(methyl methacrylate)
PMOST	Poly(*p*-methoxystyrene)
P*n*BA	Poly(*n*-butyl acrylate)
PPDFMA	Poly(pentadecafluorooctyl methacrylate)
PS	Polystyrene
PSA	Poly(stearyl acrylate)
POSS	Polyhedral oligomeric silsesquioxane
PStNPOSS	Poly(styrene-co-*N*-propyl-4-vinylbenzamide isobutyl POSS)
P*t*BA	Poly*(tert*-butyl acrylate)
PTHS	Poly(trihydroxy styrene)
PTMSS	Poly(trimethylsilyl styrene)
PVBA	Poly(4-vinylbenzoic acid)
RAFT	Reversible addition−fragmentation chain-transfer
RIE	Reactive ion etching
SANS	Small-angle neutron scattering
SAXS	Small-angle X-ray scattering
SEC	Size exclusion chromatography
SPs	Supramolecular polymers
TEA	Triethylamine
TEM	Transmission electron microscopy
THF	Tetrahydrofuran
TLC	Thin-layer chromatography
UPy	Ureidopyrimidinone
UV	Ultraviolet
XRD	X-ray diffraction

Contents

General Introduction

With the emergence and rapid development of the semiconductor industry, the evolution from bulky computer equipment to nowadays lightweight laptops and smartphones has greatly improved the convenience of modern life. This convenience is not merely due to the reduction in device size, but more importantly, due to the increased number of transistors that can be accommodated per unit area on a chip, thereby enhancing the operation speed of smart devices and expanding their functionalities. As the feature size of transistors continues to shrink, conventional top-down lithographic techniques face increasing challenges in achieving feature sizes below 10 nm. The fundamental limitation arises from the diffraction limit of light, as described by the Rayleigh equation[1]:

$$R = k_1 \frac{\lambda}{NA}$$

where:

R = minimum resolvable feature size

λ = wavelength of the light

NA = numerical aperture of the lens system

k_1 = process-dependent factor (~ 0.25 – 0.5)

For example, when a 193 nm light source is used, the minimum achievable feature size is approximately 36 nm[1]. Although techniques such as extreme ultraviolet (EUV) lithography and electron beam lithography offer potential solutions, their high cost and complexity restrict widespread application[2].

As an alternative to top-down methods, bottom-up approaches based on molecular self-assembly have gained significant attention for constructing desired nanostructures. In 1956, Szwarc first proposed anionic polymerization based on styrene,

marking the beginning of rapid developments in (block) copolymers[3, 4]. Block copolymer (BCP) self-assembly exhibits unique advantages by enabling the formation of diverse nanostructures with domain sizes ranging from 5 to 100 nm. Specifically, well-ordered microphase-separated structures such as lamellae, hexagonally packed cylinders, gyroid phases, and body-centered cubic structures have shown great potential in applications including catalysis[5], separation[6], and nanopatterning[7]. Through selective etching of one polymer domain, microphase-separated BCPs can be converted into nanopatterns with feature sizes below 20 nm. To further achieve sub-10 nm feature sizes, a series of high χ block copolymers have been developed. However, these high χ systems are typically limited to a narrow selection of polymers containing fluorine, silicon, or hydroxyl groups. Furthermore, it is increasingly challenging to obtain feature sizes below 5 nm.

Supramolecular assembly, on the other hand, is based on non-covalent interactions such as hydrogen bonding, ionic interactions, and π-π stacking[8]. Supramolecular monomers form supramolecular polymers through these reversible and dynamic interactions, accompanied by the formation of various assembled structures. Unlike block copolymers composed of covalent bonds, the relatively weak and dynamic interactions of supramolecular polymers endow them with self-healing capabilities and functional behaviors in biological materials and responsive systems. Due to the directional nature of these supramolecular interactions, rigid nanocylinders are relatively easy to prepare. Although the interaction strength of individual supramolecular bonds is weak, the resulting nanocylinders can exhibit remarkable mechanical robustness. Furthermore, when two complementary supramolecular blocks co-assemble via supramolecular interactions, Janus nanocylinders can be prepared, i.e. nanocylinders with two faces of different compositions[9]. The objective of this thesis is to probe whether such Janus nanocylinders can be transferred from solution onto silicon substrates, resulting in well-defined nanocylinder patterns. Notably, nanocylinders formed through hydrogen bonding could display exceptional mechanical stability, and the fabrication strategy would not rely on the incompatibility between two polymer

blocks. This implies that even when the length of each segment is very short, feature sizes below 5 nm could be achieved. Additionally, the chemical contrast between the two segments of the Janus nanocylinder should provide the necessary selectivity for etching, enabling the fabrication of linear nanopatterns.

In this thesis, Chapter I provides a general overview of nanopatterning strategies based on block copolymers and supramolecular polymers, with a detailed description of lamellar and cylindrical morphologies. In Chapter II, a series of complementary hydrogen-bonded polymers were synthesized and characterized as a prerequisite for supramolecular nanopatterning based on polymer co-assembly strategies. In Chapter III, photo-responsive nanocylinders were synthesized and characterized, and their assembly behaviors in solution and on surface were investigated. Chapter IV focuses on the coassembly and characterization of pH-responsive nanocylinders to study the behavior of pH-responsiveness.

References

(1) Lin, B. J. Immersion lithography and its impact on semiconductor manufacturing. *J. Microlith., Microfab., Microsyst.* **2004**, *3*, 377-395.

(2) Nickmans, K.; Schenning, A. P. H. J. Directed self-assembly of liquid-crystalline molecular building blocks for sub-5 nm nanopatterning. *Adv. Mater.* **2018**, *30*, 1703713.

(3) Szwarc, M.; Levy, M.; Milkovich, R. Polymerization initiated by electron transfer to monomer. A new method of formation of block polymers[1]. *J. Am. Chem. Soc.* **1956**, *78*, 2656-2657.

(4) Szwarc, M. 'Living' Polymers. *Nature* **1956**, *178*, 1168-1169.

(5) Hsueh, H. Y.; Huang, Y. C.; Ho, R. M.; Lai, C. H.; Makida, T.; Hasegawa, H. Nanoporous gyroid nickel from block copolymer templates via electroless plating. *Adv.*

Mater. **2011**, *23*, 3041-3046.

(6) Car, A.; Stropnik, C.; Yave, W.; Peinemann, K. V. Tailor-made polymeric membranes based on segmented block copolymers for CO2 separation. *Adv. Funct. Mater.* **2008**, *18*, 2815-2823.

(7) Kim, H. C.; Park, S. M.; Hinsberg, W. D. Block copolymer based nanostructures: materials, processes, and applications to electronics. *Chem. Rev.* **2010**, *110*, 146-177.

(8) De Greef, T. F.; Smulders, M. M.; Wolffs, M.; Schenning, A. P.; Sijbesma, R. P.; Meijer, E. W. Supramolecular polymerization. *Chem. Rev.* **2009**, *109*, 5687-5754.

(9) Han, S.; Pensec, S.; Yilmaz, D.; Lorthioir, C.; Jestin, J.; Guigner, J. M.; Niepceron, F.; Rieger, J.; Stoffelbach, F.; Nicol, E.; Colombani, O.; Bouteiller, L. Straightforward preparation of supramolecular Janus nanorods by hydrogen bonding of end-functionalized polymers. *Nat. Commun.* **2020**, *11*, 4760.

Chapter I: Bibliography

1.1 Introduction

Since its proposal in 1965 by Gordon E. Moore, Moore's law has profoundly influenced the track of the semiconductor industry. It supposes that the number of transistors on a chip doubles approximately every two years, resulting in exponential increases in computing power and energy efficiency[1]. Although it was originally an empirical observation, Moore's law evolved into an industry-driving reference for the technological advancement.

Maintaining this rapid scaling has presented tremendous challenges, particularly in the field of lithographic patterning. As device features approach sub-10 nm scales, traditional photolithography techniques struggle with resolution limitations, line edge roughness, and pattern collapse[2, 3]. Advanced methods such as extreme ultraviolet lithography (EUV) and multiple patterning have been explored to overcome these hurdles, but each carries significant cost and complexity[4]. Consequently, bottom-up nanofabrication strategies, particularly those based on the self-assembly of block copolymers (BCPs), have obtained immense interest[5, 6].

Block copolymer self-assembly offers a promising route to fabricate highly ordered, nanoscale patterns over large areas with feature sizes ranging from 5 to 50 nm[7, 8]. BCPs consist of chemically distinct blocks in a covalent bonds-based polymer, which phase separates on the nanometer scale due to the incompatibility between the blocks[9]. This results in different morphologies, including lamellar, cylindrical, gyroid, and spherical domains, which can be harnessed for nanolithography[10], membranes[11], photonic crystals[12], and high-density data storage[13].

Nanopatterning with BCPs is particularly appealing due to its cost-effectiveness, scalability, and tunability. The domain size and morphology can be precisely tailored by adjusting parameters such as block volume fraction (f), interaction parameter (χ),

and annealing conditions[7]. Directed self-assembly (DSA) techniques, including graphoepitaxy and chemoepitaxy, further enhance pattern regularity and orientation, enabling integration with conventional lithographic processes[14, 15].

Among the available BCP morphologies, lamellar and cylindrical structures are uniquely suitable for nanopatterning applications, especially for semiconductor device fabrication[16]. Their ability to form well-defined, periodic nanostructures with controllable orientation and small domain sizes makes them possible to extend Moore's law, and even overcome current photolithography limits.

The development of BCPs nanopatterning also crosses with the emergence of supramolecular polymers (SPs), where non-covalent interactions such as hydrogen bonding[17-20], π–π stacking[21-23], metal-ligand coordination[24-26], and ionic associations[27-29] introduce a new dimension of functionality and responsiveness. Generally, supramolecular polymer nanopatterning introduces at least one polymer to achieve certain nanostructures which are driven by supramolecular interaction, or synergetic interactions of supramolecular interaction and incompatibility of two polymers. Such a kind of nanopatterning improves the phase separation of two distinct polymers or endows itself unique characteristic due to the directional supramolecular interaction.

In this chapter, we explore BCPs nanopatterning with lamellar and cylindrical morphologies. Furthermore, the SPs nanopatterning using hydrogen bonding and other supramolecular interactions is also described to show its importance in the bottom-up process.

1.2 Block copolymers-based nanopatterning

The utility of block copolymers (BCPs) for nanopatterning arises from their abilities to self-assemble into periodic and nanoscaled morphologies dictated by the chemical incompatibility between covalently linked polymer blocks[9]. Through careful control of molecular weight, volume fraction, and processing conditions, ordered microdomain structures such as lamellae, cylinders, spheres, and gyroids (Figure 1.2.1) can be achieved[7]. Among these, lamellar and cylindrical morphologies are particularly suited for nanopatterning applications due to their linear and periodic geometries, which are ideal for semiconductor line/space nanopatterns and contact/via (dot) nanopatterns[30-32].

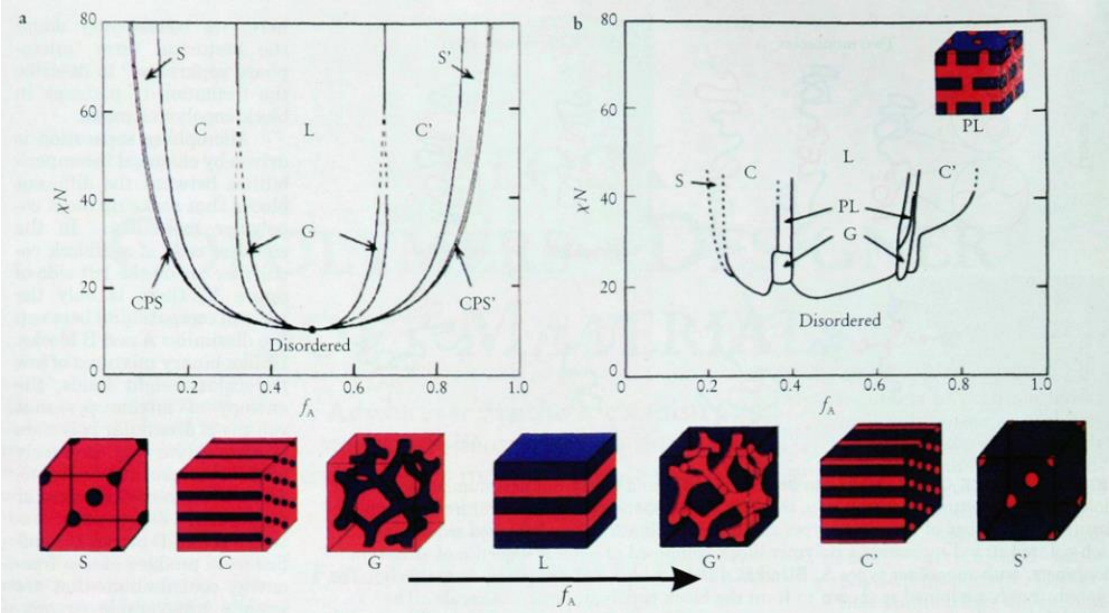

Figure 1.2.1 Phase diagrams for linear AB diblock copolymers with theory (a) and experiment (b) (figure from Bates et al. [7]).

The driving force behind microphase separation in BCPs is the Flory-Huggins interaction parameter (χ) and the overall degree of polymerization (N), with the product χN governing the order-disorder transition (ODT) of the system[7, 33, 34]. To achieve well-defined nanodomains for pattern transfer, BCP thin films are typically annealed under thermal or solvent vapor conditions to promote chain mobility and domain alignment[35].

Moreover, directed self-assembly (DSA) techniques have emerged to precisely guide the orientation and placement of BCP domains, effectively bridging the gap between bottom-up assembly and top-down lithography[4, 6, 36, 37].

1.2.1 Lamellar morphology

Lamellar structures are one of the most frequently observed and technologically relevant morphologies in symmetric diblock copolymers, where the volume fraction of each block approaches 0.5[33]. In the bulk state, lamellae adopt alternating layers of A and B domains with a period (L_0) governed by the degree of polymerization and Flory-Huggins interaction[7].

In thin films, lamellae can orient either parallel or perpendicular to the substrate, depending on surface interactions and interfacial energy balances. Parallel lamellae, although easier to form, offer limited utility for lithographic applications, where vertical (perpendicular) orientation is required for effective pattern transfer[16]. Numerous studies have focused on strategies to induce perpendicular lamellar orientation, including solvent vapor annealing[38-43], and thermal annealing techniques[44-48]. For example, Park et al. demonstrated large-area lamellar patterning using poly(styrene-*b*-methyl methacrylate) (PS-*b*-PMMA) with thermal annealing, achieving highly ordered perpendicular domains suitable for nanolithography[49]. Graphoepitaxy[50] and chemoepitaxy approaches[51], wherein predefined substrate topography or chemistry-modified surface, further enhance long-range order and domain alignments. Furthermore, many investigations have integrated lamellar BCPs nanopatterning into semiconductor processes due to their significant performances[36, 52].

To achieve small feature sizes, particularly sub-10 nm, some high χ systems are adopted. They include, but are not limited, to silicon-containing BCPs, fluorine-containing BCPs and hydroxyl-containing BCPs. For silicon-containing BCPs, the Si can either be in the main chain or side chain, with the representatives of polydimethylsiloxane and polytrimethylsilylstyrene, respectively. Cushen et al. has

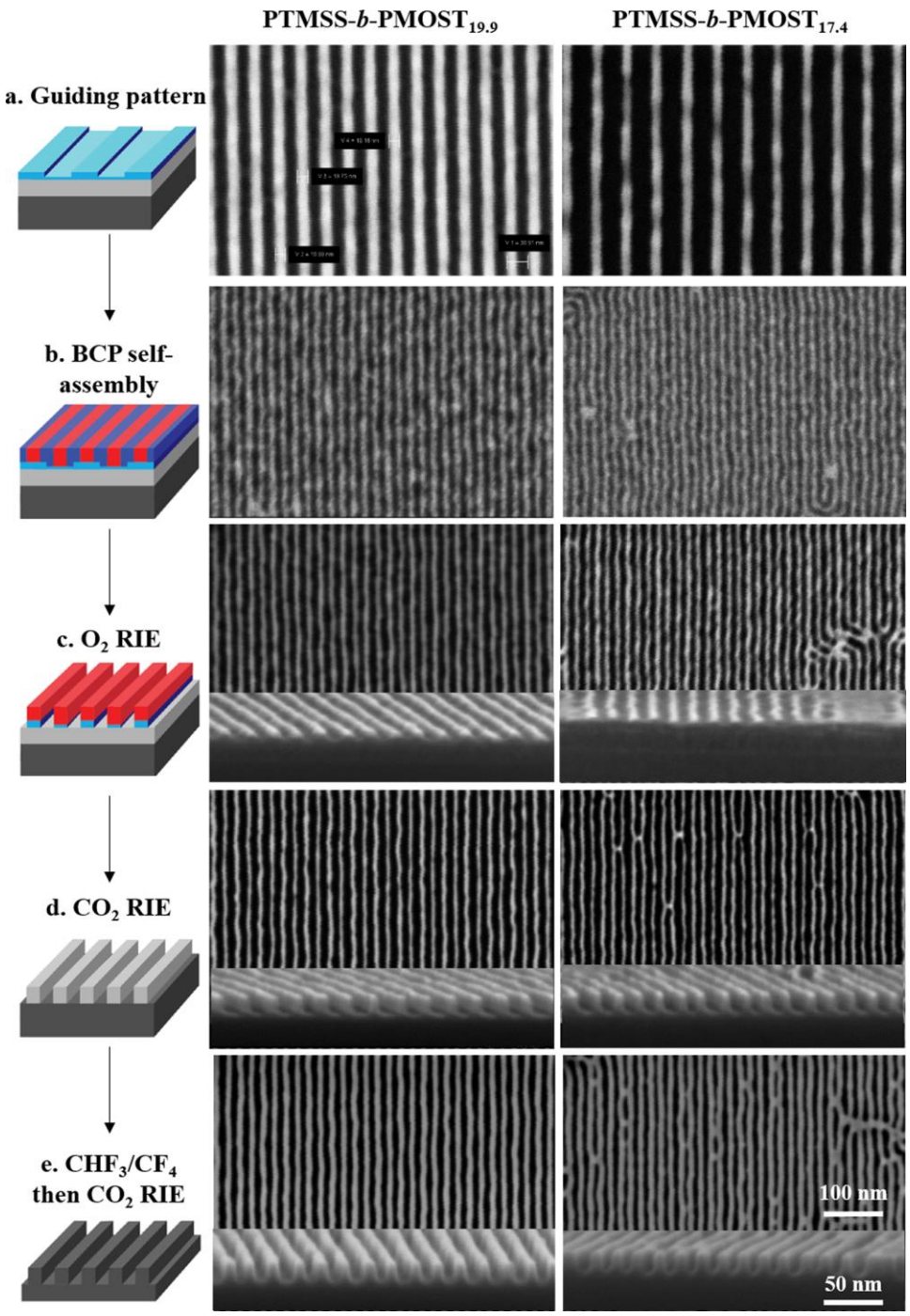

Figure 1.2.1.1 Cartoon of the pattern transfer process with combined top view and cross-section images of PTMSS-*b*-PMOST$_{19.9}$ and PTMSS-*b*-PMOST$_{17.4}$ (figure from Cushen et al. [53]).

demonstrated poly(trimethylsilylstyrene-*block*-*p*-methoxystyrene) (PTMSS-*b*-PMOST) capable of small domain sizes of 19.9 and 17.4 nm (Figure 1.2.1.1) [53]. First, a PS mat (top-coat) was put on the silicon substrate to promote perpendicular orientation. Then,

PTMSS-*b*-PMOST was spin-coated onto the substrate followed by thermal annealing. After forming perpendicular lamella, PTMSS provided intrinsic etching contrast compared with PMOST by using O_2 reactive ion etching to remove organics. With CHF_3/CF_4 etching, trenches were further obtained on the substrate. Deng et al. reported fluorine-containing BCPs via reversible addition−fragmentation chain-transfer (RAFT) polymerization to obtain sub-10 nm features[54]. The first block was poly(heptafluorobutyl methacrylate) (PHFBMA), and the second block (PStNPOSS) was synthesized by a copolymerization of styrene and *N*-propyl-4-vinylbenzamide isobutyl polyhedral oligomeric silsesquioxane. The highly incompatible blocks (poly($St_{10.4}$-*co*-$StNPOSS_{3.5}$)-*b*-$PHFBMA_{25}$) provided high χ, leading to a 5.6 nm lamellar domain size.

Kim et al. [55] investigated the effect of improving χ value between polystyrene and hydroxyl-functionalized polystyrene (Figure 1.2.1.2). With one hydroxyl in the monomer of poly(4-hydroxystyrene) (PHS), hexagonal cylinder and lamella were observed. When the volume fraction of PHS was 0.55, PHS-*b*-PS with a DP_n ~116 presented $\chi = 0.12$ at 150 °C, giving 11.8 nm lamellar domain size. With two hydroxyls in the monomer (DHS) of one block ($f_{PHS} = 0.5$), PDHS-*b*-PS with a significantly shorter $DP_n \sim 18$ displayed $\chi = 0.7$ at 170 °C and finally resulted in 5.9 nm lamellar domain size[56]. Surprisingly, χ value was increased to 1.24 at 220 ℃ with three hydroxyls in the monomer of polytrihydroxystyrene-*block*-polystyrene (PTHS-*b*-PS, DP_n ~11), obtaining a 4.5 nm domain size. Yu et al. reported a similar BCPs containing 2 hydroxyls in glycerol monomethacrylate based on poly(glycerol monomethacrylate)-*block*-polystyrene (PGM-*b*-PS) with 5.4 nm full pitch lamellar microdomains[57].

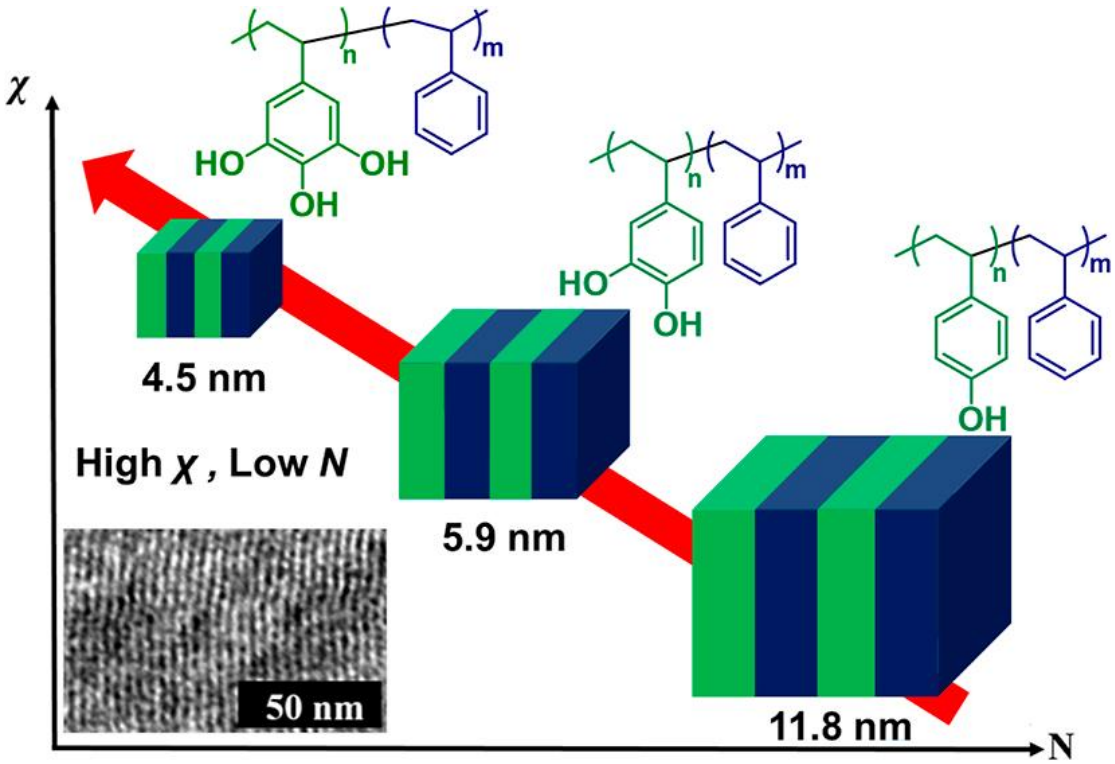

Figure 1.2.1.2 Illustration of decrease in domain spacing as PS is paired with mono-, di-, and tri-hydroxy substituted PS (figure from Mishra et al. [55]).

A completely different strategy to achieve small feature sizes is to use the microphase separation between main-chain and side-chain in comb-like homopolymers. Xu et al. [58] found that the comb-like homopolymer, poly(1-((2-acryloyloxy)ethyl)-3-alkylimidazolium bromide) (P(AOEAmI-Br)), self-assembled into lamellar and hexagonal morphologies. The microphase separation was originated from the incompatibility between the polar main chain and the apolar alkyl side chains. The domain spacing was independent on the molecular weight but depending on the length of the side chain. As shown in Figure 1.2.1.3, P($AOEA_{18}$I-Br) 19 or 62 or 85 or 159 had the same side chain (m = 18) but different DP_n (the numbers indicate the DP_n, in Figure 1.2.1.3). X-ray diffraction (XRD) showed respectively 4.10, 4.10, 4.05 and 4.10 nm domain sizes, with confirmation from transmission electron microscopy (TEM) results (4.05, 4.11, 4.15, and 4.12 nm).

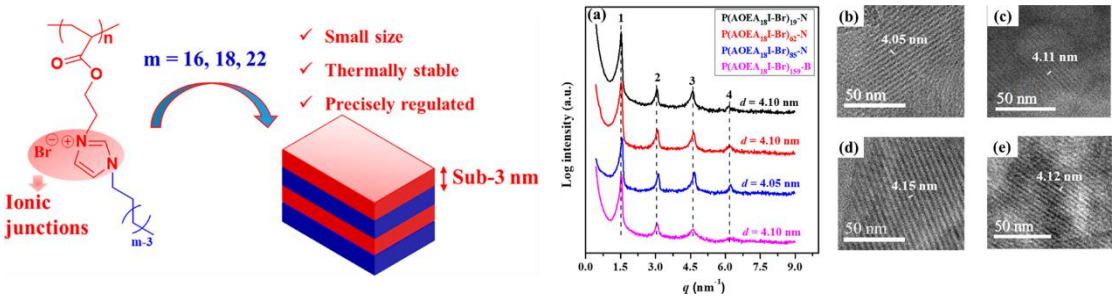

Figure 1.2.1.3 Illustration of comb-like homopolymer self-assembling into lamellar morphology (left) and corresponding XRD and TEM images (right) (figure from Zhang et al. [58]).

1.2.2 Cylindrical morphology

To form cylindrical nanodomains asymmetric diblock copolymers are used, typically when the volume fraction of one block lies between around 0.24 and 0.36[33]. The minority component self-organizes into hexagonally packed cylinders embedded in a continuous matrix of the majority block. Cylindrical morphologies are highly attractive for fabricating dense arrays of nanopores or nanodots with applications in memory devices[59-61], nanophotonics[62], and nanoporous membranes[63-65].

In thin films, the orientation of the cylindrical domains relative to the substrate — either parallel, perpendicular, or tilted — can be manipulated through substrate modification, film thickness control, and annealing protocols[66]. Perpendicular and parallel cylinder orientations are desirable for nanolithography, enabling pattern transfer of high-aspect-ratio nanodots (nanopores) or nanolines.

Pioneered by Mansky et al. with polystyrene-*block*-polybutadiene (PS-*b*-PB) [67], block copolymers nanopatterning has achieved tremendous success in the fabrication of sub-50 nm features. Park et al. [52] reported the large area (2 × 2 μm) preparation of polystyrene-*block*-poly(ethylene oxide) (PS-*b*-PEO) thin films on sapphire wafers. Firstly, the sapphire substrate formed a sawtooth pattern after the thermal treatment (Figure 1.2.2.1 A and D). The well-formed sawtooth pattern was used to guide the self-assembly of PS-*b*-PEO by graphoepitaxy. Then, the block copolymers, PS-*b*-PEO, were

spin-coated on the substrates. Finally, the well-aligned, defect-free and long-range order cylindrical nanopatterns were obtained (Figure 1.2.2.1 B, C, E, and F) after the solvent annealing with *o*-xylene vapors. The well-aligned patterns with cylindrical microdomains 3 nm in diameter indicated areal densities in an excess of 10 terabits per square inch when the nanopattern was extended.

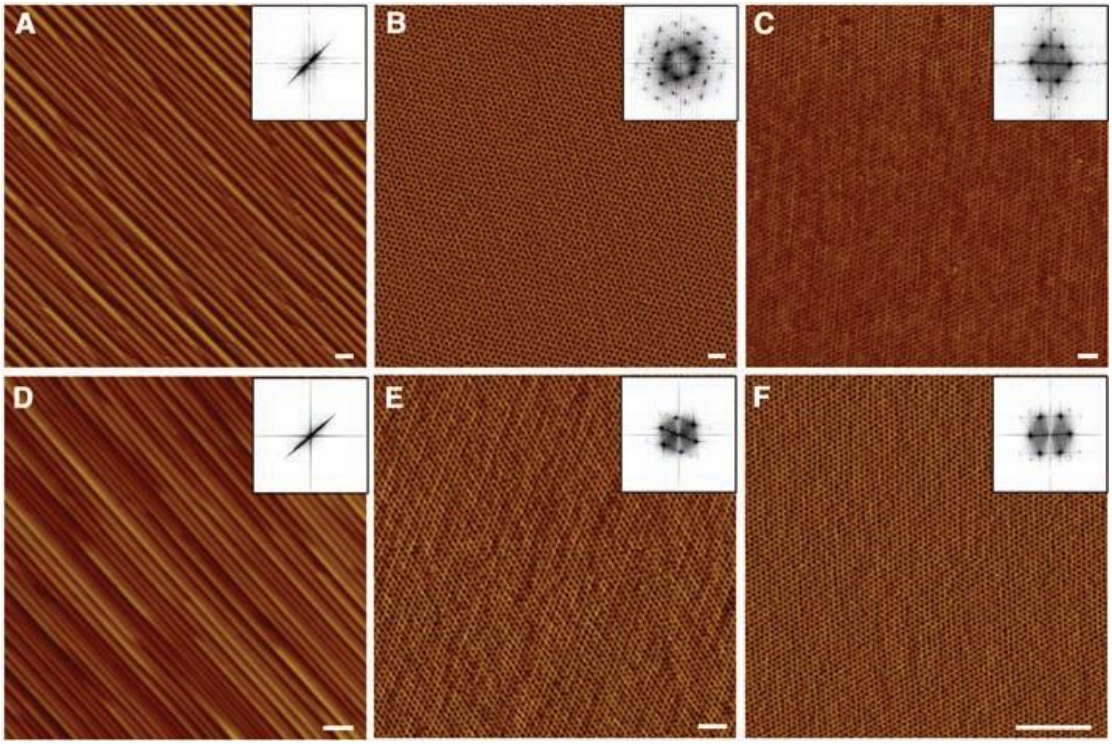

Figure 1.2.2.1 AFM figures of sawtooth patterns of sapphire substrates after thermal treatments (A and D) and cylindrical morphologies of polystyrene-*block*-poly(ethylene oxide) with molecular weights of 26.5 kg/mol (B), 25.4 kg/mol (C), 21.0 kg/mol (E) and 7.0 kg/mol (F). Scale bars, 100 nm (figure from Park et al. [52]).

To obtain certain morphologies with good order over large area, solvent vapor annealing and thermal annealing are efficient processing methods for preparing nanopatterning in thin films. Compared with thermal annealing, solvent vapor annealing has some significant advantages. Firstly, solvent vapor annealing is conducted at room or lower temperature, which is energy-efficient and easily operative. Secondly, BCPs chains create a local environment when absorbing the solvent, mitigating the disparate interfacial energies originated from the different blocks. In this

way, it allows the formation of microdomains perpendicular to the free surface of the film. Thirdly, solvent vapor annealing enhances the molecular diffusivity to reach general equilibrium more easily. Tada et al. [68] reported the self-assembly of PMMA-*b*-PMAPOSS in thin films with cylindrical dots under controlled solvent vapor annealing. As shown in Figure 1.2.2.2(a), $PMMA_{41}$-*b*-$PMAPOSS_{29}$ did not present a regular morphology, but well-ordered perpendicular cylinders were obtained when the degree of swelling was up to 175% (Figure 1.2.2.2(d)).

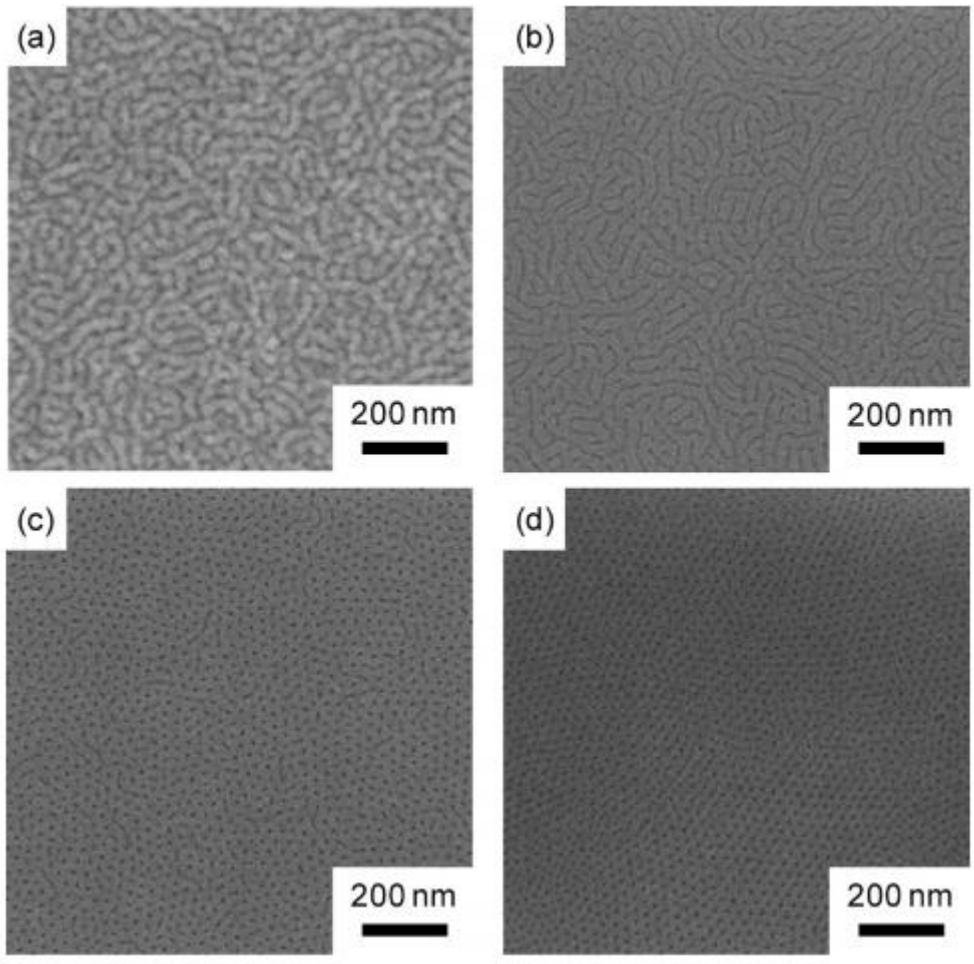

Figure 1.2.2.2 SEM images of the $PMMA_{41}$-*b*-$PMAPOSS_{29}$ films on Si substrates with 0% (a), 125% (b), 150% (c) and 175% (d) degrees of swelling (figure from Tada et al. [68]).

Thermal annealing is normally conducted with the simultaneous use of a random copolymer. A thin film of a random copolymer is used to mitigate different surface

energies and finally becomes “neutralized”. As indicated in Figure 1.2.2.3, before the transformation of PS-*b*-PMMA onto the substrate, a random copolymer PS-*r*-PMMA was grafted to achieve “neutralized” effect[35, 69]. Then, PS-*b*-PMMA was spin-casted onto the substrate followed by thermal annealing. UV was introduced later to break PMMA and PMMA was removed with the rinsing of acetic acid. Finally, nanopores with different thickness of thin films could be prepared (Figure 1.2.2.3b, c, and d). It indicated the effect of film thickness on PS-*b*-PMMA thin film self-assembly process. If the thin film was too thin, the distribution of large pores was observed (Figure 1.2.2.3b), while the film presented elongated pores for thicker film (Figure 1.2.2.3d).

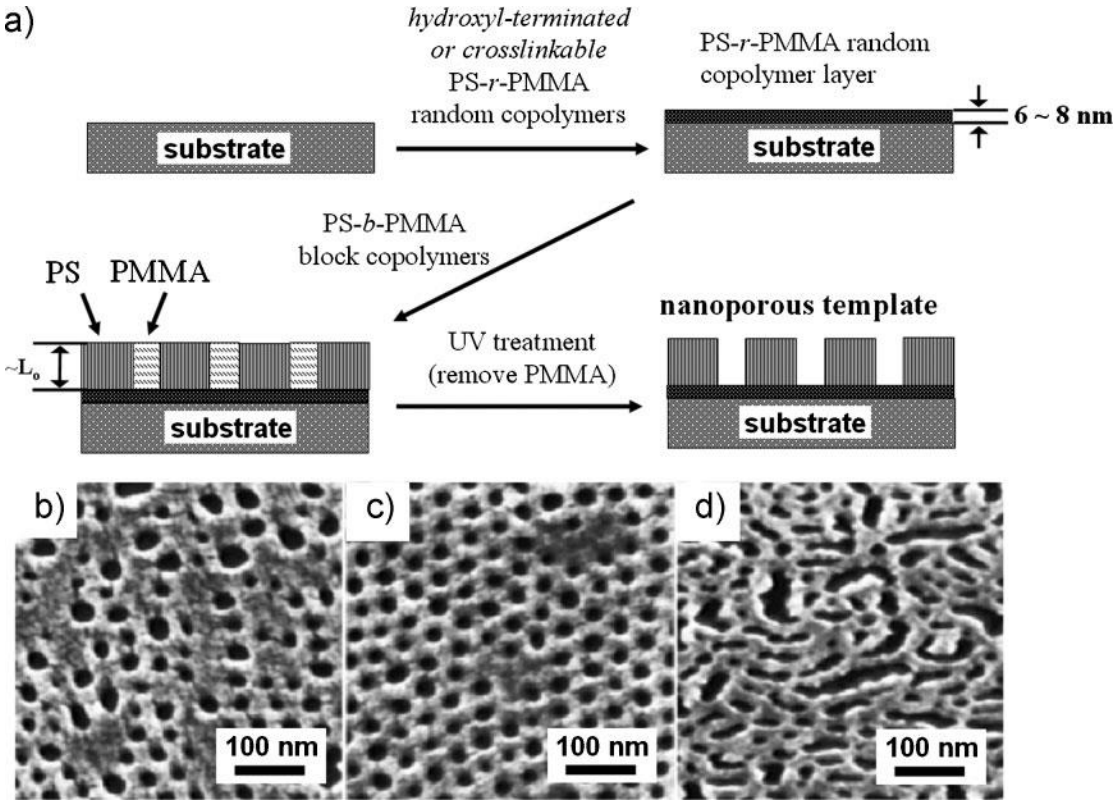

Figure 1.2.2.3 Schematics (a) and thin film thickness (b: 31nm; c: 42 nm; d: 51 nm) of preparing the nanoporous template from PS-*b*-PMMA (figure from Bang et al. [35] and Guarini et al. [69]).

Similar to lamellar morphology mentioned before, the first method to achieve sub-10 nm cylindrical domain sizes is to reduce N, while using high χ BCPs to keep χN larger than 10.5. Deng et al. [54] synthesized silicon and fluorine-containing diblock

copolymers, poly(trimethylsilyl styrene)-*block*-poly(pentadecafluorooctyl methacrylate) (PTMSS-*b*-PPDFMA), by anionic polymerization. $PTMSS_{13.6}$-*b*-$PPDFMA_{4.7}$ displayed cylindrical morphology (from SAXS) with 6.4 nm domain spacing. When the BCPs were transferred onto the Si substrate, field-emission scanning electron microscopy confirmed the cylindrical morphology with dark PTMSS and light PPDFMA (Figure 1.2.2.4). When the BCPs was dissolved at 1 wt% in toluene and spin-coated onto a silicon template with trenches, a well-organized pattern was obtained and the line width was close to 6.4 nm (from the SAXS result). The parallel nanocylinder of $PTMSS_{13.6}$-*b*-$PPDFMA_{4.7}$ was appealing since PPDFMA could be removed by O_2 reactive ion etching, while PTMSS was more resistant. It could therefore be used as a mask before etching with CHF_3/CF_4, giving rise to line/space pattern in silicon. Genabeek et al. [70] investigated the self-assembly of poly(dimethylsiloxane)-*b*-poly(lactic acid) (PDMS-*b*-PLA) synthesized via iterative exponential growth. The lowest cylindrical domain size they observed was low down to 6.5 nm in $PDMS_{23}$-*b*-PLA_{11}. AFM investigations proved the formation of cylinders in $PDMS_{27}$-*b*-PLA_{15} and $PDMS_{59}$-*b*-PLA_{33}.

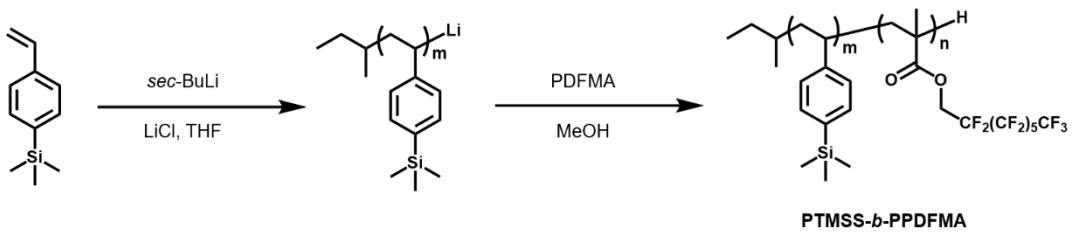

PTMSS-*b*-PPDFMA

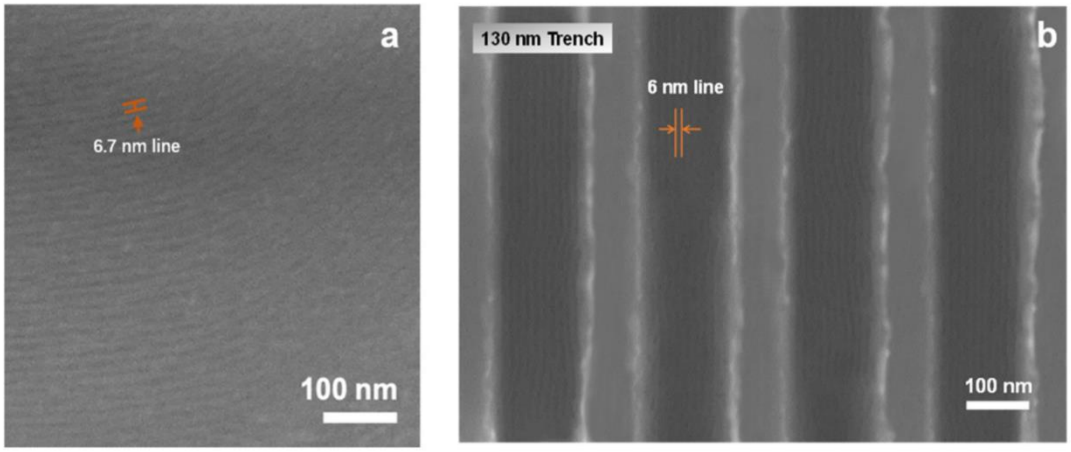

Figure 1.2.2.4 Synthetic scheme of PTMSS-*b*-PPDFMA (top) and field-emission scanning electron microscopy images of $PTMSS_{13.6}$-*b*-$PPDFMA_{4.7}$ thin film on Si wafer (a) and $PTMSS_{13.6}$-*b*-$PPDFMA_{4.7}$ line pattern in 130 nm-Si trench template (b) (figure from Deng et al. [54]).

Borsali's group developed a series of maltoheptaose-based block copolymers enabling them to self-assemble into cylindrical morphologies with ~10 nm features, which was originated from the high incompatibility between maltoheptaose (MH, containing 22 hydroxyls) and polystyrene[71, 72]. In a recent work, they reported the cylindrical morphology of self-assembly of maltoheptaose (MH) or maltotriose (MT)-based Janus bottlebrush copolymers[73]. As displayed in Figure 1.2.2.5, polystyrene was synthesized via anionic polymerization followed by end modification with a norbornene. Ring-opening metathesis polymerization combined with click chemistry with MH or MT afforded Janus-like bottlebrush BCPs. The bottlebrush BCPs self-assembled into cylindrical morphologies and the lowest domain size was low down to 8.3 nm from SAXS and confirmed by atomic force microscopy (AFM). Even though the overall molar mass is high, the domain sizes are small because they are dependent on the length of side chains.

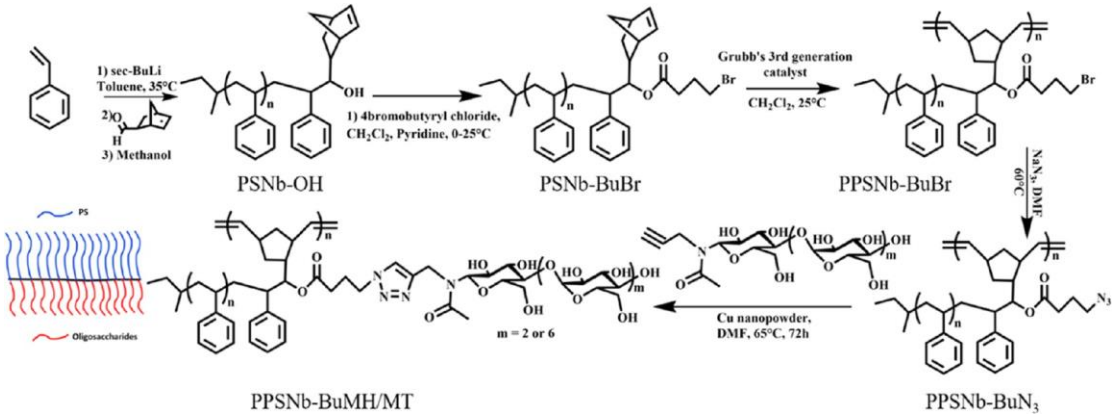

Figure 1.2.2.5 Synthesis of Janus-type bottlebrush block copolymers (figure from Mumtaz et al. [73]).

1.3 Supramolecular polymers-based nanopatterning

Supramolecular polymers are assembled from monomers held together by non-covalent interactions[74-76], such as hydrogen bonding interaction[17], π-π interaction[77], ionic bonding interaction[27] and metal-ligand binding interaction[78]. The rich dynamic behavior of supramolecular polymers endows them with promising abilities in recyclability, self-healing, stimuli responsiveness, and evolvable properties for the applications as self-healing[79], catalytic[80], optoelectronic[81] and biomedical materials[82]. With the collectively supramolecular interactions between molecules, supramolecular polymers have also comparably robust mechanical properties to covalent polymers, indicating greatly interesting investigations in surface nanopatterning.

1.3.1 Hydrogen bonding interaction

The incorporation of supramolecular interactions into block copolymer (BCP) systems has emerged as a powerful strategy to diversify nanostructure morphologies and functionalities[83, 84]. Among the various non-covalent interactions, hydrogen bonding is particularly attractive due to its directional nature, reversibility, and moderate strength, making it well-suited for dynamic, responsive, and self-healing nanostructures[76].

In hydrogen-bonded supramolecular block copolymers systems, small molecules or oligomers capable of forming hydrogen bonds are selectively incorporated into one block of a diblock copolymers[75]. This selective association effectively modifies the volume fraction, interaction, and chain mobility of the host block, thereby tuning the phase behavior and domain morphology[85]. For instance, Montarnal et al. [86] synthesized PMMA-*supra*-PS with complementary hydrogen bondings via RAFT polymerization using corresponding hydrogen bonding terminated chain transfer agents (Figure 1.3.1.1). In $PMMA_{15k}$-*supra*-PS_{30k}, the hexagonal cylinders were observed after thermal annealing on a silicon wafer. With the introduction of the mixed solvent of $MeOH/H_2O/CHCl_3$ (47.5:47.5:3), PMMA was selectively dissolved giving nanopores

with ~14 nm in diameter.

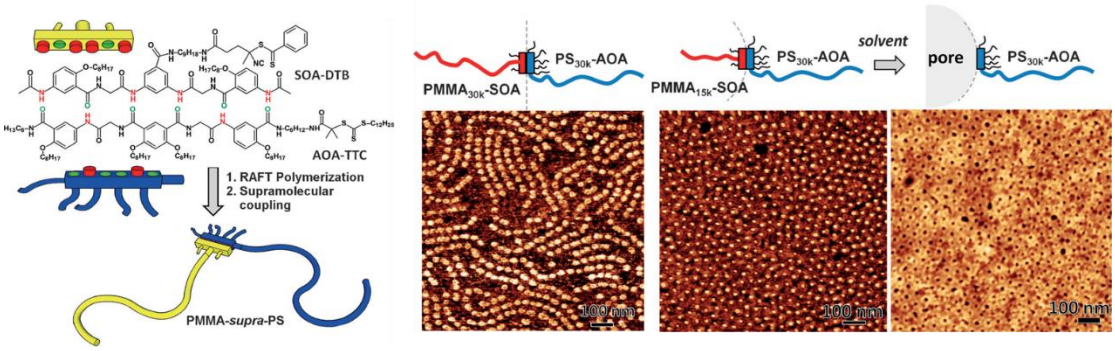

Figure 1.3.1.1 Illustration of hydrogen-bonded PMMA-*supra*-PS (left) and AFM figures (figure from Montarnal et al. [86]).

A similar study was performed by Pitet et al. [87] indicating the efficient co-assembly of ureidopyrimidinones (UPy)-ended PDMS and 1,7-diamidonaphthyridines (Napy)-ended PLA. There were no phase separations for PDMS-UG and PLA-Napy alone but lamellar morphology was observed when they were blended.

Instead of providing the junction of two blocks, hydrogen bonding can also promote the alignment of the blocks, improving line edge roughness (LER) [88]. The LER must be minimized to reduce current leakage of the final device due to a decreased gate length. As shown in Figure 1.3.1.2, PS and PMMA were connected with a urea and a rigid linker. The existence of urea with directional hydrogen bondings strictly define the boundary of PS, improving the line edge roughness.

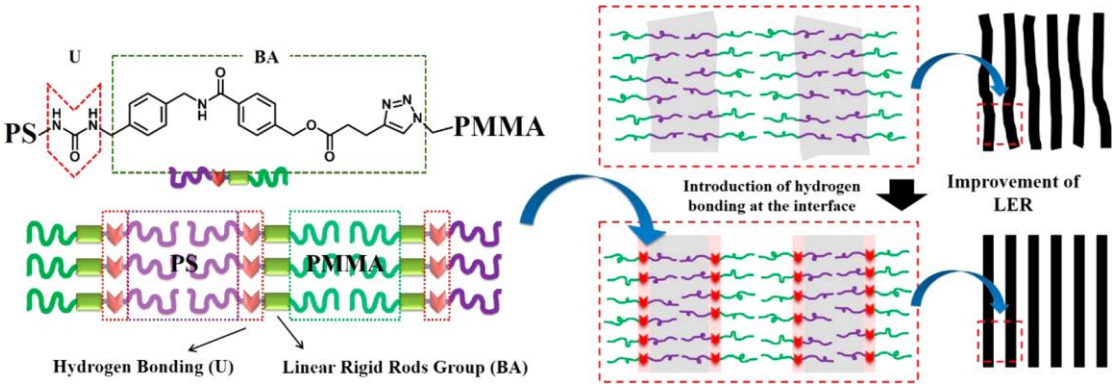

Figure 1.3.1.2 Chemical structure of PS-U-BA-PMMA and schematic showing the

improvement of LER due to hydrogen bonding (U) and rigid rod (BA) moieties located at the junction of PS and PMMA chains (figure from Lee et al. [88]).

Urea-based hydrogen bonding interaction has received increasingly attention due to the efficient and robust assembly in solution[89-91], but there are only few investigations of urea-based polymers on surface. Véchambre et al. [92] synthesized triurea-based poly(*n*-butyl acrylate) (P*n*BA) capable of self-assembling into cylindrical morphology driven by the robust hydrogen bonding interactions of triureas (Figure 1.3.1.3). Different from synergetic interaction of hydrogen bonding mentioned previously that improved the phase separation, the formation of cylindrical morphology was totally dependent on the hydrogen bonding and hydrophobic interactions. When polymer's DP_n was 36 (M_n: 5.2 kg/mol), AFM result revealed an ultrasmall distance between two adjacent cylinders, as low as 6 nm, which was in good agreement with the SAXS measurement of 7 nm.

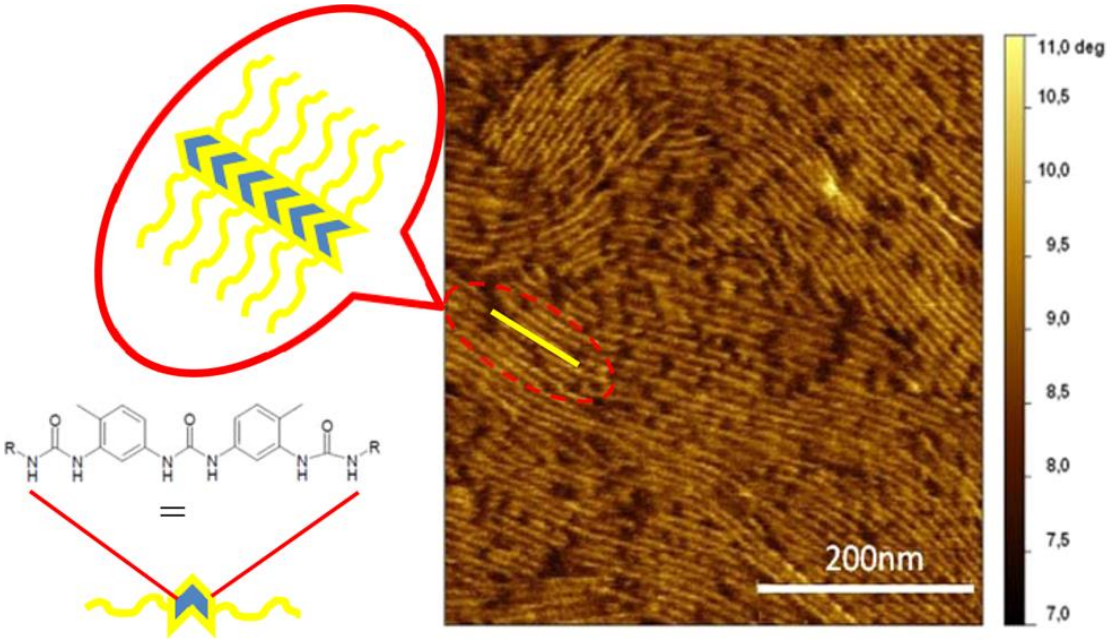

Figure 1.3.1.3 AFM image of triurea-based poly(*n*-butyl acrylate) with 5.2 kg/mol molecular weight (figure from Véchambre et al. [92]).

A third strategy is to incorporate additives (small molecules) into BCPs to form well-ordered morphology via hydrogen bonding interaction between BCPs and the

additive[93]. As shown in Figure 1.3.1.4, 1 equivalent of poly(styrene-*block*-4-vinylpyridine) (PS-*b*-PVP) combined with 1 equivalent of 2,4-hydroxybenzeneazo benzoic acid (HABA) form perpendicular cylinders after thermal annealing. The perpendicular cylinders could become parallel morphology after a further chloroform annealing. Then, methanol was introduced to remove HABA followed by the introduction of phenolic resin precursor cured by formaldehyde gas. After the pyrolysis, nanodots or parallel nanowires were obtained.

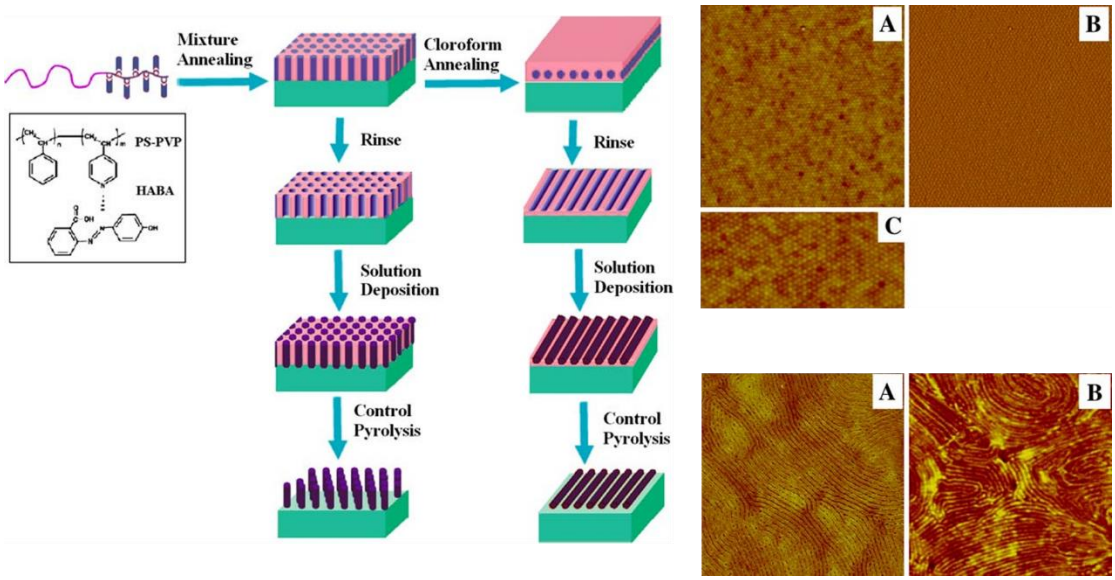

Figure 1.3.1.4 Scheme of the fabrication of highly ordered polymeric nanodot and nanowire arrays (left) and AFM figures of nanodots after pyrolysis (upper right A, B, and C. A: height image; B: phase image; C: enlarged height image) and parallel nanocylinders (or nanowires) after chloroform annealing and pyrolysis (bottom right A and B. A: height image after chloroform annealing; B: height image after pyrolysis) (figure from Liu et al. [93]).

1.3.2 Other interactions

Beyond hydrogen bonding, supramolecular interactions such as halogen bonding interaction[94, 95], ionic interaction[96], and π–π stacking interaction[83] have been explored for enhancing and diversifying BCPs nanopatterning capabilities.

Analogous to hydrogen bonding, halogen bonding also possesses a net attractive

interaction between an electron-poor halogen (i.e. iodine) and an electron-rich Lewis base (i.e. amine or pyridine derivative). Milani et al. [97] reported well-defined, ordered arrangements of cylindrical morphology with the enhancement of adding 1,8-diiodoperfluorooctane (DIPFO) into polystyrene-*block*-poly(4-vinylpyridine) (PS-*b*-P4VP). For pure PS-*b*-P4VP, SAXS experiment with broad peaks revealed a poor hexagonal morphology, which was confirmed by AFM result (Figure 1.3.2.1 bottom A). When DIPFO was introduced into PS-*b*-P4VP in 1:1 molar ratio, Raman spectrum indicated the binding with the redshift of C–I stretching band. Afterwards, the complex was drop-casted without any annealing and gave well-ordered cylindrical morphology (Figure 1.3.2.1 bottom B). By using ethanol to remove DIPFO, FTIR demonstrated the complete removal of DIPFO from the previous complex, providing the resistant nanoporous structure (Figure 1.3.2.1 bottom C). Chen et al. [95] also showed the significant ordering enhancement of the assembly of a liquid crystalline block copolymer by introducing halogen interaction.

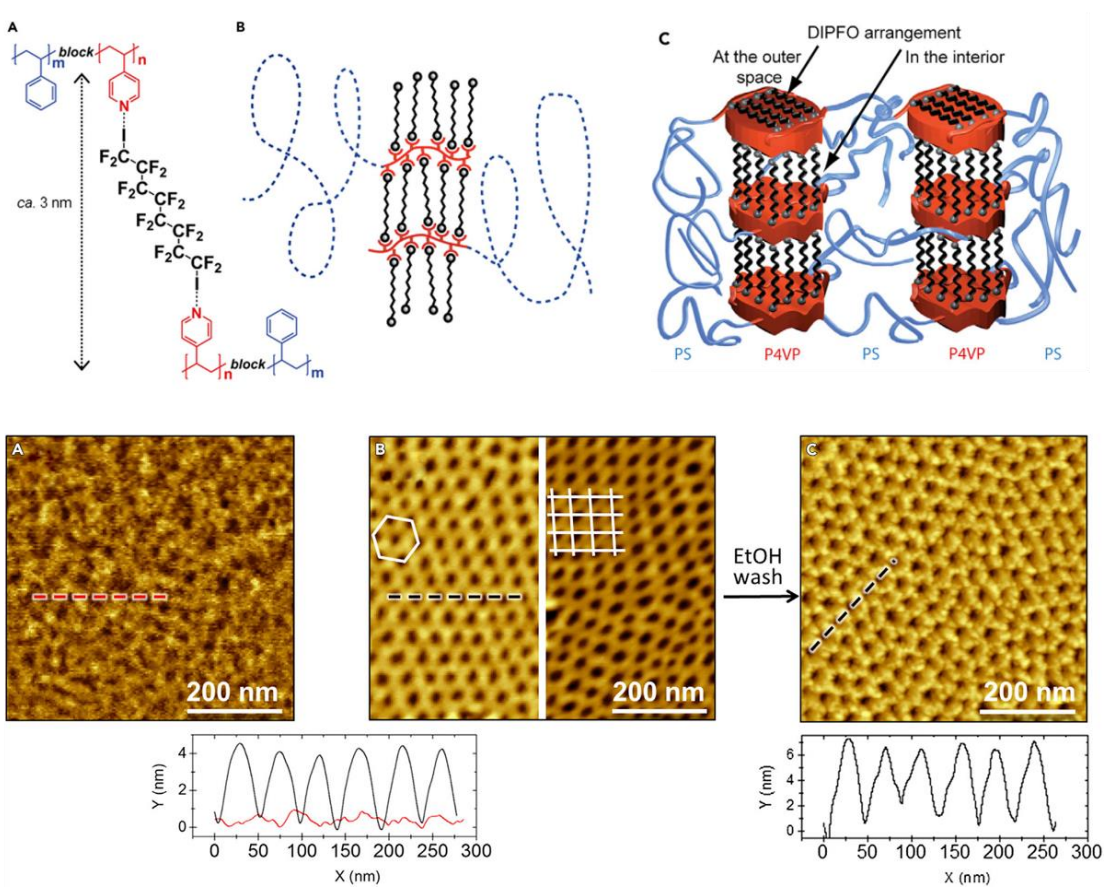

Figure 1.3.2.1 Illustrations of the halogen interaction between PS-*b*-P4VP and DIPFO (upper A, B and C), and AFM images of PS-*b*-P4VP (bottom A), complex PS-*b*-P4VP/DIPFO (bottom B) and PS-*b*-P4VP/DIPFO film after ethanol washing (bottom C) (figure from Milani et al. [97]).

Ionic interaction leverages the strong electrostatic forces between oppositely charged polymer segments or dopant molecules to drive phase separation. Ionic supramolecular systems offer high segregation strength and rapid ordering kinetics. Initiated by Wiesner et al., introducing ionic interaction into block copolymers not only controls or improves the stabilization of phase separation but also could change the phase morphologies due to the change of curvature of the interface[98, 99]. When the ionic interaction is in the middle of two blocks, it defines strictly the boundary of the two segments, which greatly improves the line edge roughness in lines nanopatterning. As displayed in Figure 1.3.2.2, PDMS-*b*-PMMA was obtained by azide–alkyne "click" coupling[100]. Triazole in the middle was further ionized using iodomethane (MeI) and then exchanged by lithium triflate (LiOTf) to introduce ionic interaction. In light of the strongly attractive ionic interaction, PDMS-*b*-PMMA presented longer range ordering. When $PDMS_{1.7k}$-*b*-$PMMA_{5.1k}$ was thermal annealed and etched, the well-ordered line features with a similar full pitch of 13 nm were obtained. Ji et al. [101] adopted a similar strategy using poly(3-hexylthiophene)-*b*-poly(methyl methacrylate) (P3HT-*b*-PMMA) to manipulate the self-assembly behavior giving the changes of nanostructures.

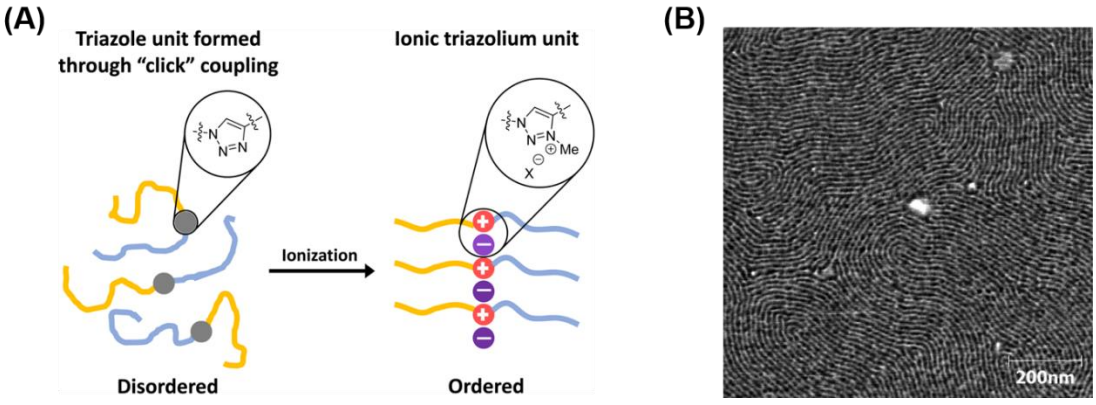

Figure 1.3.2.2 Illustration of the enhancement of phase separation by insetting ionic

interaction (A), and AFM phase image (B) of $PDMS_{1.7k}$-$b^{(\pm)}$-$PMMA_{5.1k}$ after thermal annealing and reactive ion etching (figure from Luo et al. [100]).

Park's group reported a robust strategy using ionic interaction to fabricate parallel and perpendicular cylindrical morphologies over large area[102]. As shown in Figure 1.3.2.3, end-sulfonated polystyrene (SPS), end-aminated polybutadiene (APBD), end-aminated polystyrene (APS) and end-sulfonated polybutadiene (SPBD) were prepared, respectively. SPS co-assembled with APBD to form Supra 1, and the other 2 polymers co-assembled to form Supra 2. Supra 1 and Supra 2 were dissolved in THF followed by spin-coating onto the silicon substrate. The AFM revealed the cylindrical morphologies of Supra 1 (Figure 1.3.2.3 upper right a) and Supra 2 (Figure 1.3.2.3 upper right e). Treated with benzene annealing for 5 minutes, improved nanopatterns (Figure 1.3.2.3 upper right b and f) were obtained. When annealing time was increased to 30 minutes, parallel cylinders (Figure 1.3.2.3 upper right c and g) were achieved. When simple, not end-functionalized polystyrene was blended with APBD and SPBD, macroscopic phase separations were observed due to the thermodynamically unfavorable mixing energy. This indicated the key role of ionic interaction between polystyrene and polybutadiene. After solvent annealing, Supra 1 and 2 thin films were treated with osmium tetroxide (OsO_4) to crosslink polybutadiene, followed by the immersion into a mixture of methyl ethyl ketone and hydrochloric acid to remove PS. AFM images demonstrated the formation of nanodots over large area (Figure 1.3.2.3 bottom right a and b).

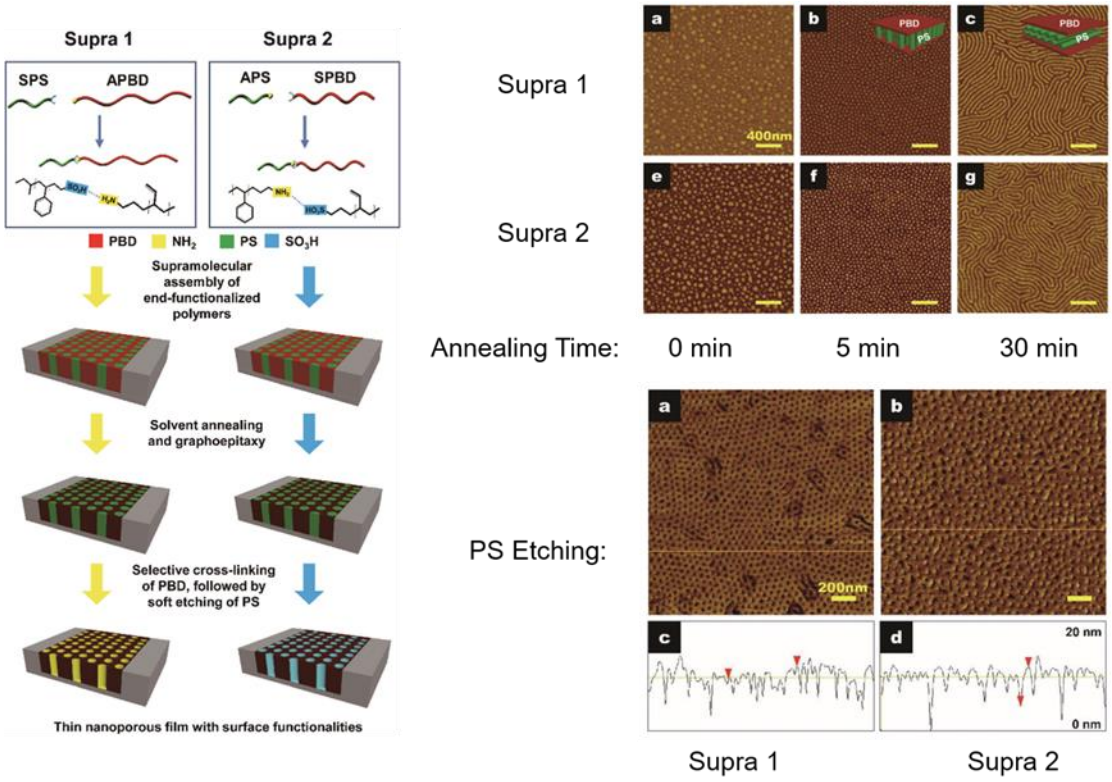

Figure 1.3.2.3 Illustration of the process of nanopatterning using Supra 1 and Supra 2 (left), and AFM images after solvent annealing of Supra 1 and Supra 2 with different time (upper right) and after etching (bottom right) (figure from Cho et al. [102]).

π–π stacking interactions offer another avenue for enhancing phase separation in BCP systems. Even though conjugated or aromatic moieties incorporated into polymers promote stacking interactions that increase stabilization, related studies[21, 83] in nanopatterning are still less investigated.

1.3.3 Conclusion

In conclusion, the supramolecular approaches in block copolymers stabilize the nanostructure or enhance the structural versatility of BCPs nanopatterning systems. Furthermore, supramolecular interactions impart BCPs with dynamic, responsive properties that make BCPs adjustable in nanopatterning. Finally, in some systems[83, 84, 102], supramolecular interaction plays a dominant role as driving force for microphase separation outplaying the morphologies that would be formed with simple BCPs

without specific supramolecular moities. When BCPs chains possessing supramolecular moities are decreased to small oligomers, due to the directional supramolecular interaction, it is promising to achieve sub-5 even sub-3 nm domain features which are desirable for top-down patterning processes.

1.4 References

(1) Moore, G. E. Cramming more components onto integrated circuits. *Electronics* **1965**, *38*, 114-117.

(2) Segalman, R. A. Patterning with block copolymer thin films. *Mater. Sci. Eng., R* **2005**, *48*, 191-226.

(3) Stoykovich, M. P.; Nealey, P. F. Block copolymers and conventional lithography. *Mater. Today* **2006**, *9*, 20-29.

(4) Chen, Y.; Xiong, S. Directed self-assembly of block copolymers for sub-10 nm fabrication. *Int. J. Extreme Manuf.* **2020**, *2*, 032006.

(5) Li, M.; Ober, C. K. Block copolymer patterns and templates. *Mater. Today* **2006**, *9*, 30-39.

(6) Ji, S.; Wan, L.; Liu, C.-C.; Nealey, P. F. Directed self-assembly of block copolymers on chemical patterns: A platform for nanofabrication. *Prog. Polym. Sci.* **2016**, *54-55*, 76-127.

(7) Bates, F. S.; Fredrickson, G. H. Block copolymers—designer soft materials. *Phys. Today* **1999**, *52*, 32-38.

(8) Kim, H. C.; Park, S. M.; Hinsberg, W. D. Block copolymer based nanostructures: materials, processes, and applications to electronics. *Chem. Rev.* **2010**, *110*, 146-177.

(9) Bates, F. S.; Fredrickson, G. H. Block copolymer thermodynamics: theory and experiment. *Annu. Rev. Phys. Chem.* **1990**, *41*, 525-557.

(10) Tang, C.; Lennon, E. M.; Fredrickson, G. H.; Kramer, E. J.; Hawker, C. J. Evolution of block copolymer lithography to highly ordered square arrays. *Science* **2008**, *322*, 429-432.

(11) Nunes, S. P. Block copolymer membranes for aqueous solution applications.

Macromolecules **2016**, *49*, 2905-2916.

(12) Liu, S.; Yang, Y.; Zhang, L.; Xu, J.; Zhu, J. Recent progress in responsive photonic crystals of block copolymers. *J. Mater. Chem. C.* **2020**, *8*, 16633-16647.

(13) Werner, J. G.; Li, Y.; Wiesner, U. Block-copolymer-architected materials in electrochemical energy storage. *Small Sci.* **2023**, *3*, 2300074.

(14) Li, W.; Müller, M. Directed self-assembly of block copolymers by chemical or topographical guiding patterns: Optimizing molecular architecture, thin-film properties, and kinetics. *Prog. Polym. Sci.* **2016**, *54-55*, 47-75.

(15) Morris, M. A. Directed self-assembly of block copolymers for nanocircuitry fabrication. *Microelectron. Eng.* **2015**, *132*, 207-217.

(16) Bates, C. M.; Maher, M. J.; Janes, D. W.; Ellison, C. J.; Willson, C. G. Block copolymer lithography. *Macromolecules* **2013**, *47*, 2-12.

(17) Sijbesma, R. P.; Beijer, F. H.; Brunsveld, L.; Folmer, B. J.; Hirschberg, J. H.; Lange, R. F.; Lowe, J. K.; Meijer, E. W. Reversible polymers formed from self-complementary monomers using quadruple hydrogen bonding. *Science* **1997**, *278*, 1601-1604.

(18) Fernandez-Castano Romera, M.; Gostl, R.; Shaikh, H.; Ter Huurne, G.; Schill, J.; Voets, I. K.; Storm, C.; Sijbesma, R. P. Mimicking active biopolymer networks with a synthetic hydrogel. *J. Am. Chem. Soc.* **2019**, *141*, 1989-1997.

(19) Danial, M.; Tran, C. M.; Young, P. G.; Perrier, S.; Jolliffe, K. A. Janus cyclic peptide-polymer nanotubes. *Nat. Commun.* **2013**, *4*, 2780.

(20) Obert, E.; Bellot, M.; Bouteiller, L.; Andrioletti, F.; Lehen-Ferrenbach, C.; Boue, F. Both water- and organo-soluble supramolecular polymer stabilized by hydrogen-bonding and hydrophobic interactions. *J. Am. Chem. Soc.* **2007**, *129*, 15601-15605.

(21) Berruee, S.; Guigner, J. M.; Bizien, T.; Bouteiller, L.; Sosa Vargas, L.; Rieger, J.

Spontaneous formation of polymeric nanoribbons in water driven by π-π interactions. *Angew. Chem. Int. Ed.* **2024**, *64*, e202413627.

(22) Burattini, S.; Greenland, B. W.; Hayes, W.; Mackay, M. E.; Rowan, S. J.; Colquhoun, H. M. A supramolecular polymer based on tweezer-type π–π stacking interactions: molecular design for healability and enhanced toughness. *Chem. Mater.* **2010**, *23*, 6-8.

(23) Hoeben, F. J.; Jonkheijm, P.; Meijer, E. W.; Schenning, A. P. About supramolecular assemblies of π-conjugated systems. *Chem. Rev.* **2005**, *105*, 1491-1546.

(24) Rowan, S. J.; Beck, J. B. Metal-ligand induced supramolecular polymerization: a route to responsive materials. *Faraday Discuss.* **2005**, *128*, 43-53.

(25) Beck, J. B.; Ineman, J. M.; Rowan, S. J. Metal/ligand-induced formation of metallo-supramolecular polymers. *Macromolecules* **2005**, *38*, 5060-5068.

(26) Ahmadi, M.; Seiffert, S. Coordination geometry preference regulates the structure and dynamics of metallo-supramolecular polymer networks. *Macromolecules* **2021**, *54*, 1388-1400.

(27) Noro, A.; Hayashi, M.; Matsushita, Y. Design and properties of supramolecular polymer gels. *Soft Matter* **2012**, *8*, 6416-6429.

(28) Lin, X.; Grinstaff, M. W. Ionic supramolecular assemblies. *Isr. J. Chem.* **2013**, *53*, 498-510.

(29) Aboudzadeh, M. A.; Munoz, M. E.; Santamaria, A.; Marcilla, R.; Mecerreyes, D. Facile synthesis of supramolecular ionic polymers that combine unique rheological, ionic conductivity, and self-healing properties. *Macromol. Rapid. Commun.* **2012**, *33*, 314-318.

(30) Black, C. T.; Ruiz, R.; Breyta, G.; Cheng, J. Y.; Colburn, M. E.; Guarini, K. W.; Kim, H. C.; Zhang, Y. Polymer self assembly in semiconductor microelectronics. *IBM*

J. Res. Dev. **2007**, *51*, 605-633.

(31) Park, C.; Yoon, J.; Thomas, E. L. Enabling nanotechnology with self assembled block copolymer patterns. *Polymer* **2003**, *44*, 6725-6760.

(32) Ruiz, R.; Kang, H.; Detcheverry, F. A.; Dobisz, E.; Kercher, D. S.; Albrecht, T. R.; de Pablo, J. J.; Nealey, P. F. Density multiplication and improved lithography by directed block copolymer assembly. *Science* **2008**, *321*, 936-939.

(33) Bates, F. S.; Schulz, M. F.; Khandpur, A. K.; Förster, S.; Rosedale, J. H.; Almdal, K.; Mortensen, K. Fluctuations, conformational asymmetry and block copolymer phase behaviour. *Faraday Discuss.* **1994**, *98*, 7-18.

(34) Bates, F. S. Polymer-polymer phase behavior. *Science* **1991**, *251*, 898-905.

(35) Bang, J.; Jeong, U.; Ryu du, Y.; Russell, T. P.; Hawker, C. J. Block copolymer nanolithography: translation of molecular level control to nanoscale patterns. *Adv. Mater.* **2009**, *21*, 4769-4792.

(36) Stoykovich, M. P.; Muller, M.; Kim, S. O.; Solak, H. H.; Edwards, E. W.; de Pablo, J. J.; Nealey, P. F. Directed assembly of block copolymer blends into nonregular device-oriented structures. *Science* **2005**, *308*, 1442-1446.

(37) Darling, S. B. Directing the self-assembly of block copolymers. *Prog. Polym. Sci.* **2007**, *32*, 1152-1204.

(38) Ma, S. Y.; Ahn, H.; Lee, D. H. Catalytically active metal nanomeshes fabricated by block copolymer self-assembly on unidirectionally aligned soft topographic patterns. *ACS Appl. Nano Mater.* **2024**, *7*, 7533-7542.

(39) Jin, C.; Olsen, B. C.; Luber, E. J.; Buriak, J. M. Nanopatterning via solvent vapor annealing of block copolymer thin films. *Chem. Mater.* **2016**, *29*, 176-188.

(40) Xiong, S.; Wan, L.; Ishida, Y.; Chapuis, Y. A.; Craig, G. S.; Ruiz, R.; Nealey, P. F.

Directed self-assembly of triblock copolymer on chemical patterns for sub-10-nm nanofabrication via solvent annealing. *ACS Nano* **2016**, *10*, 7855-7865.

(41) Wan, L.; Ji, S.; Liu, C. C.; Craig, G. S.; Nealey, P. F. Directed self-assembly of solvent-vapor-induced non-bulk block copolymer morphologies on nanopatterned substrates. *Soft Matter* **2016**, *12*, 2914-2922.

(42) Selkirk, A.; Prochukhan, N.; Lundy, R.; Cummins, C.; Gatensby, R.; Kilbride, R.; Parnell, A.; Baez Vasquez, J.; Morris, M.; Mokarian-Tabari, P. Optimization and control of large block copolymer self-assembly via precision solvent vapor annealing. *Macromolecules* **2021**, *54*, 1203-1215.

(43) Kim, K.; Park, S.; Kim, Y.; Bang, J.; Park, C.; Ryu, D. Y. Optimized solvent vapor annealing for long-range perpendicular lamellae in PS-*b*-PMMA films. *Macromolecules* **2016**, *49*, 1722-1730.

(44) Lane, A. P.; Yang, X.; Maher, M. J.; Blachut, G.; Asano, Y.; Someya, Y.; Mallavarapu, A.; Sirard, S. M.; Ellison, C. J.; Willson, C. G. Directed self-assembly and pattern transfer of five nanometer block copolymer lamellae. *ACS Nano* **2017**, *11*, 7656-7665.

(45) Lee, J. E.; Park, J. S.; Yang, G. G.; Choi, H. J.; Lim, J.; Kim, J.; Choi, B.; Ko, M.; Jeon, N.; Kim, J. H.; Jin, H. M. Transient, reusable top-coats for the vertical orientation of high-χ block copolymers for nanopatterning. *ACS Appl. Nano Mater.* **2023**, *6*, 16790-16797.

(46) Nakatani, R.; Takano, H.; Chandra, A.; Yoshimura, Y.; Wang, L.; Suzuki, Y.; Tanaka, Y.; Maeda, R.; Kihara, N.; Minegishi, S.; Miyagi, K.; Kasahara, Y.; Sato, H.; Seino, Y.; Azuma, T.; Yokoyama, H.; Ober, C. K.; Hayakawa, T. Perpendicular orientation control without interfacial treatment of RAFT-synthesized high-χ block copolymer thin films with sub-10 nm features prepared via thermal annealing. *ACS Appl. Mater. Interfaces* **2017**, *9*, 31266-31278.

(47) Pang, Y.; Jin, X.; Huang, G.; Wan, L.; Ji, S. Directed self-assembly of styrene-methyl acrylate block copolymers with sub-7 nm features via thermal annealing. *Macromolecules* **2019**, *52*, 2987-2994.

(48) Shi, L. Y.; Lan, J.; Lee, S.; Cheng, L. C.; Yager, K. G.; Ross, C. A. Vertical lamellae formed by two-step annealing of a rod-coil liquid crystalline block copolymer thin film. *ACS Nano* **2020**, *14*, 4289-4297.

(49) Kim, S. O.; Solak, H. H.; Stoykovich, M. P.; Ferrier, N. J.; De Pablo, J. J.; Nealey, P. F. Epitaxial self-assembly of block copolymers on lithographically defined nanopatterned substrates. *Nature* **2003**, *424*, 411-414.

(50) Jeong, S.-J.; Kim, S. O. Ultralarge-area block copolymer lithography via soft graphoepitaxy. *J. Mater. Chem.* **2011**, *21*, 5856-5859.

(51) Bates, C. M.; Seshimo, T.; Maher, M. J.; Durand, W. J.; Cushen, J. D.; Dean, L. M.; Blachut, G.; Ellison, C. J.; Willson, C. G. Polarity-switching top coats enable orientation of sub-10-nm block copolymer domains. *Science* **2012**, *338*, 775-779.

(52) Park, S.; Lee, D. H.; Xu, J.; Kim, B.; Hong, S. W.; Jeong, U.; Xu, T.; Russell, T. P. Macroscopic 10-terabit-per-square-inch arrays from block copolymers with lateral order. *Science* **2009**, *323*, 1030-1033.

(53) Cushen, J.; Wan, L.; Blachut, G.; Maher, M. J.; Albrecht, T. R.; Ellison, C. J.; Willson, C. G.; Ruiz, R. Double-patterned sidewall directed self-assembly and pattern transfer of sub-10 nm PTMSS-*b*-PMOST. *ACS Appl. Mater. Interfaces* **2015**, *7*, 13476-13483.

(54) Deng, H.; Zhou, J.; Li, X.; Yang, Z. Si containing block copolymers quickly assemble into sub-6 nm domains. *Polym. Chem.* **2022**, *13*, 6098-6107.

(55) Mishra, A. K.; Lee, J.; Kang, S.; Kim, E.; Choi, C.; Kim, J. K. Gallol-based block copolymer with a high Flory–Huggins interaction parameter for next-generation

lithography. *Macromolecules* **2022**, *55*, 10797-10803.

(56) Kwak, J.; Mishra, A. K.; Lee, J.; Lee, K. S.; Choi, C.; Maiti, S.; Kim, M.; Kim, J. K. Fabrication of sub-3 nm feature size based on block copolymer self-assembly for next-generation nanolithography. *Macromolecules* **2017**, *50*, 6813-6818.

(57) Yu, D. M.; Mapas, J. K. D.; Kim, H.; Choi, J.; Ribbe, A. E.; Rzayev, J.; Russell, T. P. Evaluation of the interaction parameter for poly(solketal methacrylate)-*block*-polystyrene copolymers. *Macromolecules* **2018**, *51*, 1031-1040.

(58) Zhang, Z. K.; Ding, S. P.; Xia, D. L.; Xu, J. T. Microphase separation with sub-3 nm microdomains in comb-like poly(n-alkyl acrylate) homopolymers facilitated by charged junction groups between the main chains and side chains. *ACS Macro Lett.* **2023**, *12*, 1005-1011.

(59) Hung, C. C.; Chiu, Y. C.; Wu, H. C.; Lu, C.; Bouilhac, C.; Otsuka, I.; Halila, S.; Borsali, R.; Tung, S. H.; Chen, W. C. Conception of stretchable resistive memory devices based on nanostructure-controlled carbohydrate-block-polyisoprene block copolymers. *Adv. Funct. Mater.* **2017**, *27*, 1606161.

(60) Chuang, T. H.; Chiang, Y. C.; Hsieh, H. C.; Isono, T.; Huang, C. W.; Borsali, R.; Satoh, T.; Chen, W. C. Nanostructure- and orientation-controlled resistive memory behaviors of carbohydrate-*block*-polystyrene with different molecular weights via solvent annealing. *ACS Appl. Mater. Interfaces* **2020**, *12*, 23217-23224.

(61) Bai, X.; Gou, X.; Zhang, J.; Liang, J.; Yang, L.; Wang, S.; Hou, X.; Chen, F. A review of smart superwetting surfaces based on shape-memory micro/nanostructures. *Small* **2023**, *19*, 2206463.

(62) Yue, L.; Yan, B.; Wang, Z. Photonic nanojet of cylindrical metalens assembled by hexagonally arranged nanofibers for breaking the diffraction limit. *Opt. Lett.* **2016**, *41*, 1336-1339.

(63) Wang, Y.; He, C.; Xing, W.; Li, F.; Tong, L.; Chen, Z.; Liao, X.; Steinhart, M. Nanoporous metal membranes with bicontinuous morphology from recyclable block-copolymer templates. *Adv. Mater.* **2010**, *22*, 2068-2072.

(64) Jackson, E. A.; Hillmyer, M. A. Nanoporous membranes derived from block copolymers: from drug delivery to water filtration. *ACS Nano* **2010**, *4*, 3548-3553.

(65) Wang, Y. Nondestructive creation of ordered nanopores by selective swelling of block copolymers: toward homoporous membranes. *Acc. Chem. Res.* **2016**, *49*, 1401-1408.

(66) Hawker, C. J.; Russell, T. P. Block copolymer lithography: merging "bottom-up" with "top-down" processes. *MRS Bull.* **2005**, *30*, 952-966.

(67) Mansky, P.; haikin, P.; Thomas, E. L. Monolayer films of diblock copolymer microdomains for nanolithographic applications. *J. Mater. Sci.* **1995**, *30*, 1987-1992.

(68) Tada, Y.; Yoshida, H.; Ishida, Y.; Hirai, T.; Bosworth, J. K.; Dobisz, E.; Ruiz, R.; Takenaka, M.; Hayakawa, T.; Hasegawa, H. Directed self-assembly of POSS containing block copolymer on lithographically defined chemical template with morphology control by solvent vapor. *Macromolecules* **2011**, *45*, 292-304.

(69) Guarini, K. W.; Black, C. T.; Yeung, S. H. I. Optimization of diblock copolymer thin film self assembly. *Adv. Mater.* **2002**, *14*, 1290-1294.

(70) van Genabeek, B.; de Waal, B. F.; Gosens, M. M.; Pitet, L. M.; Palmans, A. R.; Meijer, E. W. Synthesis and self-assembly of discrete dimethylsiloxane-lactic acid diblock co-oligomers: the dononacontamer and its shorter homologues. *J. Am. Chem. Soc.* **2016**, *138*, 4210-4218.

(71) Otsuka, I.; Tallegas, S.; Sakai, Y.; Rochas, C.; Halila, S.; Fort, S.; Bsiesy, A.; Baron, T.; Borsali, R. Control of 10 nm scale cylinder orientation in self-organized sugar-based block copolymer thin films. *Nanoscale* **2013**, *5*, 2637-2641.

(72) Liao, Y.; Chen, W. C.; Borsali, R. Carbohydrate-based block copolymer thin films: ultrafast nano-organization with 7 nm resolution using microwave energy. *Adv. Mater.* **2017**, *29*, 1701645.

(73) Mumtaz, M.; Merino, D. H.; Solano, E.; Chen, W.-C.; Borsali, R. Simple approach to synthesize carbohydrate-based Janus-type bottlebrush copolymers and their self-assemblies in sub-5 nm features in thin films. *Macromolecules* **2024**, *57*, 9595-9605.

(74) De Greef, T. F.; Smulders, M. M.; Wolffs, M.; Schenning, A. P.; Sijbesma, R. P.; Meijer, E. W. Supramolecular polymerization. *Chem. Rev.* **2009**, *109*, 5687-5754.

(75) Yang, L.; Tan, X.; Wang, Z.; Zhang, X. Supramolecular polymers: historical development, preparation, characterization, and functions. *Chem. Rev.* **2015**, *115*, 7196-7239.

(76) Aida, T.; Meijer, E. W.; Stupp, S. I. Functional supramolecular polymers. *Science* **2012**, *335*, 813-817.

(77) Burattini, S.; Colquhoun, H. M.; Fox, J. D.; Friedmann, D.; Greenland, B. W.; Harris, P. J.; Hayes, W.; Mackay, M. E.; Rowan, S. J. A self-repairing, supramolecular polymer system: healability as a consequence of donor-acceptor π–π stacking interactions. *Chem. Commun.* **2009**, 6717-6719.

(78) Wei, P.; Yan, X.; Huang, F. Supramolecular polymers constructed by orthogonal self-assembly based on host-guest and metal-ligand interactions. *Chem. Soc. Rev.* **2015**, *44*, 815-832.

(79) Campanella, A.; Dohler, D.; Binder, W. H. Self-Healing in supramolecular polymers. *Macromol. Rapid. Commun.* **2018**, *39*, 1700739.

(80) Li, Y.; Hammoud, A.; Bouteiller, L.; Raynal, M. Emergence of homochiral benzene-1,3,5-tricarboxamide helical assemblies and catalysts upon addition of an achiral monomer. *J. Am. Chem. Soc.* **2020**, *142*, 5676-5688.

(81) Li, P.; Jia, Y.; Chen, P. Design and synthesis of new type of macrocyclic architectures used for optoelectronic materials and supramolecular chemistry. *Chem. Eur. J.* **2023**, *29*, e202300300.

(82) Dong, R.; Zhou, Y.; Huang, X.; Zhu, X.; Lu, Y.; Shen, J. Functional supramolecular polymers for biomedical applications. *Adv. Mater.* **2015**, *27*, 498-526.

(83) Berrocal, J. A.; Zha, R. H.; de Waal, B. F. M.; Lugger, J. A. M.; Lutz, M.; Meijer, E. W. Unraveling the driving forces in the self-assembly of monodisperse naphthalenediimide-oligodimethylsiloxane block molecules. *ACS Nano* **2017**, *11*, 3733-3741.

(84) Zha, R. H.; de Waal, B. F.; Lutz, M.; Teunissen, A. J.; Meijer, E. W. End groups of functionalized siloxane oligomers direct block-copolymeric or liquid-crystalline self-assembly behavior. *J. Am. Chem. Soc.* **2016**, *138*, 5693-5698.

(85) Jonkheijm, P.; van der Schoot, P.; Schenning, A. P.; Meijer, E. W. Probing the solvent-assisted nucleation pathway in chemical self-assembly. *Science* **2006**, *313*, 80-83.

(86) Montarnal, D.; Delbosc, N.; Chamignon, C.; Virolleaud, M. A.; Luo, Y.; Hawker, C. J.; Drockenmuller, E.; Bernard, J. Highly ordered nanoporous films from supramolecular diblock copolymers with hydrogen-bonding junctions. *Angew. Chem. Int. Ed.* **2015**, *54*, 11117-11121.

(87) Pitet, L. M.; van Loon, A. H. M.; Kramer, E. J.; Hawker, C. J.; Meijer, E. W. Nanostructured supramolecular block copolymers based on polydimethylsiloxane and polylactide. *ACS Macro Lett.* **2013**, *2*, 1006-1010.

(88) Lee, K. S.; Lee, J.; Kwak, J.; Moon, H. C.; Kim, J. K. Reduction of line edge roughness of polystyrene-*block*-poly(methyl methacrylate) copolymer nanopatterns by Introducing hydrogen bonding at the junction point of two block chains. *ACS Appl. Mater. Interfaces* **2017**, *9*, 31245-31251.

(89) Krieg, E.; Bastings, M. M.; Besenius, P.; Rybtchinski, B. Supramolecular polymers in aqueous media. *Chem. Rev.* **2016**, *116*, 2414-2477.

(90) Simic, V.; Bouteiller, L.; Jalabert, M. Highly cooperative formation of bis-urea based supramolecular polymers. *J. Am. Chem. Soc.* **2003**, *125*, 13148-13154.

(91) Pal, A.; Karthikeyan, S.; Sijbesma, R. P. Coexisting hydrophobic compartments through self-sorting in rod-like micelles of bisurea bolaamphiphiles. *J. Am. Chem. Soc.* **2010**, *132*, 7842-7843.

(92) Véchambre, C.; Callies, X.; Fonteneau, C.; Ducouret, G.; Pensec, S.; Bouteiller, L.; Creton, C.; Chenal, J.-M.; Chazeau, L. Microstructure and self-assembly of supramolecular polymers center-functionalized with strong stickers. *Macromolecules* **2015**, *48*, 8232-8239.

(93) Liu, X.; Stamm, M. Fabrication of highly ordered polymeric nanodot and nanowire arrays templated by supramolecular assembly block copolymer nanoporous thin films. *Nanoscale Res. Lett.* **2009**, *4*, 459-464.

(94) Zheng, J.; Suwardi, A.; Wong, C. J. E.; Loh, X. J.; Li, Z. Halogen bonding regulated functional nanomaterials. *Nanoscale Adv.* **2021**, *3*, 6342-6357.

(95) Chen, Y.; Huang, S.; Wang, T.; Yu, H. Enhanced ordering and efficient photoalignment of nanostructures in block copolymers enabled by halogen bond. *Macromolecules* **2020**, *53*, 1486-1493.

(96) Park, J.; Staiger, A.; Mecking, S.; Winey, K. I. Sub-3-nanometer domain spacings of ultrahigh-χ multiblock copolymers with pendant ionic groups. *ACS Nano* **2021**, *15*, 16738-16747.

(97) Milani, R.; Houbenov, N.; Fernandez-Palacio, F.; Cavallo, G.; Luzio, A.; Haataja, J.; Giancane, G.; Saccone, M.; Priimagi, A.; Metrangolo, P.; Ikkala, O. Hierarchical self-assembly of halogen-bonded block copolymer complexes into upright cylindrical

domains. *Chem* **2017**, *2*, 417-426.

(98) Schädler, V.; Wiesner, U. Salt-controlled lamellar spacing in ionically end-capped symmetric diblock copolymers. *Macromolecules* **1997**, *30*, 6698-6701.

(99) Schöps, M.; Leist, H.; DuChesne, A.; Wiesner, U. Salt-induced switching of microdomain morphology of ionically functionalized diblock copolymers. *Macromolecules* **1999**, *32*, 2806-2809.

(100) Luo, Y.; Montarnal, D.; Treat, N. J.; Hustad, P. D.; Christianson, M. D.; Kramer, E. J.; Fredrickson, G. H.; Hawker, C. J. Enhanced block copolymer phase separation using click chemistry and ionic junctions. *ACS Macro Lett.* **2015**, *4*, 1332-1336.

(101) Ji, E.; Pellerin, V.; Rubatat, L.; Grelet, E.; Bousquet, A.; Billon, L. Self-assembly of ionizable "clicked" P3HT-*b*-PMMA copolymers: ionic bonding group/counterion effects on morphology. *Macromolecules* **2016**, *50*, 235-243.

(102) Cho, S. M.; Song, G.; Park, C.; Lee, Y.; Kang, H. S.; Lee, W.; Park, S.; Huh, J.; Ryu, D. Y.; Park, C. Surface functionalized nanostructures via position registered supramolecular polymer assembly. *Nanoscale* **2018**, *10*, 6333-6342.

Chapter II: Synthesis of a library of co-assembling polymers for nanopatterning

2.1 Introduction

The International Technology Roadmap for Semiconductors (ITRS) has identified directed self-assembly (DSA) of block copolymers (BCPs) as a promising technique for next-generation nanopatterning especially as feature sizes in semiconductor manufacturing continue to shrink beyond the limits of traditional photolithography (see Chapter I) [1-6]. Parallel to BCPs, supramolecular polymers have obtained increasing attention due to their abilities of assemblies into lamellar and cylindrical morphologies[7-9]. Our group has proved that Janus cylinders less than 10 nm diameter can be readily prepared in solution via supramolecular interaction using two complementary _4_8_ and _8_4_polymer[9], as presented in Figure 2.1.1. In this chapter, the idea is to synthesize a library of _4_8_ and _8_4_polymers for the investigation of surface nanopatterning. As shown in Figure 2.1.2, two kinds of polymers (_4_8_polymer and _8_4_polymer) with complementary hydrogen bonding co-assemble together to form Janus cylinder in solution via hydrogen bonds and hydrophobic interactions, instead of forming other nano-objects via non-Janus co-assembly or self-sorting due to the mismatched hydrogen bonding or steric hindrance. In light of the promising results, our objective is to transfer these obtained Janus nano-cylinders onto silicon substrate for a further investigation in nanopatterning. After the polymers are transferred, one component in the polymers can possibly be removed by dissolution or etching according to different uses of polymers (details are explained in section 2.4 Polymerizations).

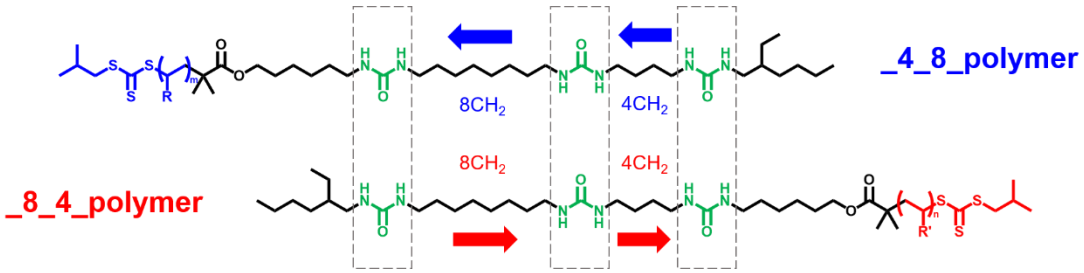

Figure 2.1.1. Chemical structures of _4_8_ and _8_4_polymer with complementary hydrogen bonds.

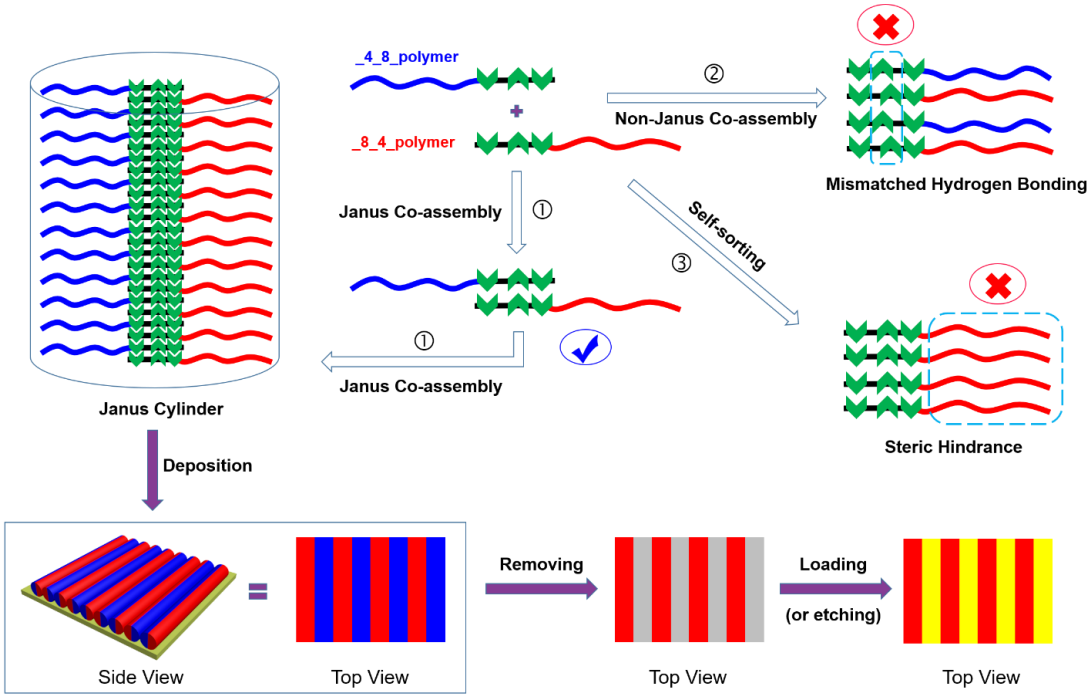

Figure 2.1.2. Illustration of the process of co-assembly and nanopatterning.

Compared to BCPs, using supramolecular polymers to do nanopatterning has significant advantages. Firstly, supramolecular polymers are (co)assembled with interactions such as hydrogen bonding, ionic bond, and π–π stacking. This indicates that supramolecular polymers can readily achieve small feature sizes with polymers of low degrees of polymerization (*N*), via the intermolecular interactions. In contrast, for conventional BCPs, it is only limited to certain types of high χ BCPs to achieve sub-10 nm feature sizes. Secondly, supramolecular polymers co-assembly reduce dramatically the number of syntheses necessary to obtain the corresponding polymers. For examples,

using 10 _4_8_polymers and 10 _8_4_polymers to co-assemble we can obtain 100 kinds of supramolecular polymers, but with BCPs' strategy, we have to do 100 polymerizations to achieve the same effect. In this way, supramolecular polymers co-assembly can establish conveniently a promising library for the investigation of nanopatterning.

In this chapter, a series of hydrogen bonding based polymers (_8_4_polymers and _4_8_polymers) are synthesized by means of RAFT polymerization for the characterizations in solution (at IMMM, Le Mans) and on surface (at ICMN, Orléans) by our collaborators, in the framework of the ANR project JASUR. The design of these polymers is described in section **2.4 Polymerizations**. To obtain these polymers, the syntheses of the functional _8_4_ and _4_8_RAFT agents are optimized in **2.2** and **2.3**.

2.2 Optimization of _8_4_ RAFT agent synthesis

The synthesis of _8_4_ RAFT agent (compound **10** in Figure 2.2.2.) was previously reported by Han et al. (Figure 2.2.1 and 2.2.2) [9]. For the synthesis of NH_3Cl-CTA (intermediate **5**), as shown in Figure 2.2.1, it is based on a general trithiocarbonate-type RAFT agent, **1**. This trithiocarbonate **1** was transformed into acyl chloride **3**, and then reacted with the protected amino alcohol **2**, forming the Boc-protected trithiocarbonate **4**. Finally, the Boc group can be deprotected by hydrochloric acid to form NH_3Cl-CTA (**5**).

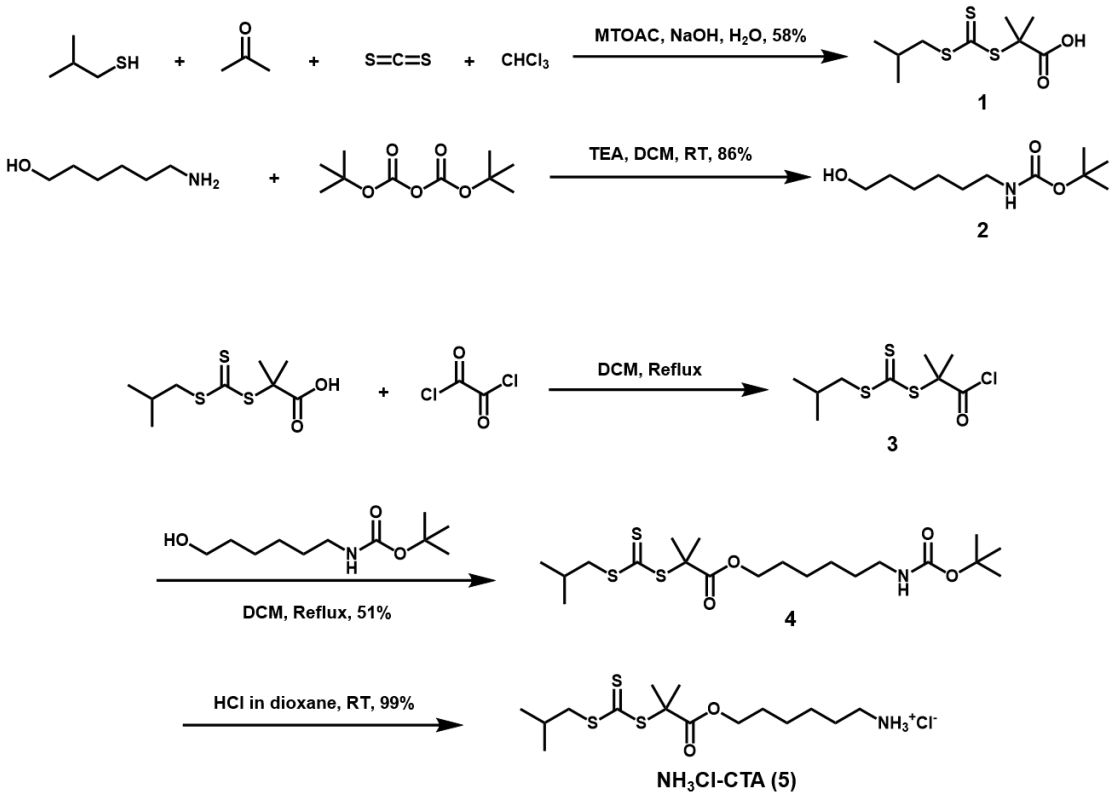

Figure 2.2.1. Synthetic route of NH_3Cl-CTA (**5**), according to Han et al. [9]

The protocole of Han et al. was used for the synthesis of intermediate **1**, except that an additional purification step by a silica column was performed. The treatments of intermediate **2**, **3**, **4,** and **5** follow the same procedures according to Han et al. [9] The yields of these reactions in Figure 2.2.1 were a little lower but comparable to those reported.

The synthesis of intermediate **9** is performed via two steps by successive reactions between isocyanates and amines as explained in Figure 2.2.2. In this process, $8CH_2$ and $4CH_2$ spacers were successfully embedded between ureas functions to form intermediate **9**, followed by its coupling reaction with NH_3Cl-CTA (**5**) to form _8_4_CTA (**10**).

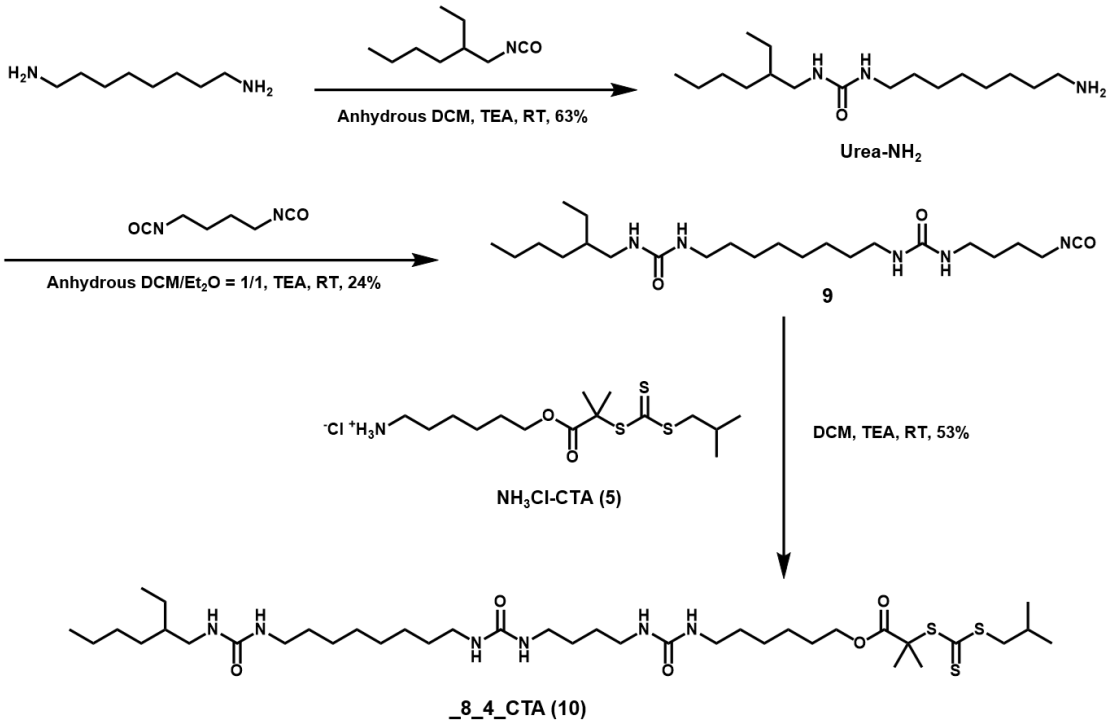

Figure 2.2.2. Synthetic route of _8_4_CTA, according to Han et al. [9]

Sadly, obtaining Urea-NH_2 did not succeed when following the reported procedure. In the initial scheme (Figure 2.2.2), 10 equivalents of 1,8-diaminooctane were added to react with 2-ethylhexyl isocyanate. This caused large consumption of 1,8-diaminooctane and more importantly, the product (Urea-NH_2) was not easy to purify due to the existence of large excess of 1,8-diaminooctane when performing a flash column. Moreover, the yield of the next reaction to obtain intermediate **9** was only 24%, which was too low to make a larger scale preparation for the use in the later polymerization. Therefore, we tested a new synthetic route (Figure 2.2.3) to synthesize _8_4_CTA.

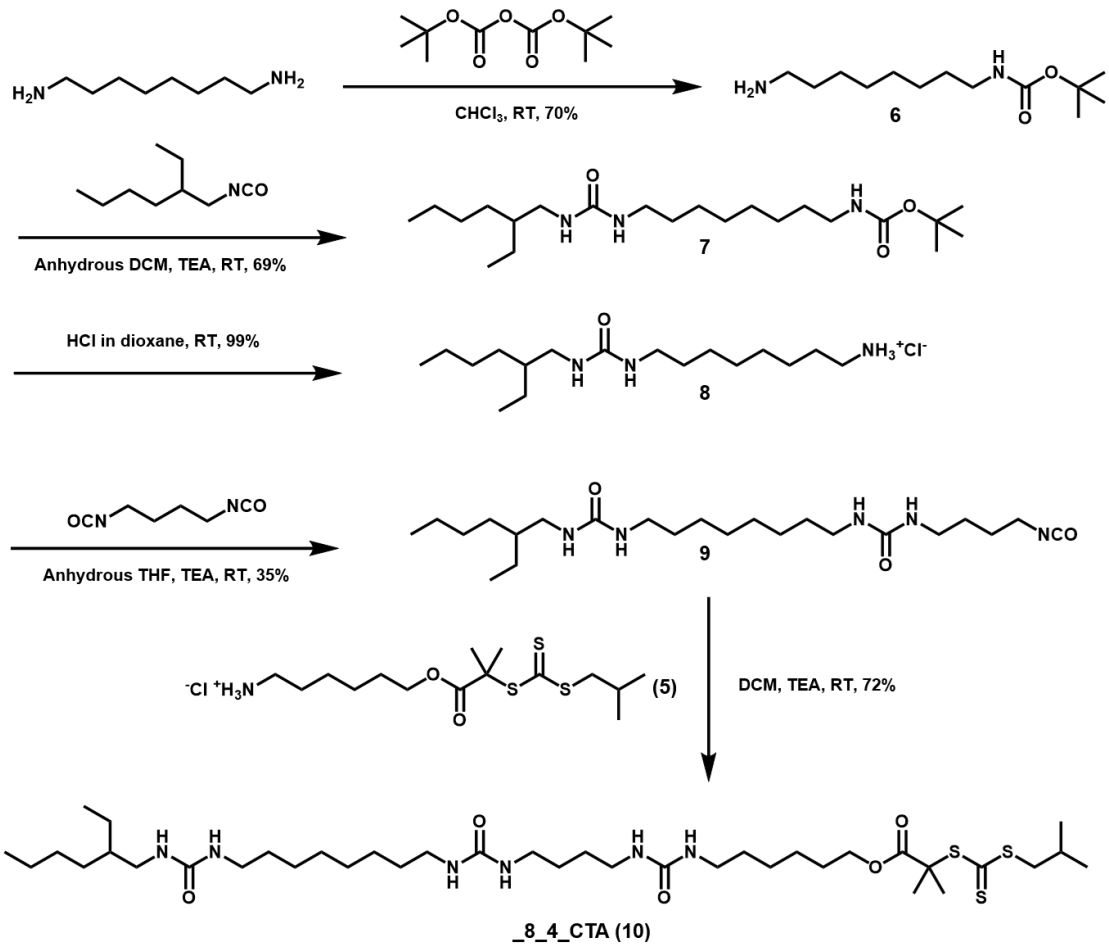

Figure 2.2.3. Adapted synthesis route of _8_4_CTA (**10**).

2.2.1 Protecting group strategy for intermediate 8

As shown in Figure 2.2.3, 1,8-diaminooctane was mono-protected by Boc group, followed by a reaction with 2-ethylhexyl isocyanate to form intermediate **7**. When the Boc group was deprotected (nearly 100% yield), intermediate **8** was obtained. Finally, the combined yield for the 3 steps (48%) is slightly lower than the yield of the previous route (63%), but this new route is easier to reproduce and only 1 equivalent of amine **6** is used instead of 10 equivalents used in the former procedure.

2.2.2 Optimization of intermediate 9

In this reaction, firstly intermediate **8** (instead of Urea-NH_2) and TEA were dissolved in anhydrous THF (a better solvent to dissolve intermediate **8** than DCM), and then slowly added into a flask equipped with anhydrous THF, 1,4-

diisocyanatobutane and a magnetic stirring bar. The reaction was monitored by ^{1}H NMR until the disappearance of the -C**H**$_2$NH$_2$ peak at 2.67 ppm. Afterwards, the dispersion was filtered to remove triethylamine salt and the solution was concentrated by a vacuum evaporator at 20 °C. Then excess pentane was poured into the concentrated solution to precipitate. The forming white solid was filtered, and dried. Although the initial batches (intermediate **9** (batch 1 and 2)) appeared pure by NMR (Figure 2.2.2.1), the polymerizations tests (see below section 2.2.4, presence of a high molar mass shoulder in SEC) indicated it was contaminated by a small quantity of unreacted 1,4-diisocyanatobutane leading ultimately to bifunctional RAFT agents, when not removed before the next synthesis step. Therefore, in the subsequent synthesis of intermediate **9** (batch 4 to 7), the final solid was thoroughly washed with excess pentane before drying. The yield of this step has been improved to 35%.

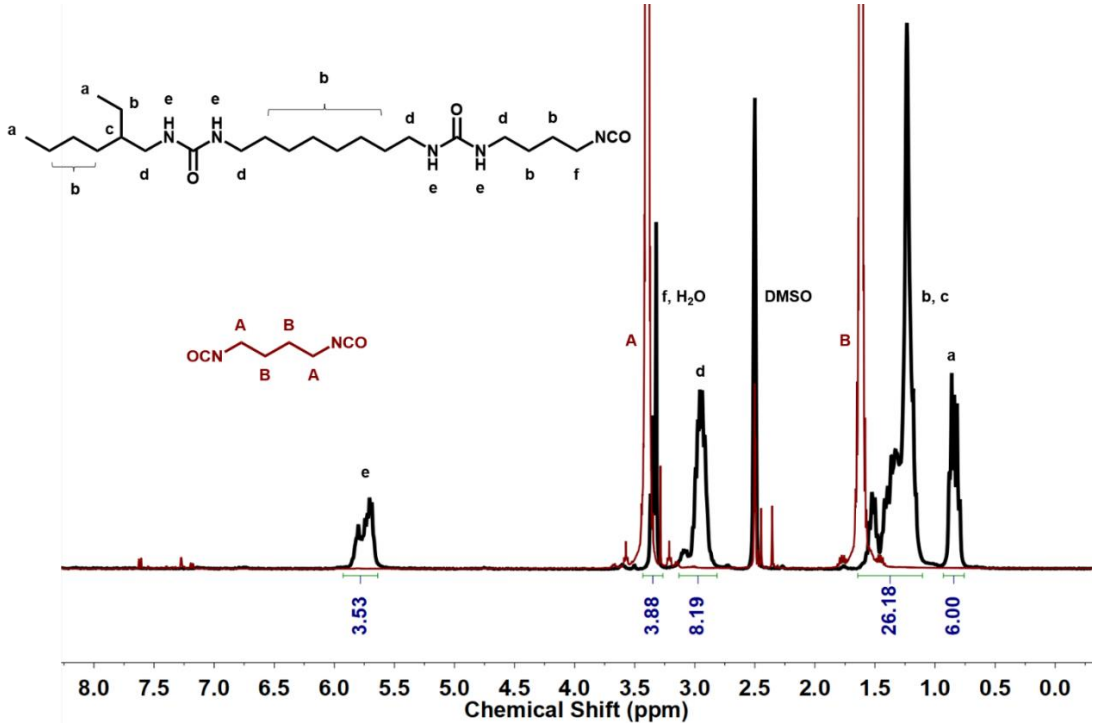

Figure 2.2.2.1 Comparison of ^{1}H NMR between intermediate **9** (batch 2) and 1,4-diisocyanatobutane (in DMSO-d$_6$).

2.2.3 Synthesis of _8_4_CTA (10)

According to the synthetic route of Han et al[9]. (Figure 2.2.2), intermediate **9** and excess intermediate **5** were added into a flask equipped with anhydrous DCM and a magnetic stirring bar. TEA in DCM was then injected. The reaction was stirred overnight at room temperature. The solution was concentrated to form a gel and then acetone was poured into the flask to precipitate the product. The formed yellow solid was washed by excess water and acetone. Afterwards, the yellow product was dried under vacuum. The first two batches (_8_4_CTA-B1 and _8_4_CTA-B2) were synthesized by using a non-washed intermediate **9**, but the following batches _8_4_CTA-B4, _8_4_CTA-B5, _8_4_CTA-B6 and _8_4_CTA-B7 were synthesized from thoroughly washed intermediate **9**.

The obtained _8_4_CTA batches were analyzed by ^{1}H NMR. As shown in Figure 2.2.3.1(a), there were some obvious impurities in 7.0 - 7.5 ppm in the first batch (_8_4_CTA-B1). Water and acetone washing for the crude product were introduced in the following batches. As indicated in Figure 2.2.3.1 (b-d), the different batches of _8_4_CTA showed that the impurities in 7.0 - 7.5 ppm were successfully removed. The yields for _8_4_CTA-B2, _8_4_CTA-B4 and _8_4_CTA-B6 were 84%, 55% and 72%, respectively. These three batches of _8_4_CTA were tested in the polymerizations.

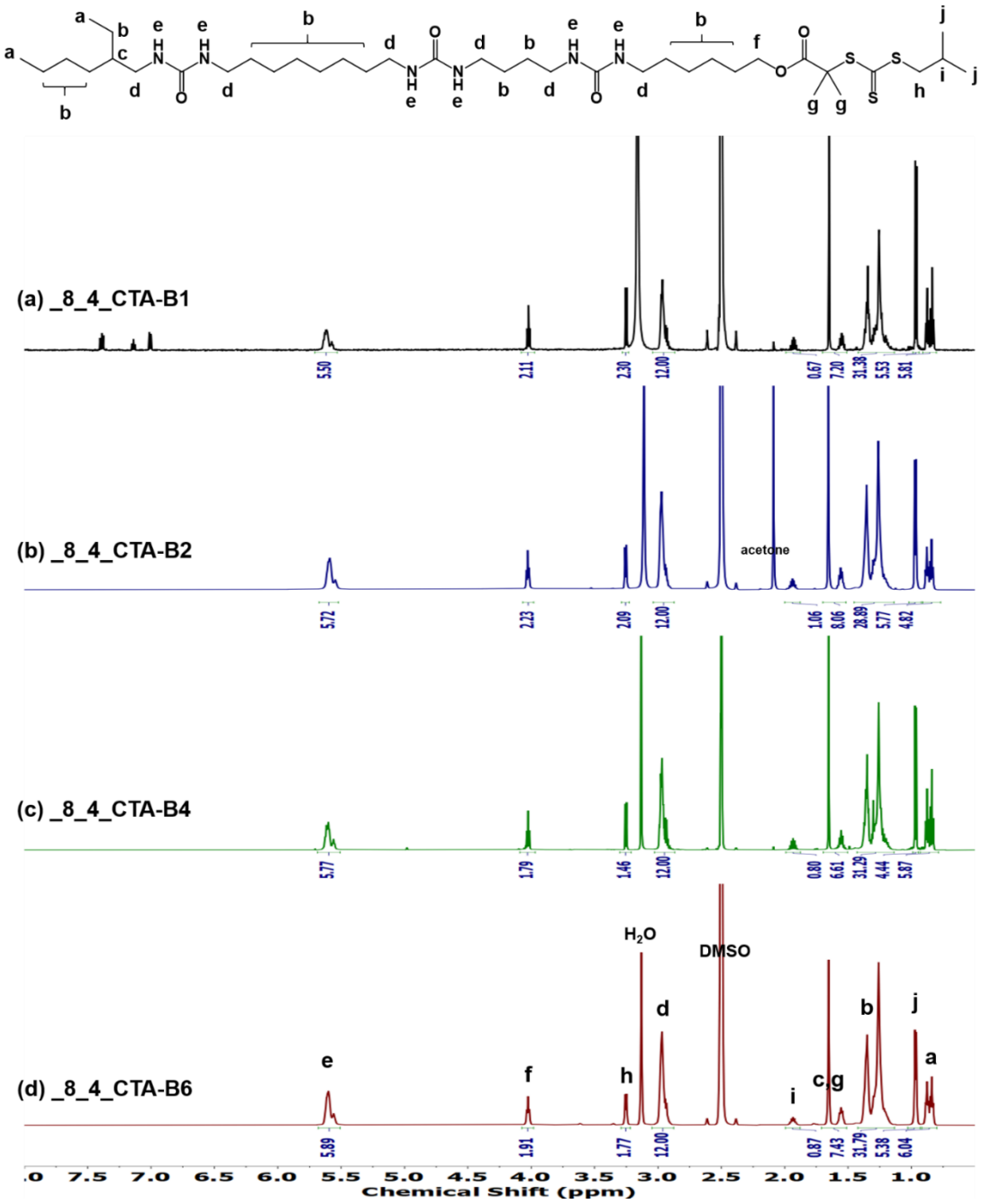

Figure 2.2.3.1 ^{1}H NMR of different batches of _8_4_CTA (in DMSO-d_6, 65 ℃).

2.2.4 Polymerization tests with _8_4_CTA (10)

Firstly, *tert*-butyl acrylate was chosen to check the purity of _8_4_CTA-B2. The polymerization of *tert*-butyl acrylate was performed at 70 °C in DMSO, with AIBN as initiator, in a round-bottom flask, which was degassed. After checking the monomer conversion (68%, corresponding to 140 min of polymerization), the polymerization was stopped by putting the flask into an ice-water bath. When the temperature reached room temperature, a solid precipitated from the solution. Then cold MeOH/H_2O (v/v = 1/1) was poured into the flask and afterwards the solid was filtered and washed by additional cold MeOH/H_2O. The polymer (_8_4_P*t*BA_{25}) was dried and then analyzed by ^{1}H NMR (Figure 2.2.4.1) and SEC (Figure 2.2.4.2). The number "25" corresponds to the number-average degree of polymerization, DP_n, determined by ^{1}H NMR using signals of b, c, g, i, k, k', m and m' (DP_n = (317.10 - 40) / 11 = 25).

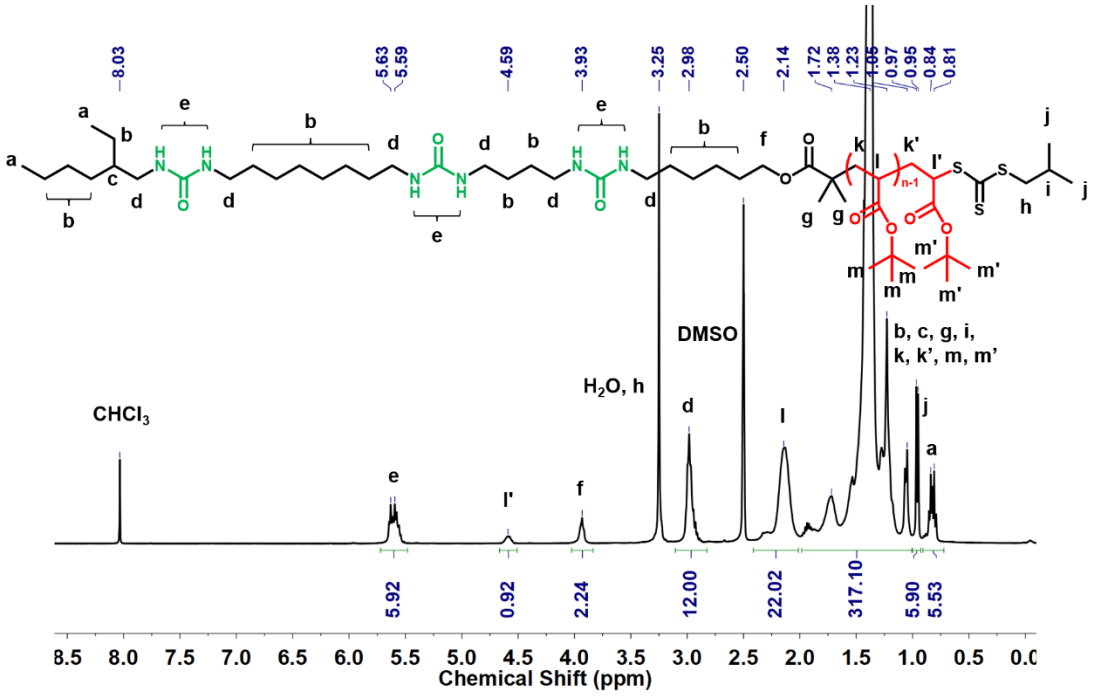

Figure 2.2.4.1. ^{1}H NMR of _8_4_P*t*BA_{25} from _8_4_CTA-B2 (in DMSO-d_6/$CDCl_3$, v/v = 1/1).

The ^{1}H NMR of _8_4_P*t*BA$_{25}$ did not contain obvious impurities, but strangely, the polymer showed a shoulder with a high molecular weight when it was analyzed by SEC. The shoulder hinted that there were side reactions occurring when the polymerization was going on.

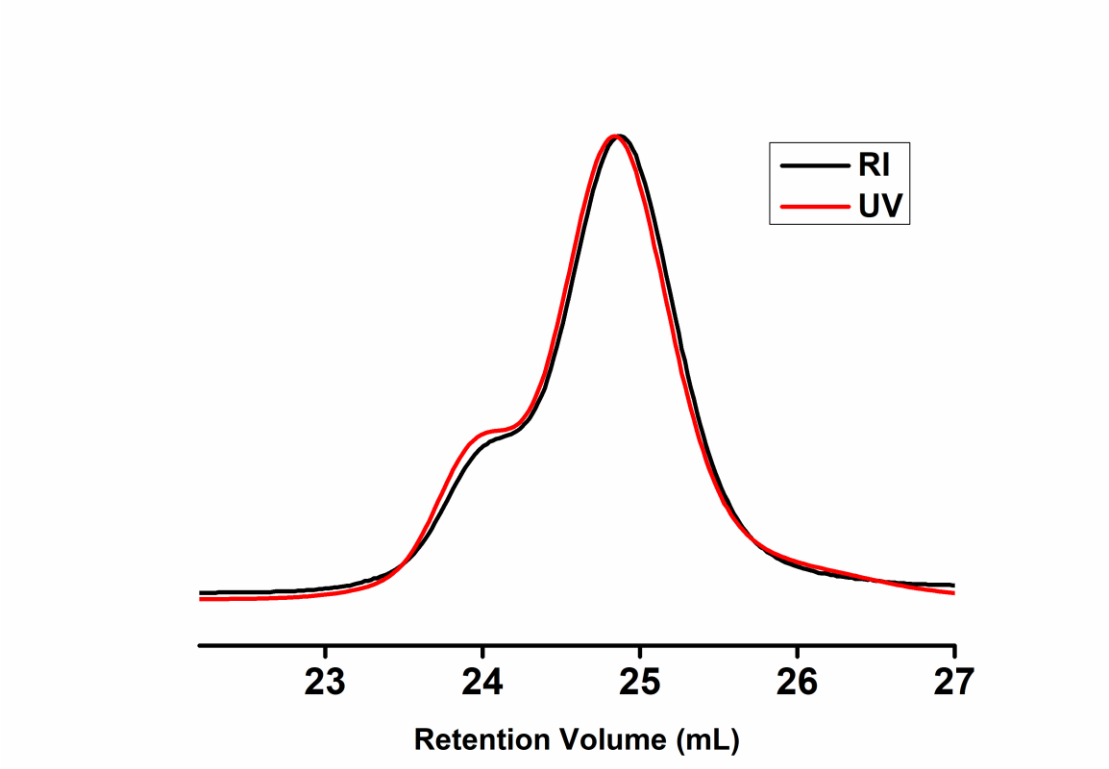

Figure 2.2.4.2. SEC figures of _8_4_P*t*BA$_{25}$ from _8_4_CTA-B2 (in THF). UV detection at 309 nm.

The fact that the shoulder's molecular weight is nearly 2 times that of the main peak for _8_4_P*t*BA$_{25}$, indicates that this shoulder may be caused by a di-trithiocarbonate. In the synthesis of _8_4_CTA-B2, since the precipitated intermediate **9** was not thoroughly washed by pentane, it is possible that the excess 1,4-diisocyanatobutane was not fully removed and then reacted with NH_3Cl-CTA (**5**) to form a di-trithiocarbonate (Figure 2.2.4.3). Since this impurity did not have the distinguished peaks compared to _8_4_CTA (**10**), it was hard to detect by ^{1}H NMR.

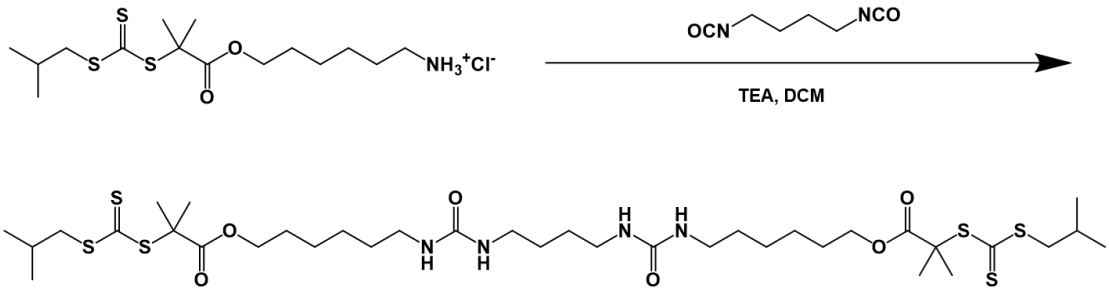

Figure 2.2.4.3. Scheme of the formation of the di-trithiocarbonate supposed to form due to excess diisocyanate remaining in compound **9**.

When realizing the shoulder in the SEC figure may be due to the formation of di-trithiocarbonate, intermediate **9** was washed by excess pentane to avoid the formation of di-trithiocarbonate (see section **2.2.2 Optimization of intermediate 9**). Following this treatment, a new batch of RAFT agent, 8_4_CTA-B4, was synthesized and thus used to perform the polymerization to verify this hypothesis.

Keeping the same polymerization conditions as before, i.e. the same ratio between monomer, _8_4_CTA, and initiator, solvent (DMSO), temperature (70°C), and the weights and volume for all reactants and the solvent, the polymerization was performed using the new batch, _8_4_CTA-B4. The polymerization was kinetically monitored for the monomer conversion and stopped when the monomer conversion was around 70% (corresponding to 140 min). Then, the polymer was precipitated and then dried. As shown in Figure 2.2.4.4, no shoulder appears in _8_4_P*t*BA$_{32}$ when using _8_4_CTA-B4. This indicated that the di-trithiocarbonate was successfully avoided after pentane washing.

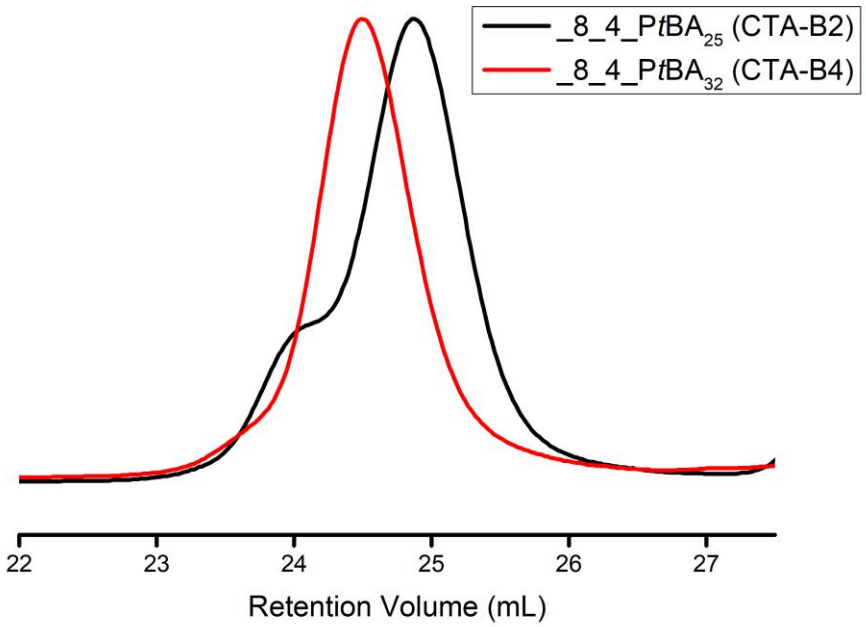

Figure 2.2.4.4. SEC figures (RI signal, in THF) of _8_4_P*t*BA$_{25}$ (black, from_8_4_CTA-B2) and _8_4_P*t*BA$_{32}$ (red, from _8_4_CTA-B4).

Therefore, it seems that the washing step for intermediate **9** removes the impurity responsible for the formation of the shoulder in the polymerization. However, it is difficult to detect the impurity from the NMR data for both intermediate **9** or for _8_4_CTA, which means that each new batch of transfer agent has to be tested in a polymerization to ensure its purity. In an alternative attempt to check the purity of the RAFT agents, we compared their DSC thermograms (Figure 2.2.4.5), but unfortunately, no significant difference could be detected.

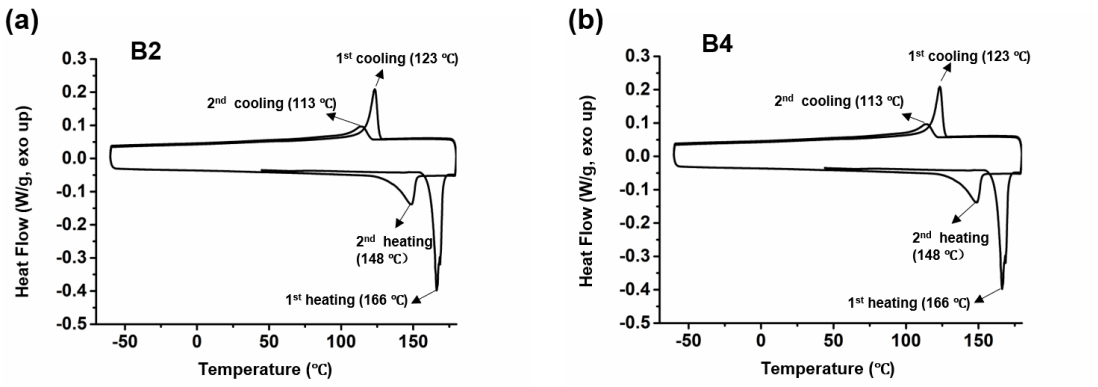

Figure 2.2.4.5. DSC of _8_4_CTA-B2 (a) and _8_4_CTA-B4 (b) (10°C/min).

In the following polymerizations (part 2.4), _8_4_CTA-B4, _8_4_CTA-B5, _8_4_CTA-B6 and _8_4_CTA-B7 were used and lead to no shoulder problems.

2.3 Optimization of _4_8_ RAFT agent synthesis

2.3.1 Synthesis of _4_8_RAFT agent with isocyanate-free route

The previously reported synthesis of _4_8_CTA is depicted in Figure 2.3.1.1. **Urea-4C-NH_2** was obtained after the mono-reaction of 1,4-diaminobutane (10 equivalents) with a good yield. After reacting with 1,8-diisocyanatooctane (2 equivalents), the product (2Urea-NCO) precipitated and was washed by a mixture of DCM and Et_2O (v/v = 1/1). Finally, when **2Urea-NCO** reacted with **NH_3Cl-CTA (5)**, precipitates formed and were then washed with DCM to form **_4_8_CTA (18)** in 55% yield.

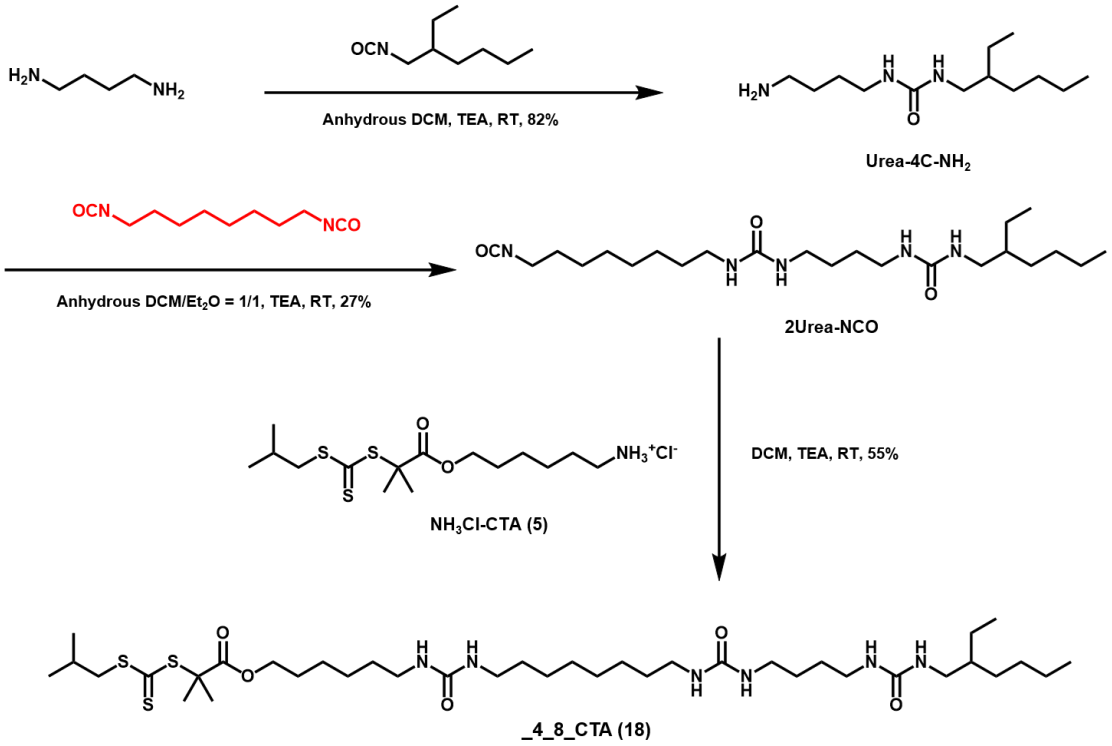

Figure 2.3.1.1. Synthetic route of _4_8_CTA (**18**), according to Han et al. [9]

Unfortunately, 1,8-diisocyanatooctane was not commercially available anymore, which meant that 2Urea-NCO and _4_8_CTA were not accessible. Considering this situation, a new synthetic route of _4_8_CTA was designed.

Instead of using highly toxic phosgene-related reagents to obtain urea, David Siefker (postdoc in the group) noticed that the reaction between amine and carbamate also provided a powerful tool to achieve urea[10-15]. Therefore, a novel synthetic route of _4_8_CTA was designed and performed as displayed in Figure 2.3.1.2. Based on NH_3Cl-CTA (**5**) that we used previously, 4-nitrophenyl chloroformate was introduced to form carbamate **11**. Then, carbamate **11** reacted with a mono-protected amine **6** to obtain intermediate **12**.

After deprotection of the Boc group, intermediate **13** was formed. At the same time, another synthetic route to synthesize intermediate **17** was designed. Starting from 1,4-diaminobutane, Boc_2O and isocyanate were introduced successively to form intermediate **15**. After Boc deprotection and the introduction of 4-nitrophenyl chloroformate, intermediate **17** was obtained. Finally, through the coupling reaction of intermediate **13** with intermediate **17**, _4_8_CTA (**18**) was obtained with a 72% yield.

It is worth noting that _4_8_CTA could be achieved with a one-pot reaction of 2 amines and 4-nitrophenyl chloroformate (or isopropenyl chloroformate), but necessarily, the symmetrical ureas would form more or less at the same time, giving the difficulty to purify the impurities because the product and by-products all contain 3 ureas, and the symmetrical ureas with 2 trithiocarbonates in both ends would affect the polymerization. Given this, the final step to obtain _4_8_CTA was designed with a coupling between an amine (or ammonium (**13**)) and an isolated carbamate (**17**).

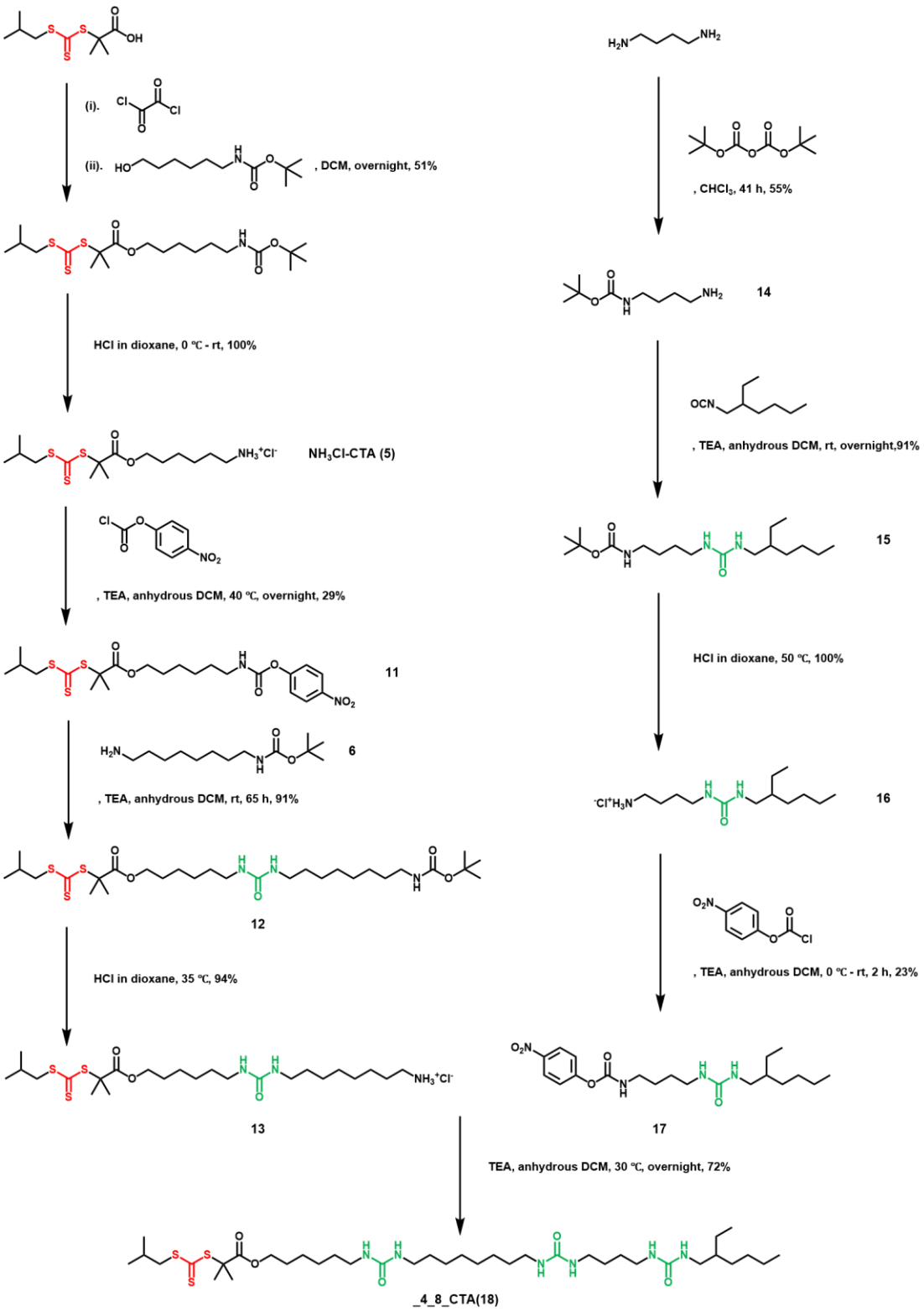

Figure 2.3.1.2. New synthetic route of _4_8_CTA **(18)**.

2.3.2 Polymerization test with _4_8_CTA (18) using *tert*-butyl acrylate

Similarly to _8_4_CTA, the synthesized _4_8_CTA was scrutinized with a polymerization of *tert*-butyl acrylate to check the purity. By keeping the same condition as for _8_4_CTA (0.6 M, DMSO and 70°C), the polymerization was performed and the polymer was precipitated from the mixture of water and methanol. From the ^{1}H NMR, except solvents, all corresponding hydrogen peaks were found. By choosing peak d as the reference and using the integrating signals of b, c, g, i, k, k', m and m', the number-average degree of polymerization could be calculated as 48.

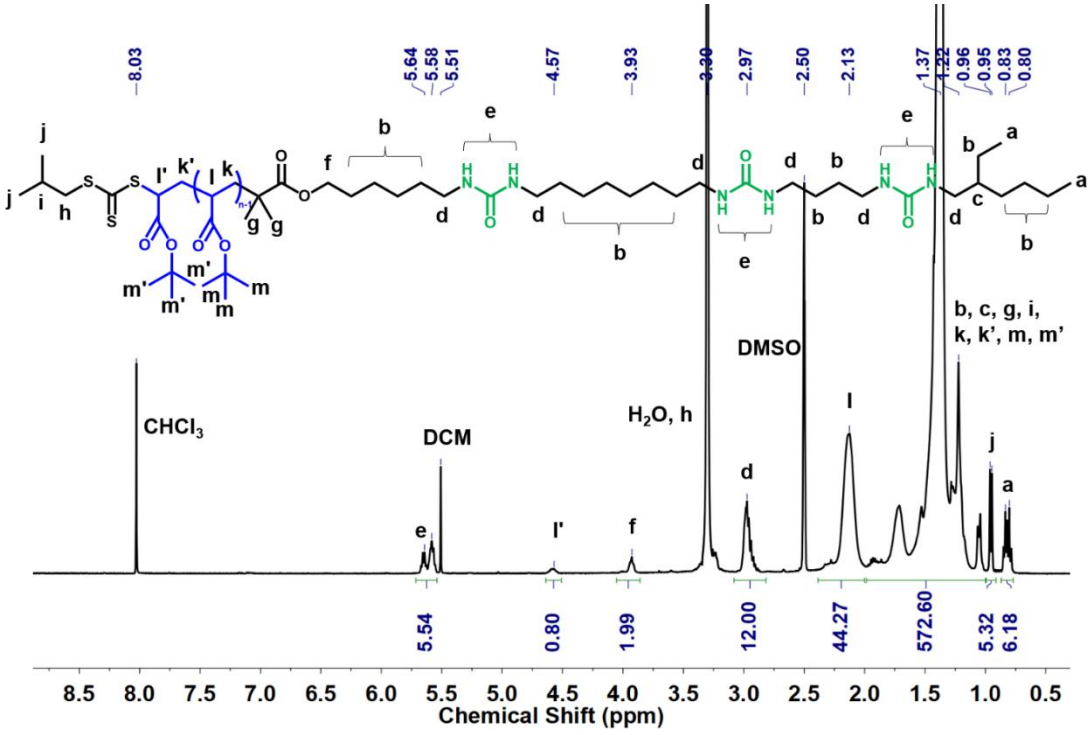

Figure 2.3.2.1. ^{1}H NMR of _4_8_P*t*BA$_{48}$ from _4_8_CTA-B1 (in DMSO-d$_6$/CDCl$_3$, v/v = 1/1).

The SEC curves showed in Figure 2.3.2.2 was monomodal with a low dispersity of 1.11. Furthermore, the number-average molar mass, M_n, from ^{1}H NMR (6.9 kg/mol) and SEC (7.0 kg/mol) corresponded well to the expected value (7.7 kg/mol).

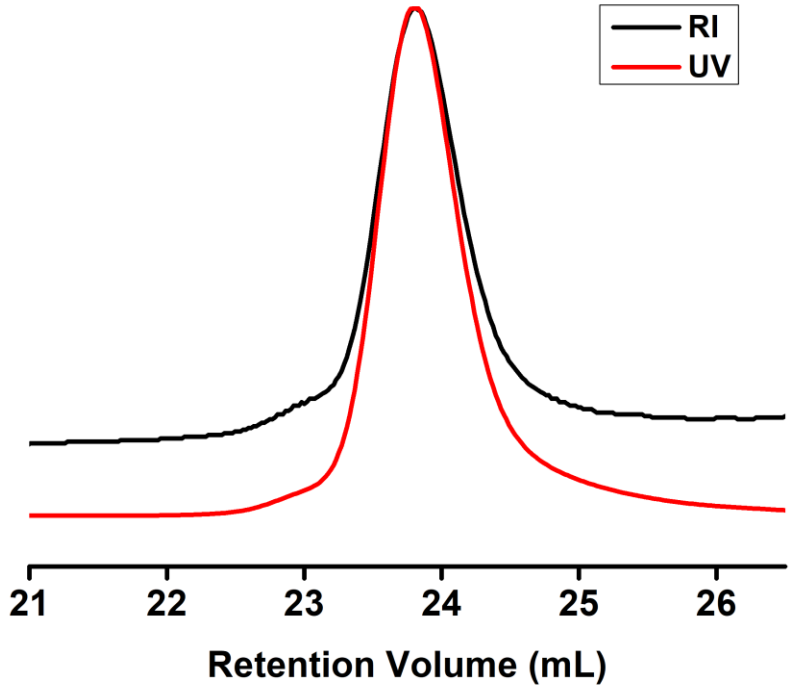

Figure 2.3.2.2. SEC figures (in THF) of _4_8_P*t*BA$_{48}$ from_4_8_CTA-B1. UV detection at 309 nm.

2.4 Polymerizations

As explained before, _4_8_polymer co-assembles with _8_4_polymer due to complementary hydrogen bonding to form Janus nanorods in solution. The objective is to transfer the Janus nanorods onto a silicon substrate to create nanopatterns with various structure and properties. Therefore, a library of _4_8_polymers and _8_4_polymers has been synthesized. The main difficulty of these polymerizations is the low solubility of the trisurea-CTAs which impose to perform the polymerizations in a strongly polar solvent (such as DMSO or DMF) and at high temperature (at least 65°C).

2.4.1 Polymerization of acrylamides using _8_4_CTA and _4_8_CTA

Acrylamides used here for polymerizations are *N,N*-dimethylacrylamide (DMAc) and *N*-acryloylmorpholine (NAM) as their corresponding _4_8_ and _8_4_polymers (Figure 2.4.1.1) have been proved as powerful and efficient compounds to form nanorods in solution[9]. The use of these hydrophilic polyacrylamides not only takes fully advantage of forming readily abundant and long nanorods in solution, but also help to understand the assembly behavior of complementary polymers when they co-assemble with other polymers.

The polymerizations of *N,N*-dimethylacrylamide and *N*-acryloylmorpholine were performed in similar ways. Herein, the synthesis of _8_4_PDMAc with a targeted DP_n of 120 was chosen as an example and discussed.

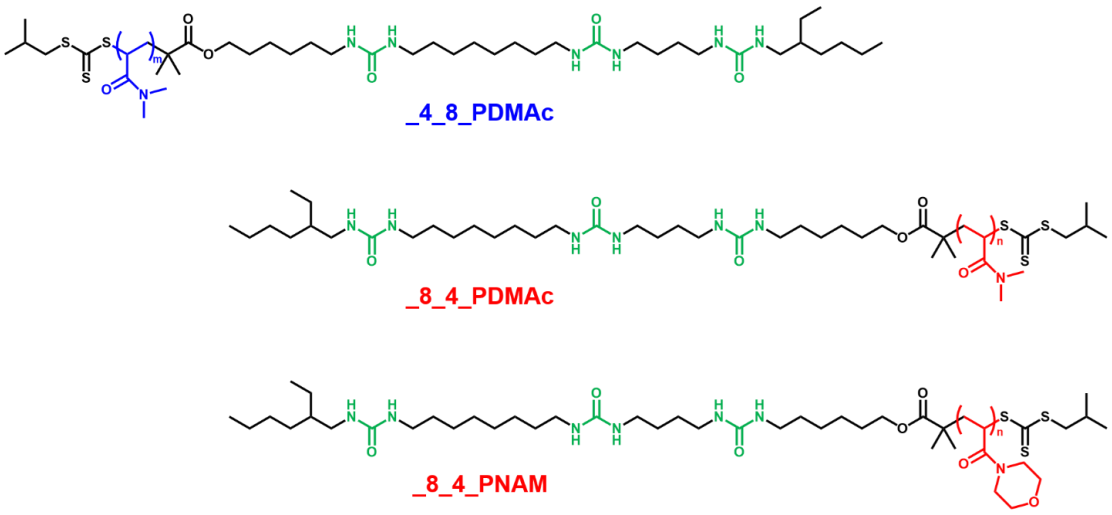

Figure 2.4.1.1. Chemical structures of _4_8_ and _8_4_polyacrylamides.

The polymerization of *N,N*-dimethylacrylamide was performed at 65 °C using DMSO as solvent, and then the polymer was purified by dialysis in water. Different *DP*s were targeted following the same procedure (see Table 2.4.1.1).

The polymerization of *N,N*-dimethylacrylamide (at a concentration of 0.2 M) was monitored by ^{1}H NMR so as to stop at 70% conversion for a targeted DP_n (120). As showed in Figure 2.4.1.2a, the near-linear plot demonstrated that the concentration of radical is rather constant during polymerization. Meanwhile, the number-average molar mass (M_n), called here *molecular weight* for reasons of simplicity, increases linearly with monomer conversion, as shown in Figure 2.4.1.2b. The SECs in figure 2.4.1.2c indicated the narrow distribution for _8_4_PDMAc$_{137}$. Finally, the polymer was purified by dialysis and then analyzed by SEC (Figure 2.4.1.2d), showing M_n = 13600 g/mol with a dispersity of 1.12.

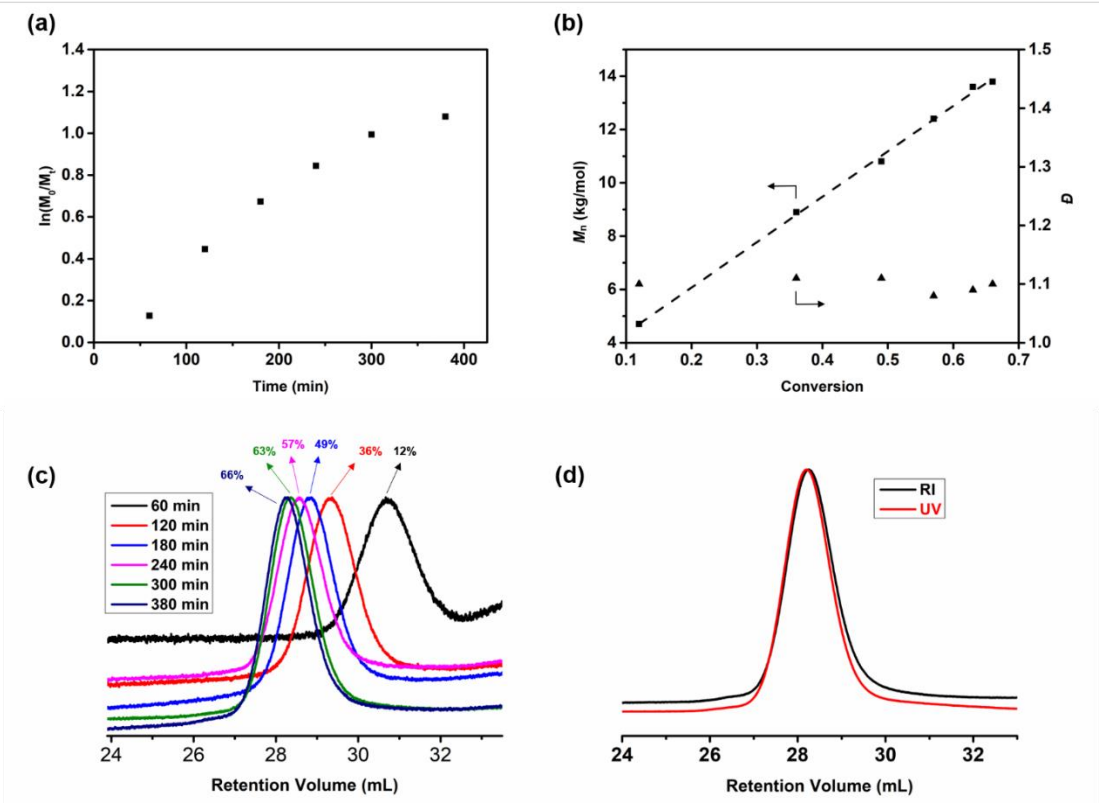

Figure 2.4.1.2. Polymerization of _8_4_PDMAc$_{137}$ using _8_4_CTA-B6 in DMSO. (a) Semilogarithmic kinetic plot. (b) Evolution of number-average molecular weight (M_n, calibrated by PMMA, dashed line was fitted with a linear regression) and dispersity ($Đ$) with conversion. (c) SEC traces evolution with time (RI detection). (d) SEC traces for purified _8_4_PDMAc$_{137}$. UV detection at 309 nm. Reaction conditions: $[M]_0/[\_8\_4\_CTA]_0/[AIBN]_0$ = 172/1/0.1, in DMSO and at 65°C.

As shown in Figure 2.4.1.3, _8_4_PDMAc$_{137}$ indicated its good purity from ^{1}H NMR. The DP_n could be calculated from the integration of peaks of b, c, g, j, k, and k' compared to the peak a (the protons of the RAFT agent count for 45 and must be subtracted from the integration).

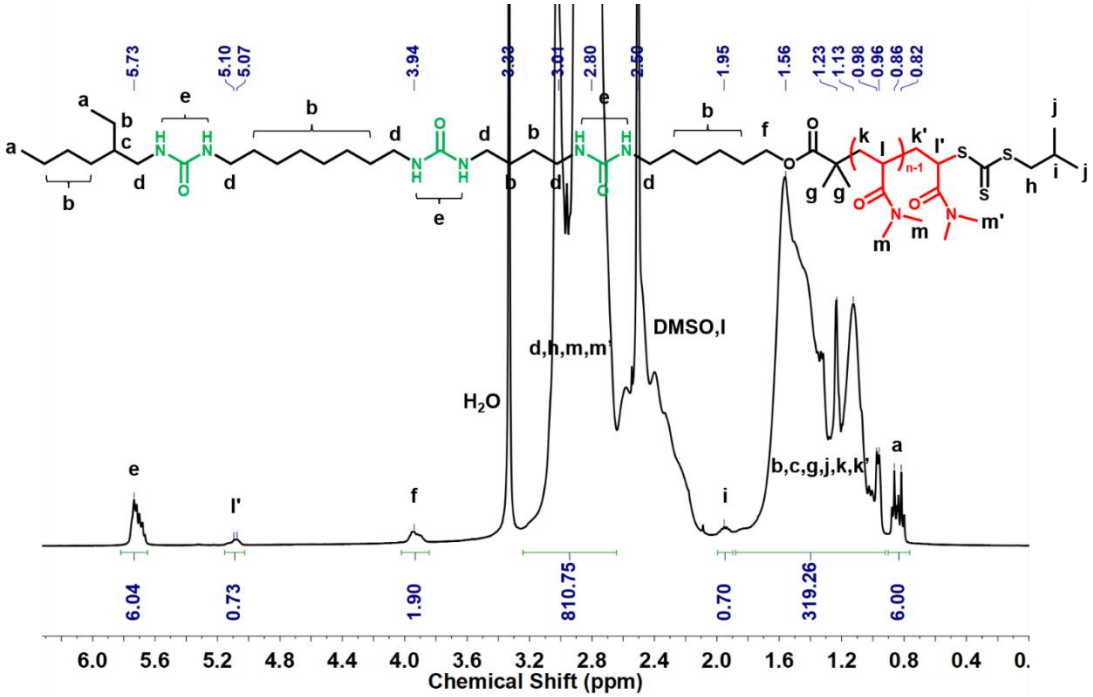

Figure 2.4.1.3. ^{1}H NMR of _8_4_PDMAc$_{137}$ (in DMSO-d$_6$).

_4_8_PDMAc$_{150}$, _4_8_PDMAc$_{80}$, _4_8_PDMAc$_{67}$ and _8_4_PNAM$_{60}$ were synthesized with a similar way, and the conditions of polymerization were given in Table 2.4.1.1.

Table 2.4.1.1. Functional poly(*N,N*-dimethylacrylamide)s (PDMAc) and poly(*N*-acryloylmorpholine) (PNAM) obtained with _4_8_ and _8_4_CTA.

Name	**RAFT Agent**	**$[M]_0/[CTA]_0/[AIBN]_0$**	**$[M]_0$ (M)**	**Temp. (°C)**	**Conv. (%)[a] *(time)***	**$DP_{n,NMR}$[b]**	**$M_{n,th}$ (g/mol)[c]**	**$M_{n,NMR}$ (g/mol)[d]**	**$M_{n,SEC}$ (g/mol)[e]**	**$Đ$**
_8_4_ PDMAc$_{137}$	_8_4_CTA -B6	172/1/0.1	0.2	65	66 *(6.3h)*	137	12100	14400	13600	1.12
_8_4_ PNAM$_{60}$	_8_4_CTA -B7	100/1/0.1	0.8	70	70 *(1.5h)*	60	10700	9300	8000	1.17
_4_8_ PDMAc$_{150}$	_4_8_CTA -SH[f]	171/1/0.2	0.2	65	67 *(3.7h)*	150	12200	15600	14900	1.17
_4_8_ PDMAc$_{80}$	_4_8_CTA -B1	114/1/0.1	0.2	65	68 *(2.7h)*	80	8500	8700	9700	1.09
_4_8_ PDMAc$_{67}$	_4_8_CTA -SH[f]	86/1/0.1	0.2	65	73 *(3.5h)*	67	7000	7400	7600	1.09

[a] Calculated by ^{1}H NMR at the time of beginning and ending.

[b, d] Calculated by ^{1}H NMR of the purified polymers.

[c] Theoretical M_n was calculated by conversion.

[e] Determined by SEC in DMF (with 1 g/L LiBr) using PMMA standards and refractive index detection.

[f] From Shuaiyuan Han[9].

With $[M]_0$ = initial monomer concentration and $[CTA]_0$ = initial chain transfer agent concentration.

2.4.2 Polymerization of acrylates using _8_4_CTA and _4_8_CTA

Polyacrylates here used mostly are hydrophobic polymers except PHEA. The chemical structures based on _4_8_ and _8_4_ are given in Figure 2.4.2.1.

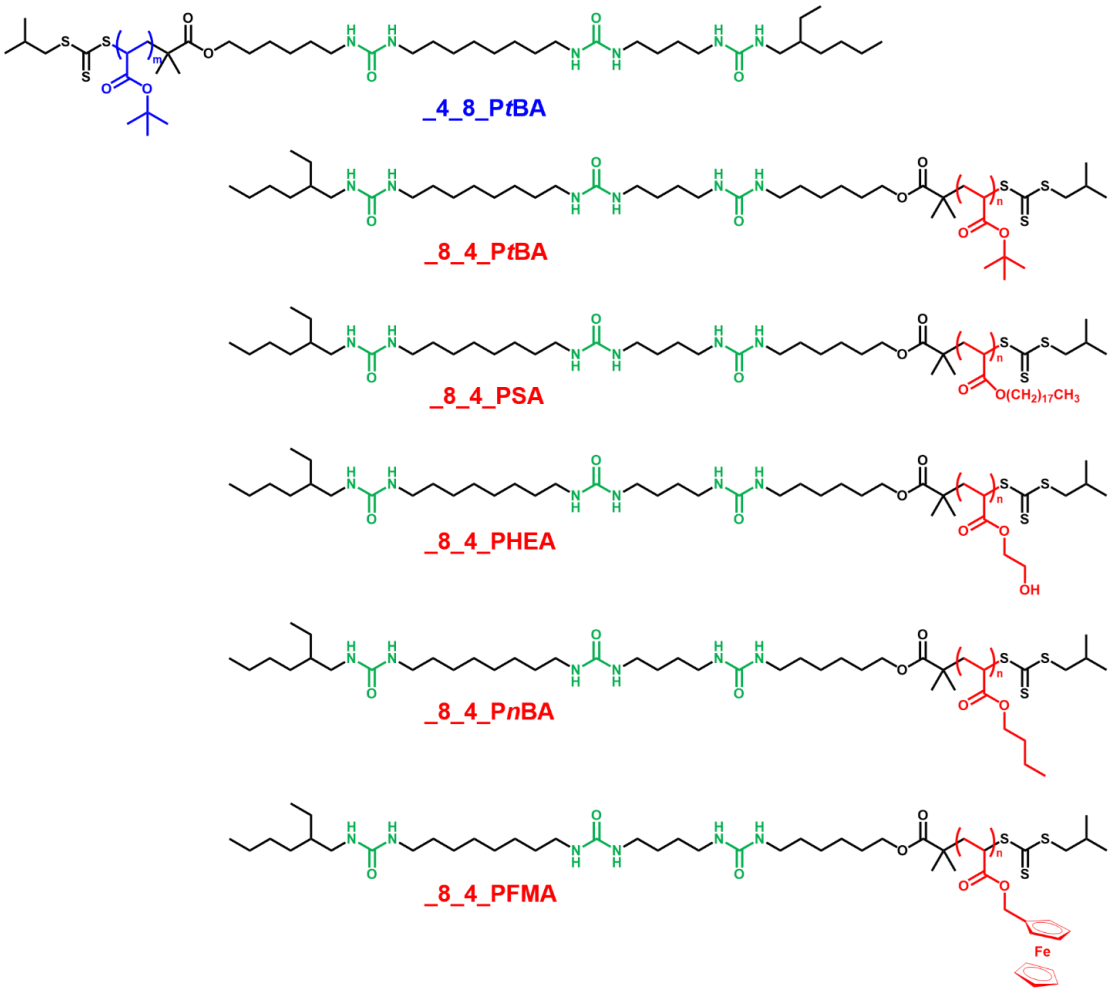

Figure 2.4.2.1. _4_8_ and _8_4_polyacrylates synthesized using the corresponding RAFT agents.

These polymers are synthesized to match with corresponding PDMAc since PDMAc has shown its good ability to form Janus nanorods when it co-assembles with complementary polymers. According to the literature, non-Janus poly(*n*-butyl acrylate) (P*n*BA) nanorods display good surface behavior when transferred onto Si substrate and analyzed by AFM, with a diameter of ~ 6 nm when DP_n is 36[16]. It would thus be interesting to investigate it by the co-assembly with PDMAc. Also, poly(*tert*-butyl

acrylate) (P*t*BA) is promising when co-assembling with PDMAc since there is a good phase contrast in AFM due to the T_g gap between PDMAc (~ 125 °C) and P*t*BA (~ 52 °C), and P*t*BA is not as sticky as P*n*BA (T_g ~ -50 °C).

Poly(stearyl acrylate) (PSA) is a hydrophobic polymer that is hardly soluble in polar solvents (such as methanol) due to the long alkyl side chain. Therefore, we hope to be able to dissolve selectively PDMAc away from PDMAc/PSA nanopatterns, thus providing a simple access to regular trenches on Si wafers.

Like PDMAc, poly(2-hydroxyethyl acrylate) (PHEA) is a hydrophilic polymer due to the existence of the hydroxyl in side chain. However, hydroxyls in PHEA can be crosslinked with glutaraldehyde vapors[17]. In this case, after crosslinking of PHEA, PDMAc should be readily removed by dissolution from PDMAc/PHEA nanopatterns.

Ferrocene-containing polymers have obtained a great attention due to not only its redox responsive property[18-22] but also "etching contrast" when it is combined with other polymers[23, 24]. It is interesting to note that ferrocene-containing polymers keep the iron oxide in its position while other polymers are pyrolyzed at a high temperature. In this way, ferrocene-containing polymers have the natural advantage to provide "etching contrast" in nanopatterning. Ferrocenemethyl acrylate (FMA) was synthesized in two steps according to a reported protocol[25] in an overall yield of 24%.

Globally, the polymerization procedures were similar to the synthesis of the polyacrylamides, yet differing by monomer concentration and temperature due to the low polymerization rate of PDMAc. Except PHEA, all hydrophobic polymers were purified by precipitations in poor solvents. PHEA was obtained from dialysis against water and following freeze-drying. The detailed conditions of polymerizations of these polymers are listed in Table 2.4.2.1. SEC figures are shown in Figure 2.4.2.2.

From Table 2.4.2.1, we observed that P*t*BA gave a good dispersity (less than 1.15) and, generally, there is a good agreement of observed molecular weights between NMR and SEC. For PSA, DP_n = 33 and 73 were synthesized for a preliminary test of co-

assembly. Finally, a large scale (1.7 g) of _8_4_PSA$_{42}$ with a 1.14 dispersity was synthesized for a further investigation of our collaborators. In the case of PHEA, high *DP*s were targeted to probe the influence on the self-assembly. Remarkably, PHEA with a DP_n ~1300 could be achieved with a 1.67 dispersity, and the dispersity of PHEA$_{600}$ was low down to 1.25.

Table 2.4.2.1. Functional polyacrylates based on corresponding _4_8_ and _8_4_CTA.

Name	RAFT Agent	$[M]_0/[CTA]_0/[AIBN]_0$	$[M]_0$ (M)	Temp. (°C)	Conv. (%)[a] *(time)*	$DP_{n, NMR}$[b]	$M_{n, th}$ (kg/mol)[c]	$M_{n, NMR}$ (kg/mol)[d]	$M_{n, SEC}$ (kg/mol)[e]	*Đ*
_8_4_P*t*BA$_{32}$	_8_4_CTA-B4	43/1/0.1	0.6	70	73 *(2.3h)*	32	4.8	4.9	5.0	1.15
_4_8_P*t*BA$_{62}$	_4_8_CTA-B1	172/1/0.1	0.6	70	55 *(8.7h)*	62	13.0	8.7	8.8	1.13
_4_8_P*t*BA$_{48}$	_4_8_CTA-B1	86/1/0.1	0.6	70	63 *(3h)*	48	7.7	6.9	7.0	1.11
_8_4_PSA$_{73}$	_8_4_CTA-B4	86/1/0.1	0.5	70	78 *(2.8h)*	73	22.6	24.5	23.3	1.40
_8_4_PSA$_{42}$	_8_4_CTA-B7	50/1/0.1	0.5	70	74 *(2.5h)*	42	12.8	14.4	12.8	1.14
_8_4_PSA$_{33}$	_8_4_CTA-B5	43/1/0.1	0.5	70	77 *(1.4h)*	33	11.6	11.5	12.7	1.23
_8_4_PHEA$_{1300}$	_8_4_CTA-B7	2857/1/0.2	2	65	64 *(24h)*	1300	212.9	151.6	135.6	1.67
_8_4_PHEA$_{600}$	_8_4_CTA-B6	900/1/0.4	2	65	65 *(2.3h)*	600	68.7	70.4	85.2	1.25
_8_4_PHEA$_{47}$	_8_4_CTA-B7	100/1/0.1	0.8	70	65 *(3h)*	47	8.3	6.2	8.0	1.31
_8_4_PFMA$_{69}$	_8_4_CTA-B6	86/1/0.2	0.5	70	82 *(20h)*	69	20.0	19.4	6.8	1.41
_8_4_P*n*BA$_{41}$	_8_4_CTA-B4	86/1/0.1	0.6	70	65 *(8h)*	41	8.0	6.0	6.8	1.31

[a] Calculated by ^{1}H NMR at the time of beginning and ending.

[b, d] Calculated by ^{1}H NMR of the purified polymers.

[c] Theoretical M_n was calculated by conversion.

[e] Determined by SEC in THF using PMMA standards and refractive index detection. PHEA was determined by SEC in DMF (with 1 g/L LiBr) using PMMA standards and refractive index detection.

With $[M]_0$ = initial monomer concentration and $[CTA]_0$ = initial chain transfer agent concentration.

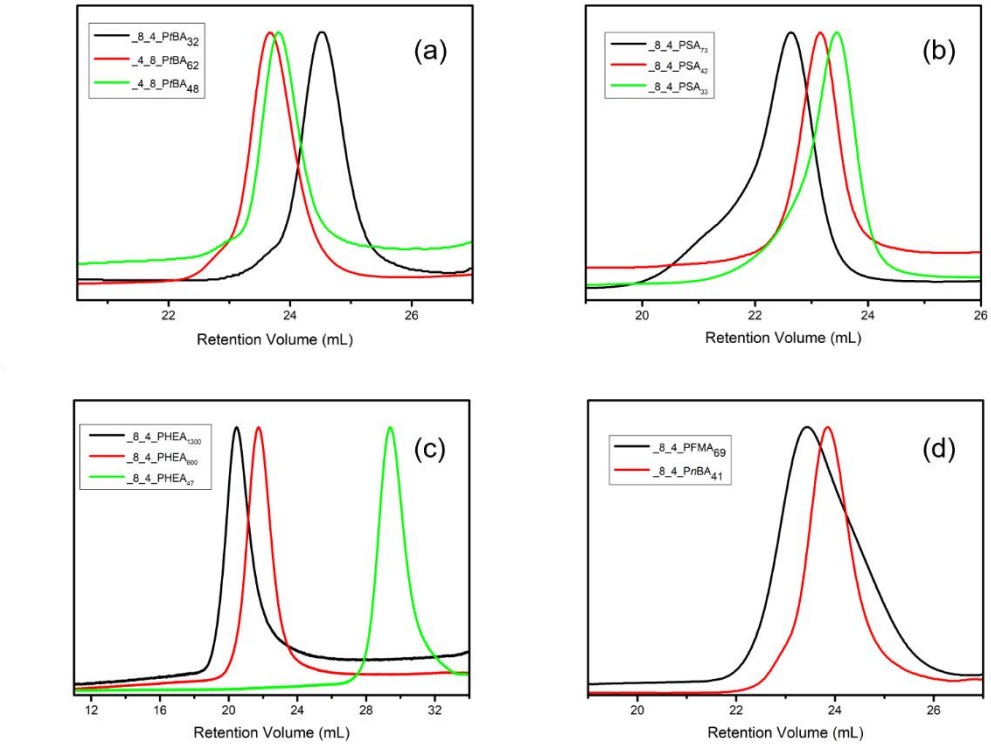

Figure 2.4.2.2. SEC figures of _4_8_ and _8_4_polyacrylates (PHEA in DMF, others in THF).

2.4.3 Polymerization of styrene derivatives using _8_4_CTA and _4_8_CTA

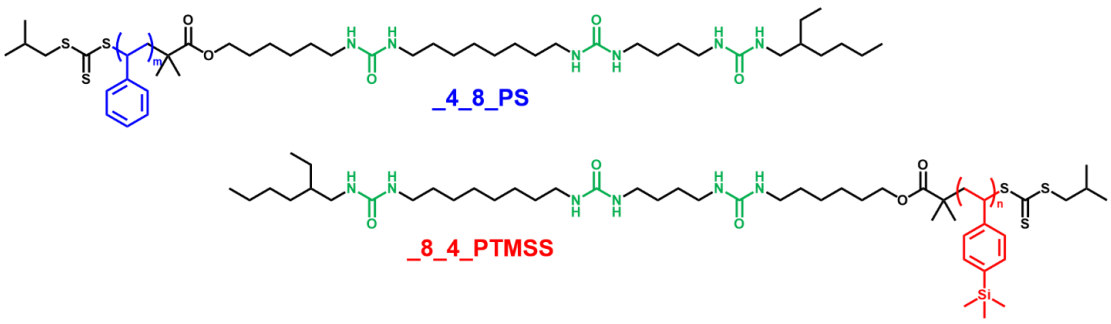

Figure 2.4.3.1. _4_8_ PS and _8_4_PTMSS synthesized by corresponding RAFT agents.

Figure 2.4.3.1 shows the chemical structures of _4_8_PS and _8_4_PTMSS. Polystyrene has been used as a classical polymer in nanopatterning and will therefore be a useful reference[2, 26-29]. When a silicon atom is introduced into the styrene monomer, it enhances the etching contrast with other polymers. Indeed, O_2 reactive ion etching (RIE) would remove PDMAc while PTMSS would be oxidized with a lower rate. 4-trimethylsilyl styrene was synthesized according to a reported protocol[30] in good yield (68%).

The polymerizations of styrene or 4-trimethylsilyl styrene were performed with more initiator since they are “lazy monomers” (have low propagation constants, k_p). The monomer conversions reached 62% after 55 hours and 38% after 7 hours. Even though the propagation is slow, the dispersity is still low.

Table 2.4.3.1. Polystyrene derivatives based on corresponding _4_8_ and _8_4_CTA.

Name	RAFT Agent	$[M]_0/[CTA]_0/[AIBN]_0$	$[M]_0$ (M)	Temp. (℃)	Conv. (%)[a] *(time)*	$DP_{n,NMR}$[b]	$M_{n,th}$ (kg/mol)[c]	$M_{n,NMR}$ (kg/mol)[d]	$M_{n,SEC}$ (kg/mol)[e]	*Đ*
_8_4_PTMSS$_{61}$	_8_4_CTA-B7	86/1/0.3	1	70	62 *(55h)*	61	10.1	11.5	9.6	1.12
_4_8_PS$_{33}$	_4_8_CTA-B1	150/1/0.3	2	75	38 *(7h)*	33	6.7	4.2	4.0	1.09

[a] Calculated by ^{1}H NMR at the time of beginning and ending.

[b, d] Calculated by ^{1}H NMR of the purified polymers.

[c] Theoretical M_n was calculated by conversion.

[e] Determined by SEC in THF using PS standards and refractive index detection.

With $[M]_0$ = initial monomer concentration and $[CTA]_0$ = initial chain transfer agent concentration.

The SEC analyses (Figure 2.4.3.2) revealed unimodal distributions. A small shoulder is visible at the high molar mass side for PTMSS and could result from termination reactions; but low dispersity and an experimental M_n close to the theoretical one indicated that the polymerization was globally well controlled.

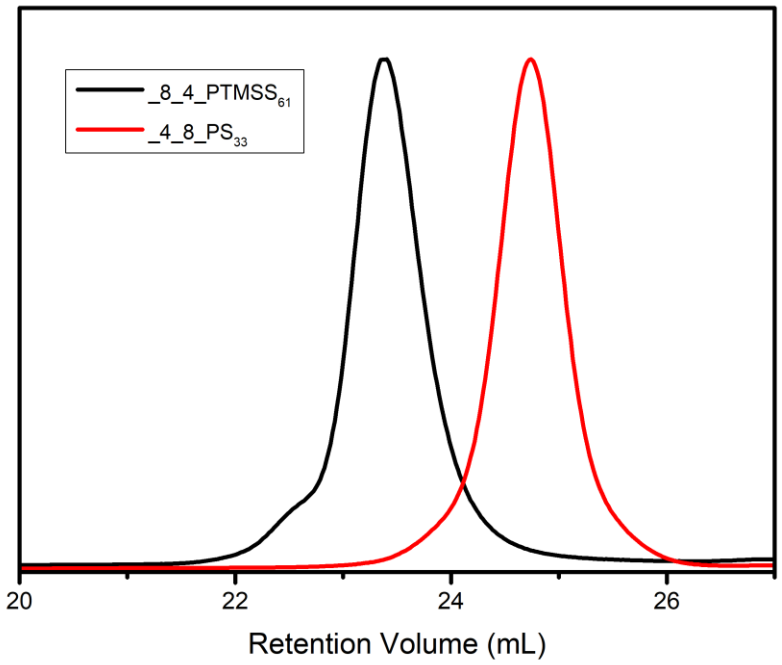

Figure 2.4.3.2. SEC figures of _8_4_PTMSS$_{61}$ and _4_8_PS$_{33}$ (in THF).

2.5 Conclusions

In this chapter, the syntheses of RAFT agents are optimized and several batches of RAFT agents have been prepared. Afterwards, a series of _4_8_ and _8_4_polymers was synthesized via RAFT polymerization according to their expected behavior in nanopatterning. The polymers are characterized by ^{1}H NMR and SEC and have been transmitted to our collaborators.

The self-assembly of these polymers in solution is currently studied at IMMM (Le Mans). In particularly, based on _4_8_PDMAc and _8_4_PHEA, they have explored the influence of experimental conditions (polymer concentration, rate of water addition, temperature) to optimize the self-assembly process[31]. They found that: (1) there was no significant changes for the coassembly process with a quick (100 mL/h) and slow (0.5 mL/h) rate of water addition; (2) lowering polymer concentration (from 100 g/L to 10 g/L) would reduce amounts of nanocylinders; (3) increasing temperature (from 20 ℃ to 80 ℃) weakens hydrogen bonds and improves hydrophobic interaction thus decreasing nanocylinders yield and triggering the formation of spheres. They have also probed the influence of the degree of polymerization of the polymers on the length and diameter of the nanorods[32]. By using _4_8_PDMAc$_{80}$ coassemble with _8_4_PHEA$_{47}$ and _8_4_PHEA$_{500}$, nanocylinders are observed but when increasing DP_n largely, _4_8_PDMAc$_{500}$/_8_4_PHEA$_{600}$ and _4_8_PDMAc$_{1300}$/_8_4_PHEA$_{1300}$ do not show nanocylinders due to the strong steric hindrance.

The deposition of the pre-assembled Janus nanorods on surfaces is currently studied at ICMN (Orléans) by dip-coating and Langmuir-Blodgett deposition.

2.6 Experimental Section

2.6.1. Chemicals and Solvents

The following chemicals were used directly without purification. 1, 3, 5-Trioxane (97%, Fluka), sodium hydroxide (NaOH, ≥98%, Sigma-Aldrich), 2-methyl-1-propanethiol (92%, Sigma-Aldrich), methyltrioctylammonium chloride (Aliquat 336, Aldrich), carbon disulfide (99.9%, Acros Organics), 6-amino-1-hexanol (95%, ABCR), trimethylamine (TEA, ≥99.5%, Sigma-Aldrich), di-tert-butyl dicarbonate (95%, TCI), hydrochloric acid (35%, VWR), HCl in dioxane (4 M, TCI), magnesium sulfate (VWR), oxalyl chloride (≥99%, Sigma-Aldrich), 1,8-diaminooctane (98%, Sigma-Aldrich), 2-ethylhexyl isocyanate (98%, Sigma-Aldrich), 1,4-diisocyanatobutane (97%, Sigma-Aldrich), sodium sulfate (Supelco), 1,4-diaminobutane (99%, Sigma-Aldrich), 4-nitrophenyl chloroformate (90%, Fluorochem), 4-bromostyrene (≥95%, TCI), chlorotrimethylsilane (≥98%, Sigma-Aldrich), magnesium turnings (≥99.5%, Sigma-Aldrich), ferrocenecarboxaldehyde (98%, Sigma-Aldrich), sodium borohydride (≥95%, TCI), ammonium chloride (≥99%, Thermo Scientific), acryloyl chloride (96%, Fisher Scientific), sodium chloride (Supelco).

Toluene (100%, VWR), acetone (≥99%, Sigma-Aldrich), chloroform (≥99.8%, VWR), pentane (≥98%, Sigma-Aldrich), hexane (≥98%, Sigma-Aldrich), dichloromethane (≥99%, Sigma-Aldrich), ethyl acetate (≥99.5%, Sigma-Aldrich), dioxane (99.8%, Sigma-Aldrich), tetrahydrofuran (≥99%, Sigma-Aldrich), dimethyl sulfoxide (≥99.9%, Fisher Chemical), methanol (≥99.9%, Carlo Erba).

N,N-Dimethylacrylamide (DMAc, 99%, Sigma-Aldrich), *N*-acryloylmorpholine (NAM, 97%, Sigma-Aldrich), *n*-butyl acrylate (≥99%, Sigma-Aldrich) and *tert*-butyl acrylate (98%, Sigma-Aldrich) were purified on a basic aluminium oxide column to remove the inhibitors. 2,2'- Azobis(2-methylpropionitrile) (AIBN, 98%, Sigma-Aldrich) and stearyl acrylate (≥97%, TCI) were recrystallized from methanol. Styrene (≥99%, Sigma-Aldrich) and 2-hydroxylethyl acrylate (≥95%, TCI) were distilled before

the uses. The anhydrous dichloromethane (DCM), tetrahydrofuran (THF) and toluene were obtained from a solvent purification system (MBraun SPS).

2.6.2 Characterizations

Nuclear Magnetic Resonance (NMR). ^{1}H and ^{13}C NMR spectra were obtained in deuterated solvents using Bruker 300, 400 or 600 MHz NMR spectrometer. All ^{1}H NMR spectra were referenced to the peak at 7.26 ppm (in $CDCl_3$), 5.32 ppm (in CD_2Cl_2), 3.58 ppm (in THF-d_8) and 2.5 ppm (in DMSO-d_6). ^{13}C NMR spectra were referenced to the peak at 77.16 ppm (in $CDCl_3$) and 39.52 ppm (in DMSO-d_6). For monomer consumption in polymerization, the integration of trioxane or toluene was set as a reference to calculate the monomer conversion.

Size Exclusion Chromatography (SEC). Polymers with a ~3 mg/mL concentration were analyzed by SEC using DMF (+ 1 g/L LiBr) or THF as eluent phase. PDMAc, PNAM, PHEA were analyzed in DMF, while P*t*BA, P*n*BA, PSA, PFMA, PS and PTMSS were analyzed in THF. For SEC in DMF, the columns were thermostated at 60 °C, and the flow rate was set at 0.8 mL/min. For SEC in THF, the columns were thermostated at 40 °C, and the flow rate was set at 1 mL/min. The eluent contained toluene (20 drops in 100 mL DMF) as an internal standard. Polymers in DMF were detected by a differential refractive index detector (RI) and a Diode Array UV Detector (309 nm). Polymers in THF were detected by a differential refractive index (RI) detector Viscoteck 3580 and a Diode Array UV Detector (309 nm) Shimadzu SPD20-AV. Excepted for PS and PTMSS calibrating for which a PS calibration was used (refractive index detector), the average molar masses of all other polymers were calculated using a PMMA calibration (refractive index detector).

2.6.3 Synthesis of _8_4_and _4_8_RAFT agents

Synthesis of intermediate 1. Under argon atmosphere and mechanical stirring, a NaOH aqueous solution (20 mL, 50 wt%, 250 mmol) was added dropwise to a solution of 2-methyl-1-propanethiol (24 mL, 221 mmol), acetone (140 mL, 1.9 mol)

and methyltrioctylammonium chloride (4 mL, 22.5 mmol) kept in an ice-water bath. After the end of the addition, the reaction was stirred for 30 min. A solution of carbon disulfide (14 mL, 220 mmol) in acetone (40 mL) was slowly added into the mixture (within about 5 minutes), the solution was stirred for another 30 min. Chloroform (28 mL, 333 mmol) was added in one portion, and 65 mL of an aqueous NaOH solution (50 wt%, 815 mmol) was added dropwise. The reaction mixture was stirred overnight at room temperature. 325 mL of water was added to the resulting reaction mixture, followed by 165 mL of concentrated HCl to acidify the reaction to pH=1-2. The remaining acetone was removed by purging with argon. The yellow solid was collected by filtration and then washed with distilled water to remove the salt. Then the yellow solid was recrystallized from an acetone/pentane (1/10) solution. The crystallized solid was purified over silica gel column using DCM as eluent to obtain a brown solid (32 g, 58 %). ^{1}H NMR (300 MHz, $CDCl_3$) δ 3.21 (d, 2H), 2.04 – 1.93 (m, 1H), 1.73 (s, 6H), 1.01 (d, 6H). ^{13}C NMR (101 MHz, $CDCl_3$) δ 221.09, 179.10, 55.74, 45.54, 28.01, 25.36, 22.22.

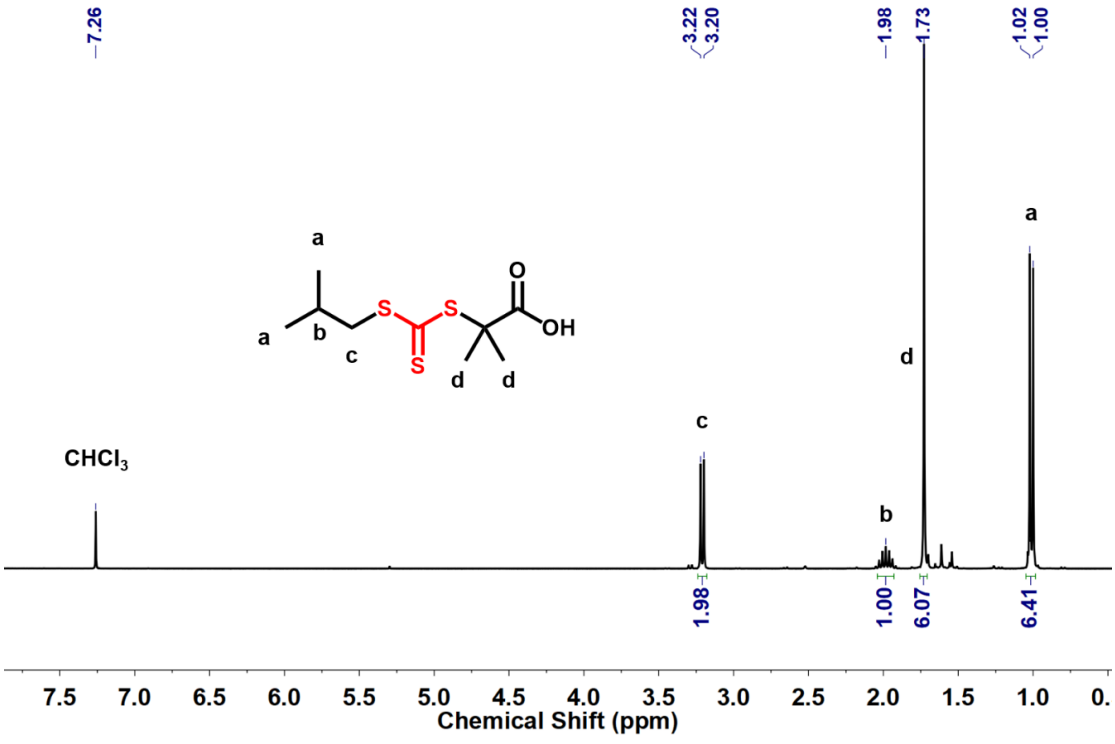

Figure 2.6.3.1. ^{1}H NMR of intermediate **1** (in $CDCl_3$).

Synthesis of intermediate 2. 6-Amino-1-hexanol (25.0 g, 214 mmol, 1.00 eq), triethylamine (22.7 g, 225 mmol, 1.05 eq) and a magnetic stirring bar were added into a 1 L round-bottom flask. After the addition of DCM (500 mL), di-tert-butyl dicarbonate (48.9 g, 225 mmol, 1.05 eq) dissolved in DCM (100 mL) was slowly dropped into the 1 L round-bottom flask. The reaction was stirred overnight at room temperature and the mixture was washed with HCl (1 M, 500 mL) and then DI water (200 mL × 3). The organic layer was dried by anhydrous magnesium sulfate and the solvent was removed under reduced pressure, giving a colorless waxy solid (30.2 g, 65.1%). ^{1}H NMR (400 MHz, $CDCl_3$) δ 4.51 (br, 1H), 3.63 (t, 2H), 3.11 (q, 2H), 1.76 – 1.24 (m, 17H). ^{13}C NMR (101 MHz, $CDCl_3$) δ 156.20, 79.24, 62.88, 40.51, 32.75, 30.24, 28.58, 26.54, 25.42.

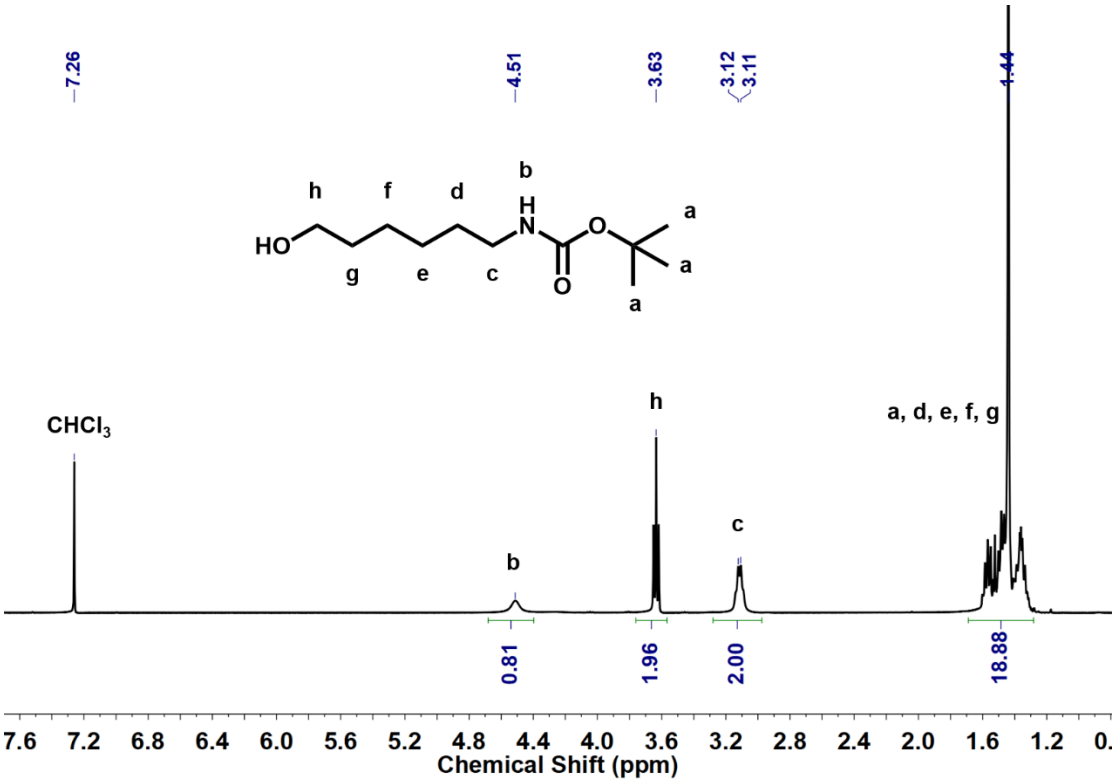

Figure 2.6.3.2. ^{1}H NMR of intermediate **2** (in $CDCl_3$).

Synthesis of intermediate 3 and 4. To a solution of intermediate **1** (7.44 g, 29.3 mmol, 1 eq) in DCM (30 mL) cooled in an ice-water bath was dropwise added a DCM solution (30 mL) of oxalyl chloride (7.4 mL, 89.9 mmol, 3 eq). After 5 hours, a dark

reddish solution was formed and the solution was evaporated to obtain intermediate **3**. The intermediate **3** was dissolved in 20 mL of DCM in a 100 mL round-bottom flask cooled with an ice-water bath. Then a solution of intermediate **2** (9.5 g, 43.8 mmol, 1.5 eq) in 50 mL of DCM was slowly dropped into the flask. The solution was placed under reflux overnight. Afterwards, the solvent was removed under reduced pressure. The remaining oil was purified by flash column chromatography on silica gel using EA/Hex (1:6) as an eluent to obtain a yellow viscous liquid (6.7 g, 51%). ^{1}H NMR (300 MHz, $CDCl_3$) δ 4.50 (br, 1H), 4.07 (t, 2H), 3.18 (d, 2H), 3.08 (q, 2H), 2.05 – 1.87 (m, 1H), 1.76 – 1.53 (m, 8H), 1.53 – 1.38 (m, 11H), 1.38 – 1.24 (m, 4H), 0.99 (d, 6H). ^{13}C NMR (101 MHz, $CDCl_3$) δ 221.73, 173.11, 156.08, 79.16, 66.06, 56.16, 45.31, 40.63, 30.10, 28.56, 28.41, 28.06, 26.52, 25.77, 25.51, 22.16.

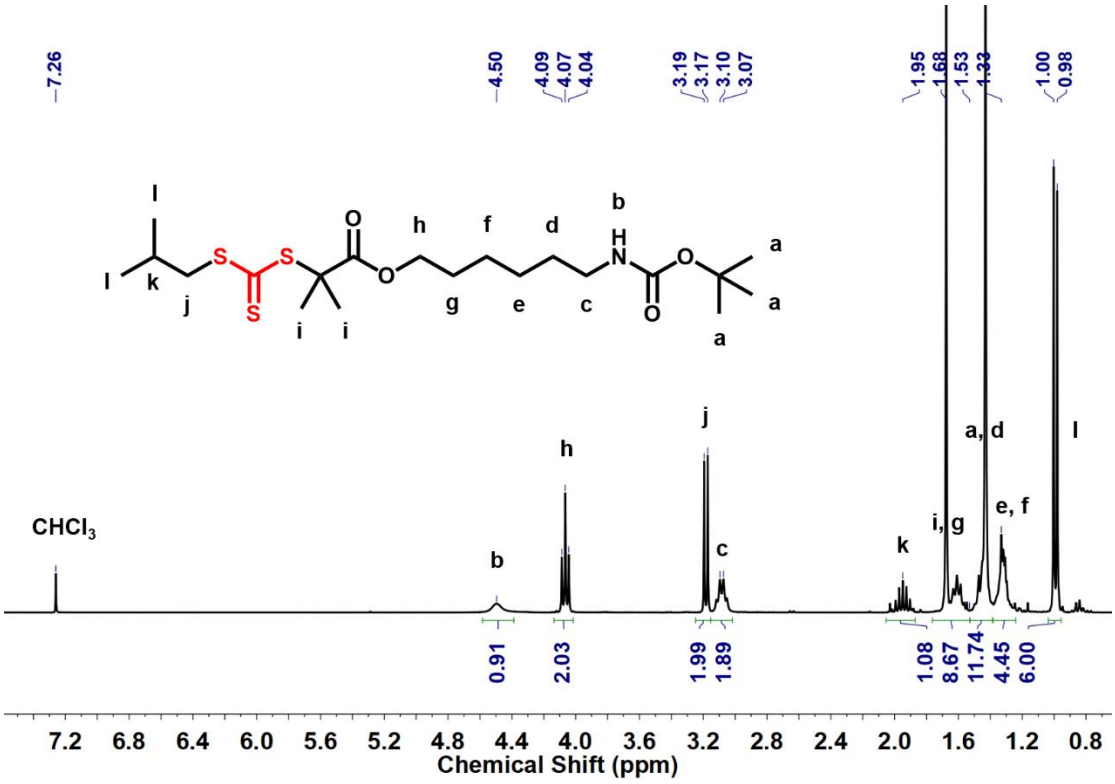

Figure 2.6.3.3. ^{1}H NMR of intermediate **4** (in $CDCl_3$).

Synthesis of NH_3Cl-CTA (5). A magnetic stirring bar and intermediate **4** (4.5 g, 10 mmol, 1 eq) dissolved in dioxane (40 mL) were added into a 100 mL round-bottom flask cooled with an ice-water bath. Then 15 mL of 4 M HCl in dioxane was dropwise

added into the flask. The mixture was stirred at 60 ℃ overnight. A bright yellow oil (3.87 g, 100%) was obtained by evaporating the solvent. ^{1}H NMR (300 MHz, Chloroform-*d*) δ 8.29 (br, 3H), 4.07 (t, 2H), 3.19 (d, 2H), 3.06 – 2.89 (m, 2H), 2.04 – 1.87 (m, 1H), 1.84 – 1.58 (m, 10H), 1.50 – 1.30 (m, 4H), 1.00 (d, 6H). ^{13}C NMR (101 MHz, $CDCl_3$) δ 221.81, 173.16, 65.83, 56.20, 45.35, 39.96, 28.21, 28.09, 27.67, 26.18, 25.54, 25.43, 22.19.

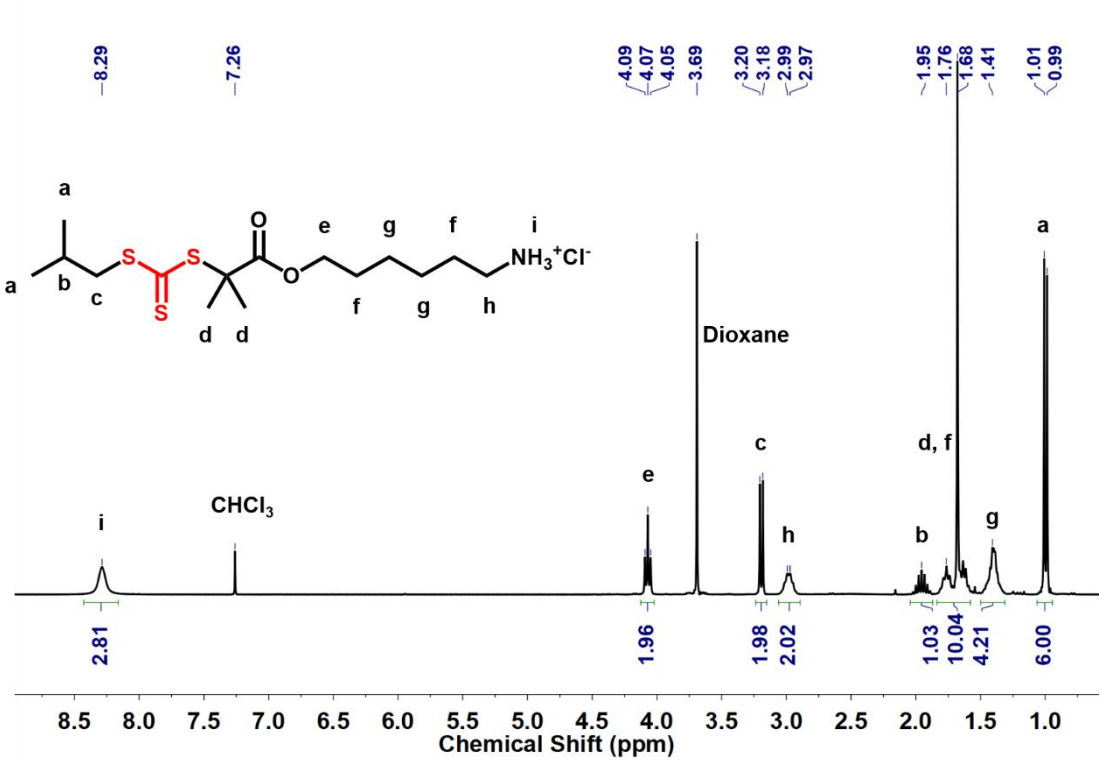

Figure 2.6.3.4. ^{1}H NMR of intermediate **5** (in $CDCl_3$).

Synthesis of intermediate 6. 1,8-diaminooctane (30 g, 208 mmol, 5 eq) and a magnetic stirring bar were added into a 1L round-bottom flask. After the addition of chloroform (500 mL), di-tert-butyl dicarbonate (9.08 g, 41.7 mmol, 1.00 eq) was dissolved in chloroform (40 mL) and then slowly dropped into the 1L round-bottom flask. The reaction was stirred at room temperature for 64 h. The filtrate was filtered, and the solution was collected and dried by anhydrous sodium sulfate. The white waxy product (7.1 g, 70%) was obtained by flash column chromatography on silica gel using

$CHCl_3$/MeOH (100/5-60/40) as an eluent. ^{1}H NMR (300 MHz, $CDCl_3$) δ 4.51 (br, 1H), 3.16 – 3.00 (m, 2H), 2.74 – 2.60 (m, 2H), 1.53 – 1.20 (m, 23H).

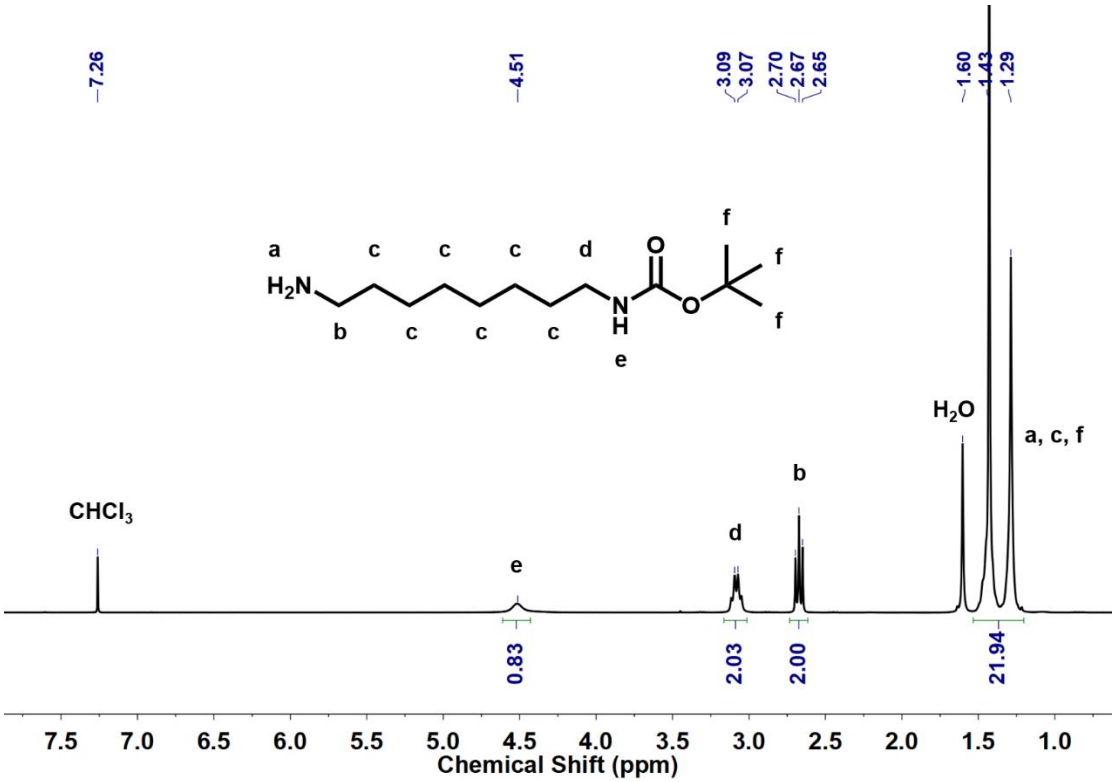

Figure 2.6.3.5. ^{1}H NMR of intermediate **6** (in $CDCl_3$).

Synthesis of intermediate 7. To a solution of intermediate **6** (7.1 g, 29 mmol, 1.02 eq) and triethylamine (3.02 g, 30 mmol, 1.05 eq) in anhydrous DCM (100 mL) was slowly added a DCM solution (20 mL) of 2-ethylhexyl isocyanate (4.42 g, 28.5 mmol, 1.00 eq). The reaction was performed at room temperature overnight. The solution was washed with 0.1 M HCl (125 mL ×2), DI water (100 mL) and brine (100 mL). Afterwards, the solution was dried by anhydrous Na_2SO_4 and then the solvent was evaporated giving a colorless viscous liquid (7.9 g, 69%). ^{1}H NMR (400 MHz, $CDCl_3$) δ 4.62 (m, 3H), 3.21 – 2.96 (m, 6H), 1.59 – 1.17 (m, 30H), 0.98 – 0.80 (m, 6H). ^{13}C NMR (101 MHz, $CDCl_3$) δ 158.60, 77.48, 77.16, 76.84, 43.60, 40.68, 39.95, 31.15, 30.31, 30.11, 29.22, 29.19, 29.08, 28.58, 26.84, 24.35, 23.19, 14.22, 11.06.

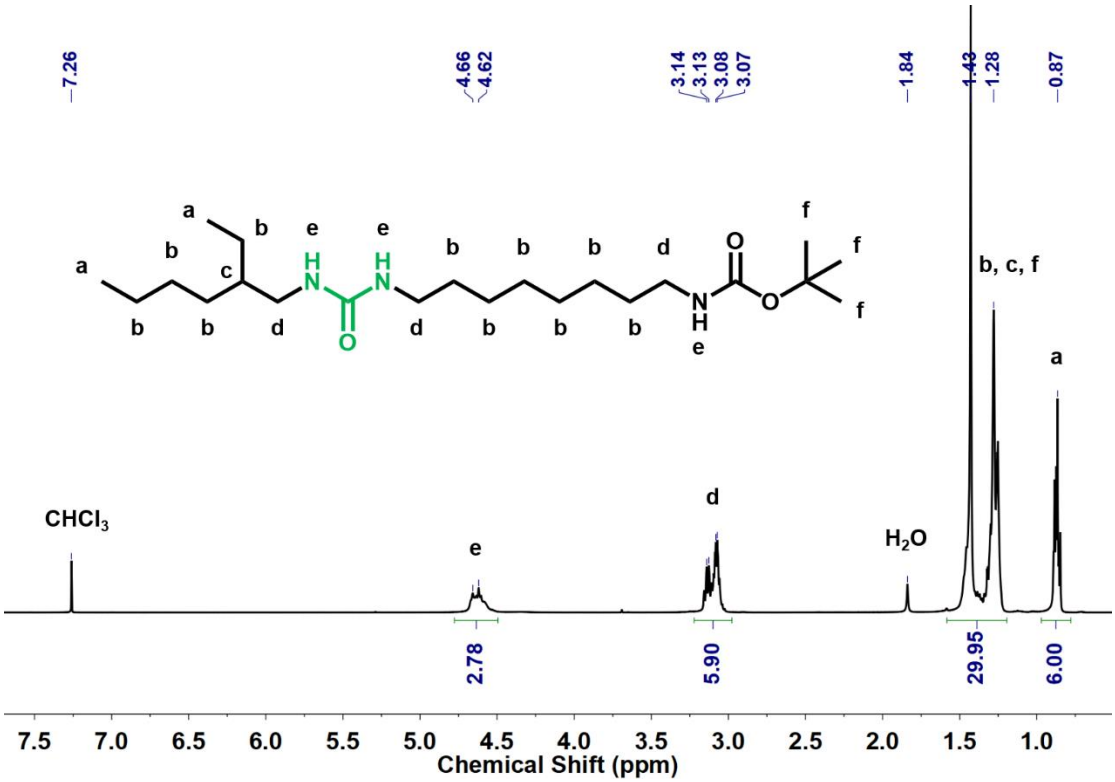

Figure 2.6.3.6. ^{1}H NMR of intermediate **7** (in $CDCl_3$).

Synthesis of intermediate 8. A magnetic stirring bar and intermediate **7** (4.44 g, 11.1 mmol, 1 eq) dissolved in dioxane (30 mL) were added into a 100 mL round-bottom flask cooled with an ice-water bath. Then 8.3 mL of 4 M HCl in dioxane was slowly added into the flask. The mixture was stirred at room temperature overnight. A bright yellow oil (3.68 g, 98.7%) was obtained after evaporating the solvent. ^{1}H NMR (400 MHz, DMSO-d_6) δ 7.98 (t, 3H), 6.88 – 6.09 (br, 2H), 3.17 – 2.86 (m, 4H), 2.83 – 2.65 (m, 2H), 1.67 – 1.01 (m, 21H), 0.96 – 0.73 (m, 6H). ^{13}C NMR (101 MHz, DMSO-d_6) δ 158.28, 41.83, 40.15, 38.72, 30.40, 30.03, 28.53, 28.47, 28.42, 26.89, 26.21, 25.75, 23.63, 22.53, 13.96, 10.80.

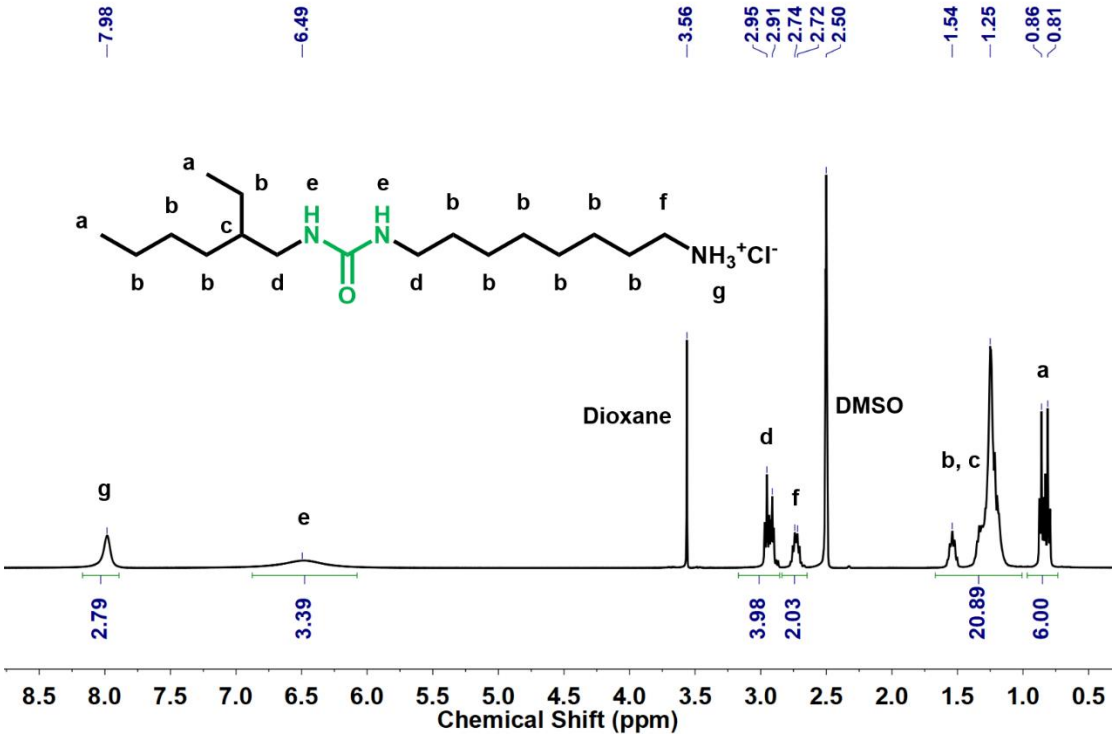

Figure 2.6.3.7. ^{1}H NMR of intermediate **8** (in DMSO-d_6).

Synthesis of intermediate 9. Intermediate **8** (1.58 g, 4.72 mmol, 1.00 eq), triethylamine (2.62 mL, 1.91 mmol, 4 eq), a magnetic stirring bar and 94 mL of anhydrous THF were added into a 250 mL round-bottom flask. The solution (0.05 M) was stirred over 30 minutes to totally convert $NH3^{+}Cl^{-}$ to amine. A white precipitate was formed during the stirring. Then the mixture (liquid and solid) was transferred to a 150 mL dropping funnel and then slowly added (if the addition was blocked, using a long needle to help) into a dried 250 mL round-bottom flask which was previously charged with 1,4-diisocyanatobutane (1.32 g, 9.44 mmol, 2 eq), 47 mL of anhydrous THF. The remaining mixture was transferred to the dropping funnel by 50 mL of anhydrous THF and then added to the 250 mL flask again. After 160 minutes, the reaction was stopped and the solution was filtered by a Büchner funnel. The solution was condensed to about 5 mL and then 200 mL of pentane was added into the flask. A white solid was formed. After filtration, the solid was washed by 200 mL of pentane and dried under vacuum at 25 °C giving a white solid (0.71 g, 35%). ^{1}H NMR (400 MHz, THF-d_8) δ 5.48 (br, 4H), 3.32 (t, 2H), 3.20 – 2.97 (m, 8H), 1.67 – 1.11 (m, 25H),

1.04 – 0.69 (m, 6H). ^{13}C NMR (101 MHz, THF-d_8) δ 159.19, 159.05, 66.99, 66.77, 43.32, 43.16, 41.15, 40.41, 40.29, 39.67, 31.82, 31.20, 29.79, 29.74, 29.41, 28.57, 27.29, 24.88, 24.73, 23.83, 14.28, 11.18.

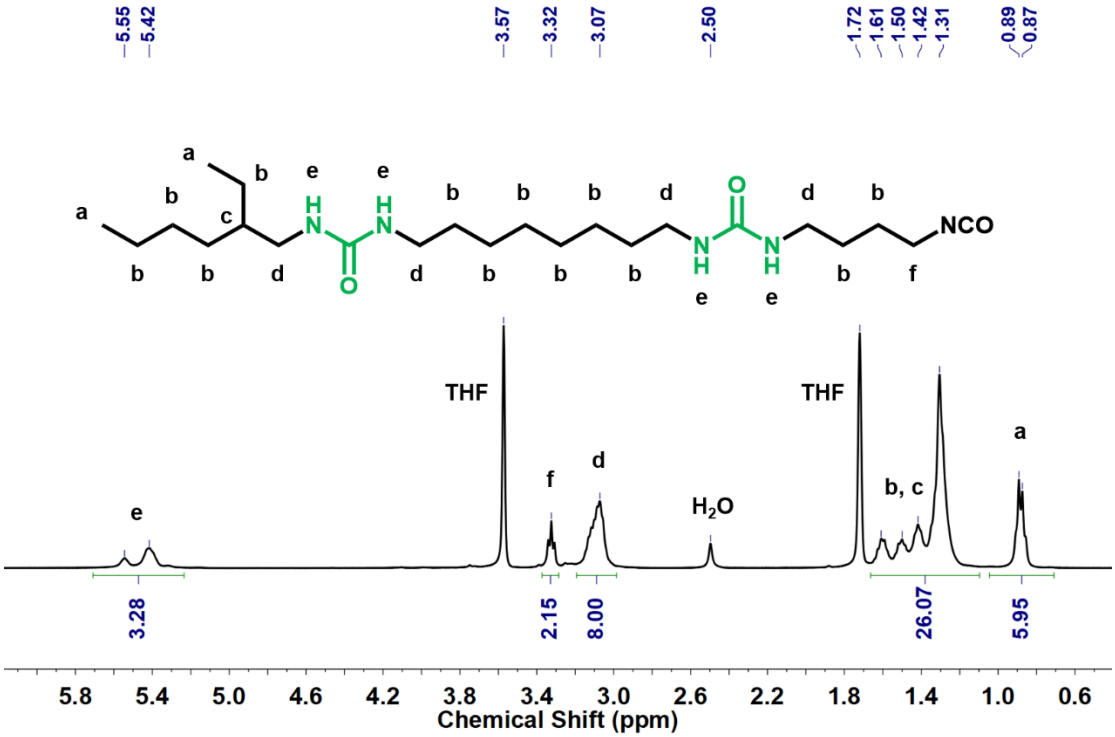

Figure 2.6.3.8. ^{1}H NMR of intermediate **9** (in THF-d_8).

Synthesis of _8_4_CTA (10). Intermediate **9** (0.88 g, 2.0 mmol, 1 eq), NH_3Cl-CTA (0.74 g, 2.2 mmol, 1.1 eq), triethylamine (0.41 g, 4.1 mmol, 2.1 eq), a magnetic stirring bar and 80 mL of DCM were added into a 100 mL round-bottom flask. The reaction was performed at room temperature for 18 hours. Afterwards, the solution was concentrated to gel and then 50 mL of acetone was poured into the flask. A yellow solid precipitated and then was washed with 50 mL of acetone, 250 mL DI water and 200 mL of acetone in a fritted funnel. The yellow solid (1.14 g, 72%) was dried at 40 °C under vacuum for 2 days. ^{1}H NMR (600 MHz, DMSO-d_6) δ 5.68 – 5.52 (m, 6H), 4.02 (t, 2H), 3.25 (d, 2H), 3.05 – 2.88 (m, 12H), 1.99 – 1.87 (m, 1H), 1.70 – 1.50 (m, 7H), 1.42 – 1.13 (m, 32H), 0.97 (d, 6H), 0.90 – 0.81 (m, 6H). ^{13}C NMR (151 MHz, DMSO-d_6) δ 221.53, 171.35, 157.97, 157.83, 157.82, 65.17, 55.89, 44.30, 41.93, 39.52, 30.27,

29.74, 29.73, 29.66, 28.46, 28.18, 27.61, 27.33, 27.31, 27.20, 26.05, 26.03, 25.71, 24.88, 24.78, 23.53, 22.16, 21.24, 13.50, 10.48. (some peaks overlap with DMSO).

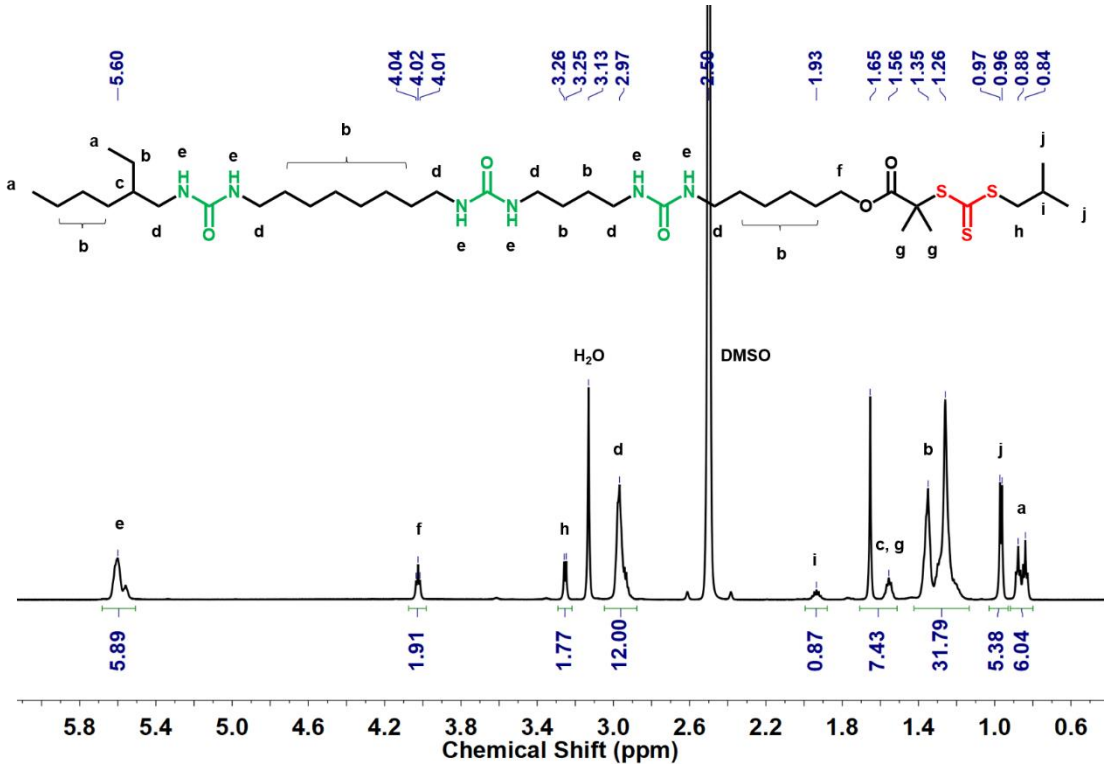

Figure 2.6.3.9. ^{1}H NMR of _8_4_CTA (in DMSO-d_6, 65°C).

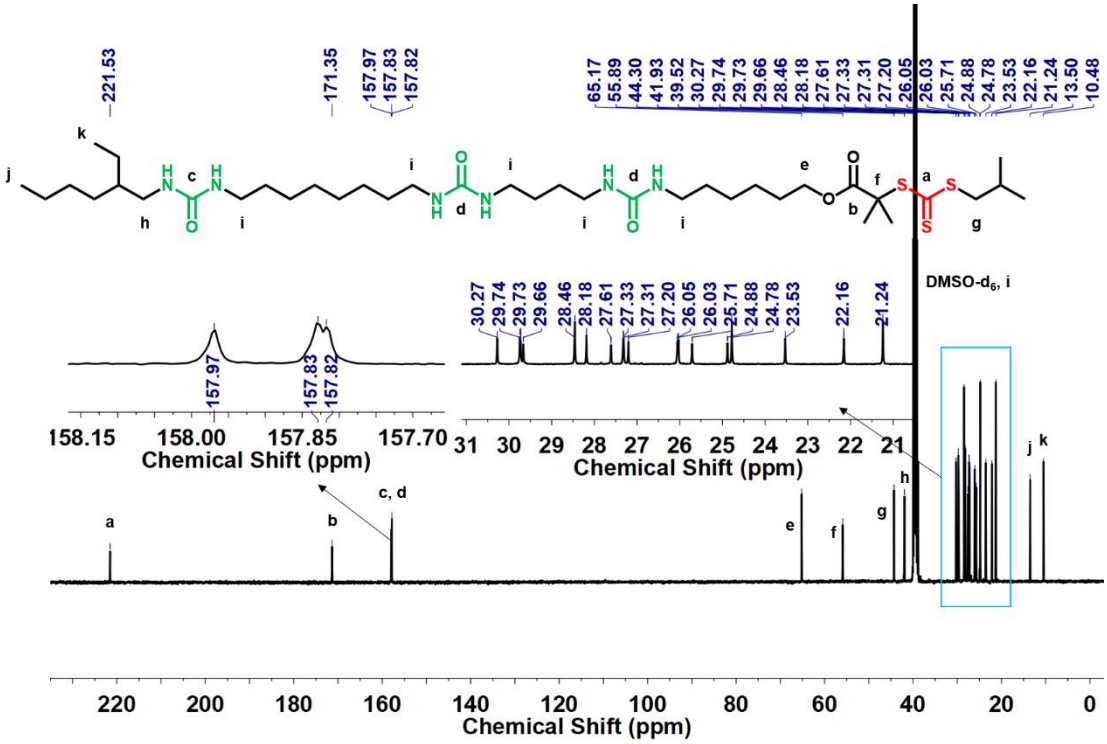

Figure 2.6.3.10. ^{13}C NMR of _8_4_CTA (in DMSO-d_6, 65°C).

Synthesis of intermediate 11. NH_3Cl-CTA (5.76 g, 14.9 mmol, 1 eq), triethylamine (1.8 g, 17.8 mmol, 1.2 eq), and a magnetic stirring bar were added into a 250 mL round-bottom flask. After the addition of DCM (100 mL), 4-nitrophenyl chloroformate (3.16 g, 15.6 mmol, 1.05 eq) dissolved in DCM (25 mL) was slowly dropped into the 250 mL round-bottom flask. The reaction was stirred overnight at 40 ℃ and the mixture was washed with Na_2CO_3 solution (50 mL) and then brine (50 mL × 2). The organic layer was dried by anhydrous sodium sulfate and the solvent was removed under reduced pressure. The yellow solid (2 g, 29%) was obtained by flash column chromatography on silica gel using DCM/PE (3/1) as an eluent. ^{1}H NMR (400 MHz, Chloroform-d) δ 8.23 (d, 2H), 7.31 (d, 2H), 5.19 (br, 1H), 4.09 (t, 2H), 3.34 – 3.23 (m, 2H), 3.19 (d, 2H), 2.02 – 1.87 (m, 1H), 1.78 – 1.51 (m, 10H), 1.39 (s, 4H), 0.99 (d, 6H). ^{13}C NMR (101 MHz, Chloroform-d) δ 221.84, 173.16, 156.12, 153.21, 144.81, 125.22, 122.05, 65.94, 56.18, 45.34, 41.38, 29.70, 28.33, 28.05, 26.35, 25.67, 25.50, 22.14.

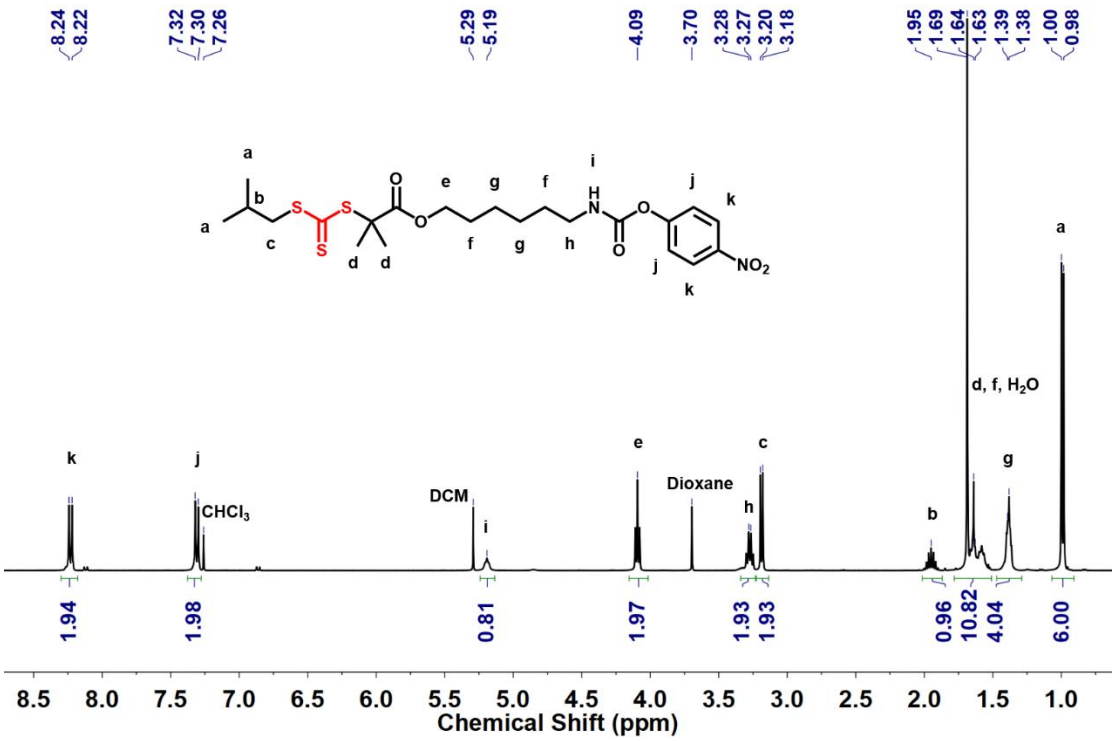

Figure 2.6.3.11. ^{1}H NMR of intermediate **11** (in $CDCl_3$).

Synthesis of intermediate 12. To a solution of intermediate **6** (0.794 g, 3.25 mmol, 1 eq) and triethylamine (0.395 g, 3.91 mmol, 1.2 eq) in anhydrous DCM (30 mL) was slowly added a DCM solution (20 mL) of intermediate **11** (1.68 g, 3.25 mmol, 1 eq). The reaction was stirred at room temperature for 65 h. Afterwards, the solution was washed by 0.1 M NaOH (50 mL), HCl (0.3 mL of concentrated HCl in 50 mL DI H_2O) and brine (50 mL). The organic layer was dried by anhydrous sodium sulfate and the solvent was removed under reduced pressure. The yellow solid (1.84 g, 91%) was obtained by a silica column using DCM/EA(0% - 50%) as an eluent. ^{1}H NMR (400 MHz, DMSO-d_6) δ 6.73 (br, 1H), 5.69 (t, 2H), 4.00 (t, 2H), 3.23 (d, 2H), 3.01 – 2.82 (m, 6H), 1.98 – 1.82 (m, 1H), 1.63 (s, 6H), 1.58 – 1.13 (m, 29H), 0.95 (d, 6H). ^{13}C NMR (101 MHz, DMSO-d_6) δ 221.68, 171.69, 170.26, 158.01, 155.52, 77.20, 65.43, 59.71, 55.97, 54.87, 44.34, 39.52, 30.04, 29.99, 29.45, 28.79, 28.73, 28.24, 27.87, 27.49, 26.34, 26.24, 26.00, 25.20, 24.95, 21.55, 20.72, 14.06 (some peaks overlap with DMSO).

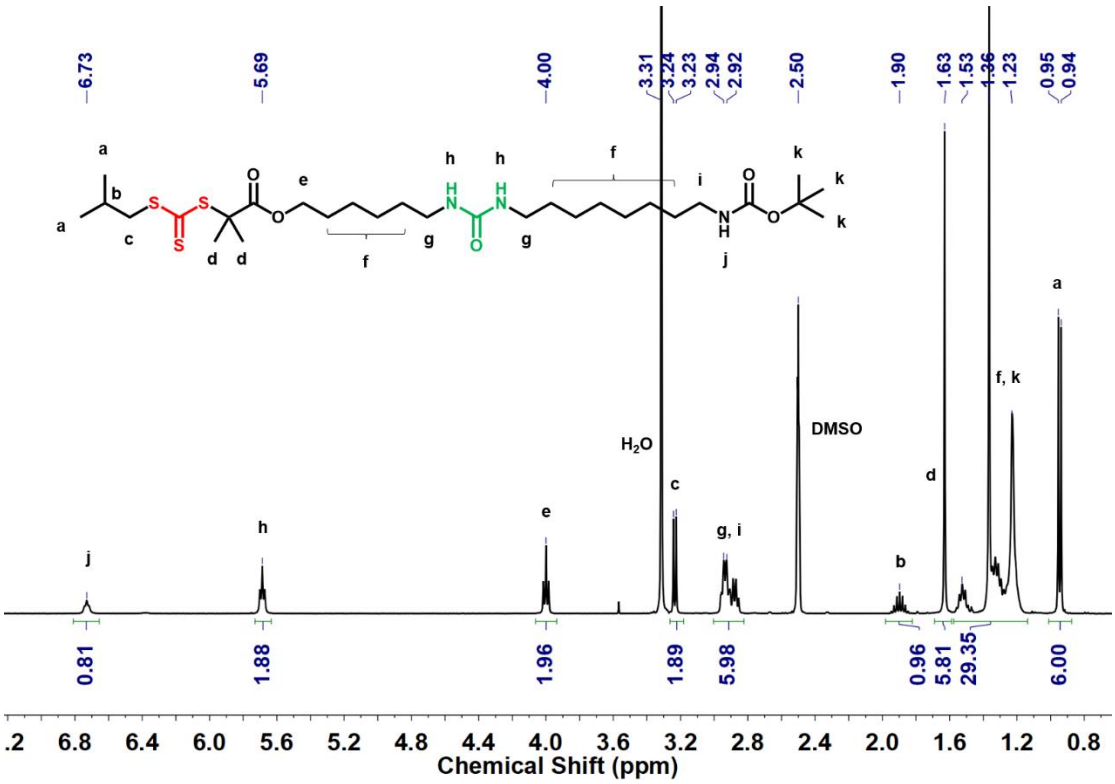

Figure 2.6.3.12. ^{1}H NMR of intermediate **12** (in DMSO-d_6).

Synthesis of intermediate 13. A magnetic stirring bar and intermediate **12** (1.65 g, 26.6 mmol, 1 eq) dissolved in dioxane (20 mL) were added into a 100 mL round-bottom flask cooled with an ice-water bath. Then 2 mL of 4 M HCl in dioxane was slowly added into the flask. After addition, the mixture was stirred at 35 ℃ overnight. A yellow solid (1.39 g, 94%) was obtained after evaporating the solvent. ^{1}H NMR (300 MHz, DMSO-d_6) δ 8.00 (s, 3H), 5.75 (br, 2H), 3.99 (t, 2H), 3.22 (d, 2H), 2.94 (q, 4H), 2.82 – 2.65 (m, 2H), 2.00 – 1.79 (m, 1H), 1.69 – 1.11 (m, 26H), 0.94 (d, 6H). ^{13}C NMR (75 MHz, DMSO-d_6) δ 221.73, 171.72, 158.15, 66.35, 65.46, 56.01, 44.36, 29.97, 28.53, 28.47, 27.87, 27.51, 26.88, 26.23, 26.00, 25.77, 25.20, 24.97, 21.58 (some peaks overlap with DMSO).

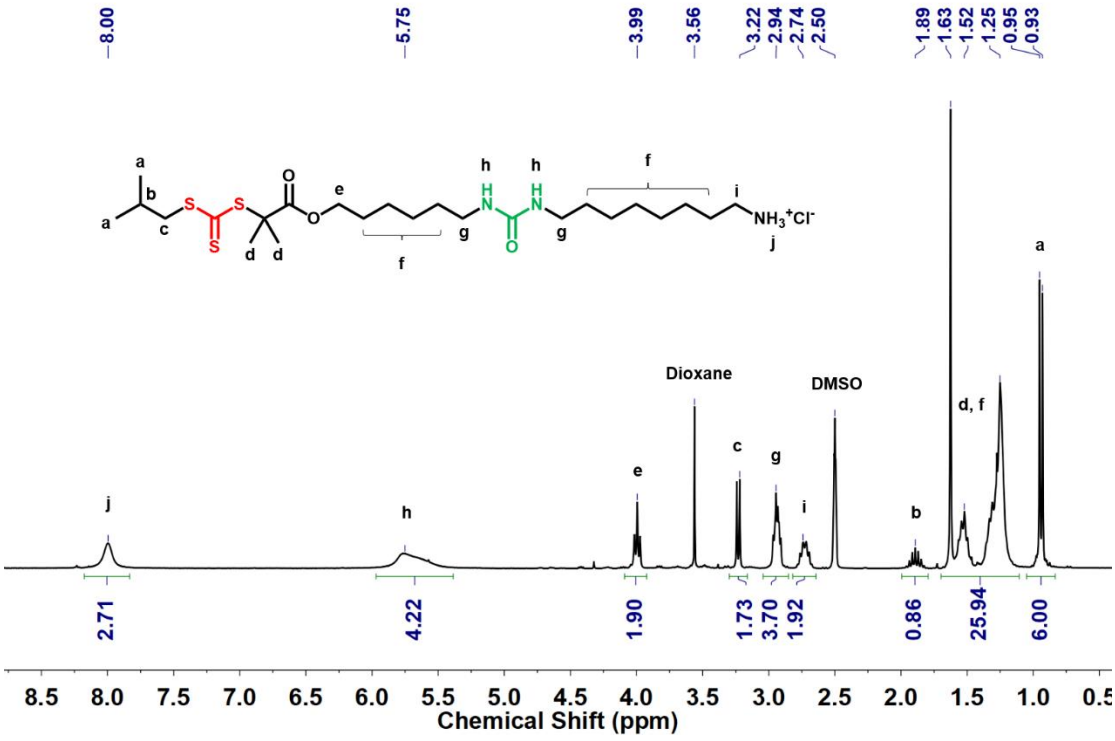

Figure 2.6.3.13. ^{1}H NMR of intermediate **13** (in DMSO-d_6).

Synthesis of intermediate 14. 1,4-diaminobutane (30 g, 341 mmol, 5 eq) and a magnetic stirring bar were added into a 1 L round-bottom flask. After the addition of chloroform (500 mL), di-tert-butyl dicarbonate (14.86 g, 68.2 mmol, 1.00 eq) was dissolved in chloroform (40 mL) and then slowly dropped into the 1 L round-bottom

flask. The reaction was stirred at room temperature for 41 h, filtered, and the solution was collected and dried by anhydrous sodium sulfate. The white waxy product (7.06 g, 55%) was obtained by flash column chromatography on silica gel using $CHCl_3$/MeOH (100/5-60/40) as an eluent. ^{1}H NMR (400 MHz, Chloroform-d) δ 4.79 (br, 1H), 3.07 (q, 2H), 2.66 (t, 2H), 1.51 – 1.27 (m, 15H). ^{13}C NMR (101 MHz, $CDCl_3$) δ 156.08, 79.00, 41.82, 40.46, 30.86, 28.48, 27.53.

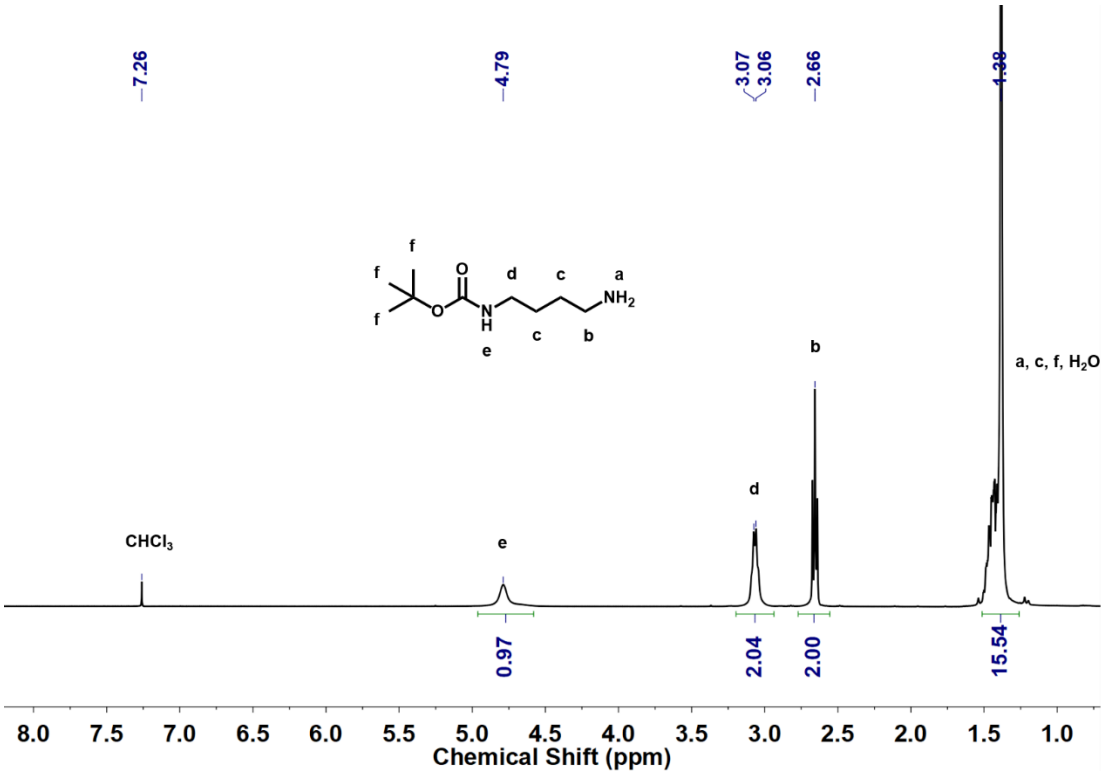

Figure 2.6.3.14. ^{1}H NMR of intermediate **14** (in $CDCl_3$).

Synthesis of intermediate 15. To a solution of intermediate **14** (4.11 g, 21.9 mmol, 1.05 eq) and triethylamine (2.21 g, 21.9 mmol, 1.05 eq) in anhydrous DCM (100 mL) was slowly added a DCM solution (20 mL) of 2-ethylhexyl isocyanate (3.23 g, 20.8 mmol, 1.00 eq). The reaction was performed at room temperature overnight. The solution was washed with 1 M HCl (30 mL), DI water (50 mL × 2) and brine (50 mL). Afterwards, the solution was dried by anhydrous Na_2SO_4 and then the solvent was evaporated giving a colorless viscous solid (6.84 g, 91%). ^{1}H NMR (400 MHz, DMSO-d_6) δ 6.77 (s, 1H), 5.69 (d, 2H), 2.92 (q, 6H), 1.46 – 1.00 (m, 22H), 0.92 – 0.74 (m, 6H).

^{13}C NMR (101 MHz, DMSO-d$_6$) δ 158.16, 155.54, 77.26, 41.85, 30.42, 28.41, 28.25, 27.51, 27.04, 23.62, 22.52, 13.95, 10.77.

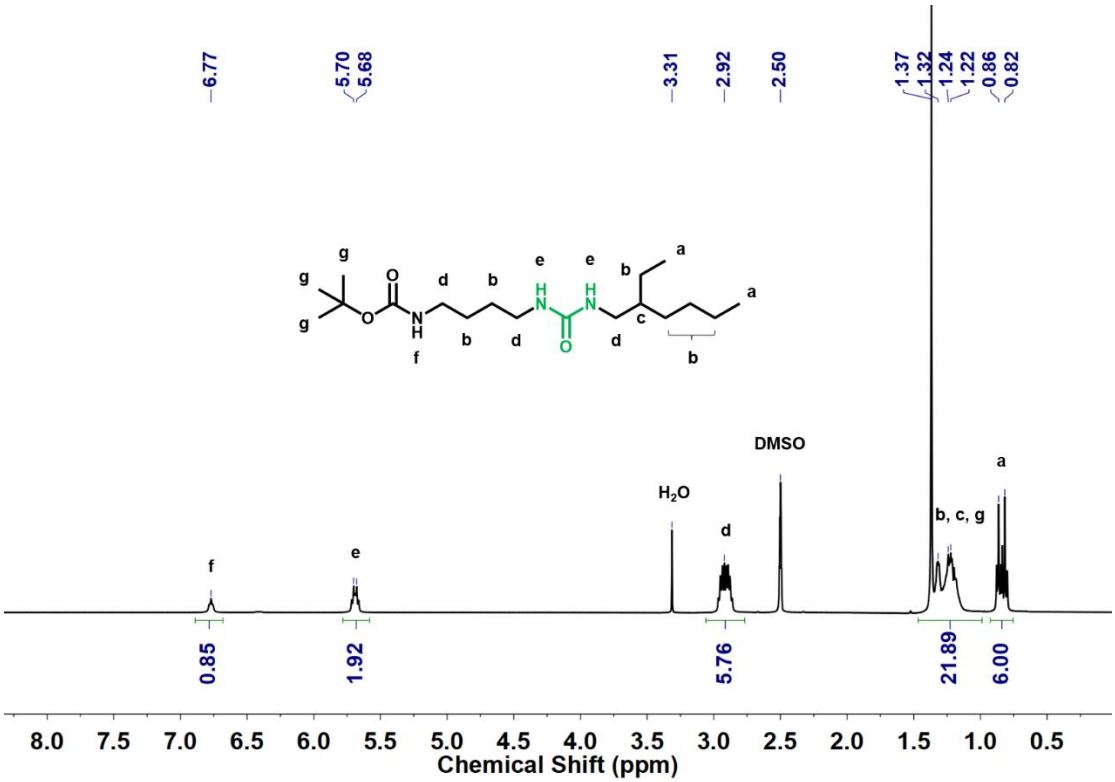

Figure 2.6.3.15. ^{1}H NMR of intermediate **15** (in DMSO-d$_6$).

Synthesis of intermediate 16. A magnetic stirring bar and intermediate **15** (6.07 g, 17.7 mmol, 1 eq) dissolved in dioxane (60 mL) were added into a 100 mL round-bottom flask cooled with an ice-water bath. Then 13.3 mL of 4 M HCl (3 eq) in dioxane was slowly added into the flask. The mixture was stirred at 50 ℃ overnight. A yellow gel (4.93 g, 100%) was obtained after evaporating the solvent. ^{1}H NMR (400 MHz, DMSO-d$_6$) δ 8.02 (br, 3H), 4.76 (br, 2H), 3.12 – 2.85 (m, 4H), 2.82 – 2.63 (m, 2H), 1.62 – 1.48 (m, 2H), 1.47 – 1.34 (m, 2H), 1.33 – 1.11 (m, 9H), 0.95 – 0.70 (m, 6H). ^{13}C NMR (101 MHz, DMSO-d$_6$) δ 158.41, 66.36, 41.96, 39.41, 38.62, 38.50, 30.41, 28.42, 27.11, 24.42, 23.61, 22.54, 14.00, 10.79.

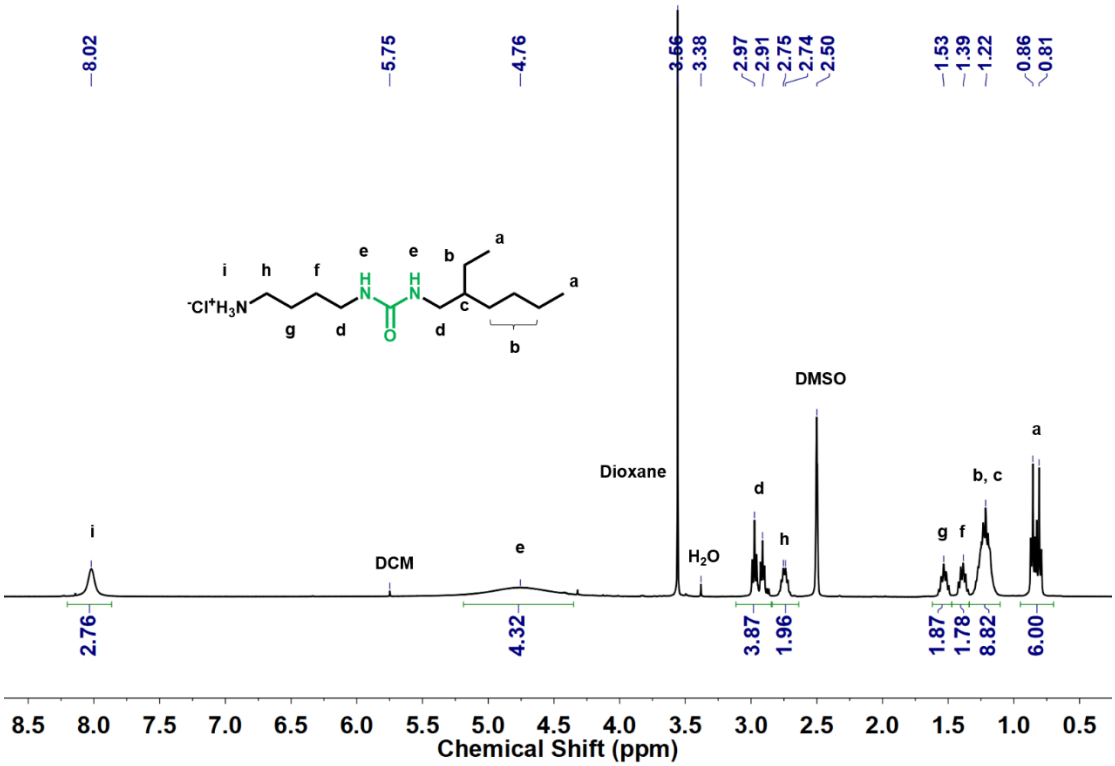

Figure 2.6.3.16. ^{1}H NMR of intermediate **16** (in DMSO-d_6).

Synthesis of intermediate 17. Intermediate **16** (2.93 g, 10.5 mmol, 1 eq), triethylamine (2.65 g, 26.2 mmol, 2.5 eq), and a magnetic stirring bar were added into a 250 mL round-bottom flask. After the addition of DCM (100 mL), 4-nitrophenyl chloroformate (2.33 g, 11.5 mmol, 1.1 eq) dissolved in DCM (30 mL) was slowly dropped into the 250 mL round-bottom flask cooled with an ice-water bath. The reaction was stirred at room temperature for 2 hours, and then the mixture was washed with diluted HCl solution (50 mL, 3 eq) and then brine (50 mL). The organic layer was dried by anhydrous sodium sulfate and the solvent was removed under reduced pressure. The yellow gel (0.99 g, 23%) was obtained by flash column chromatography on silica gel using DCM/EA (0% - 50%) as an eluent. ^{1}H NMR (400 MHz, DMSO-d_6) δ 8.25 (d, 2H), 8.04 (t, 1H), 7.39 (d, 2H), 5.87 – 5.61 (m, 2H), 3.24 – 2.83 (m, 6H), 1.60 – 1.06 (m, 13H), 0.96 – 0.71 (m, 6H). ^{13}C NMR (101 MHz, DMSO-d_6) δ 158.21, 156.29, 153.06, 144.04, 125.12, 122.37, 41.87, 40.36, 39.43, 30.41, 28.41, 27.47, 26.57, 23.62, 22.52, 13.95, 10.77.

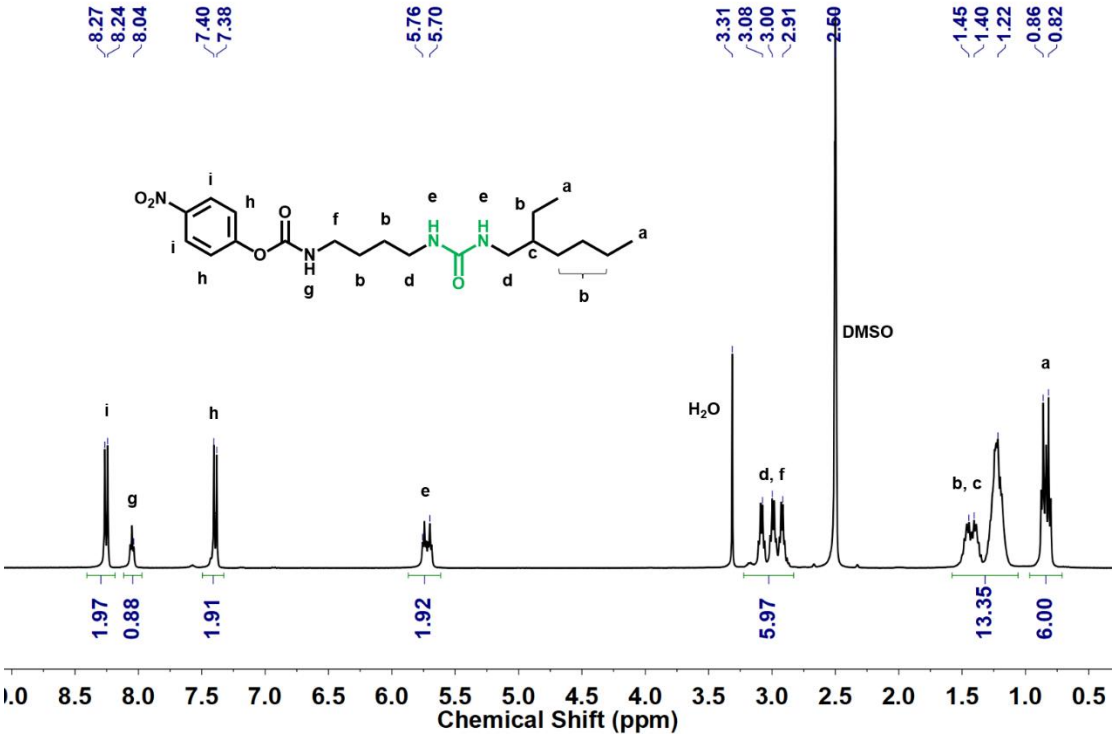

Figure 2.6.3.17. ^{1}H NMR of intermediate **17** (in DMSO-d_6).

Synthesis of _4_8_CTA (18). To a solution of intermediate **13** (1.29 g, 2.32 mmol, 1 eq), triethylamine (0.281 g, 2.78 mmol, 1.2 eq) in anhydrous DCM (50 mL) was slowly added an anhydrous DCM solution (20 mL) of intermediate **17** (0.945 g, 2.32 mmol, 1 eq). The reaction was performed at room temperature for 16 hours. Afterwards, the solution was concentrated to gel and then 80 mL of acetone was poured into the flask. A yellow solid precipitated and then was washed with 150 mL DI water, 10 mL THF, and 150 mL of acetone in a fritted funnel. The yellow solid (1.31 g, 72%) was dried at 40 °C under vacuum. ^{1}H NMR (600 MHz, DMSO-d_6) δ 5.78 – 5.51 (m, 6H), 4.02 (t, 2H), 3.26 (d, 2H), 3.07 – 2.85 (m, 12H), 1.97 – 1.89 (m, 1H), 1.71 – 1.50 (m, 7H), 1.45 – 1.14 (m, 32H), 0.97 (d, 6H), 0.90 – 0.78 (m, 6H). ^{13}C NMR (151 MHz, DMSO-d_6) δ 221.53, 171.33, 157.96, 157.82, 157.81, 65.16, 55.89, 44.30, 41.95, 30.27, 29.71, 29.65, 28.44, 28.17, 27.60, 27.31, 27.30, 27.19, 26.04, 25.68, 24.87, 24.78, 23.52, 22.14, 21.23, 13.49, 10.46 (some peaks overlap with DMSO).

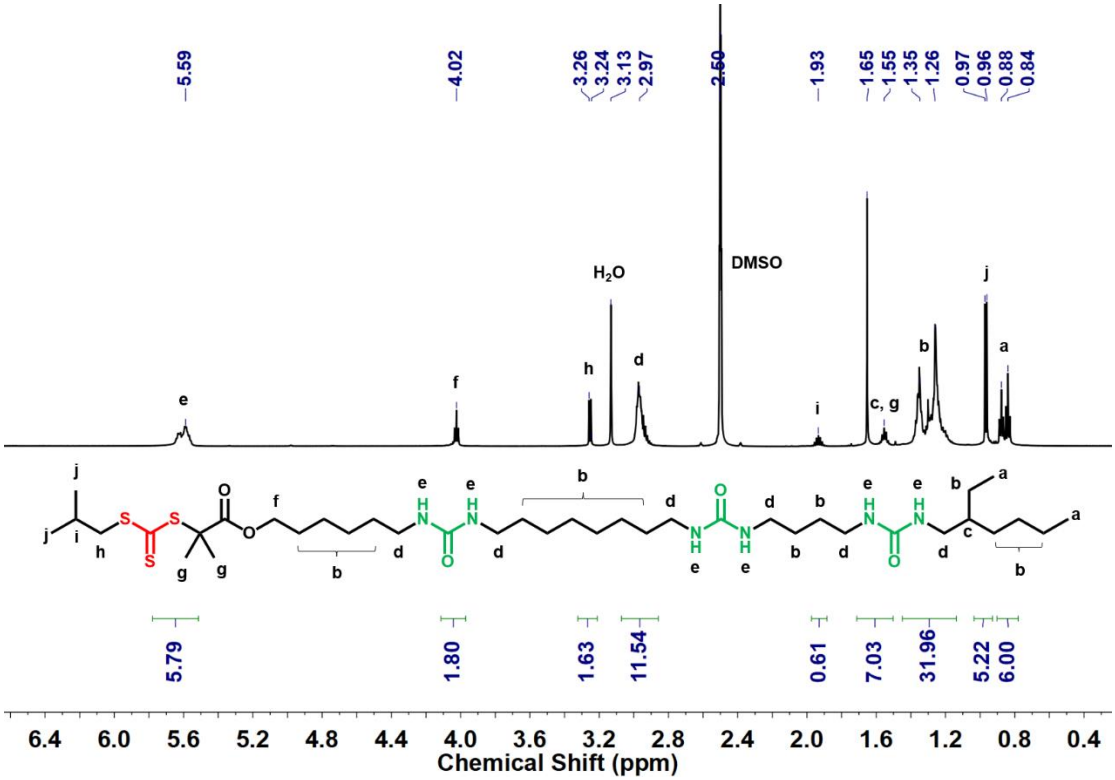

Figure 2.6.3.18. ^{1}H NMR of _4_8_CTA (in DMSO-d_6, 65°C).

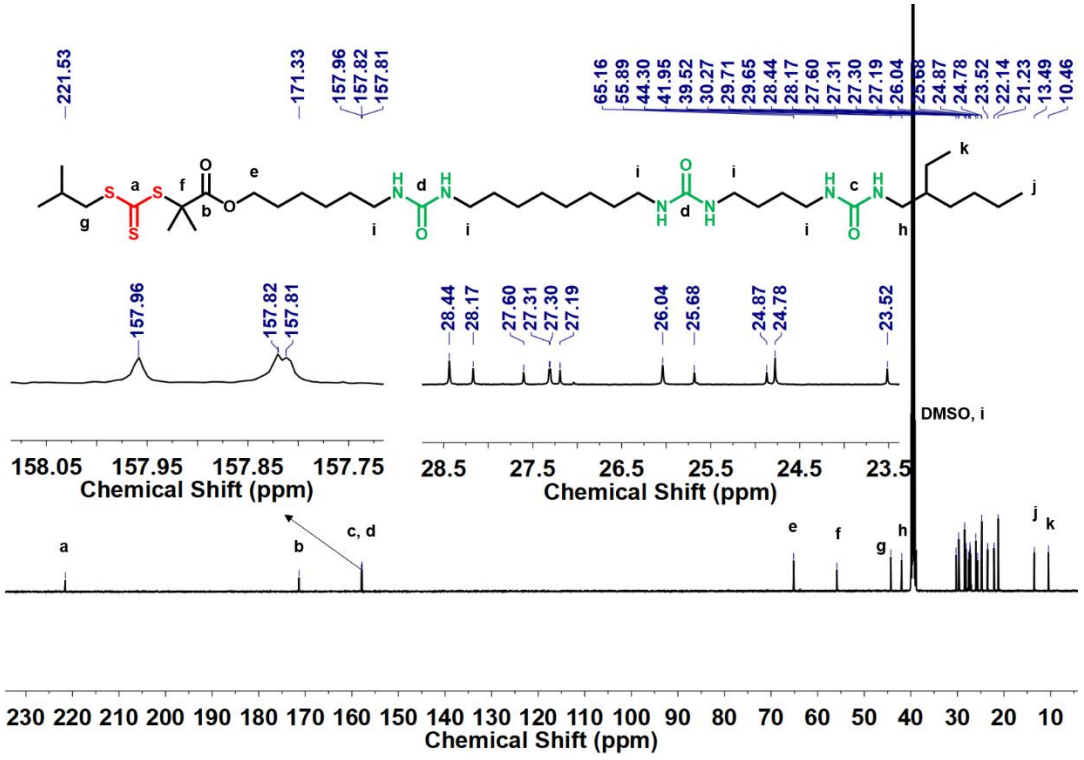

Figure 2.6.3.19. ^{13}C NMR of _4_8_CTA (in DMSO-d_6, 65°C).

2.6.4 Synthesis of monomers

Synthesis of 4-trimethylsilyl styrene (TMSS). Synthesis was adapted from Langel et al[30].A 100 mL Schlenk tube containing 4-bromostyrene (2.28 g, 12.5 mmol), chlorotrimethylsilane (1.35 g, 12.5 mmol), magnesium turning (0.6 g, 25 mmol), 20 mL of anhydrous THF, and a magnetic stirring bar was plunged into an ultrasonic bath after 3 cycles of freeze-pump-thaw process. After 3 hours, the cap was open. The mixture was washed by 20 mL saturated sodium chloride (aq) and then extracted by diethyl ether (3 × 30 mL). The organic layers were combined and dried by anhydrous Na_2SO_4. The colorless oil (1.5 g, 68%) was obtained after flash column chromatography by using hexane.^{1}H NMR (400 MHz, Chloroform-*d*) δ 7.50 (d, 2H), 7.41 (d, 2H), 6.73 (dd, 10.9 Hz, 1H), 5.79 (d, 1H), 5.26 (d, 1H), 0.28 (s, 9H). ^{13}C NMR (101 MHz, $CDCl_3$) δ 140.29, 138.11, 137.03, 133.70, 125.66, 114.22, -0.98.

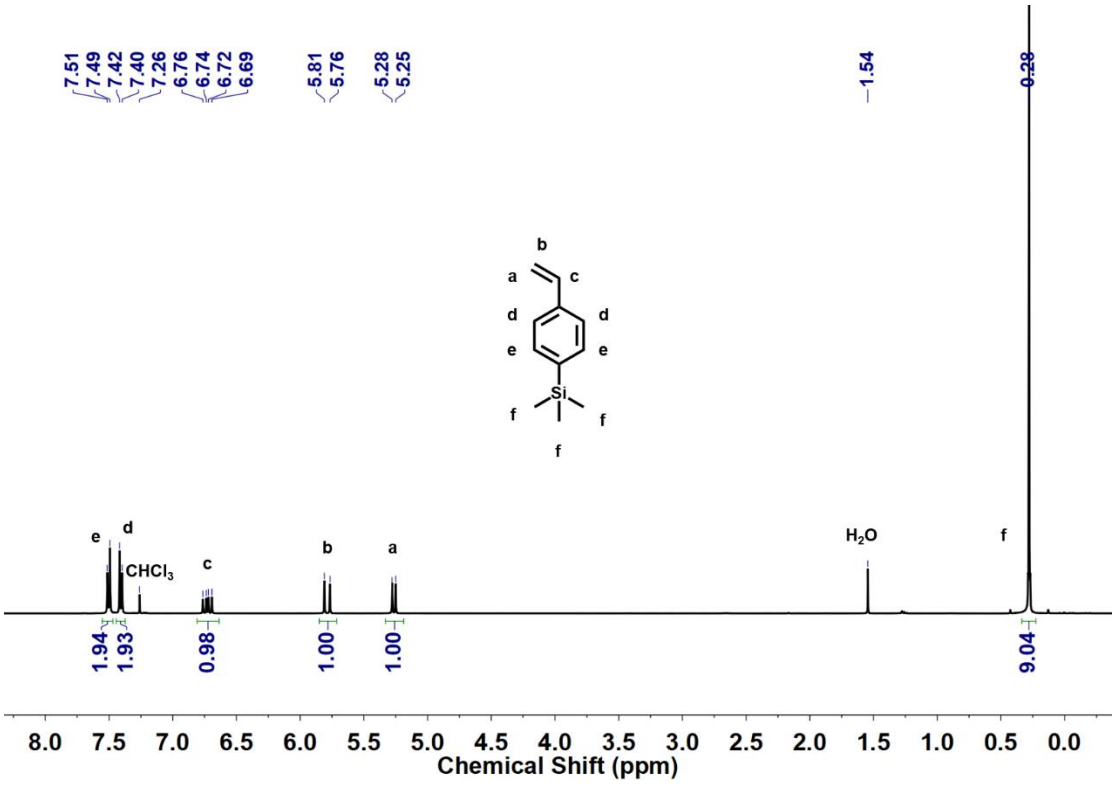

Figure 2.6.4.1 ^{1}H NMR of 4-trimethylsilyl styrene (in $CDCl_3$).

Synthesis of hydroxymethylferrocene (Fc-OH). Synthesis was adapted from Hardy et al[25]. A magnetic stirring bar and ferrocenecarboxaldehyde (10.1 g, 47.19 mol,

1eq) dissolved in methanol (300 mL) were added into a 500 mL round-bottom flask cooled with an ice-water bath. Sodium borohydride (4.52 g, 119.48 mmol, 2.5 eq) was slowly added portionwise over 2 hours to the flask. The reaction was stirred overnight before adding 250 mL of ammonium chloride (0.5 M). The solution was stirred for another 30 minutes. The solution was extracted with DCM (3 × 200 mL), then the organic layers were combined and dried by anhydrous Na_2SO_4. The yellow solid (8.9 g, 87%) was obtained after flash column chromatography using hexane/EA (20% - 30%). ^{1}H NMR (400 MHz, Chloroform-*d*) δ 4.33 (d, 2H), 4.28 – 4.10 (m, 9H), 1.55 (t, 1H). ^{13}C NMR (101 MHz, $CDCl_3$) δ 88.60, 68.44, 68.41, 68.00, 60.91.

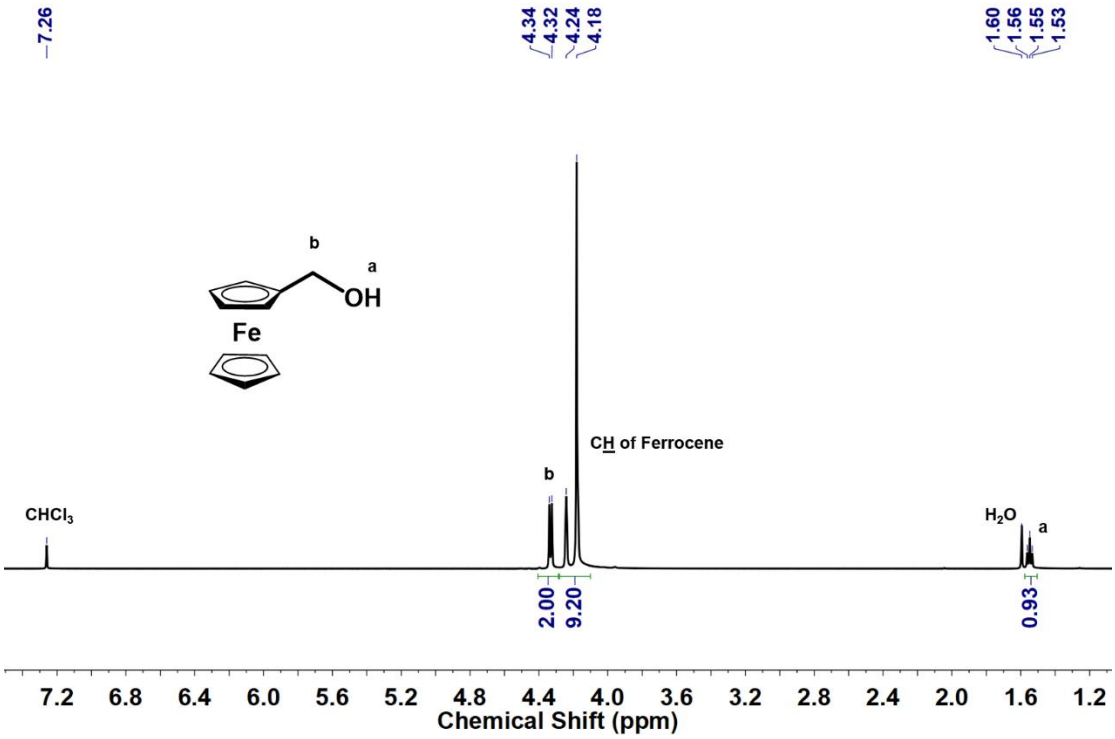

Figure 2.6.4.2.^{1}H NMR of hydroxymethylferrocene (in $CDCl_3$).

Synthesis of ferrocenemethyl acrylate (FMA). Synthesis was adapted from Hardy et al[25]. To a solution of Fc-OH (5 g, 23.1 mmol, 1 eq) and triethylamine (28 g, 277 mmol, 12 eq) in anhydrous DCM (100 mL) cooled with an ice-water bath was slowly added an anhydrous DCM solution (50 mL) of acryloyl chloride (6.25 g, 69.4 mmol, 3 eq). The reaction was stirred for 24 hours before washing with 50 mL of brine.

The yellow solid (1.78 g, 28%) was obtained after flash column chromatography using hexane/EA (3%). ^{1}H NMR (400 MHz, Chloroform-*d*) δ 6.41 (d, 1H), 6.11 (dd, 10.4 Hz, 1H), 5.81 (d, 1H), 4.98 (s, 2H), 4.29 (s, 2H), 4.21 – 4.15 (m, 7H). ^{13}C NMR (101 MHz, $CDCl_3$) δ 166.17, 130.90, 128.63, 81.43, 69.73, 68.95, 68.72, 63.05.

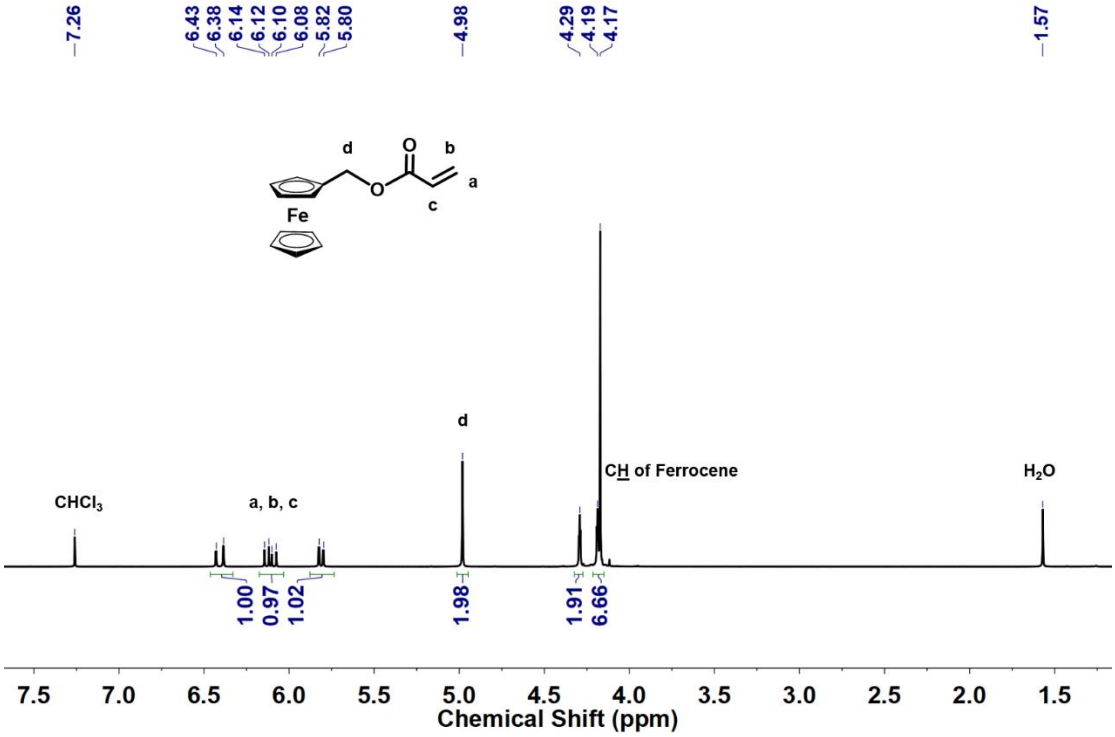

Figure 2.6.4.3. ^{1}H NMR of ferrocenemethyl acrylate (in $CDCl_3$).

2.6.5 Synthesis of _8_4_and _4_8_polymers

Polymerization of *N,N*-dimethylacrylamide using _8_4_CTA (DP_n = 137). A 100 mL round-bottom flask equipped with a magnetic stirring bar was charged with *N,N*-dimethylacrylamide (700 mg, 7.07 mmol, 172 eq), _8_4_CTA-B6 (32 mg, 0.041 mmol, 1 eq), DMSO (34 mL) and toluene (0.075 mL, 0.707 mmol, 17.2 eq). Then, the solution was bubbled with N_2 at 65 °C for 1 hour and afterwards AIBN (0.674 mg in 1 mL DMSO, 0.0042 mmol, 0.1 eq) in a 1 mL syringe was injected into the flask under the protection of N_2. The solution was bubbled with N_2 for another 10 minutes. After 380 minutes, the flask was plunged into an ice-water bath and the cap was opened after several minutes. 66% for the final conversion was determined by ^{1}H NMR (relative

integration of the internal reference peak at 7.15 ppm and CH_2=CH peak at 5.6 ppm). The polymer solution was performed by dialysis with 1 kDa membrane and a further freeze-drying step to give a light yellow powder (0.31 g, 60%). SEC: M_n = 13.6 kg/mol, $Đ$: 1.12. ^{1}H NMR (400 MHz, DMSO-d_6) δ 5.81 – 5.65 (m, 6H), 5.16 – 5.04 (m, 1H), 3.94 (t, 2H), 3.24 – 2.65 (m, 811H), 2.00 – 1.90 (m, 1H), 1.87 – 0.92 (m, 319H), 0.90 – 0.75 (m, 6H).

_4_8_PDMAc$_{150}$ was synthesized similarly to _8_4_PDMAc$_{137}$. M_n: 14.9 kg/mol, $Đ$: 1.17. ^{1}H NMR (400 MHz, DMSO-d_6) δ 5.78 – 5.64 (m, 6H), 5.18 – 5.00 (m, 1H), 3.95 (t, 2H), 3.23 – 2.64 (m, 888H), 2.01 – 1.89 (m, 1H), 1.79 – 0.93 (m, 345H), 0.89 – 0.75 (m, 6H).

_4_8_PDMAc$_{80}$ was synthesized similarly to _8_4_PDMAc$_{137}$. M_n: 9.7 kg/mol, $Đ$: 1.09. ^{1}H NMR (400 MHz, DMSO-d_6) δ 5.78 – 5.66 (m, 6H), 5.15 – 5.02 (m, 1H), 3.93 (t, 2H), 3.22 – 2.65 (m, 489H), 2.02 – 1.89 (m, 1H), 1.82 – 0.93 (m, 205H), 0.90 – 0.71 (m, 6H).

_4_8_PDMAc$_{67}$ was synthesized similarly to _8_4_PDMAc$_{137}$. M_n: 7.6 kg/mol, $Đ$: 1.09. ^{1}H NMR (400 MHz, DMSO-d_6) δ 5.79 – 5.65 (m, 6H), 5.17 – 5.00 (m, 1H), 3.94 (t, 2H), 3.21 – 2.64 (m, 414H), 2.00 – 1.88 (m, 1H), 1.81 – 0.92 (m, 179H), 0.88 – 0.76 (m, 6H).

_8_4_PNAM$_{60}$ was synthesized similarly to _8_4_PDMAc$_{137}$. M_n: 8.0 kg/mol, $Đ$: 1.17. ^{1}H NMR (300 MHz, DMSO-d_6) δ 5.78 – 5.62 (m, 6H), 4.08 – 3.02 (m, 695H), 3.02 – 2.83 (m, 12H), 2.05 – 1.00 (m, 159H), 0.99 – 0.91 (m, 6H), 0.91 – 0.75 (m, 6H).

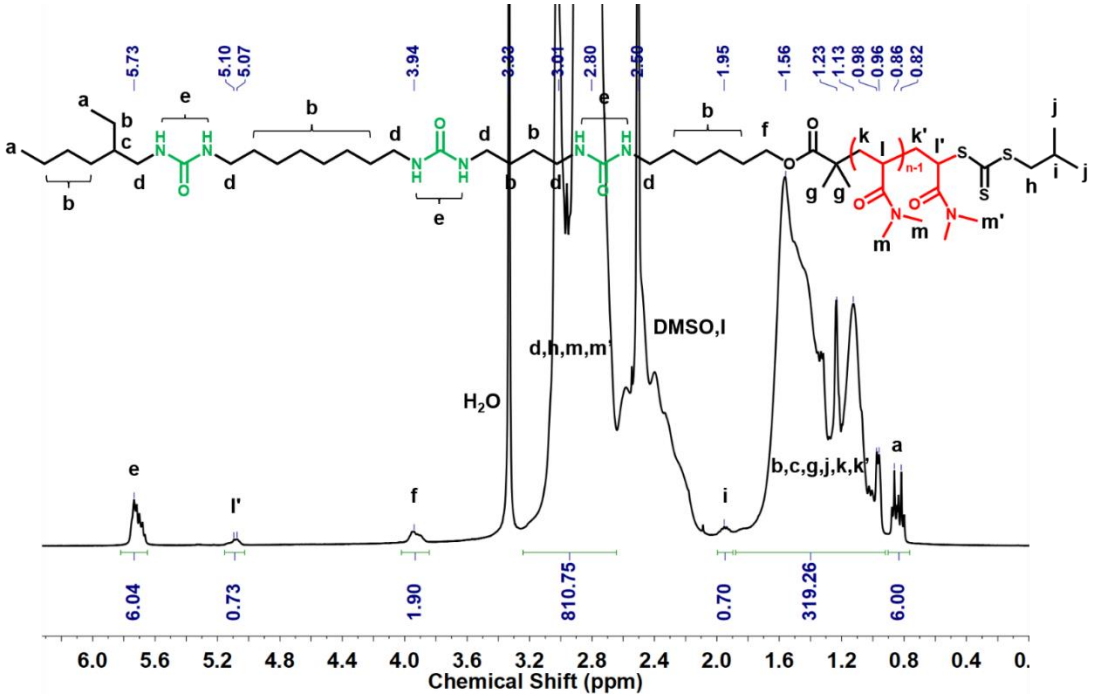

Figure 2.6.5.1. ^{1}H NMR of _8_4_PDMAc$_{137}$ (in DMSO-d$_6$).

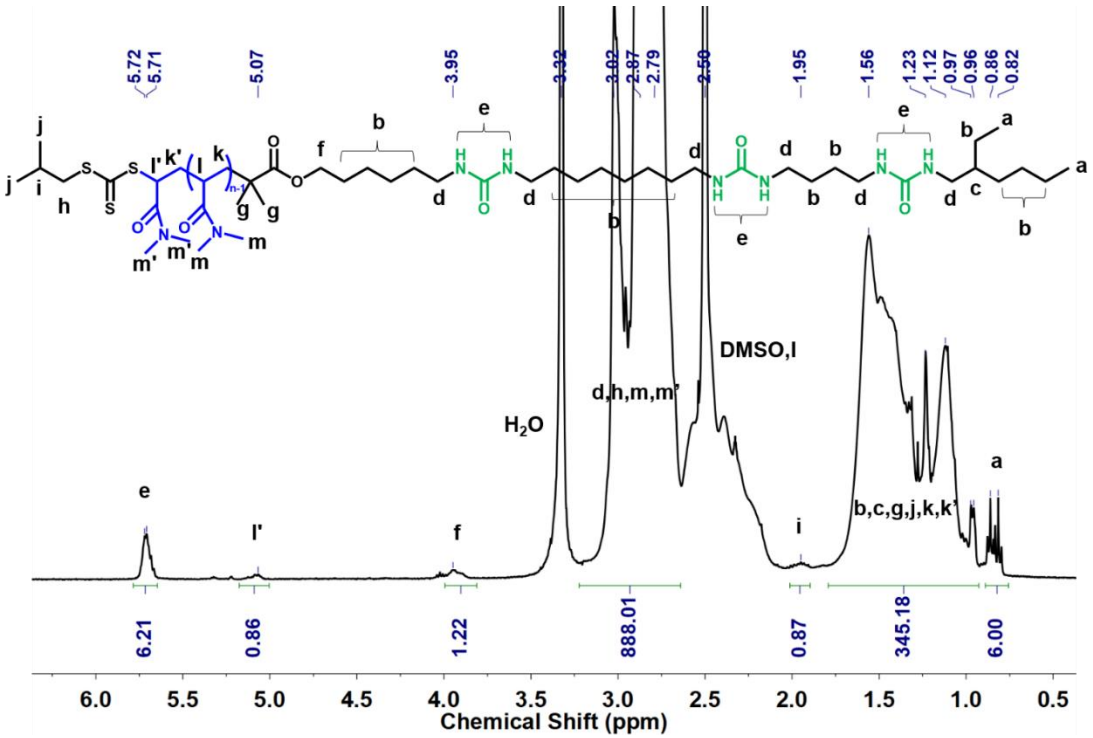

Figure 2.6.5.2. ^{1}H NMR of _4_8_PDMAc$_{150}$ (in DMSO-d$_6$).

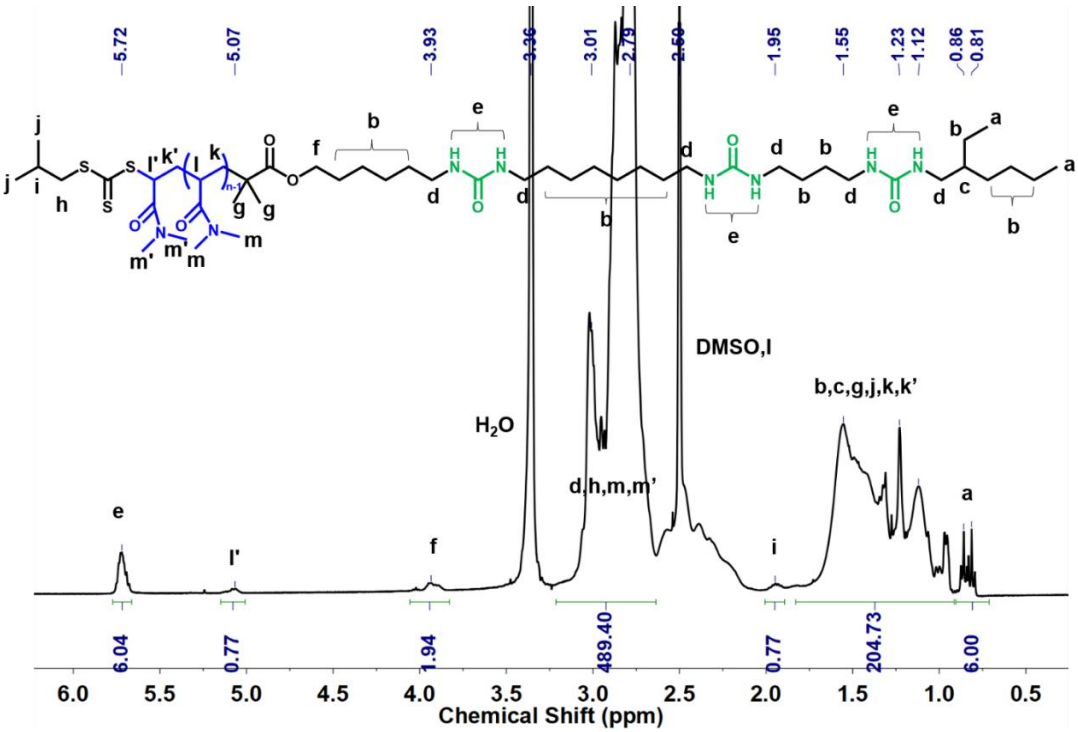

Figure 2.6.5.3. ^{1}H NMR of _4_8_PDMAc$_{80}$ (in DMSO-d$_6$).

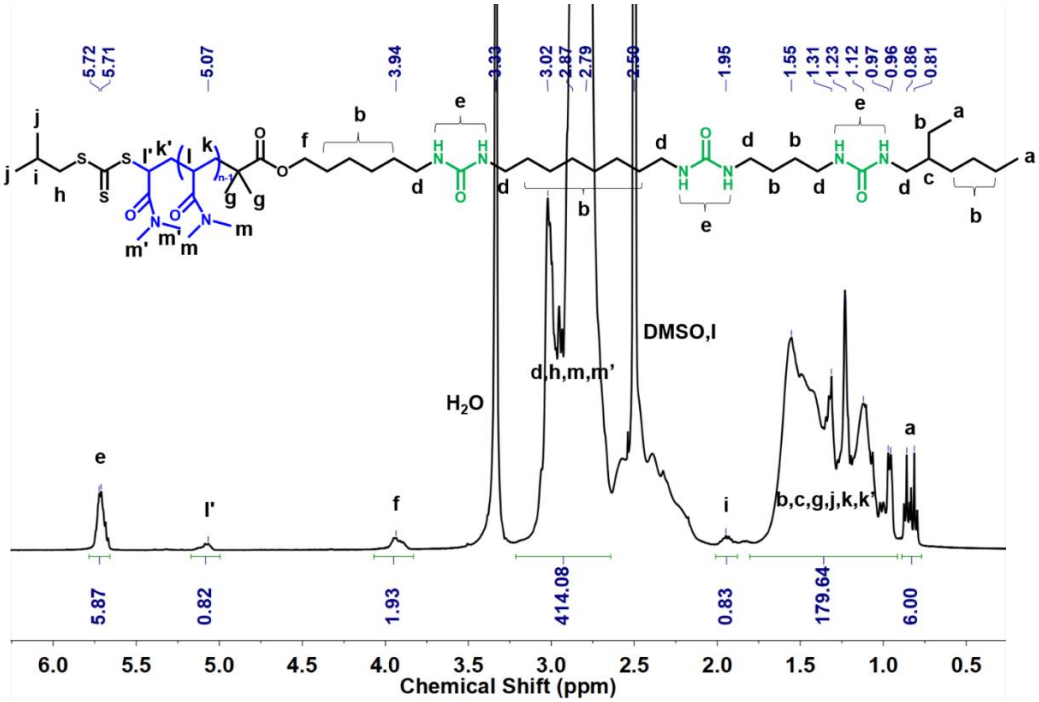

Figure 2.6.5.4. ^{1}H NMR of _4_8_PDMAc$_{67}$ (in DMSO-d$_6$).

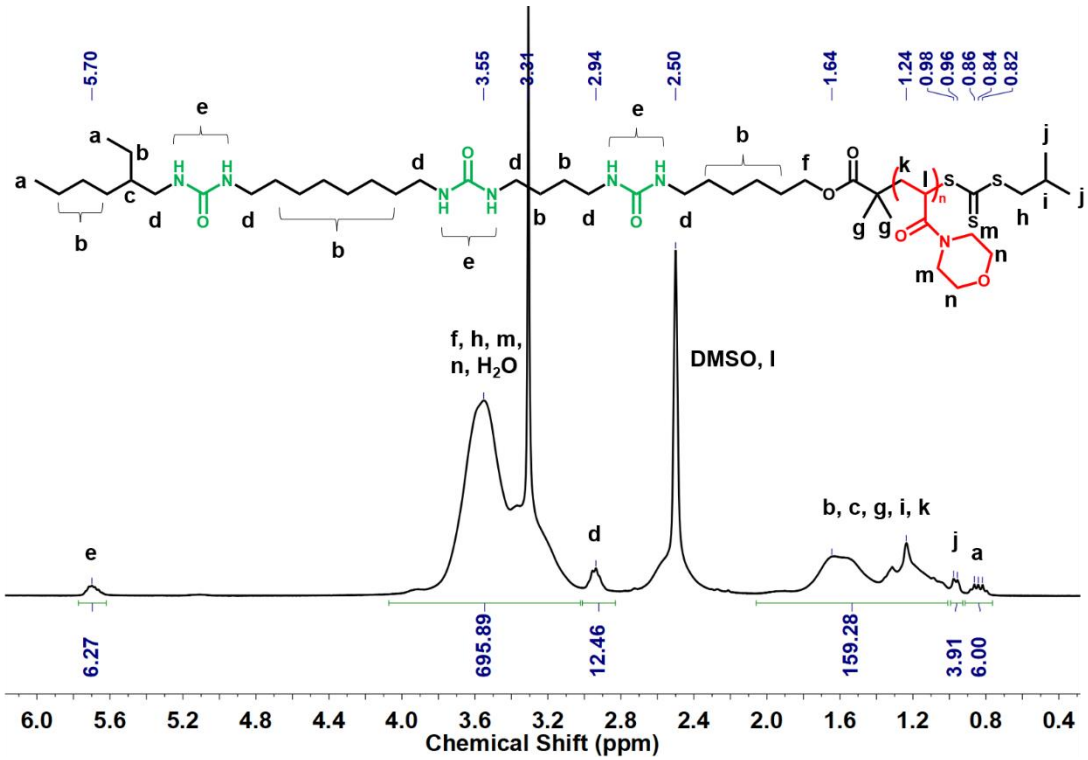

Figure 2.6.5.5. ^{1}H NMR of _8_4_PNAM$_{60}$ (in DMSO-d$_6$).

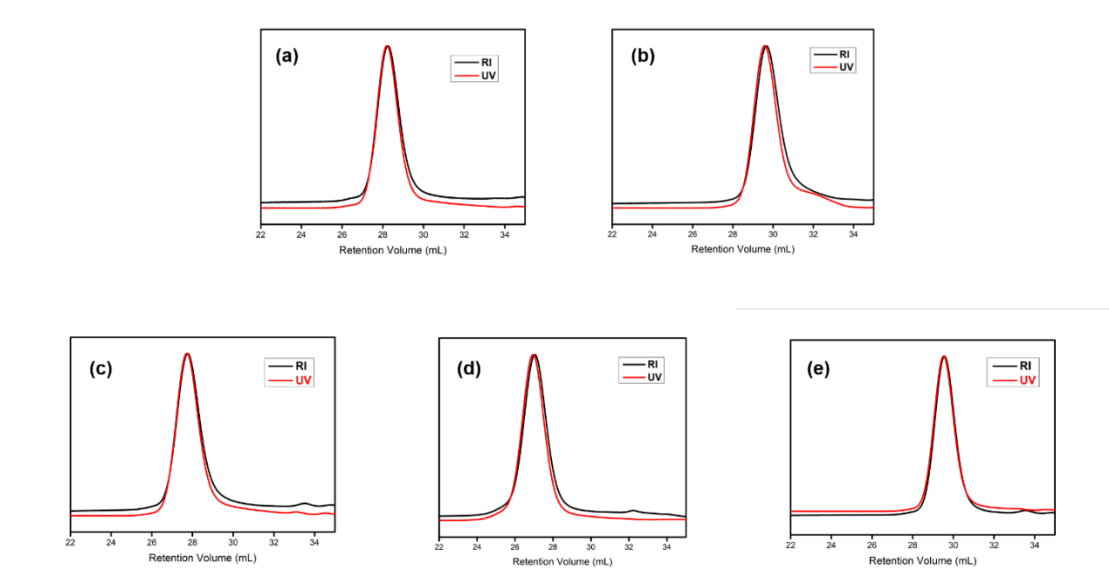

Figure 2.6.5.6. SEC figures of _8_4_PDMAc$_{137}$ (a), _8_4_PNAM$_{60}$ (b), _4_8_PDMAc$_{150}$ (c), _4_8_PDMAc$_{80}$ (d) and _4_8_PDMc$_{67}$ (e) (in DMF).

Polymerization of *n*-butyl acrylate using _8_4_CTA (DP_n = 41). A 100 mL round-bottom flask equipped with a magnetic stirring bar was charged with *n*-butyl acrylate (700 mg, 5.47 mmol, 86 eq), _8_4_CTA-B4 (50.2 mg, 0.064 mmol, 1 eq), 1, 3, 5-trioxane (internal standard, 27.5 mg, 0.307 mmol, 4.8 eq) and DMSO (7 mL). Then, the solution was bubbled with N_2 at 70 ℃ for 1 hour and afterwards AIBN (1.04 mg in 1 mL DMSO, 0.0064 mmol, 0.1 eq) in 1 mL syringe was injected into the flask under the protection of N_2. The solution was bubbled with N_2 for another 10 minutes. After 480 minutes, the flask was plunged into an ice-water bath and the cap was opened after several minutes. 65% for the final conversion was determined by ^{1}H NMR. 80 mL cold MeOH/H_2O (v/v = 1/1) was poured into the flask and then the precipitate was filtered. The solid was washed by 40 mL cold MeOH/H_2O (v/v = 1/1) and then dried at 70 ℃ under vacuum overnight to give a light yellow powder (0.195 g, 39%). M_n: 6.0 kg/mol, $Đ$: 1.31. ^{1}H NMR (400 MHz, $V_{DMSO\text{-}d6}/V_{CDCl3}$ = 1/1) δ 5.72 – 5.46 (m, 6H), 4.79 – 4.62 (m, 1H), 4.22 – 3.70 (m, 84H), 3.09 – 2.84 (m, 12H), 2.40 – 2.01 (m, 30H), 1.99 – 1.13 (m, 266H), 1.11 – 0.66 (m, 139H).

_8_4_P*t*BA$_{32}$, _4_8_P*t*BA$_{62}$, and _4_8_P*t*BA$_{48}$ were synthesized similarly to _8_4_P*n*BA$_{41}$.

_8_4_P*t*BA$_{32}$ (M_n: 4.9 kg/mol, $Đ$: 1.15). ^{1}H NMR (400 MHz, $V_{DMSO\text{-}d6}/V_{CDCl3}$ = 1/1) δ 5.69 – 5.48 (m, 6H), 4.66 – 4.50 (m, 1H), 3.93 (t, 2H), 3.09 – 2.87 (m, 12H), 2.42 – 2.00 (m, 29H), 1.98 – 1.01 (m, 391H), 0.96 (d, J = 6.7 Hz, 6H), 0.88 – 0.75 (m, 6H).

_4_8_P*t*BA$_{62}$ (M_n: 8.7 kg/mol, $Đ$: 1.13). ^{1}H NMR (400 MHz, $V_{DMSO\text{-}d6}/V_{CDCl3}$ = 1/1) δ 5.73 – 5.55 (m, 6H), 4.69 – 4.53 (m, 1H), 3.94 (t, 2H), 3.07 – 2.87 (m, 12H), 2.41 – 2.00 (m, 56H), 1.99 – 1.01 (m, 720H), 0.96 (d, J = 6.7 Hz, 6H), 0.91 – 0.75 (m, 6H).

_4_8_P*t*BA$_{48}$ (M_n: 6.9 kg/mol, $Đ$: 1.11). ^{1}H NMR (400 MHz, $V_{DMSO\text{-}d6}/V_{CDCl3}$ = 1/1) δ 5.72 – 5.54 (m, 6H), 4.65 – 4.50 (m, 1H), 3.93 (t, 2H), 3.08 – 2.81 (m, 12H), 2.38 – 2.00 (m, 44H), 1.98 – 1.01 (m, 573H), 0.95 (d, J = 6.6 Hz, 6H), 0.88 – 0.76 (m, 6H).

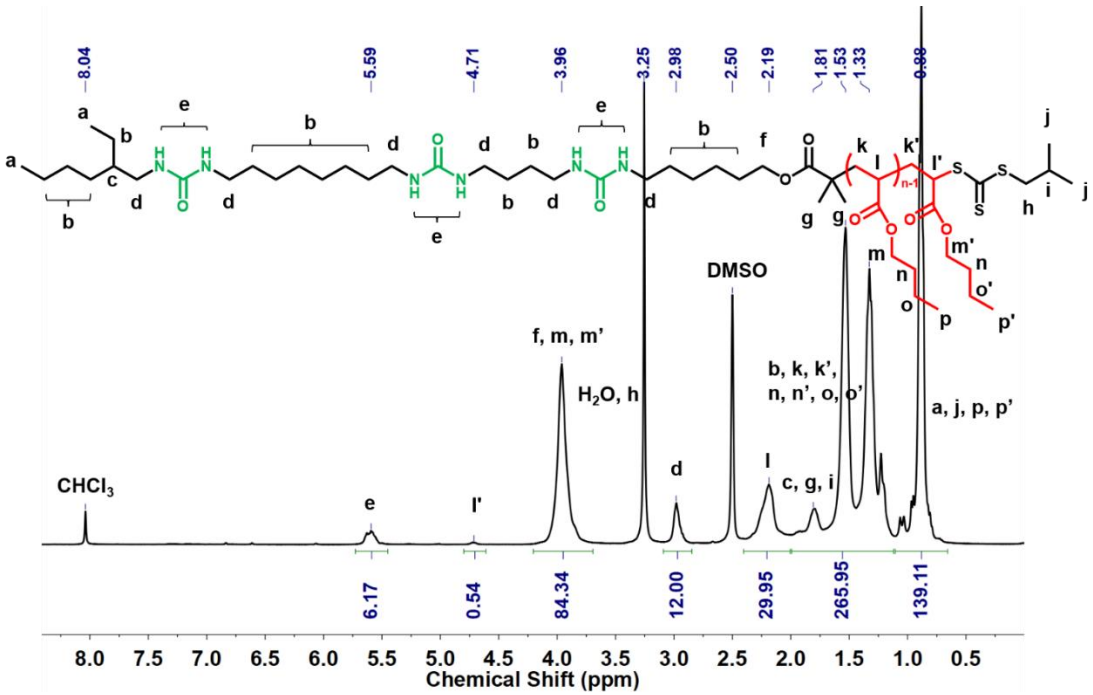

Figure 2.6.5.7. ^{1}H NMR of _8_4_P*n*BA$_{41}$ ($V_{DMSO\text{-}d6}/V_{CDCl3}$ = 1/1).

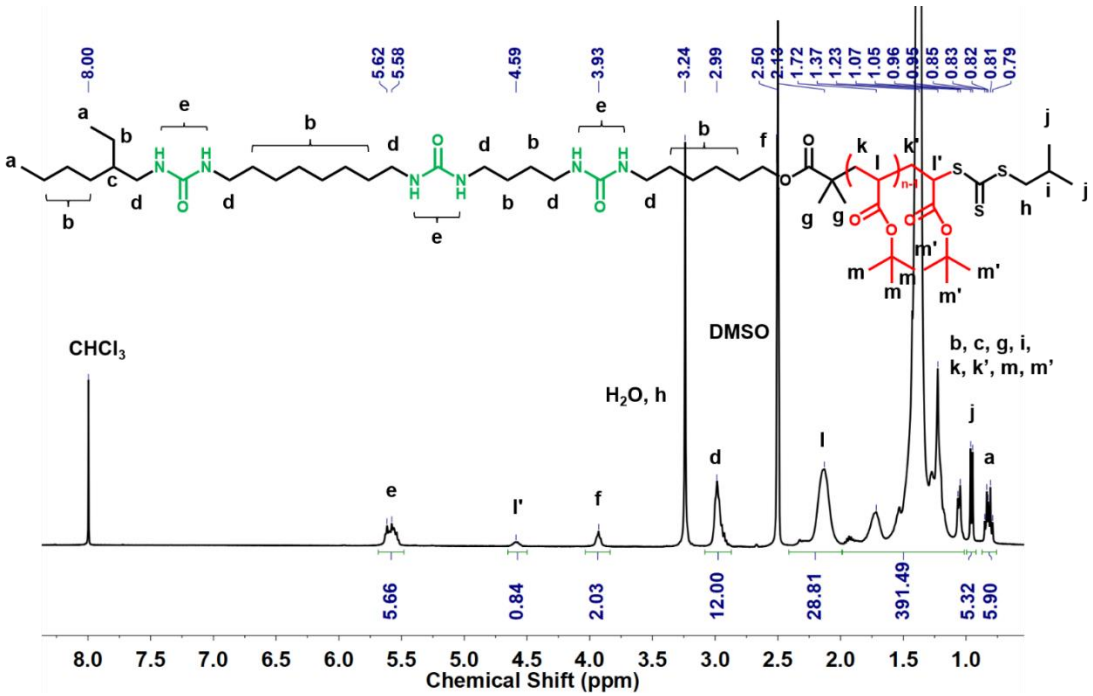

Figure 2.6.5.8. ^{1}H NMR of _8_4_P*t*BA$_{32}$ ($V_{DMSO\text{-}d6}/V_{CDCl3}$ = 1/1).

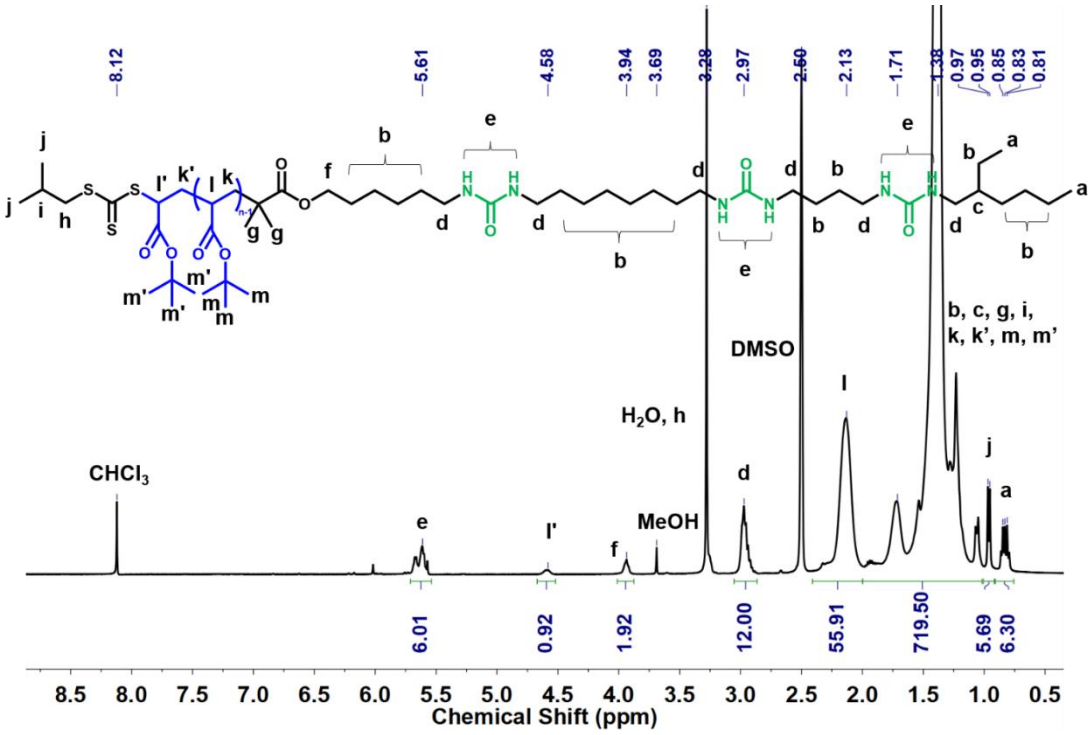

Figure 2.6.5.9. ^{1}H NMR of _4_8_P*t*BA$_{62}$ ($V_{DMSO\text{-}d6}/V_{CDCl3}$ = 1/1).

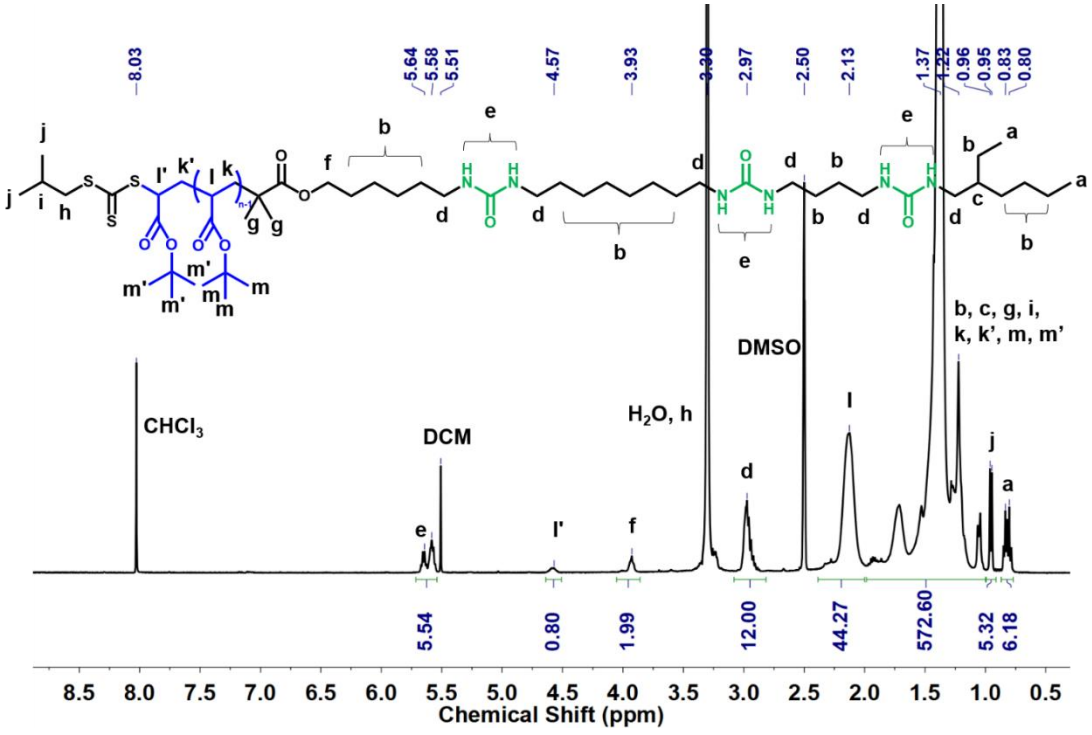

Figure 2.6.5.10. ^{1}H NMR of _4_8_P*t*BA$_{48}$ ($V_{DMSO\text{-}d6}/V_{CDCl3}$ = 1/1).

Polymerization of stearyl acrylate by _8_4_CTA (DP_n = 42). The synthesis of _8_4_PSA_{42} was described in detail as follows. _8_4_PSA_{73} and _8_4_PSA_{33} followed the same method. A 100 mL round-bottom flask equipped with a magnetic stirring bar was charged with stearyl acrylate (3 g, 9.23 mmol, 50 eq), _8_4_CTA-B7 (146 mg, 0.185 mmol, 1 eq), 1, 3, 5-trioxane (83 mg, 0.922 mmol, 5 eq) and a mixture of DMSO/toluene (v/v = 9/9 mL). Then, the solution was bubbled with N_2 at 70 ℃ for 30 minutes and afterwards AIBN (3.03mg in DMSO/toluene, 0.0185mmol, v/v = 0.5/0.5 mL, 0.1 eq) in 1 mL syringe was injected into the flask under the protection of N_2. The solution was bubbled with N_2 for another 10 minutes. After 150 minutes, the flask was plunged into an ice-water bath and the cap was opened after several minutes. 74% for the final conversion was determined by ^{1}H NMR. 80 mL methanol was poured into the flask and the precipitate was filtered. The solid was dissolved in DCM/toluene (v/v = 2/2 mL) and precipitated for 4 times in methanol. The white powder (1.7g, 72%) was filtered and then dried under vacuum overnight. M_n: 12.8 kg/mol, $Đ$: 1.14. ^{1}H NMR (400 MHz, $V_{DMSO\text{-}d6}/V_{CDCl3}$ = 1/5) δ 5.50 – 5.25 (m, 6H), 4.79 – 4.65 (m, 1H), 4.13 – 3.68 (m, 86H), 3.19 (d, 2H), 3.10 – 2.94 (m, 12H), 2.40 – 2.05 (m, 29H), 2.00 – 0.50 (m, 1684H).

Two other PSA were synthesized accordingly.

_8_4_PSA_{73} (M_n: 23.3 kg/mol, $Đ$: 1.40**)**. ^{1}H NMR (400 MHz, $V_{DMSO\text{-}d6}/V_{CDCl3}$ = 1/5) δ 5.52 – 5.19 (m, 6H), 4.79 – 4.64 (m, 1H), 4.26 – 3.56 (m, 148H), 3.18 (d, J = 4.2 Hz, 2H), 3.10 – 2.93 (m, 12H), 2.37 – 2.04 (m, 72H), 2.01 – 0.57 (m, 2764H).

_8_4_PSA_{33} (M_n: 11.5 kg/mol, $Đ$: 1.23**)**. ^{1}H NMR (400 MHz, $V_{DMSO\text{-}d6}/V_{CDCl3}$ = 1/5) δ 5.50 – 5.21 (m, 6H), 4.80 – 4.62 (m, 1H), 4.23 – 3.62 (m, 68H), 3.18 (d, J = 4.7 Hz, 2H), 3.09 – 2.93 (m, 12H), 2.43 – 2.04 (m, 34H), 2.02 – 0.59 (m, 1304H).

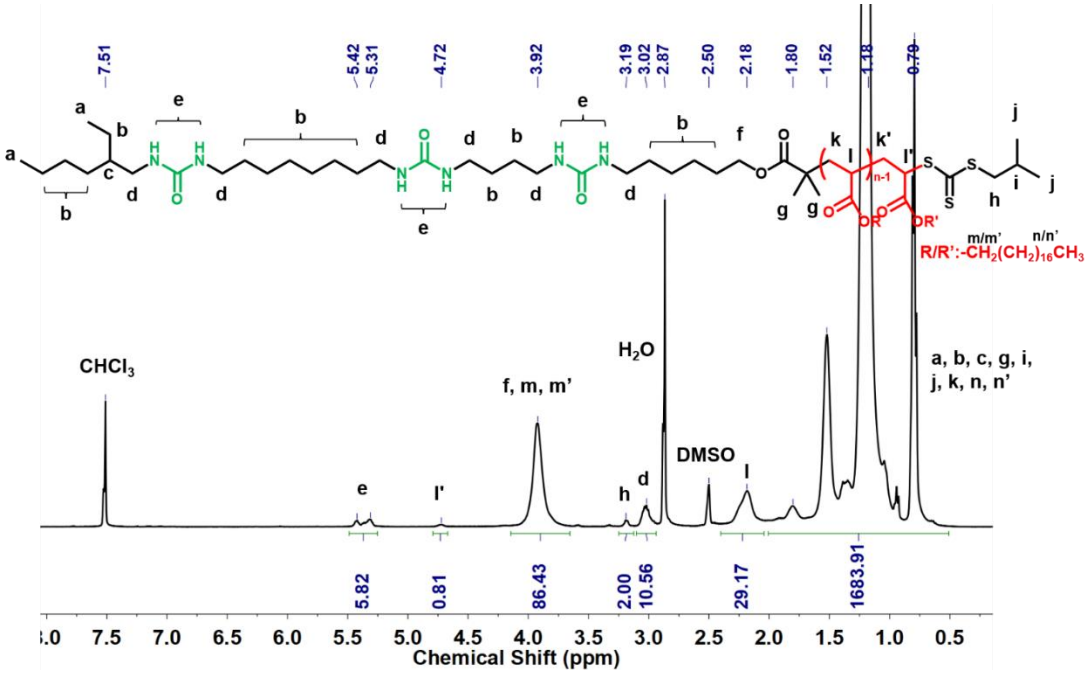

Figure 2.6.5.11. ^{1}H NMR of _8_4_PSA$_{42}$ ($V_{DMSO\text{-}d6}/V_{CDCl3}$ = 1/5).

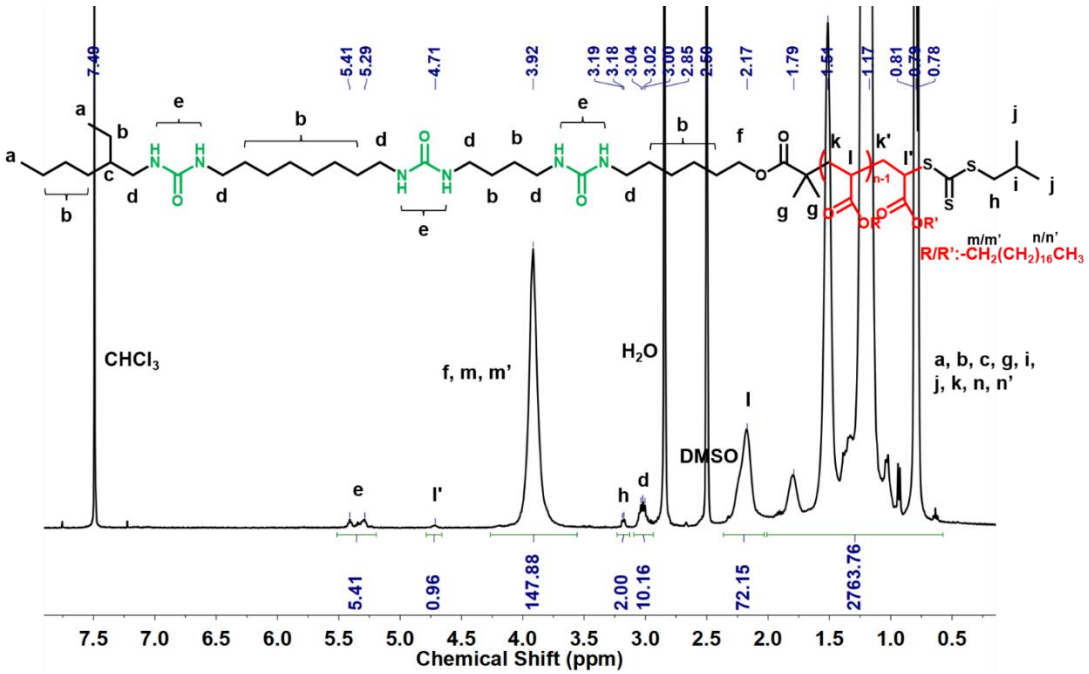

Figure 2.6.5.12. ^{1}H NMR of _8_4_PSA$_{73}$ ($V_{DMSO\text{-}d6}/V_{CDCl3}$ = 1/5).

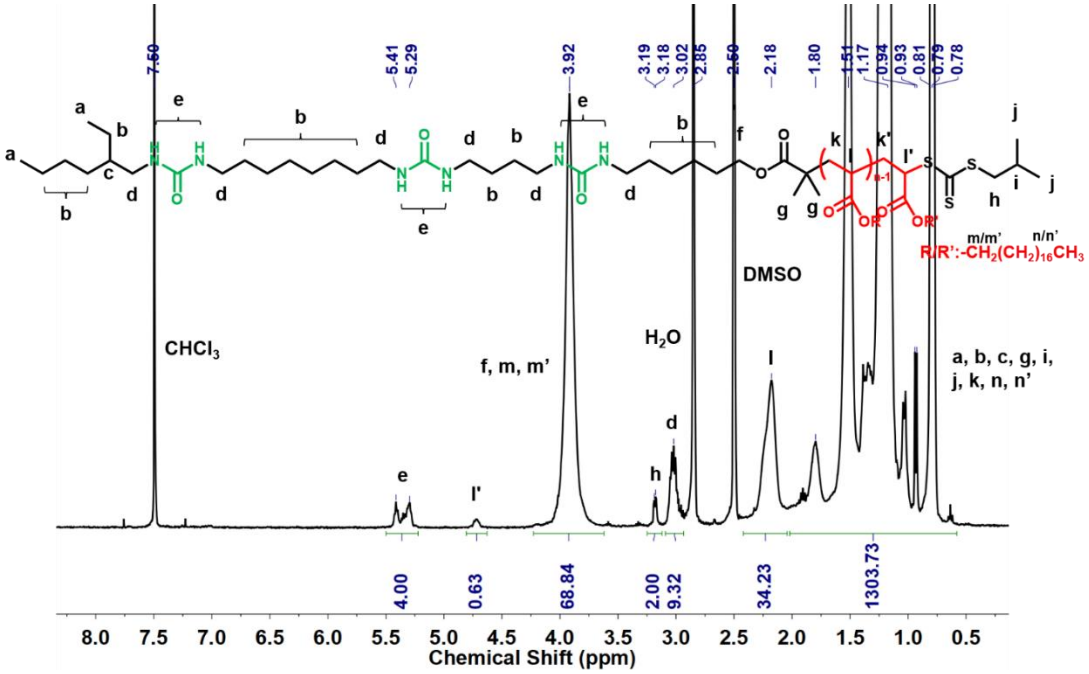

Figure 2.6.5.13. ^{1}H NMR of _8_4_PSA$_{33}$ ($V_{DMSO\text{-}d6}/V_{CDCl3}$ = 1/5).

Polymerization of 2-hydroxyethyl acrylate by _8_4_CTA (DP_n = 600). The synthesis of _8_4_PHEA$_{600}$ was described in detail as follows. _8_4_PHEA$_{1300}$ and _8_4_PHEA$_{47}$ followed the similar way. A 50 mL round bottom flask equipped with a magnetic stirring bar was charged with HEA (4 g, 34.5 mmol, 900 eq), _8_4_CTA-B6 (30.2 mg, 0.0382 mmol, 1 eq), DMSO (12.2 mL) and trioxane (155 mg, 1.72 mmol, 45 eq) used as internal standard. Then, the solution was bubbled with N_2 at 65°C for 30 min before injection of 2 mL of a 1.26 mg/mL stock solution of AIBN in DMSO (2.52 mg AIBN, 0.4 eq). The mixture was then degassed for another 10 min under N_2. Aliquots of 0.7 mL were withdrawn periodically from the reaction mixture to determine the conversion by ^{1}H NMR and molar mass by SEC. After 140 minutes, the flask was plunged into an ice-water bath and the cap was opened. A final conversion of 65% was determined by ^{1}H NMR. A yellow polymer (2.5 g, 95%) was obtained after dialysis (3.5k Da membrane) and freeze-drying. M_n: 85.2 kg/mol, $Đ$: 1.25. ^{1}H NMR (400 MHz, DMSO-d_6) δ 5.81 – 5.60 (m, 6H), 4.91 – 4.52 (m, 600H), 4.35 – 3.77 (m, 1178H), 3.68 – 3.42 (m, 1174H), 3.03 – 2.84 (m, 12H), 2.45 – 2.06 (m, 557H), 2.02 – 0.93 (m, 1165H), 0.92 – 0.74 (m, 6H).

_8_4_PHEA$_{1300}$ (M_n: 135.6 kg/mol, $Đ$: 1.67). ^{1}H NMR (400 MHz, DMSO-d_6) δ 5.81 – 5.62 (m, 6H), 5.02 – 4.51 (m, 1297H), 4.33 – 3.78 (m, 2531H), 3.69 – 3.43 (m, 2488H), 3.00 – 2.83 (m, 12H), 2.41 – 2.05 (m, 1151H), 2.03 – 0.93 (m, 2479H), 0.90 – 0.75 (m, 6H).

_8_4_PHEA$_{47}$ (M_n: 8.0 kg/mol, $Đ$: 1.31). ^{1}H NMR (400 MHz, DMSO-d_6) δ 5.80 – 5.62 (m, 6H), 4.90 – 4.60 (m, 47H), 4.18 – 3.79 (m, 94H), 3.71 – 3.43 (m, 92H), 3.03 – 2.85 (m, 12H), 2.41 – 2.05 (m, 47H), 2.03 – 1.02 (m, 129H), 0.97 (d, J = 6.7 Hz, 6H), 0.90 – 0.76 (m, 6H).

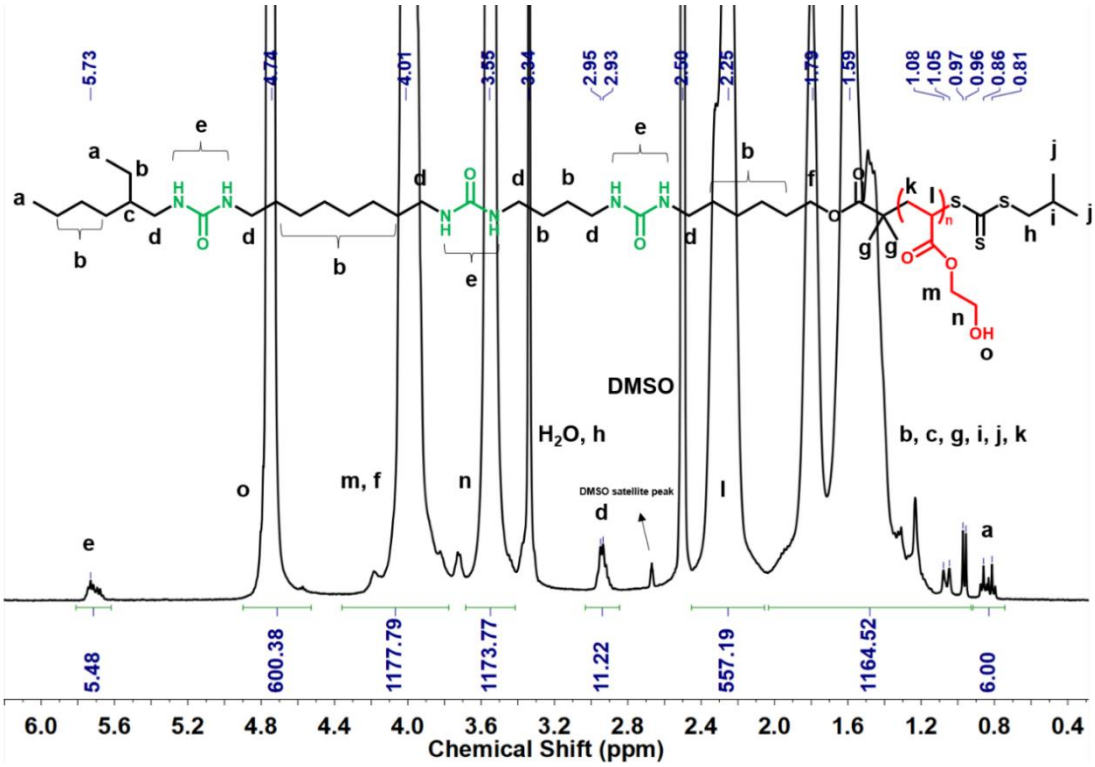

Figure 2.6.5.14. ^{1}H NMR of _8_4_PHEA$_{600}$ (in DMSO-d$_6$).

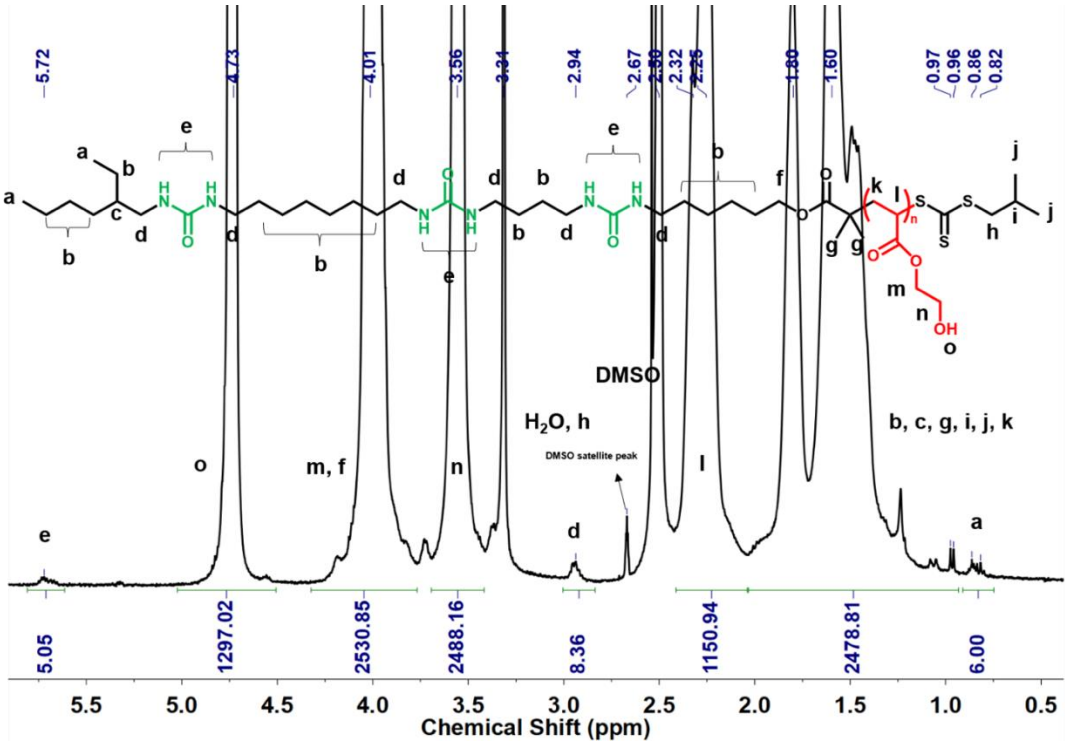

Figure 2.6.5.15. ^{1}H NMR of _8_4_PHEA$_{1300}$ (in DMSO-d$_6$).

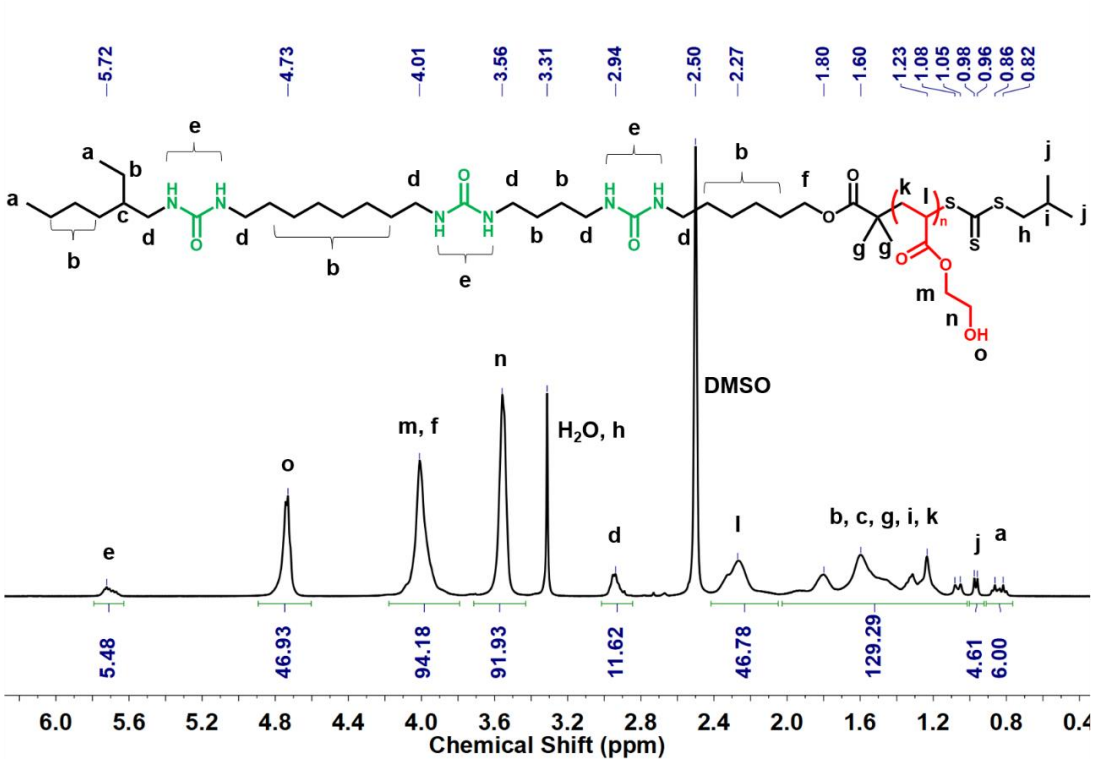

Figure 2.6.5.16. ^{1}H NMR of _8_4_PHEA$_{47}$ (in DMSO-d$_6$).

Polymerization of ferrocenemethyl acrylate (FMA) by _8_4_CTA (DP_n = 69). A 50 mL round bottom flask equipped with a magnetic stirring bar was charged with FMA (0.927 g, 3.43 mmol, 86 eq), _8_4_CTA-B6 (31.5 mg, 0.04 mmol, 1 eq), DMF (6 mL) and trioxane (17 mg, 0.189 mmol, 4.8 eq) used as internal standard. Then, the solution was bubbled with N_2 at 70°C for 45 min before injection of 0.8 mL of a 1.63 mg/mL stock solution of AIBN in DMSO (1.3 mg AIBN, 0.2 eq). The mixture was then degassed for another 10 min under N_2. Aliquots of 0.7 mL were withdrawn periodically from the reaction mixture to determine the conversion by ^{1}H NMR and molar mass by SEC. After 20 hours, the flask was plunged into an ice-water bath and the cap was opened. A final conversion of 82% was determined by ^{1}H NMR. A yellow polymer (0.32 g, 40%) was obtained after 4 times' precipitations from hexane. M_n: 6.8 kg/mol, $Đ$: 1.41. ^{1}H NMR (400 MHz, $V_{DMSO\text{-}d6}/V_{CDCl3}$ = 1/1) δ 5.76 – 5.52 (m, 6H), 5.11 – 4.55 (m, 140H), 4.47 – 3.83 (m, 683H), 3.16 – 2.87 (m, 12H), 2.29 – 1.90 (m, 51H), 1.84 – 0.90 (m, 143H), 0.86 – 0.67 (m, 6H).

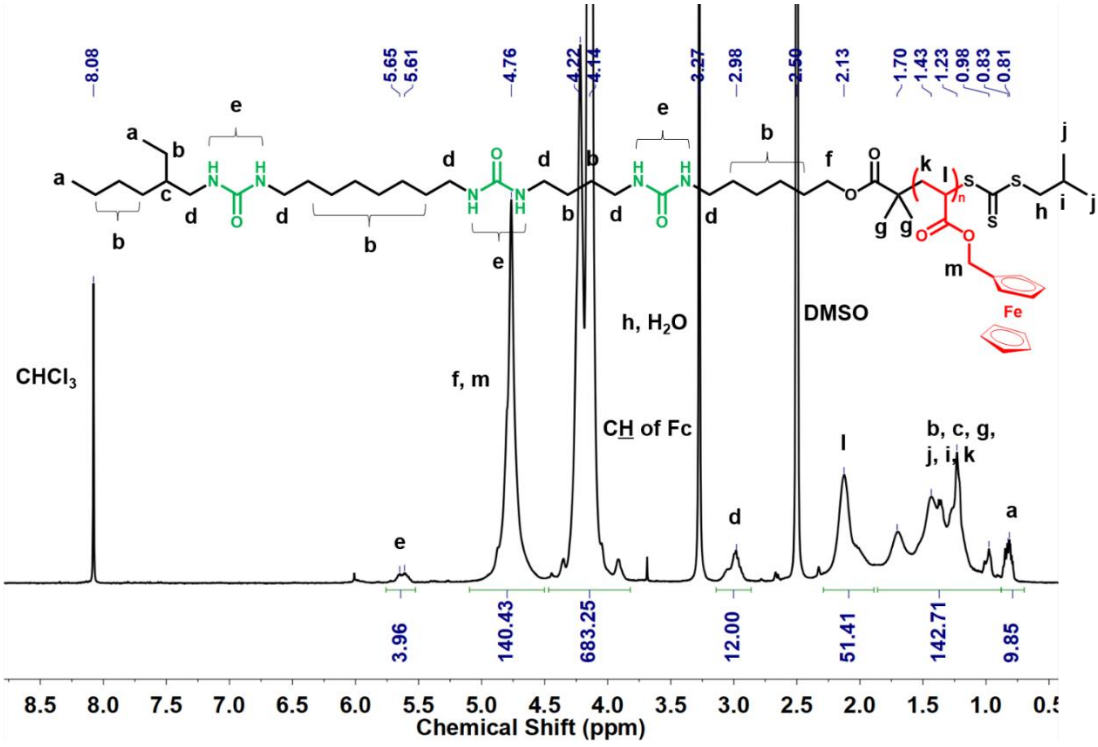

Figure 2.6.5.17. ^{1}H NMR of _8_4_$PFMA_{69}$ ($V_{DMSO\text{-}d6}/V_{CDCl3}$ = 1/1).

Polymerization of styrene by _4_8_CTA (DP_n = 33). A 100 mL round-bottom flask equipped with a magnetic stirring bar was charged with styrene (2 g, 19.2 mmol, 150 eq), _4_8_CTA-B1 (101 mg, 0.128 mmol, 1 eq), 1, 3, 5-trioxane (internal standard, 86.5 mg, 0.961 mmol, 7.5 eq) and DMSO (6.4 mL). Then, the solution was bubbled with N_2 at 75 ℃ for 30 minutes and afterwards AIBN (6.31 mg in 1 mL DMSO, 0.0385 mmol, 0.3 eq) in 1 mL syringe was injected into the flask under the protection of N_2. The solution was bubbled with N_2 for another 10 minutes. After 7 hours, the flask was plunged into an ice-water bath and the cap was opened after several minutes. 40% for the final conversion was determined by ^{1}H NMR. 80 mL cold MeOH was poured into the flask and then the precipitate was filtered. The yellow polymer (0.173 g, 19%) was obtained for another 2 precipitations in cold MeOH. M_n: 4.0 kg/mol, $Đ$: 1.09. ^{1}H NMR (400 MHz, $V_{DMSO\text{-}d6}/V_{CDCl3}$ = 1/1) δ 7.40 – 6.15 (m, 160H), 5.78 – 5.48 (m, 6H), 3.07 – 2.86 (m, 12H), 2.39 – 0.68 (m, 151H).

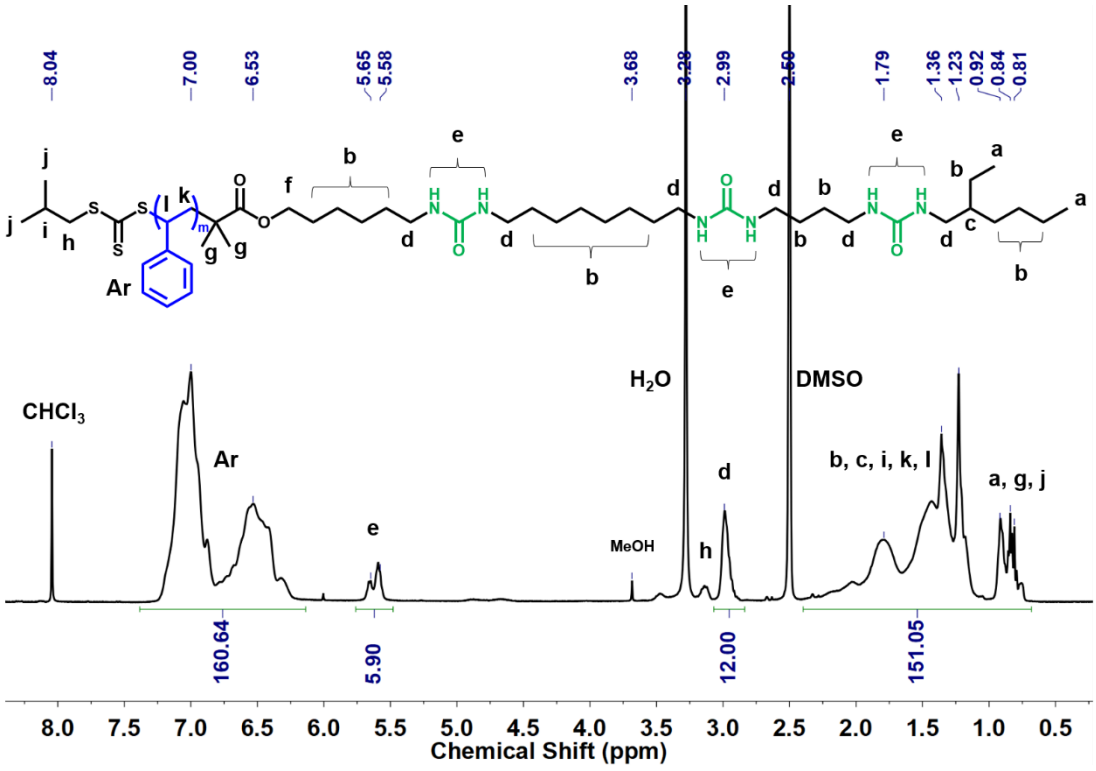

Figure 2.6.5.18. ^{1}H NMR of _4_8_PS_{33} ($V_{DMSO\text{-}d6}/V_{CDCl3}$ = 1/1).

_8_4_PTMSS$_{61}$ was synthesized similarly to _4_8_PS$_{33}$. M_n: 9.6 kg/mol, $Đ$: 1.12. ^{1}H NMR (400 MHz, $V_{DMSO\text{-}d6}/V_{CDCl3}$ = 1/2 δ 7.72 – 6.02 (m, 214H), 5.65 – 5.44 (m, 6H), 4.03 (t, 2H), 3.06 – 2.86 (m, 12H), 2.29 – 0.61 (m, 266H), 0.47 – -0.32 (m, 550H).

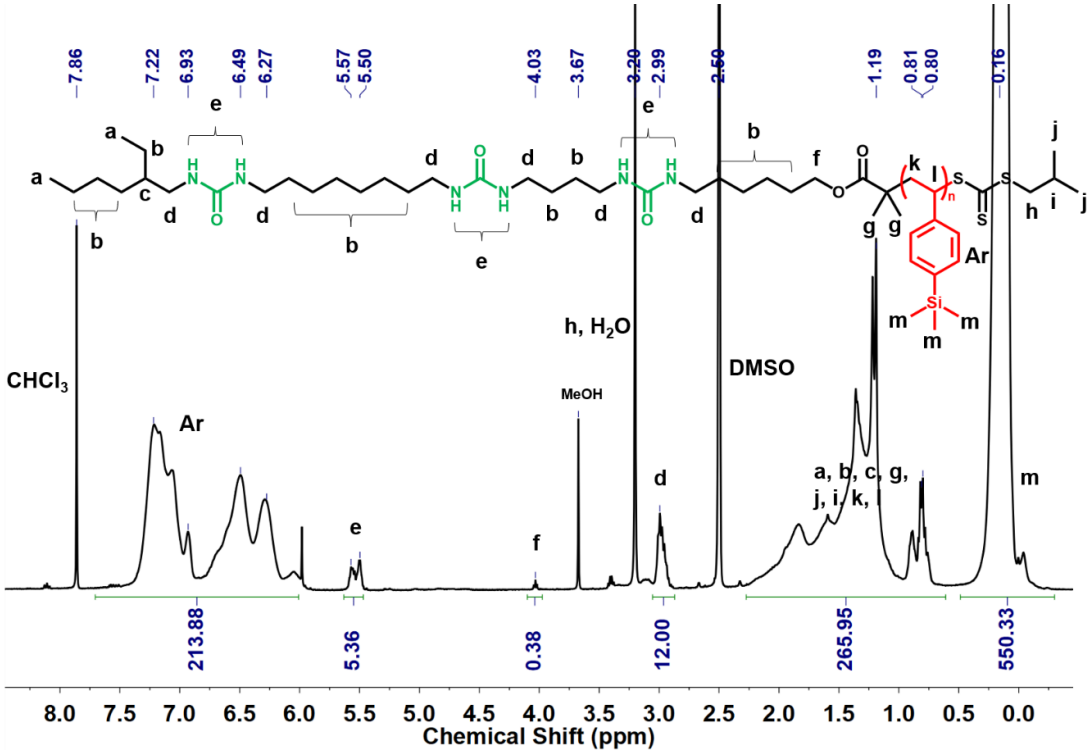

Figure 2.6.5.19. ^{1}H NMR of _8_4_PTMSS$_{61}$ ($V_{DMSO\text{-}d6}/V_{CDCl3}$ = 1/2).

2.7 References

(1) Nickmans, K.; Schenning, A. P. H. J. Directed self-assembly of liquid-crystalline molecular building blocks for sub-5 nm nanopatterning. *Adv. Mater.* **2018**, *30*, 1703713.

(2) Bang, J.; Jeong, U.; Ryu du, Y.; Russell, T. P.; Hawker, C. J. Block copolymer nanolithography: translation of molecular level control to nanoscale patterns. *Adv. Mater.* **2009**, *21*, 4769-4792.

(3) Park, S.; Lee, D. H.; Xu, J.; Kim, B.; Hong, S. W.; Jeong, U.; Xu, T.; Russell, T. P. Macroscopic 10-terabit-per-square-inch arrays from block copolymers with lateral order. *Science* **2009**, *323*, 1030-1033.

(4) Mansky, P.; Liu, Y.; Huang, E.; Russell, T. P.; Hawker, C. Controlling polymer-surface interactions with random copolymer brushes. *Science* **1997**, *275*, 1458-1460.

(5) Stoykovich, M. P.; Muller, M.; Kim, S. O.; Solak, H. H.; Edwards, E. W.; de Pablo, J. J.; Nealey, P. F. Directed assembly of block copolymer blends into nonregular device-oriented structures. *Science* **2005**, *308*, 1442-1446.

(6) Tavakkoli, K. G. A.; Gotrik, K. W.; Hannon, A. F.; Alexander-Katz, A.; Ross, C. A.; Berggren, K. K. Templating three-dimensional self-assembled structures in bilayer block copolymer films. *Science* **2012**, *336*, 1294-1298.

(7) Pal, A.; Karthikeyan, S.; Sijbesma, R. P. Coexisting hydrophobic compartments through self-sorting in rod-like micelles of bisurea bolaamphiphiles. *J. Am. Chem. Soc.* **2010**, *132*, 7842-7843.

(8) Danial, M.; Tran, C. M.; Young, P. G.; Perrier, S.; Jolliffe, K. A. Janus cyclic peptide-polymer nanotubes. *Nat. Commun.* **2013**, *4*, 2780.

(9) Han, S.; Pensec, S.; Yilmaz, D.; Lorthioir, C.; Jestin, J.; Guigner, J. M.; Niepceron, F.; Rieger, J.; Stoffelbach, F.; Nicol, E.; Colombani, O.; Bouteiller, L. Straightforward

preparation of supramolecular Janus nanorods by hydrogen bonding of end-functionalized polymers. *Nat. Commun.* **2020**, *11*, 4760.

(10) Gallou, I.; Eriksson, M.; Zeng, X.; Senanayake, C.; Farina, V. Practical synthesis of unsymmetrical ureas from isopropenyl carbamates. *J. Org. Chem.* **2005**, *70*, 6960-6963.

(11) Liu, Q.; Luedtke, N. W.; Tor, Y. A simple conversion of amines into monosubstituted ureas in organic and aqueous solvents. *Tetrahedron Lett.* **2001**, *42*, 1445-1447.

(12) Kitteringham, J.; Shipton, M. R.; Voyle, M. A simple method for the synthesis of unsymmetrical ureas. *Synth. Commun.* **2000**, *30*, 1937-1943.

(13) Tomkinson, N. C.; Bridgeman, E. A simple method for the preparation of di-, tri- and tetrasubstituted non-symmetrical ureas. *Synlett* **2006**, 243-246.

(14) Evans, A. J.; Matthews, S. E.; Cowley, A. R.; Beer, P. D. Anion binding by calix[4]arene ferrocene ureas. *Dalton Trans.* **2003**, 24, 4644-4650.

(15) Diss, M. L.; Kennan, A. J. Facile production of mono-substituted urea side chains in solid phase peptide synthesis. *Biopolymers* **2007**, *86*, 276-281.

(16) Véchambre, C.; Callies, X.; Fonteneau, C.; Ducouret, G.; Pensec, S.; Bouteiller, L.; Creton, C.; Chenal, J.-M.; Chazeau, L. Microstructure and self-assembly of supramolecular polymers center-functionalized with strong stickers. *Macromolecules* **2015**, *48*, 8232-8239.

(17) Wang, W.; Jin, X.; Zhu, Y.; Zhu, C.; Yang, J.; Wang, H.; Lin, T. Effect of vapor-phase glutaraldehyde crosslinking on electrospun starch fibers. *Carbohydr. Polym.* **2016**, *140*, 356-361.

(18) Xiao, Z.-P.; Cai, Z.-H.; Liang, H.; Lu, J. Amphiphilic block copolymers with aldehyde and ferrocene-functionalized hydrophobic block and their redox-responsive micelles. *J. Mater. Chem.* **2010**, *20*, 8375-8381.

(19) Szillat, F.; Schmidt, B. V.; Hubert, A.; Barner-Kowollik, C.; Ritter, H. Redox-switchable supramolecular graft polymer formation via ferrocene-cyclodextrin assembly. *Macromol. Rapid. Commun.* **2014**, *35*, 1293-1300.

(20) Saleem, M.; Wang, L.; Yu, H.; Zain ul, A. Synthesis of ferrocene boronic acid-based block copolymers via RAFT polymerization and their micellization, redox responsive and glucose sensing properties. *Arabian J. Chem.* **2019**, *12*, 800-815.

(21) Jiang, X.; Li, R.; Feng, C.; Lu, G.; Huang, X. Triple-stimuli-responsive ferrocene-containing homopolymers by RAFT polymerization. *Polym. Chem.* **2017**, *8*, 2773-2784.

(22) Yan, Q.; Yuan, J.; Cai, Z.; Xin, Y.; Kang, Y.; Yin, Y. Voltage-responsive vesicles based on orthogonal assembly of two homopolymers. *J. Am. Chem. Soc.* **2010**, *132*, 9268-9270.

(23) Hardy, C. G.; Ren, L.; Ma, S.; Tang, C. Self-assembly of well-defined ferrocene triblock copolymers and their template synthesis of ordered iron oxide nanoparticles. *Chem. Commun.* **2013**, *49*, 4373-4375.

(24) Wu, G.; Deng, H. High etch resistant ferrocene-containing block copolymers with 5 nm patterning capability. *J. Photopolym. Sci. Technol.* **2020**, *33*, 537-540.

(25) Hardy, C. G.; Ren, L.; Tamboue, T. C.; Tang, C. Side-chain ferrocene-containing (meth)acrylate polymers: Synthesis and properties. *J. Polym. Sci., Part A:Polym. Chem.* **2011**, *49*, 1409-1420.

(26) Park, M.; Harrison, C.; Chaikin, P. M.; Register, R. A.; Adamson, D. H. Block copolymer lithography: periodic arrays of ~10^{11} holes in 1 square centimeter. **1997**, *276*, 1401-1404.

(27) Tang, C.; Lennon, E. M.; Fredrickson, G. H.; Kramer, E. J.; Hawker, C. J. Evolution of block copolymer lithography to highly ordered square arrays. *Science* **2008**, *322*, 429-432.

(28) Cushen, J.; Wan, L.; Blachut, G.; Maher, M. J.; Albrecht, T. R.; Ellison, C. J.; Willson, C. G.; Ruiz, R. Double-patterned sidewall directed self-assembly and pattern transfer of sub-10 nm PTMSS-*b*-PMOST. *ACS Appl. Mater. Interfaces* **2015**, *7*, 13476-13483.

(29) Cushen, J. D.; Bates, C. M.; Rausch, E. L.; Dean, L. M.; Zhou, S. X.; Willson, C. G.; Ellison, C. J. Thin film self-assembly of poly(trimethylsilylstyrene-*b*-D,L-lactide) with sub-10 nm domains. *Macromolecules* **2012**, *45*, 8722-8728.

(30) Langle, S.; David-Quillot, F.; Balland, A.; Abarbri, M.; Duchêne, A. General access to para-substituted styrenes. *J. Organomet. Chem.* **2003**, *671*, 113-119.

(31) Kalem, S.; Siefker, D.; Ji, M.; Guigner, J. M.; Schweins, R.; Pensec, S.; Rieger, J.; Bouteiller, L.; Nicol, E.; Colombani, O. Supramolecular Janus nanocylinders: controlling their characteristics by the self-assembly process. *Macromol. Rapid. Commun.* **2025**, *46*, 2400492.

(32) Kalem, S.; Ji, M.; Gonzalez, A. V.; Siefker, D.; Guigner, J. M.; Schweins, R.; Pensec, S.; Rieger, J.; Bouteiller, L.; Nicol, E.; Colombani, O. Tuning the diameter of supramolecular nanocylinders: balancing long and short polymer arms for optimized self-assembly. *J. Polym. Sci.* **2025**, *doi.org/10.1002/pol.20250561*.

Chapter III: Synthesis and characterization of photo-responsive nanocylinders

3.1 Introduction

As mentioned in the previous chapters, there are two strategies to achieve small features in nanolithography, using high χ low N systems in block copolymers or using (co)assembly in supramolecular polymers. However, for block copolymers, it is always accompanied with harsh conditions such as etching[1, 2] or pyrolysis[3, 4] to remove one block of polymers in the assembled nanostructures. For supramolecular polymers, one block could be mildly removed by selective solvents[5] but such sub-10 nm feature is still not achieved. Combining these two strategies, the introduction of a cleavable linker within BCPs or SPs might be suitable to achieve small features (sub-10 nm) and mild removal of one polymer block. In some studies, introducing a photo-cleavable linker into BCPs has proved the feasibility to remove one block with mild treatments after photo-cleavage, but small features (sub-10 nm) are not achieved[6-8].

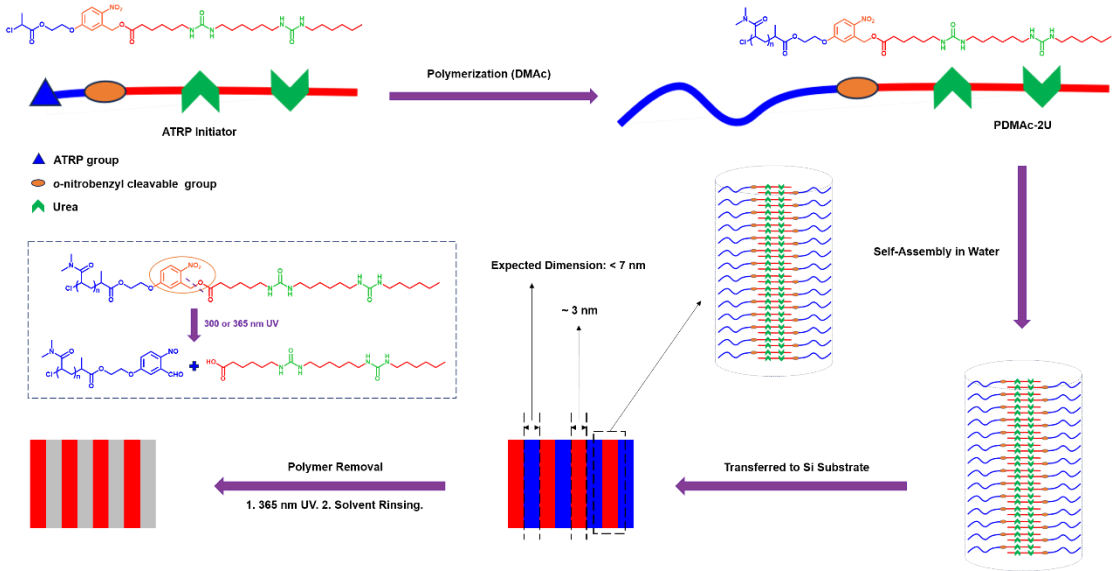

Figure 3.1.1 Illustration of the expected behavior of photo-cleavable PDMAc-2U after surface deposition and UV irradiation.

Herein, we designed a photocleavable linker (*o*-nitrobenzyl ester) inserted at the junction between a bisurea sticker and poly(*N,N*-dimethylacrylamide). Such polymers should lead to the formation of nanocylinders in water[9], as reported for a simpler system developed in our group beforehand. The aim is to investigate photo-responsive behavior on surface. *o*-nitrobenzyl alcohol derivatives have shown good cleavage behavior when they are exposed to UV[10] (absorb one photon) or near-infrared (absorb two-photon) [11-13]. As shown in Figure 3.1.1, an ATRP initiator with an *o*-nitrobenzyl ester and a bisurea was synthesized, followed by the polymerization of *N,N*-dimethylacrylamide to form PDMAc-2U. The supramolecular self-assembly of PDMAc-2U in water and its photo-responsiveness were investigated. Afterward, assemblies were transferred onto silicon substrate for the investigation of surface nanopatterning. By introducing UV irradiation and solvent rinsing, we expect to remove PDMAc to obtain line pattern with sub-10 nm features.

3.2 Results and discussions

3.2.1 Synthesis of bisurea-functionalized ATRP initiator

As shown in Scheme 3.2.1.1, starting from an *o*-nitrobenzyl aldehyde (1), the phenol was functionalized as a phenolic ether[14-17] instead of phenolic ester due to the instability of phenolic ester in acidic or basic condition. After the reduction of the aldehyde function to form TBDMSO-Ar-OH (3), an esterification was performed to give Boc-protected amine (4). When TBAF was added afterwards, the hydroxyl group was deprotected to form HO-Ar-Boc (5).

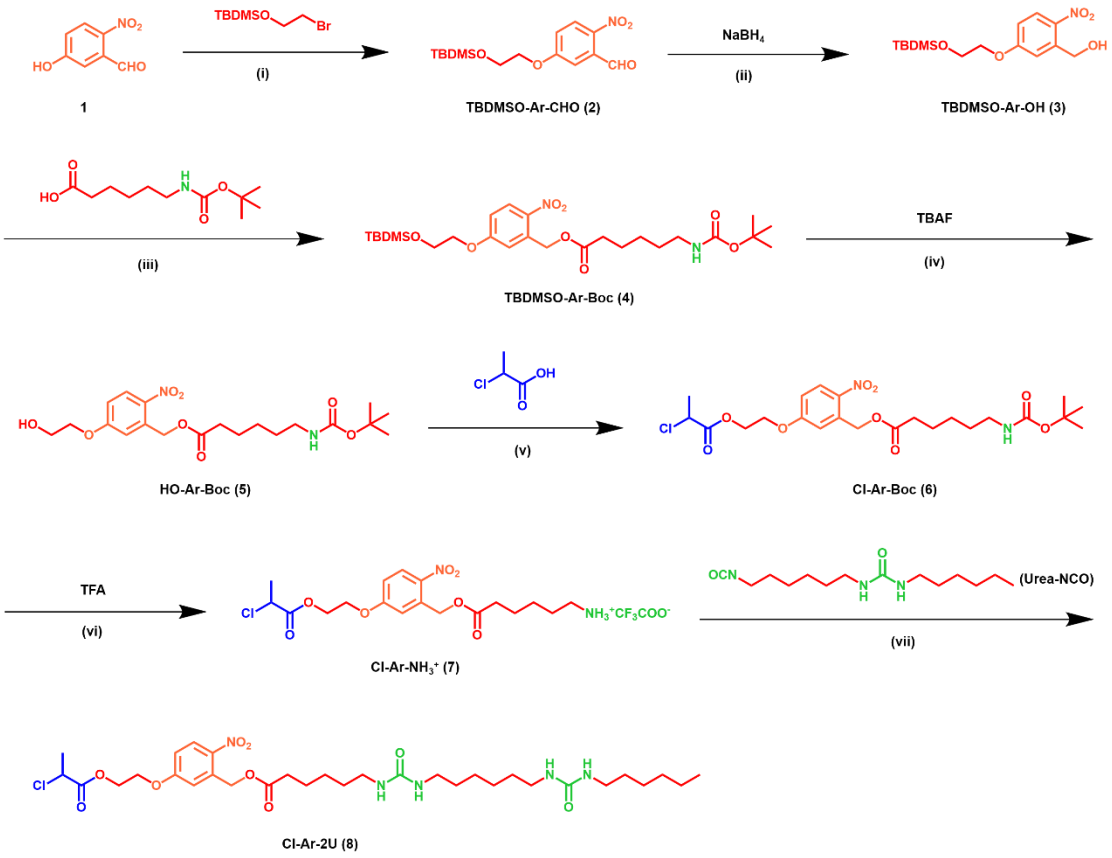

Scheme 3.2.1.1. Synthesis of bisurea-functionalized ATRP initiator. Conditions and yields of the different steps are as follows: (i): K_2CO_3, KI, DMF, 90°C, overnight, 86%; (ii): THF/MeOH, 40 min, 85%; (iii): anhydrous DCM, DMAP, DCC, 25 h, 65%; (iv): THF, 5 h, 79%; (v): anhydrous THF, DMAP, DCC, 23 h, 92%; (vi): anhydrous DCM, 20 min, 98 %; (vii): anhydrous DCM, TEA, 1 h, 60%.

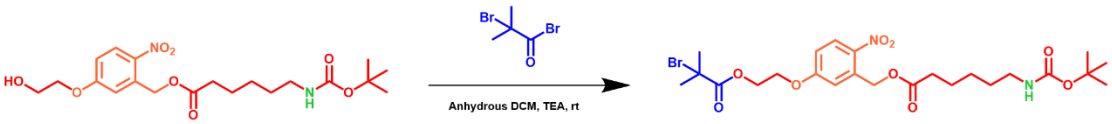

Scheme 3.2.1.2. Initial attempt to esterify HO-Ar-Boc (5) with an acyl bromide.

Step (v) was a challenging reaction. According to previous study, the yield of esterification by acyl bromide[18] was low (25%). In an attempt to improve the yield of such esterification, the reaction (Scheme 3.2.1.2) was performed with 2 equivalents of 2-bromo-2-methylpropionyl bromide, and the reaction was finished after 15 hours. The product was separated by a silica column (83% yield) and analyzed by NMR.

From the ^{1}H NMR of figure 3.2.1.1, a surprising thing was the disappearance of the carbamate proton and the appearance of peak n at 1.80 - 2.0 ppm. An additional carbon peak from carbonyl at 176.71 ppm confirmed that the expected product is not formed: it seems that both the O from hydroxyl and the N from carbamate attack the acyl bromide due to its strong electrophilicity. In fact, this probably explains why the yield was low in the reported study using acyl bromide[18]. Therefore, an acyl bromide or acyl chloride was not an option for the esterification anymore.

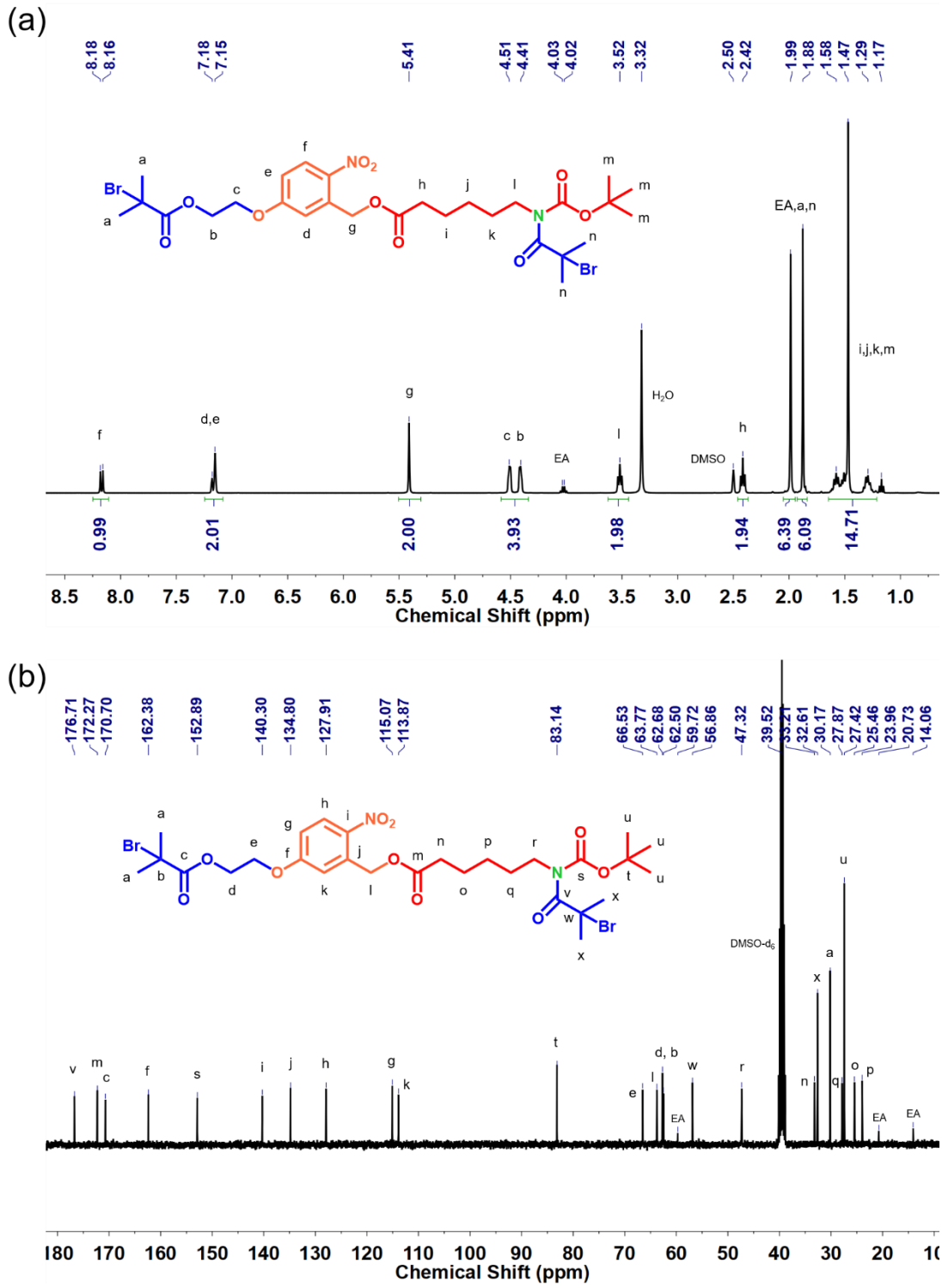

Figure 3.2.1.1. ^{1}H NMR (a) and ^{13}C NMR (b) of the product of the reaction between HO-Ar-Boc (5) and 2-bromo-2-methylpropionyl bromide.

Starting with an acid, Wooley group reported a 43% yield after 81 hours using DCC/DMAP in DCM[19]. Later, Maynard et al improved the yield to 72% when 2-

chloropropionic acid was used with DCC/DMAP and DMF as the solvent[20]. Thus, DCM and DMF were both chosen to test the reaction between HO-Ar-Boc (5) and 2-chloropropionic acid. For the reaction in DCM, only 12% yield was obtained. When reaction was in DMF, a significant amount of HO-Ar-Boc (5) remained according to the TLC after 17 hours, indicating again low conversion. Finally, when anhydrous THF was used for the reaction, amazingly, HO-Ar-Boc (5) was totally consumed after 23 hours and a colorless solid with 92% yield was obtained. The colorless solid was the product Cl-Ar-Boc (6), confirmed by ^{1}H NMR (Figure 3.4.3.9 and 3.4.3.10). This reaction indicated a strong solvent effect.

After obtaining Cl-Ar-Boc (6), it was treated with TFA to remove the Boc group, giving Cl-Ar-NH_3^+ (7). Then Cl-Ar-NH_3^+ (7) was reacted with Urea-NCO (which was synthesized[21] in advance) in the presence of triethylamine. During the reaction, a colorless solid formed. The reaction was monitored by FTIR to check the disappearance the N=C=O peak at 2270 cm^{-1}. The formed solid was continuously washed by chloroform, diethyl ether, water, acetonitrile and ethyl acetate, with a further step of recrystallization in chloroform, giving a colorless solid with a yield of 60%. The synthesis was repeated and therefore 2 batches were obtained (see experimental part).

3.2.2 Synthesis and characterization of photo-responsive PDMAc-2U

The radical polymerization of *N,N*-dimethylacrylamide (DMAc) using trithiocarbonate RAFT agents has demonstrated good control[22, 23]. In contrast, the ATRP process for DMAc is still challenging, mainly due to two reasons[24]. First, binding of the catalyst by monomeric or polymeric amide groups can lead to the deactivation of the catalyst. Second, the halide in the polymer chain may be replaced by DMAc due to the nucleophilicity of the amide. Several studies reported ATRP polymerization of DMAc by changing different ligands[25, 26], revealing that the best catalyst complex was CuCl/Me_6TREN, which normally gave a dispersity lower than 1.30[27]. In addition to ligands, Stö1ver group pointed out that solvents such as alcohols (methanol, ethanol, isopropyl alcohol, etc.) lowered the dispersity (less than 1.10) for DMAc[24] and for *N*-

isopropylacrylamide[28], which was confirmed by Liu et al[29]. Based on these studies, the polymerization of DMAc was attempted with CuCl/Me_6TREN in isopropyl alcohol (i-PrOH) (0.5 M for monomer concentration and 0.006 M for initiator concentration) at 60 ℃ (Scheme 3.2.2.1. and Table 3.2.2.2. line 1). Even though the previously cited publications described the polymerization at room temperature, in our case a temperature of 60 °C was chosen to properly dissolve the initiator. However, only 12% monomer conversion after 17 hours indicated the deactivation of catalyst in the early stage of polymerization. The high temperature may probably accelerate the deactivation of the catalyst. Considering this, lowering moderately the temperature of polymerization seems necessary. Furthermore, in the reported studies[27, 30], a high monomer concentration may also be necessary to speed up the polymerization before the deactivation of the catalyst. To find a suitable solvent and temperature for dissolving initiator Cl-Ar-2U (8), solubility tests were performed when increasing temperature from 35 ℃ to 60 ℃, as shown in Table 3.2.2.1.

Table 3.2.2.1. The lowest temperature for solubilization of Cl-Ar-2U in different solvents (×: not soluble at 60°C).

Initiator concentration	**DMAc**	**DMF**	**DMSO**	**Toluene**	**Dioxane**	**H_2O**	**i-PrOH**	**BuOH**
0.012 M	35 ℃	35 ℃	35 ℃	×	×	×	×	×
0.08 M	45 ℃	45 ℃	45 ℃	×	×	×	×	×

Therefore, the polymerization was performed in DMF at 45 ℃ with CuCl/Me_6TREN as catalyst complex to obtain bisurea-terminated PDMAc.

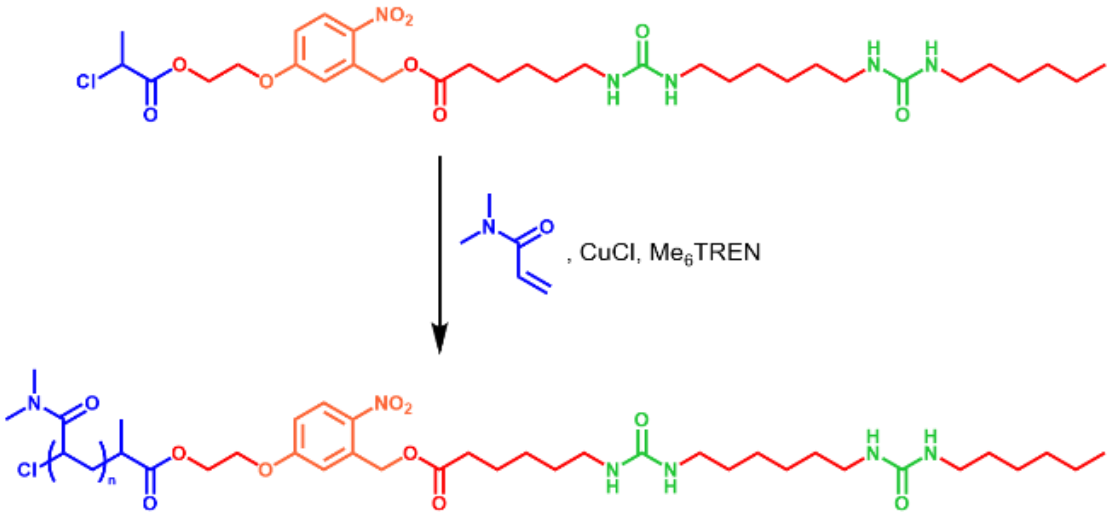

Scheme 3.2.2.1 The polymerization condition of DMAc using bisurea-terminated ATRP initiator.

The detailed polymerization condition of DMAc and characteristics of polymer are listed in Table 3.2.2.2 (lines 2-5) and a typical monitoring of the polymerization ($PDMAc_{18}$-2U) by ^{1}H NMR is shown in Figure 3.2.2.1. The low monomer conversion is attributed to the fast deactivation of the catalyst. During the polymerization, the initiation and propagation were fast, followed by a quick deactivation of the catalyst at short reaction times. A mixture of solvents (DMF and i-PrOH) was tested to see if the presence of the alcohol could reduce this problem but it was not successful (see Table 3.2.2.2 (line 6)).

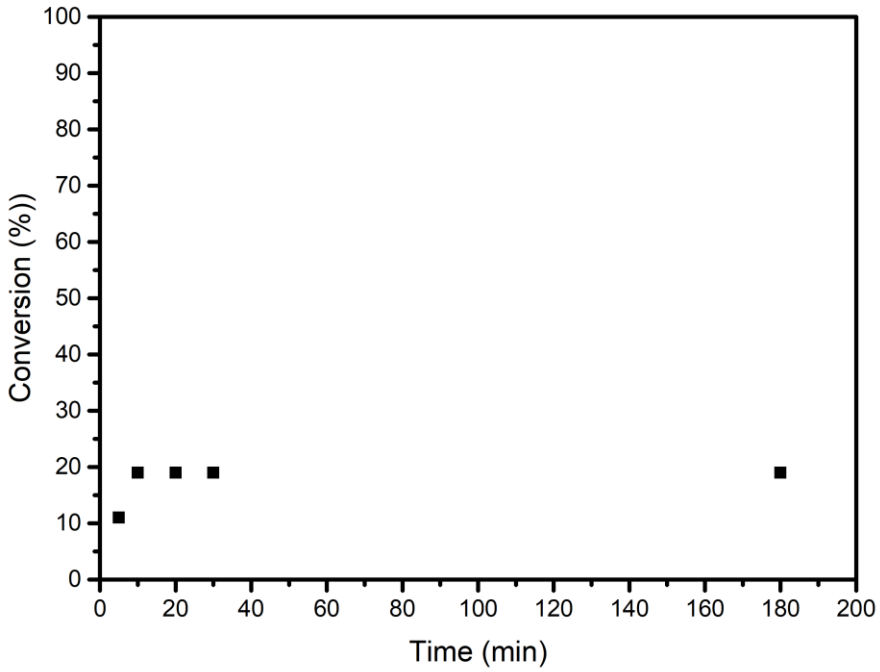

Figure 3.2.2.1. Monomer conversion during synthesis of $PDMAc_{18}$-2U monitored by NMR.

$PDMAc_{18}$-2U and $PDMAc_{83}$-2U in Table 3.2.2.2 displayed good agreements of theoretical molecular weight ($M_{n,\,th}$) and observed NMR molecular weight ($M_{n,\,NMR}$). The big gap of molecular weights between $M_{n,\,th}$ and $M_{n,\,NMR}$ in $PDMAc_{35}$-2U and $PDMAc_{100}$-2U may result from a purity problem of the initiator batch Cl-Ar-2U-B2, which was not as pure as Cl-Ar-2U-B1.

Table 3.2.2.2. Polymerization condition and characteristics of bisurea-terminated PDMAc, PDMAc-2U, synthesized by ATRP in DMF.

Entry	Initiator Batch	$[M]_0/[I]_0/[CuCl]_0/[Me_6TREN]_0$	Solvent	$[M]_0$ (M)	Temp. (℃)	Time (h)	Conv. (%)[a]	DP_{NMR}[b]	$M_{n,th}$ (kg/mol)[c]	$M_{n,NMR}$ (kg/mol)[d]	$M_{n,SEC}$ (kg/mol)[e]	$Đ$
PDMAc$_x$-2U	B1	80/1/1/1	i-PrOH	0.5	60	17	12	-	1.7	-	2.2	1.21
PDMAc$_{18}$-2U	B1	83/1/1/1	DMF	3	45	3	19	18	2.3	2.5	2.5	1.26
PDMAc$_{35}$-2U	B2	40/1/1/1	DMF	2	45	0.5	26	35	1.7	4.2	4.5	1.30
PDMAc$_{83}$-2U	B1	200/1/1/1	DMF	3	45	0.5	38	83	8.2	8.9	9.5	1.28
PDMAc$_{100}$-2U	B2	107/1/1/1	DMF	3	45	0.17	35	100	4.3	10.6	9.6	1.24
PDMAc$_{51}$-2U	B1	200/1/1/1	DMF/i-PrOH (v/v = 3/1)	3	45	0.5	16	51	3.9	5.7	5.8	1.29

[a] Calculated by ^{1}H NMR monitoring during polymerization.

[b, d] Calculated by ^{1}H NMR of the final purified polymers.

[c] Theoretical M_n was calculated by conversion.

[e] Determined by SEC in DMF using PMMA standards and refractive index detection.

-: not determined.

SEC indicated that the dispersity of PDMAc-2Us was less than 1.30 (Figure 3.2.2.2 and Table 3.2.2.2). For $PDMAc_{18}$-2U, a shoulder at the low molecular weight side was observed by SEC, more strongly visible in UV (Figure 3.2.2.2b), which indicates that the shoulder may be originated from the termination (combination) of the initiator due to the fast initiation. In the later syntheses, polymers $PDMAc_{35}$-2U, $PDMAc_{83}$-2U and $PDMAc_{100}$-2U were dialyzed against methanol instead of water, which may explain the absence of the impurity.

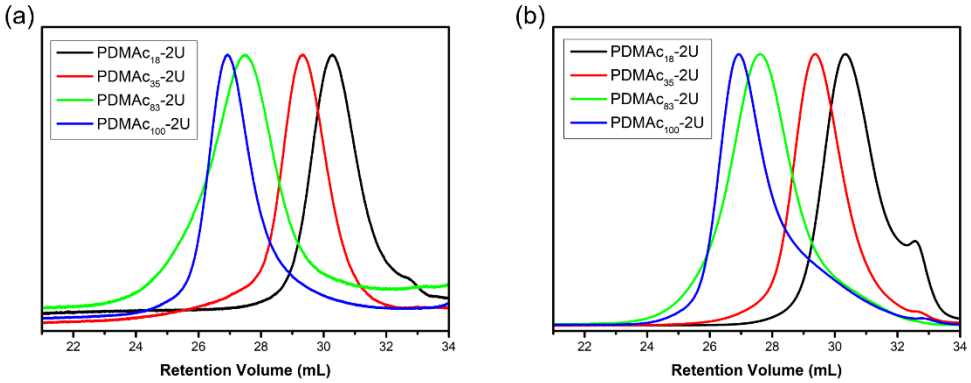

Figure 3.2.2.2. SEC figures of PDMAc-2Us synthesized in DMF with RI (a) and UV (311 nm) (b) signals.

3.2.3 Self-assembly and photo-responsiveness of PDMAc-2U in solution

Three PDMAc-2Us varying in the length of the PDMAc block were dissolved in water to investigate whether these polymers produce spontaneously nanocylinders in water, as expected[9]. Cryo-TEM suggested the formation of nanocylinders of PDMAc-2U. As shown in Figure 3.2.3.1, the shortest $PDMAc_{18}$-2U formed abundant nanocylinders with ~ 7 nm diameter. With the increasing of DP_n, in addition to the cylinders, a majority of many tiny spheres were observed in samples $PDMAc_{35}$-2U and $PDMAc_{100}$-2U.

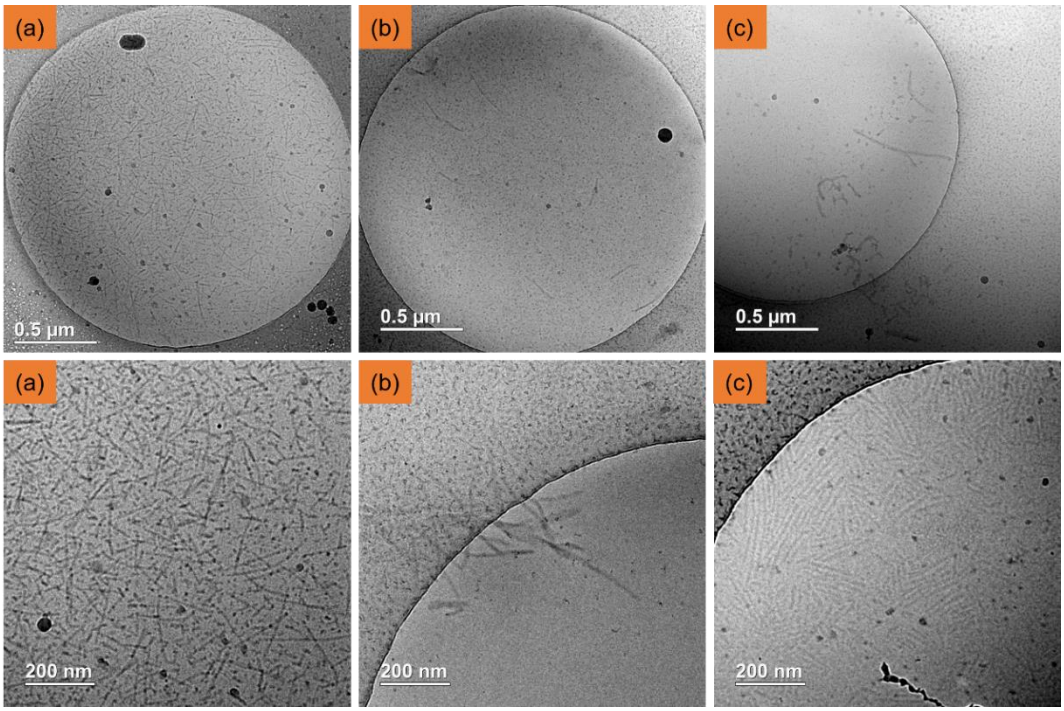

Figure 3.2.3.1. Cryo-TEM of $PDMAc_{18}$-2U (a), $PDMAc_{35}$-2U (b) and $PDMAc_{100}$-2U (c) at 1 wt% in water.

To quantify nanocylinders of PDMAc-2Us, PDMAc-2U with DP_n 18, 35 and 100 were analyzed by small-angle X-ray scattering (SAXS). As displayed in Figure 3.2.3.2, $PDMAc_{18}$-2U had a good fitting with a cylindrical micelle model with a diameter of 10 nm and a length of 40 nm, which was in good agreement with cryo-TEM morphology. For $PDMAc_{35}$-2U and $PDMAc_{100}$-2U, the scattered intensity due to nanocylinders decreased dramatically. The remaining signal ($\sim q^{-3}$) is probably due to the presence of large aggregates. Therefore, the cylinders visible on the cryo-TEM images only represent a small fraction of the sample (Figure3.2.3.1b and c).

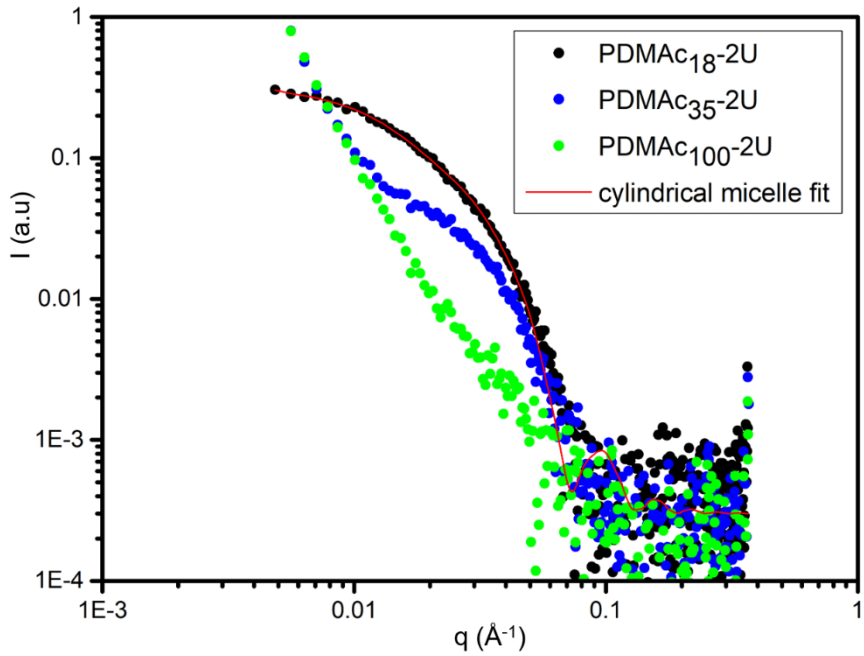

Figure 3.2.3.2. Small-angle X-ray scattering figures of PDMAc-2Us at 1 wt% in water (the red line corresponds to a cylinder model fit).

$PDMAc_{18}$-2U was selected to inspect the photo-cleavage behavior in solution at 300 nm. The cleavage was examined by UV-visible spectroscopy and SEC. Two solvents were considered: DMF where the polymers are expected to be molecularly dissolved, and H_2O where the polymers are self-assembled. UV-visible spectroscopy revealed the good efficiency of cleavage of *o*-nitrobenzyl (ONB) ester, verified by the absorbance loss (peak at 311 nm) after 8 minutes (Figure 3.2.3.3 a and c). For the cleavage in H_2O, in addition to the decrease of peak intensity at 311 nm attributed to *o*-nitrobenzyl (ONB) ester, a considerable increase of peak intensity at 350 nm originated from *o*-nitrobenzyl aldehyde, which was consistent with reported studies[10, 31, 32]. Overall, SEC confirmed the successful photocleavage after 30 min of irradiation due to the shifts of the polymer distribution in DMF and H_2O, as displayed in Figure 3.2.3.3b and d. However, in water, after 20 minutes of UV irradiation, the appearance of a shoulder at the high molecular weight side suggested that a side reaction occurred in water (Figure 3.2.3.3d). This may be due to a coupling of polymer chains, for instance through

radicals[10] produced by photocleavage. The coupling could be favored in water because of the proximity of the chains in the assemblies compared to non-assembled chains in DMF.

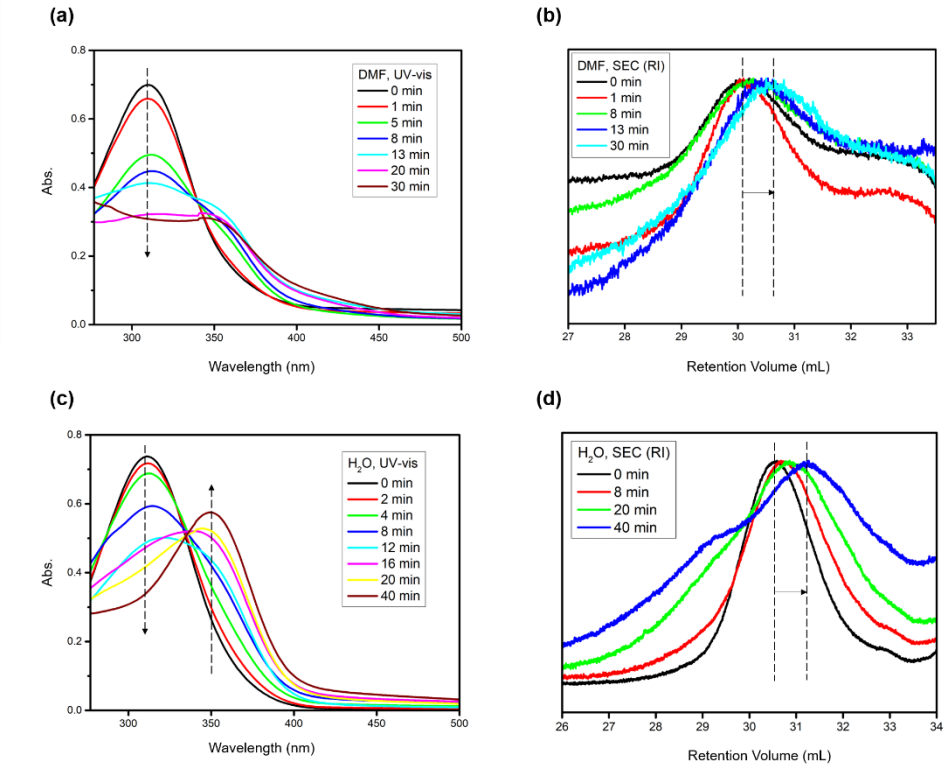

Figure 3.2.3.3. UV-visible spectroscopy (a and c) and SEC (b and d) figures of photo-cleavage kinetics of PDMAc$_{18}$-2U in DMF (a and b, 0.2 mg/mL) and H_2O (c and d, 1.3 mg/mL). The aliquots in DMF were directly injected into SEC. PDMAc$_{18}$-2Us cleaved in water were freeze-dried before injections into SEC (in DMF).

PDMAc-2Us were further investigated by SAXS for cleavage behavior. As shown in Figure 3.2.3.4a, a strong decrease in intensity was observed for PDMAc$_{18}$-2U after 6 hours of UV irradiation indicating the breaking of bonds and dissolution of the polymer chains. The residual signal was either due to aggregates formed by bisureas or simply due to inappropriate blank subtraction. For PDMAc$_{35}$-2U, few and smaller objects are formed compared to PDMAc$_{18}$-2U, but they disappeared after irradiation. For PDMAc$_{100}$-2U, no significant assemblies were found (before and after irradiation).

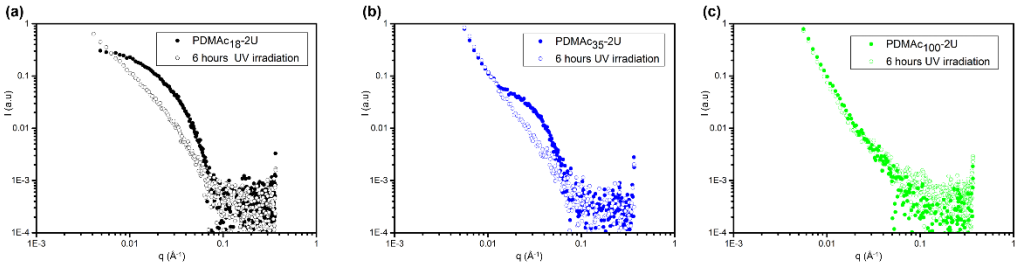

Figure 3.2.3.4. Small-angle X-ray scattering figures of PDMAc-2Us before and after 6 hours of UV irradiation with DP_n 18 (a), 35 (b) and 100 (c) at 1 wt% in water.

3.2.4 Photo-responsiveness of self-assembly of PDMAc-2U on surface

Considering that only $PDMAc_{18}$-2U formed cylindrical micelle, this polymer was chosen for surface deposition with the hope to observe nanocylinders patterning. Keeping the same solvent (water) but at low concentration (1 g/L), the polymer solution was dropped onto a clean silicon substrate. After a fast evaporation in a hood, the substrate was analyzed by atomic force microscopy. As shown in Figure 3.2.4.1, many nanocylinders were observed on a large area. By drawing a line in the Figure 3.2.4.1b, the total distance of 5 adjacent nanocylinder gives 36.6 nm, indicating the average distance between nanocylinders is ~ 7 nm, which is in good agreement with the observed diameter from cryo-TEM and SAXS.

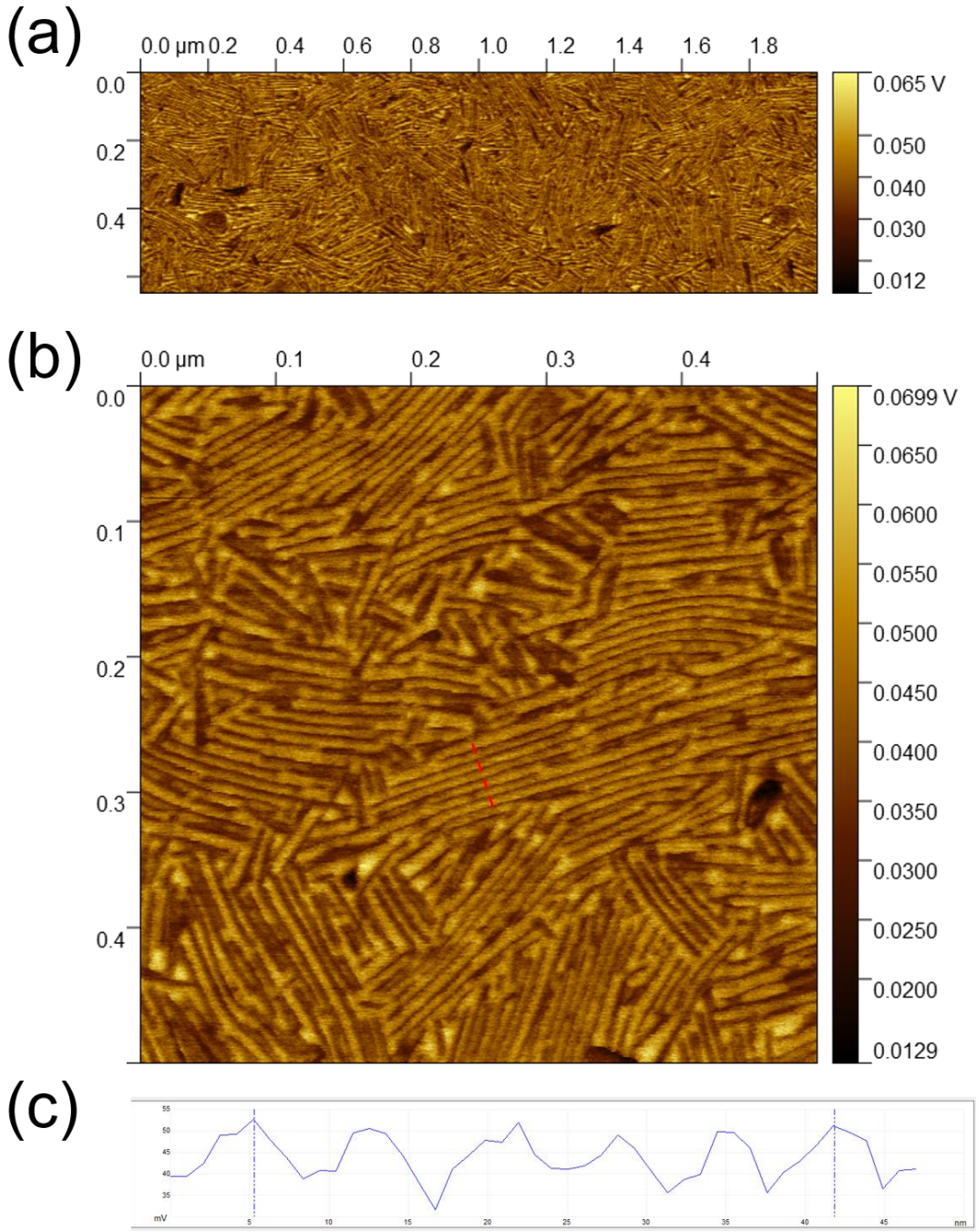

Figure 3.2.4.1. AFM figures of $PDMAc_{18}$-2U after deposition on silicon substrate (adhesion mode).

The substrate was afterwards irradiated under 365 nm UV for 40 minutes. No significant evolution was visible (Figure 3.2.4.2) which is expected since the role of UV irradiation was just to cleave *o*-nitrobenzyl ester, which should not induce the segment motion of the chain and thus the re-organization of the polymer.

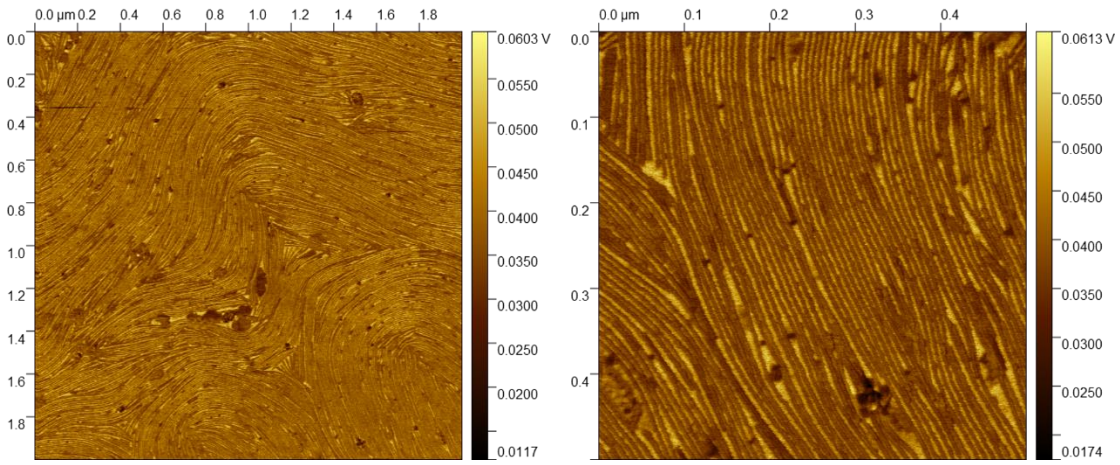

Figure 3.2.4.2. AFM figures of the film of $PDMAc_{18}$-2U after 40 minutes of UV irradiations (adhesion mode).

After 40 minutes of UV irradiation, several solvents were used to try to remove PDMAc. Firstly, the substrate was immersed into the poor solvent of PDMAc, pentane, for 1 minute. AFM figure (Figure 3.2.4.3b) did not present significant changes on nanocylinders, suggesting pentane is a too poor solvent to remove PDMAc. Then, one drop of water was used to rinse the film: some parts of the silicon surface were exposed, even though some regions kept the film. This demonstrated that water was too strong for removing PDMAc, since the sticker was also dissolved.

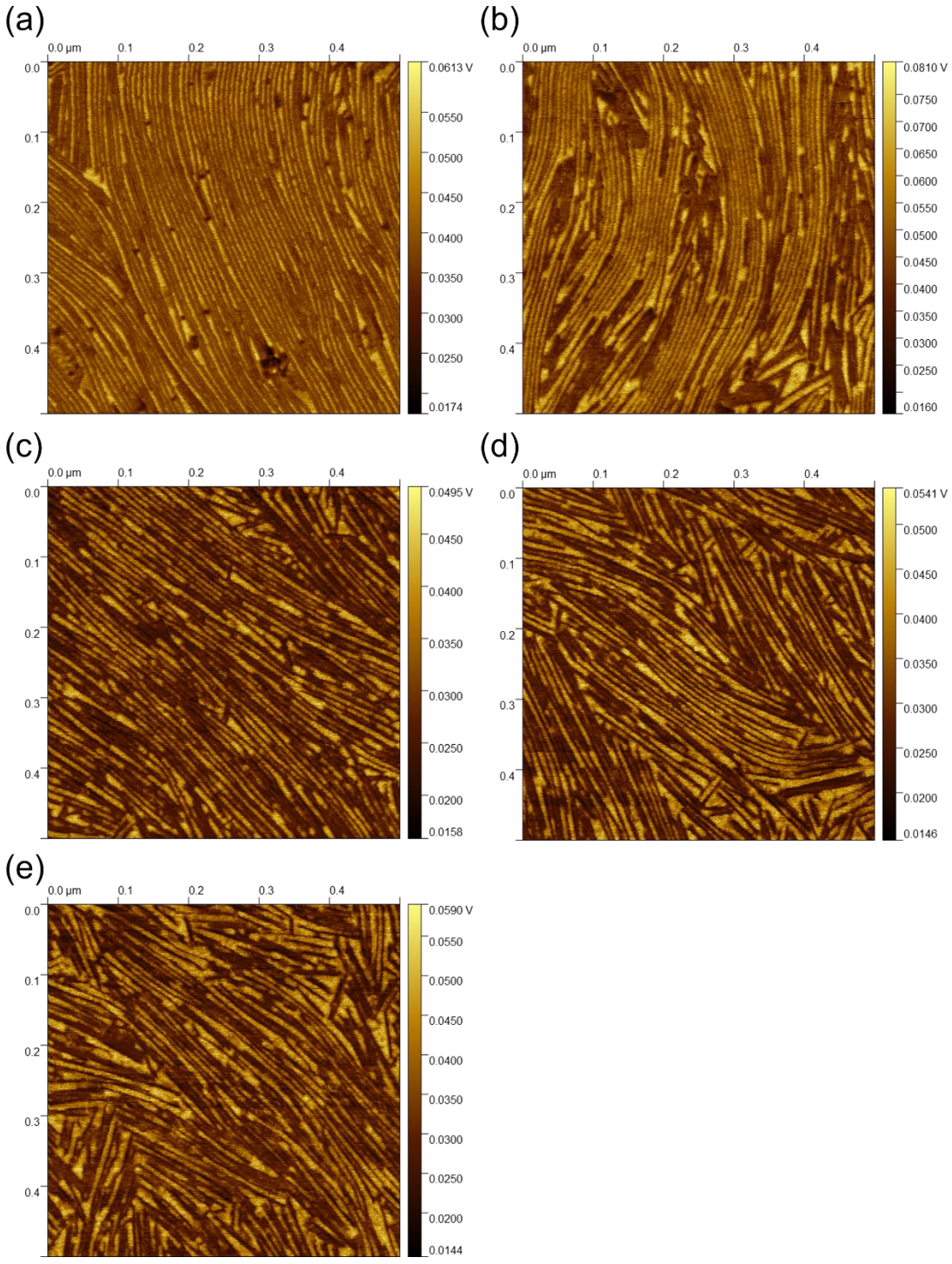

Figure 3.2.4.3. AFM figures of the film of $PDMAc_{18}$-2U before (a) and after solvent treatment using pentane (b) or EA (c: 1 drop rinsing; d: 5 drops rinsing; e: 1 minute soaking) to remove PDMAc (adhesion mode).

Finally, several trials using ethyl acetate to remove PDMAc were performed. When a film after 40 minutes of irradiation was rinsed with 1 drop (Figure 3.2.4.3c) or 5 drops (Figure 3.2.4.3d) of ethyl acetate, still, no obvious changes were observed. However, the film was strongly affected with the observation of cracks after soaking the substrate in ethyl acetate for 1 minute (Figure 3.2.4.4c top), even though nanorods were still found on some unaffected regions (Figure 3.2.4.4c bottom and Figure 3.2.4.3e). This indicated that 1 minute soaking in ethyl acetate was probably too strong for the selective removal of cleaved PDMAc.

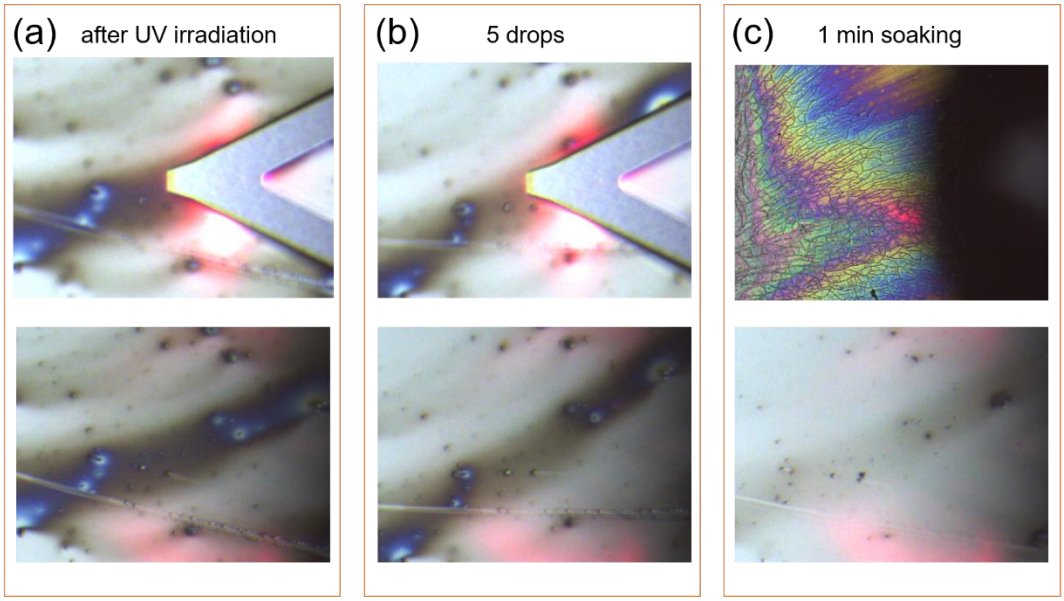

Figure 3.2.4.4. Optical images of the film before (a) and after (b and c) using EA treatments.

3.3 Conclusions

In this chapter, an ATRP initiator incorporating both a photo-cleavable group and a bisurea sticker was synthesized, followed by the polymerization of DMAc to access PDMAc-2U. The polymers were then characterized by ^{1}H NMR and SEC. The self-assembly behavior of PDMAc-2U in water was investigated using cryo-TEM and SAXS: nanocylinders were formed spontaneously in water for a degree of polymerization of 18. After UV irradiation, the nanocylinders were not detected anymore, revealing the good efficiency of the photocleavage behavior. Finally, the surface behavior of $PDMAc_{18}$-2U was studied. The nanocylinders tend to pack together and form parallel features of width ~ 7 nm. After UV irradiation, several solvents were used to try to remove PDMAc, but keep the sticker on the surface. This final step still needs to be optimized. If successful, this strategy should give access to arrays of nm-thick lines placed at regular distances below 10 nm.

3.4 Supporting information

3.4.1 Chemicals and Solvents

The following chemicals were used directly without purification. 5-Hydroxy-2-nitrobenzaldehyde (98%, Sigma-Aldrich), (2-bromoethoxy)- *tert* -butyldimethylsilane (> 96%, TCI Europe), potassium carbonate (K_2CO_3, ≥99.0%, Sigma-Aldrich), potassium iodide (KI, ≥99.0%, Sigma-Aldrich), sodium borohydride (> 95.0%, TCI Europe), 6-(boc-amino)hexanoic acid (>95.0%, TCI Europe), 4-(dimethylamino)pyridine (≥99%, Sigma-Aldrich), *N,N'*-dicyclohexylcarbodiimide (99%, Sigma-Aldrich), tetrabutylammonium fluoride solution (TBAF, 1M in tetrahydrofuran, Sigma-Aldrich), 2 - chloropropionic acid (92%, Sigma-Aldrich), trifluoroacetic acid (for synthesis, Sigma-Aldrich), hexamethylene diisocyanate (≥99.0%, Sigma-Aldrich), hexylamine (99%, Sigma-Aldrich), triethylamine ((≥99.5%, Sigma-Aldrich), celite (filter aid, Sigma-Aldrich), sodium hydrogen carbonate (>99.7%, Thermo Scientific), sodium chloride (≥99%, VWR), sodium sulfate (99%, Thermo Scientific), hydrochloric acid (37%, Sigma-Aldrich), tris(2-dimethylaminoethyl)amine (ABCR, 98%), anisole (99%, Acros Organics) and glacial acetic acid (>99.7%, Thermo Scientific).

N,N-Dimethylformamide (DMF, ≥99.8%, Honeywell), hexane (≥98%, Sigma-Aldrich), ethyl acetate (EA, ≥99.5%, Sigma-Aldrich), tetrahydrofuran (THF, ≥99%, Sigma-Aldrich), methanol (MeOH, ≥99.9%, Carlo Erba), dichloromethane (DCM, ≥99%, Sigma-Aldrich), chloroform ($CHCl_3$, ≥99.8%, VWR), diethyl ether (DE, ≥99.5%, Sigma-Aldrich), acetonitrile (ACN, ≥99.9%, Sigma-Aldrich) and ethanol (96.0 – 97.2%, Sigma-Aldrich) were used as received. Anhydrous DCM and THF were obtained from a solvent purification system (MBraun SPS).

N,N-Dimethylacrylamide (DMAc, 99%, Sigma-Aldrich) was purified on a basic aluminum oxide column to remove the inhibitor. Copper(I) chloride (CuCl, >98.0%,

TCI Europe) was stirred overnight in glacial acetic acid and then filtered through a Buchner funnel, followed by washing with ethanol (3 times) and diethyl ether (3 times), drying under vacuum and finally storing under nitrogen.

3.4.2 Characterizations

Nuclear Magnetic Resonance (NMR). ^{1}H and ^{13}C NMR spectra were obtained in deuterated solvents using Bruker 300 or 400 MHz NMR spectrometer, with 5 mm diameter tubes, at 298 K. All ^{1}H NMR spectra were referenced to the peak at 7.26 ppm (in $CDCl_3$) and 2.50 ppm (in DMSO-d_6). ^{13}C NMR spectra were referenced to the peak at 77.16 ppm (in $CDCl_3$) and 39.52 ppm (in DMSO-d_6). For monomer consumption in polymerization, the integration of anisole was set as a reference to calculate the monomer conversion.

Size Exclusion Chromatography (SEC). PDMAc-2Us with different DP_n were dissolved in DMF with ~ 3 mg/mL concentration to do SEC. The columns of DMF SEC were thermostated at 60°C and the flow rate was set as 0.8 mL/min. Polymers in DMF were detected by a differential refractive index detector (RI) and a Diode Array UV Detector (311 nm). The average molar masses of polymers were obtained by PMMA calibration with refractive index detector.

UV Reactor. The photo-cleavage of polymers were performed under a Rayonet UV reactor equipped with 16 lamps with a maximum irradiation at 300 nm. Polymers were dissolved in DMF or H_2O with stirring during photo-cleavage.

UV-Visible Spectroscopy. Polymer solutions were prepared in cuvette holders with a path length of 2 or 10 mm to perform UV-visible spectroscopy equipped with JASCO-670.

Fourier Transformed InfraRed (FTIR) spectroscopy. The filtrates of Urea-NCO before and during the reaction were filtered with 0.2 μm filters and then injected into a CaF_2 cell to determine the disappearance of N=C=O peak at 2270 cm^{-1}.

Cryo-TEM. Samples were flash frozen in liquid ethane and observed at -180 °C on a JEOL JEM-2100 LaB_6 microscope operating at 200 kV under low-dose conditions (10 electrons $Å^{-2}$ s^{-1}). Digital images were recorded on a Gatan Ultrascan 1000 CCD camera.

Atomic Force Microscopy (AFM). Silicon substrates were cleaned by acetone, ethanol and water in sequence before uses. AFM imaging was performed in air at room temperature in PeakForce Quantitative Nanomechanical Mapping (QNM) mode on an AFM Dimension Icon with ScanAsyst from Bruker, USA, using ScanAsyst-Air silicon-nitride cantilevers (resonance frequency: 70 kHz, spring constant: 0.4 N/m) with a nominal tip radius of 2 nm.

3.4.3 Synthesis of ATRP initiator (Cl-Ar-2U)

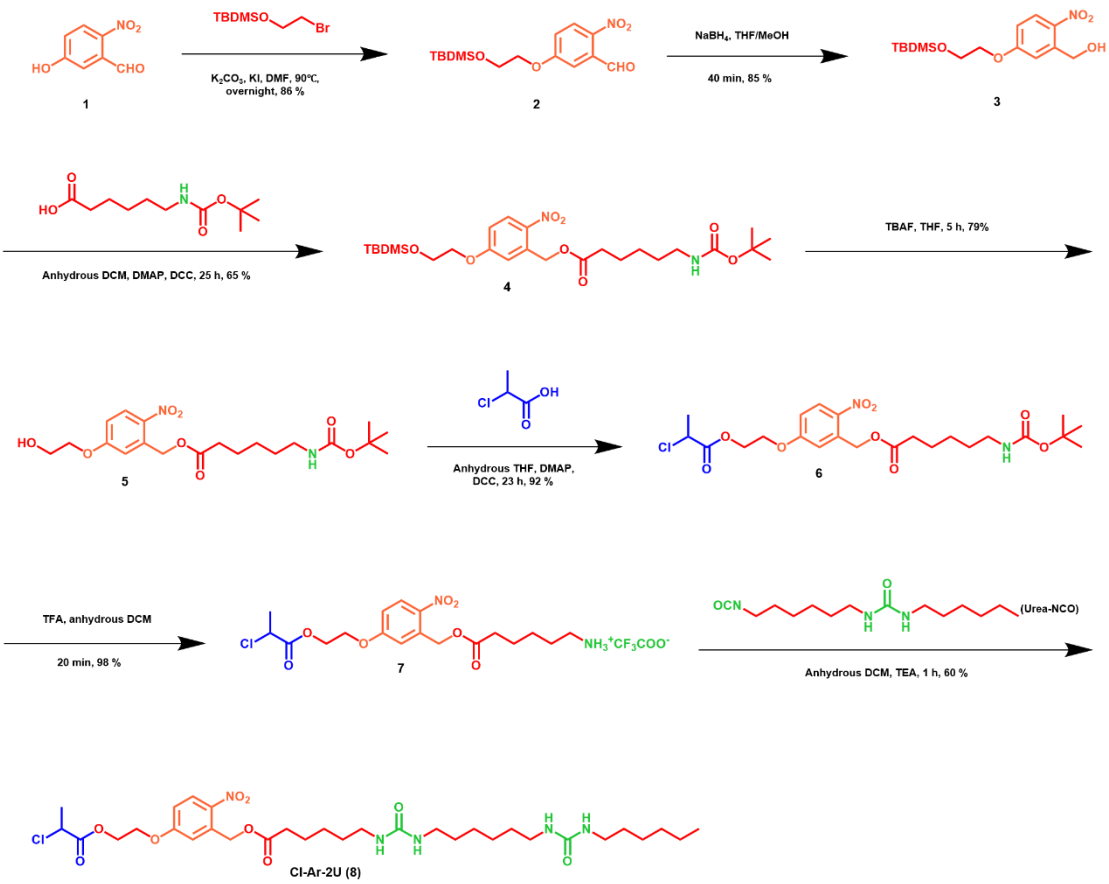

Scheme 3.4.3.1 Synthetic route of bisurea-based ATRP initiator (Cl-Ar-2U).

Synthesis of intermediate of TBDMSO-Ar-CHO (2). Synthesis was adapted from Zong et al[33]. To a solution of 5-hydroxy-2-nitrobenzaldehyde (10 g, 60 mmol, 1 eq), K_2CO_3 (16.5 g, 120 mmol, 2 eq) and KI (1.99 g, 12 mmol, 0.2 eq) in DMF (250 mL) was dropwise added (2-bromoethoxy)-*tert*-butyldimethylsilane (17.1 g, 72 mmol, 1.2 eq). The solution was stirred at 90 ℃ for 17 hours. After cooling down to room temperature, the solution was filtered through celite and then diluted with DI water (200 mL). Afterwards, the aqueous solution was extracted with EA (250 mL × 3). The combined organic layers were washed by saturated $NaHCO_3$ and NaCl. The organic layer was dried by anhydrous sodium sulfate and the solvent was removed under reduced pressure. The yellow solid (16.8 g, 86%) was obtained by flash column chromatography on silica gel using EA (0% - 8%) in hexane as the eluent.

^{1}H NMR (300 MHz, Chloroform-*d*) δ 10.42 (s, 1H), 8.11 (d, 1H), 7.30 (d, 1H), 7.15 (dd, 1H), 4.18 (t, 2H), 3.98 (t, 2H), 0.86 (s, 9H), 0.06 (s, 6H).

^{13}C NMR (75 MHz, $CDCl_3$) δ 188.50, 163.66, 142.26, 134.40, 127.27, 119.04, 114.07, 77.16, 70.72, 61.71, 25.90, 18.40, -5.20.

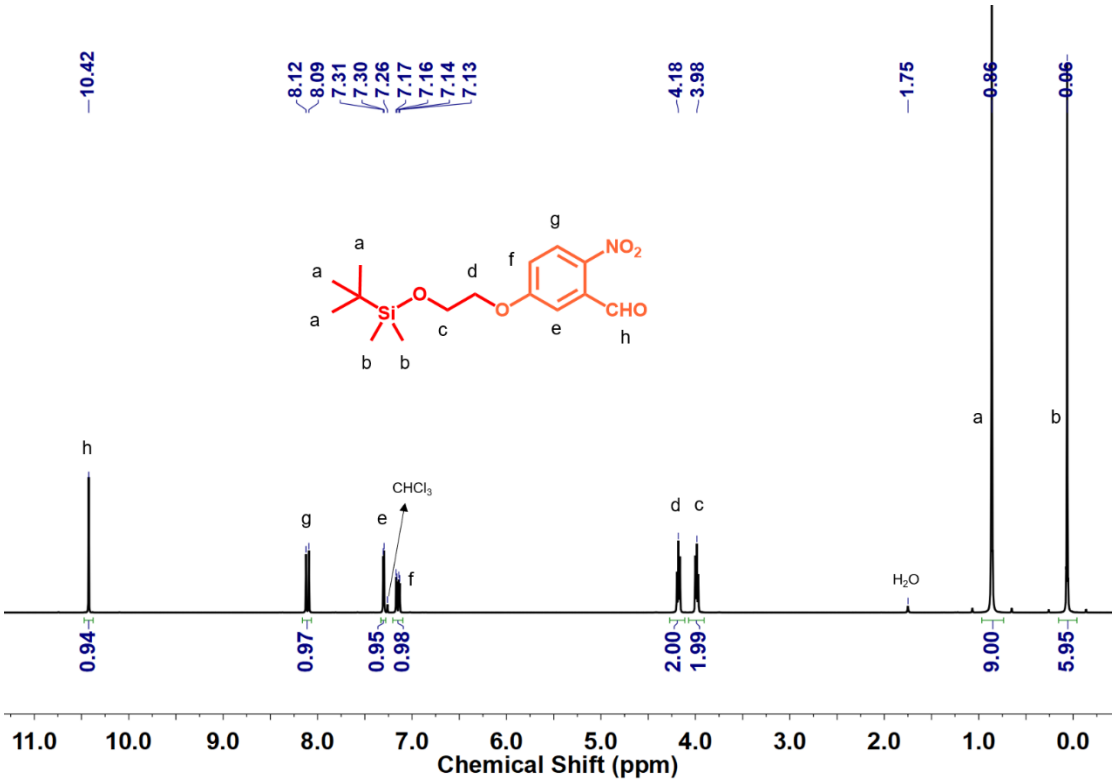

Figure 3.4.3.1. ^{1}H NMR of TBDMSO-Ar-CHO (**2**, in $CDCl_3$).

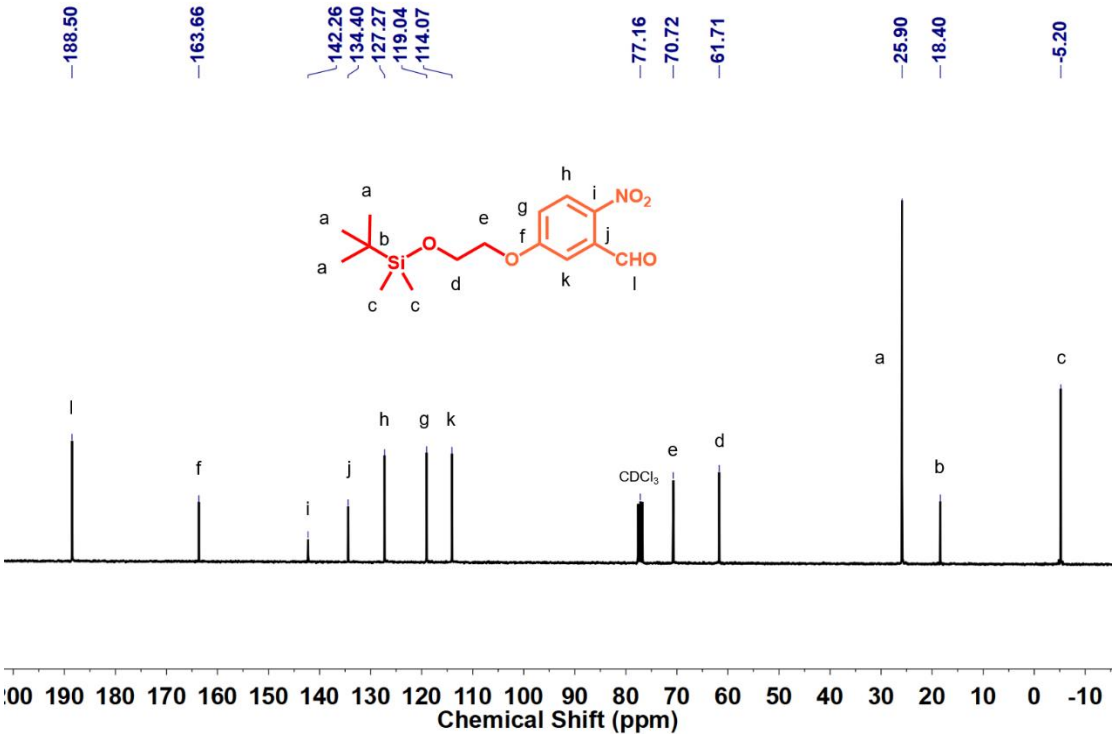

Figure 3.4.3.2. ^{13}C NMR of TBDMSO-Ar-CHO (**2**, in $CDCl_3$).

Synthesis of intermediate of TBDMSO-Ar-OH (3). Synthesis was adapted from Hardy et al[34]. TBDMSO-Ar-CHO (10.4 g, 32 mmol, 1 eq) THF/MeOH (70/70 mL) and a magnetic stirring bar were added into a 250 mL round bottom flask which was cooled at 0 ℃. Under the protection of nitrogen, sodium borohydride (1.28 g, 33.7 mmol, 1.05 eq) was added portionwise. The reaction was monitored by TLC and finished after 40 minutes until TBDMSO-Ar-CHO was totally consumed. The solution was evaporated and 50 mL of EA and 150 mL of hydrochloric acid (1 M) were added, followed by stirring 30 minutes. The aqueous solution was extracted by EA (150 mL × 2). Afterwards, the combined organic layers were washed by saturated $NaHCO_3$ (100 mL) and NaCl (100 mL). The organic layer was dried by anhydrous sodium sulfate and the solvent was removed under reduced pressure. The crude product was purified by flash column chromatography on silica gel using EA (10% - 15%) in hexane as the eluent to afford a yellow solid (8.9 g, 85%).

^{1}H NMR (400 MHz, DMSO-d_6) δ 8.12 (d, 1H), 7.35 (d, 1H), 7.02 (d, 2.9 Hz, 1H), 5.56 (t, 1H), 4.85 (d, 2H), 4.17 (t, 2H), 3.96 (t, 2H), 0.86 (s, 9H), 0.07 (s, 6H).

^{13}C NMR (101 MHz, DMSO-d_6) δ 163.06, 142.35, 139.29, 127.48, 113.23, 112.72, 70.00, 61.41, 60.21, 25.76, 18.00, -5.21.

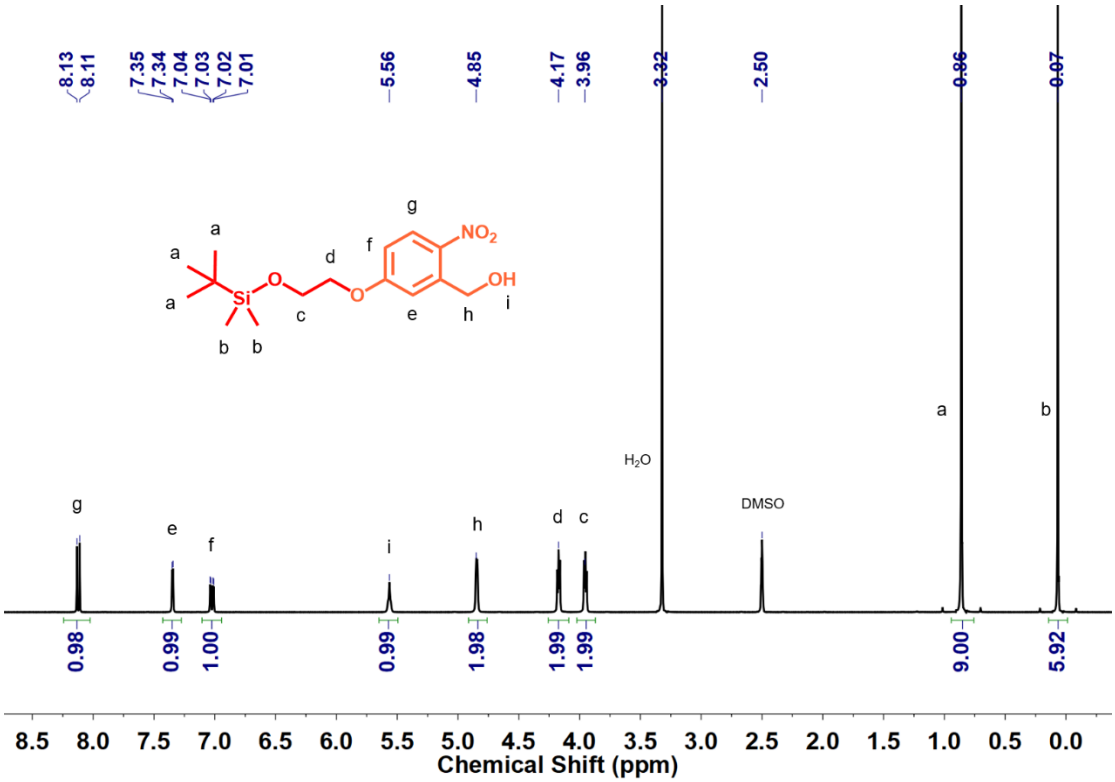

Figure 3.4.3.3. ^{1}H NMR of TBDMSO-Ar-OH (**3**, in DMSO-d$_6$).

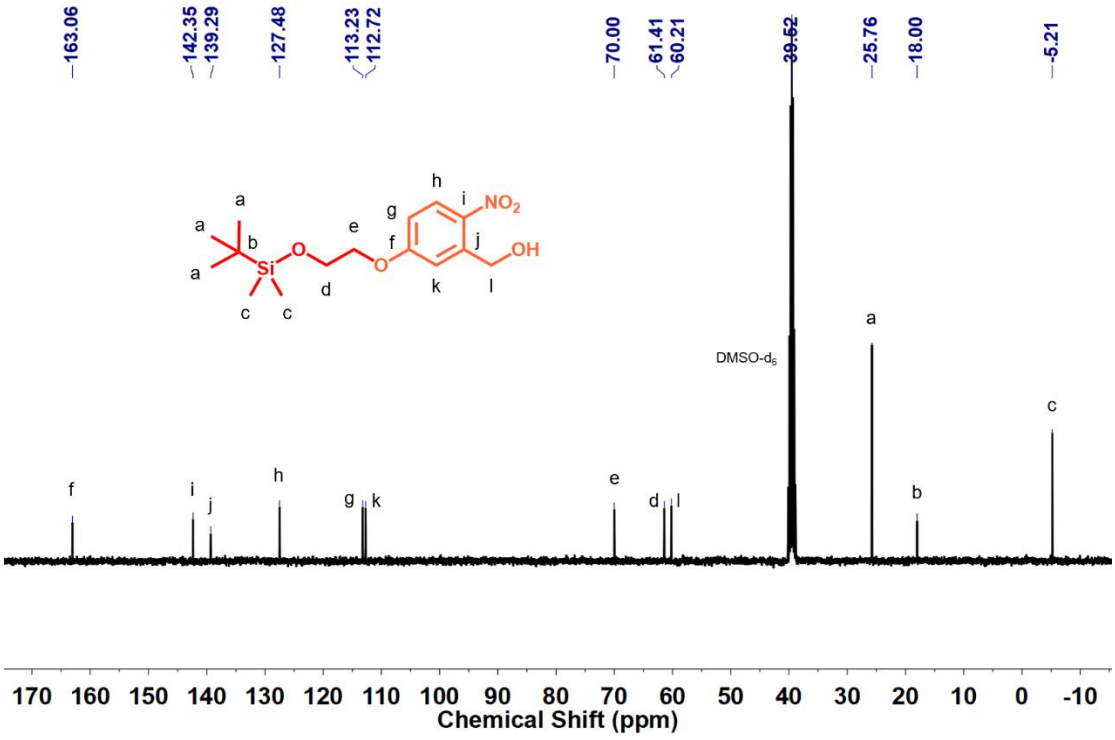

Figure 3.4.3.4. ^{13}C NMR of TBDMSO-Ar-OH (**3**, in DMSO-d$_6$).

Synthesis of intermediate of TBDMSO-Ar-Boc (4). To a 50 mL round bottom flask equipped with a magnetic stirring bar was added 6-(Boc-amino)hexanoic acid (0.85 g, 3.68 mmol, 1.2 eq), DMAP (0.19 g, 1.56 mmol, 0.5 eq), DCC (0.94 g, 4.56 mmol, 1.5 eq) and 20 mL of anhydrous DCM. The solution was cooled at 0 ℃ and stirred for 5 minutes before dropwise adding a solution of TBDMSO-Ar-OH (1 g, 3.06 mmol, 1 eq) in anhydrous DCM (10 mL). After 25 hours, the solution was washed with 20 mL of DI water and then dried by anhydrous sodium sulfate. After evaporating the solvent, the crude product was purified by flash column chromatography on silica gel using EA (10% - 25%) in hexane as the eluent to afford a yellow liquid (1.08 g, 65%).

^{1}H NMR (400 MHz, DMSO-d_6) δ 8.17 (d, 1H), 7.12 (d, 2H), 6.73 (s, 1H), 5.42 (s, 2H), 4.19 (t, 2H), 3.94 (t, 2H), 2.99 – 2.80 (m, 2H), 2.40 (t, 2H), 1.63 – 1.16 (m, 15H), 0.85 (s, 9H), 0.05 (s, 6H).

^{13}C NMR (101 MHz, DMSO-d_6) δ 172.31, 162.90, 155.52, 139.89, 134.95, 127.94, 114.62, 113.68, 77.24, 70.16, 62.45, 61.39, 39.60, 33.37, 29.12, 28.23, 25.71, 24.13, 17.97, -5.28.

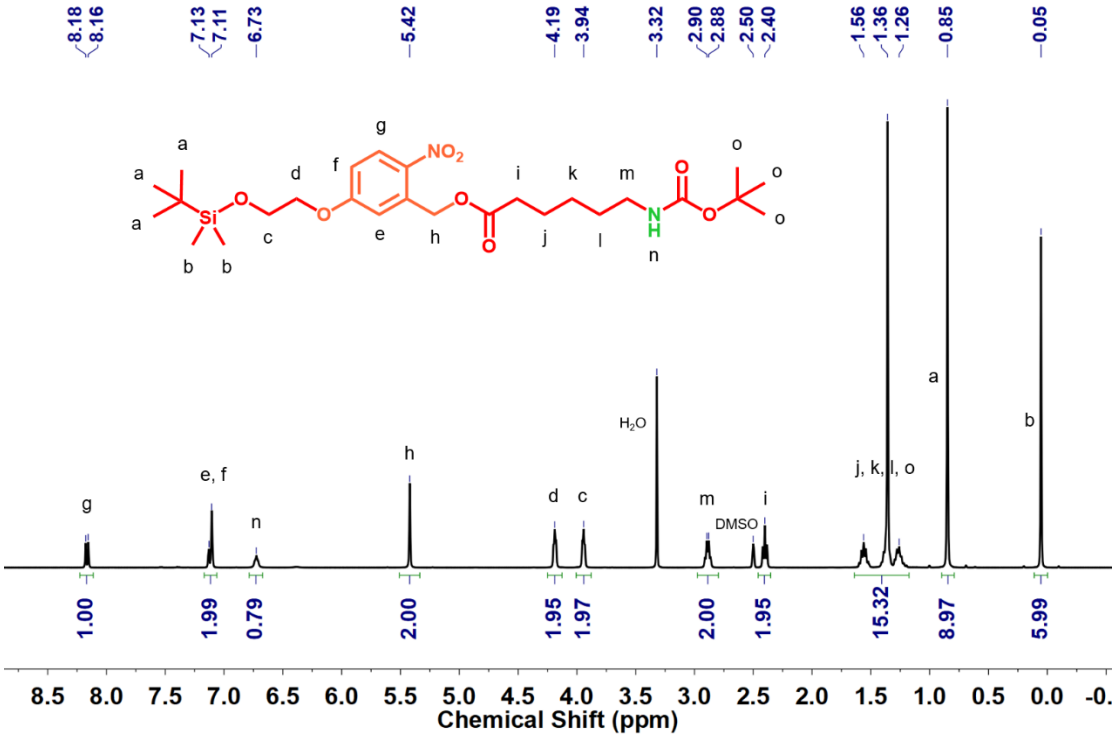

Figure 3.4.3.5. ^{1}H NMR of TBDMSO-Ar-Boc (**4**, in DMSO-d$_6$).

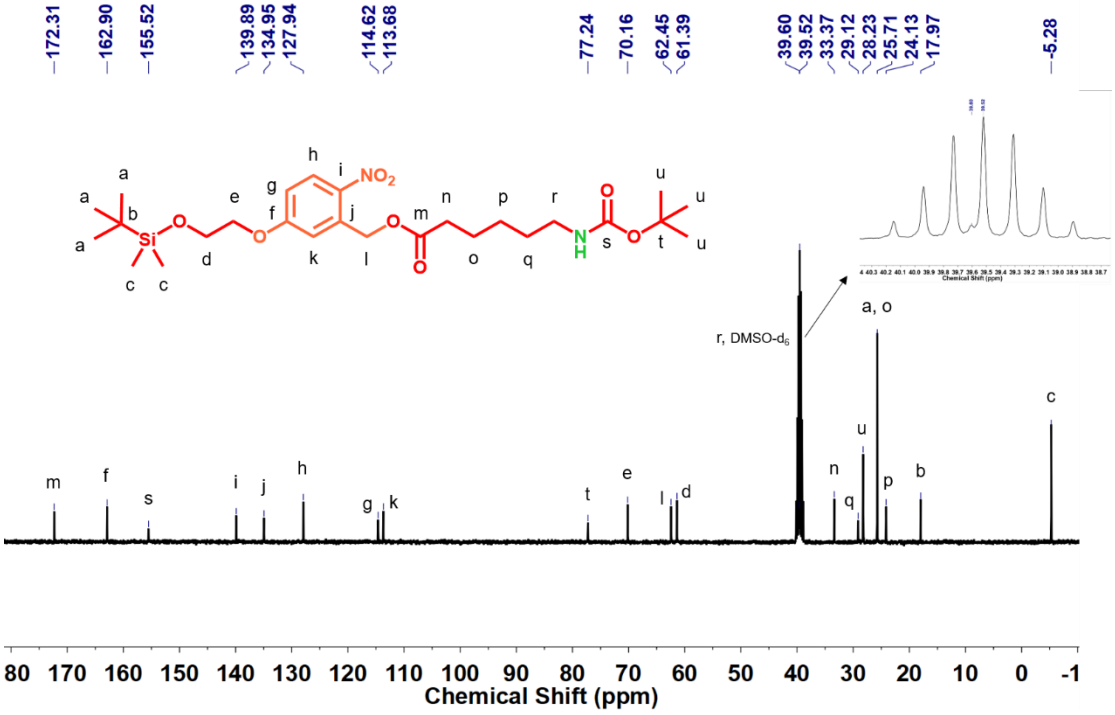

Figure 3.4.3.6. ^{13}C NMR of TBDMSO-Ar-Boc (**4**, in DMSO-d$_6$).

Synthesis of intermediate of HO-Ar-Boc (5). TBDMSO-Ar-Boc (6.2 g, 11.5 mmol, 1 eq), 100 mL of THF and a magnetic stirring bar were added into a 250 mL round bottom flask. Afterwards, a solution of TBAF (1 M solution in THF, 12.1 mL, 12.1 mmol, 1.05 eq) in THF (20 mL) was dropwise added into the flask. The reaction was monitored by TLC. TBDMSO-Ar-Boc was totally consumed after 5 hours. After evaporation of the solvent, the crude product was purified by flash column chromatography on silica gel using EA (0% - 40%) in DCM as the eluent to afford a yellowish liquid (3.85 g, 79%).

^{1}H NMR (400 MHz, DMSO-d_6) δ 8.17 (d, 1H), 7.12 (d, 2H), 6.74 (s, 1H), 5.42 (s, 2H), 4.94 (t, 1H), 4.15 (t, 2H), 3.84 – 3.68 (m, 2H), 2.89 (q, 2H), 2.41 (t, 2H), 1.62 – 1.21 (m, 15H).

^{13}C NMR (101 MHz, DMSO-d_6) δ 172.44, 163.02, 155.56, 139.87, 134.89, 127.94, 114.80, 113.72, 77.29, 70.59, 62.53, 59.28, 39.63, 33.31, 29.12, 28.25, 25.71, 24.13.

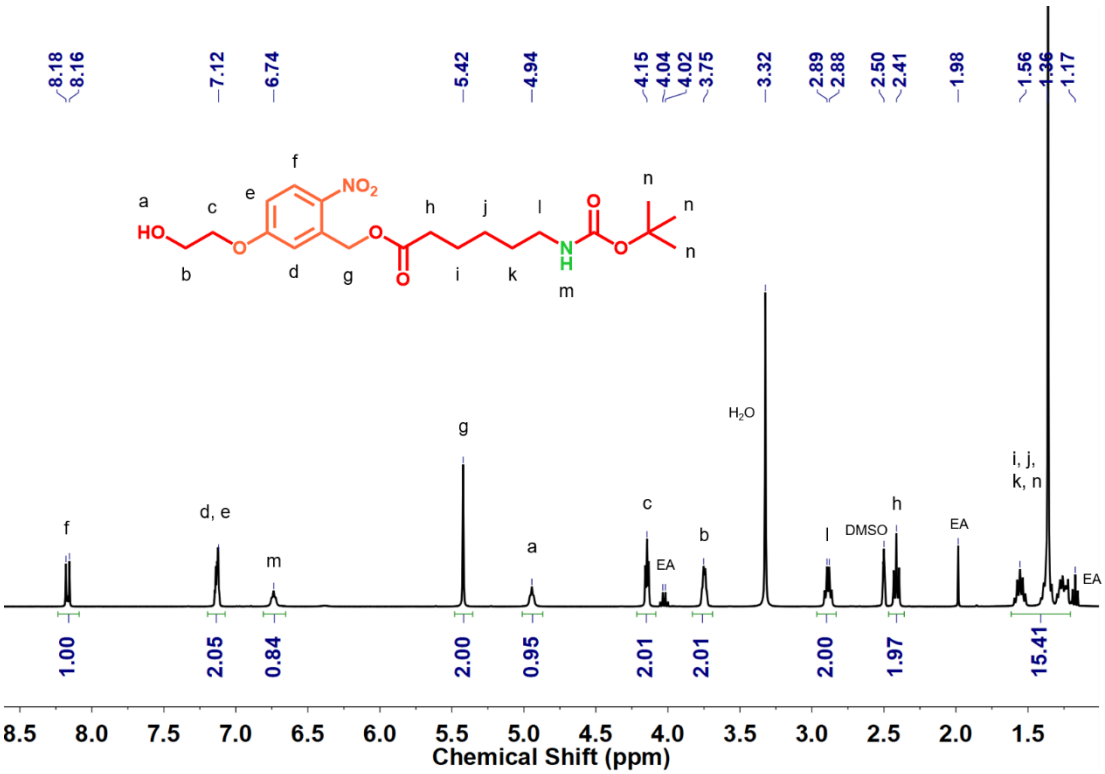

Figure 3.4.3.7. ^{1}H NMR of HO-Ar-Boc (**5**, in DMSO-d$_6$).

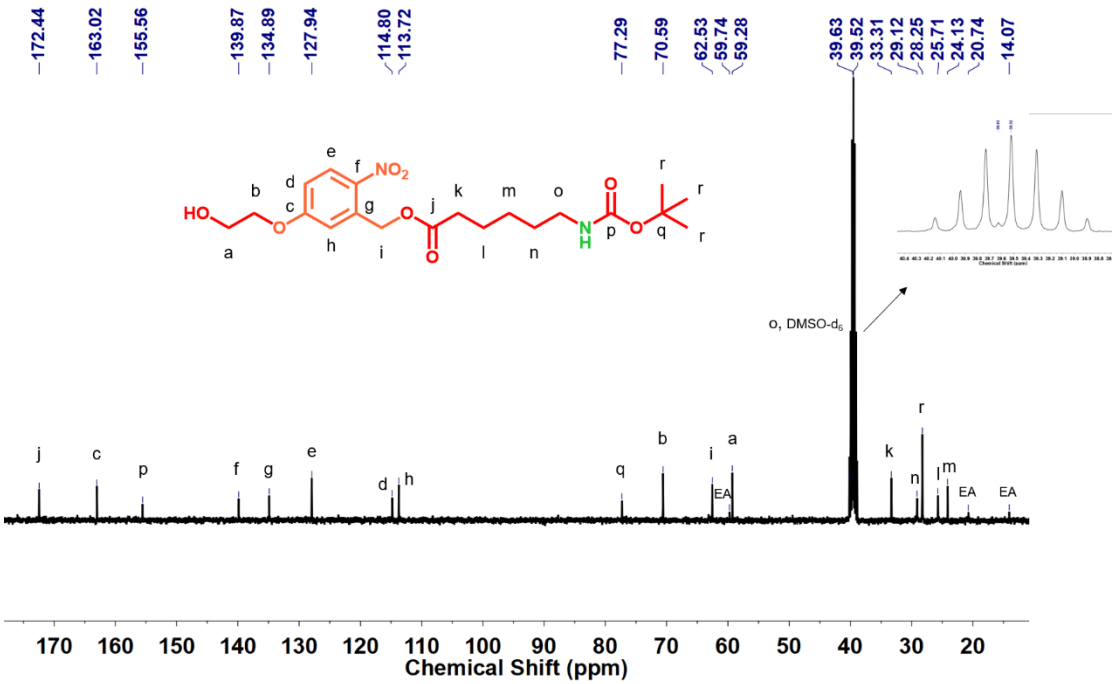

Figure 3.4.3.8. ^{13}C NMR of HO-Ar-Boc (**5**, in DMSO-d$_6$).

Synthesis of intermediate of Cl-Ar-Boc (6). To a 100 mL round bottom flask equipped with a magnetic stirring bar was added 2-chloropropionic acid (0.5 g, 4.63 mmol, 1.9 eq), DMAP (0.55 g, 4.51 mmol, 1.8 eq), DCC (1.45 g, 7.04 mmol, 2.9 eq) and 50 mL of anhydrous THF. The solution was cooled at 0 ℃ and stirred for 5 minutes before dropwise adding a solution of TBDMSO-Ar-OH (1 g, 2.46 mmol, 1 eq) in anhydrous THF (15 mL). The reaction was stirred for 23 hours. After evaporating the solvent, the crude product was purified by manual column on silica gel using EA (33% - 40%) in hexane as the eluent to afford a colorless solid (1.1 g, 92%).

^{1}H NMR (400 MHz, DMSO-d_6) δ 8.17 (d, 1H), 7.16 (d, 2H), 6.74 (s, 1H), 5.42 (s, 2H), 4.75 (q, 1H), 4.59 – 4.31 (m, 4H), 2.97 – 2.80 (m, 2H), 2.41 (t, 2H), 1.66 – 1.47 (m, 5H), 1.45 – 1.15 (m, 13H).

^{13}C NMR (101 MHz, DMSO-d_6) δ 172.42, 169.53, 162.28, 155.53, 140.31, 134.87, 127.92, 114.96, 113.86, 77.28, 66.56, 63.67, 62.47, 52.58, 39.61, 33.30, 29.11, 28.24, 25.70, 24.11, 21.19.

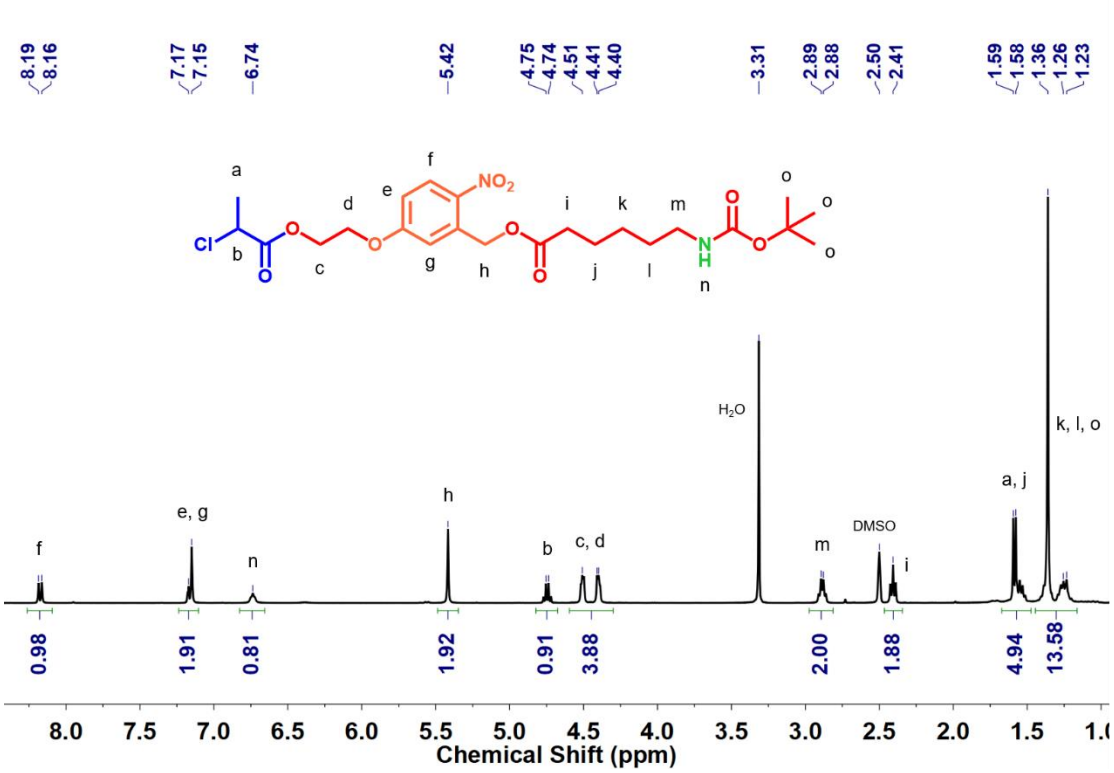

Figure 3.4.3.9. ^{1}H NMR of Cl-Ar-Boc (**6**, in DMSO-d_6).

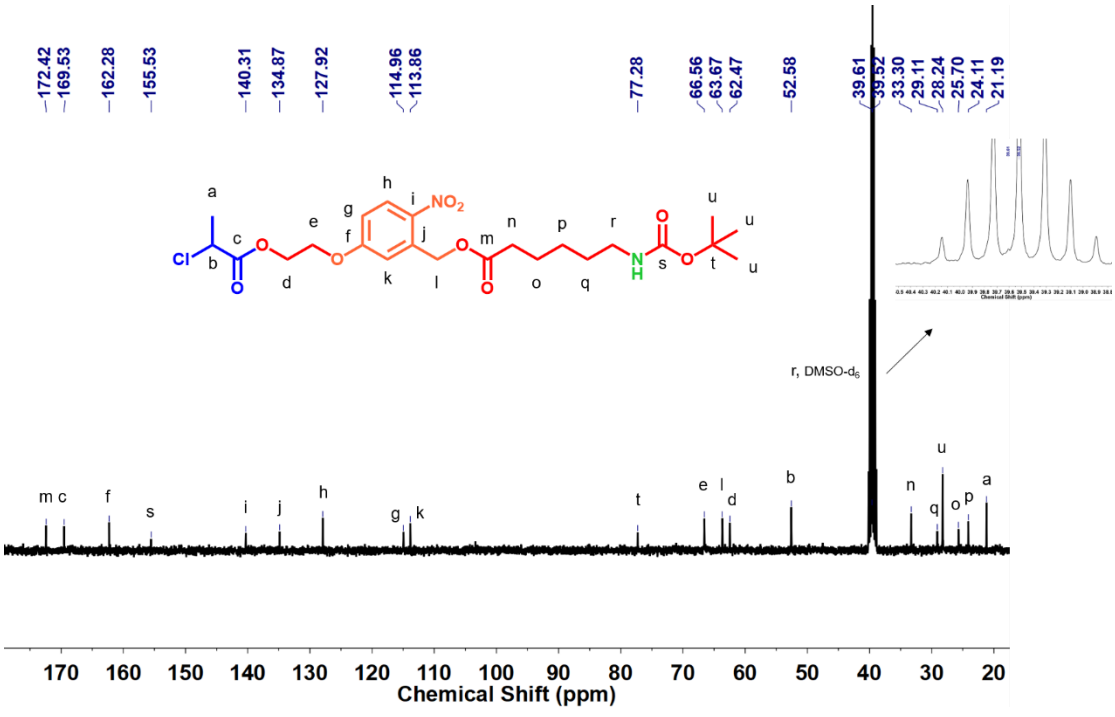

Figure 3.4.3.10. ^{13}C NMR of Cl-Ar-Boc (**6**, in DMSO-d_6).

Synthesis of intermediate of Cl-Ar-NH3$^+$ (7). To a solution of Cl-Ar-Boc (0.59 g, 1.14 mmol, 1 eq) in anhydrous DCM (20 mL) was dropwise added 2 mL of TFA (26.1 mmol, 23 eq). The reaction was monitored by TLC. Cl-Ar-Boc was totally consumed after 20 minutes. A yellow liquid (0.59 g, 98%) was obtained after evaporating the solvent.

^{1}H NMR (400 MHz, DMSO-d_6) δ 8.17 (d, 1H), 7.75 (s, 3H), 7.17 (d, 2H), 5.42 (s, 2H), 4.74 (q, 1H), 4.58 – 4.31 (m, 4H), 2.86 – 2.67 (m, 2H), 2.43 (t, 2H), 1.65 – 1.20 (m, 9H).

^{13}C NMR (101 MHz, DMSO-d_6) δ 172.35, 169.56, 162.28, 140.40, 134.73, 127.97, 115.27, 113.89, 66.60, 63.70, 62.61, 52.61, 38.63, 33.07, 26.64, 25.19, 23.84, 21.20.

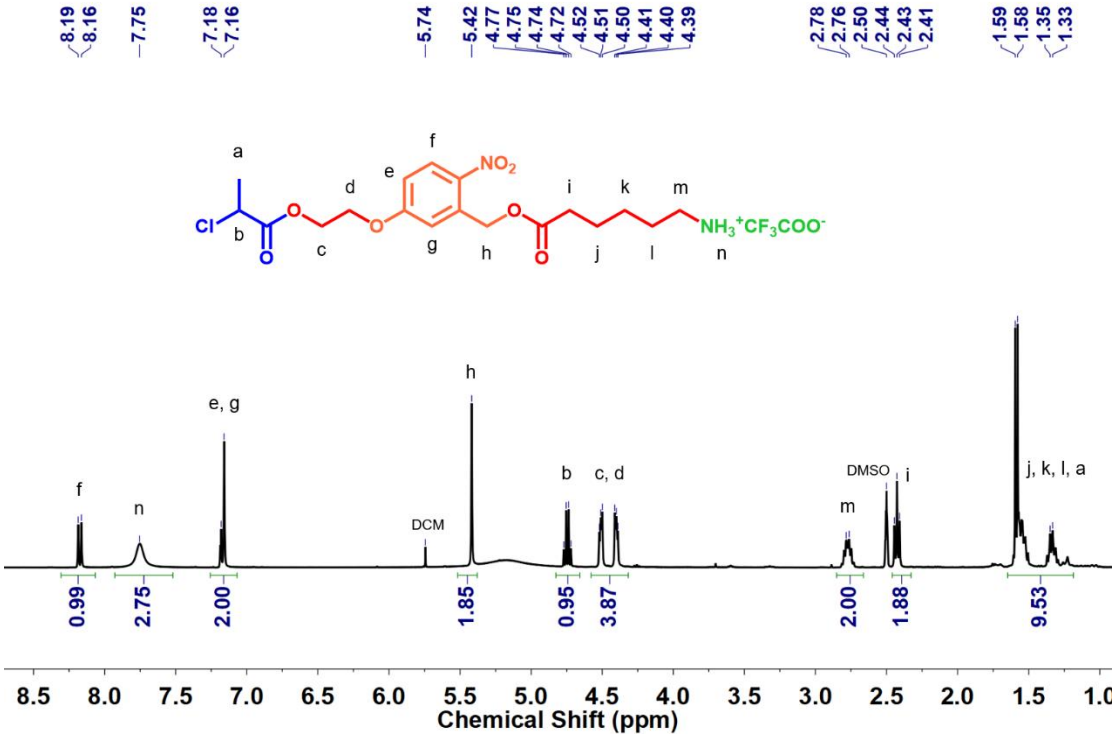

Figure 3.4.3.11. ^{1}H NMR of Cl-Ar-NH3^{+} (**7**, in DMSO-d$_6$).

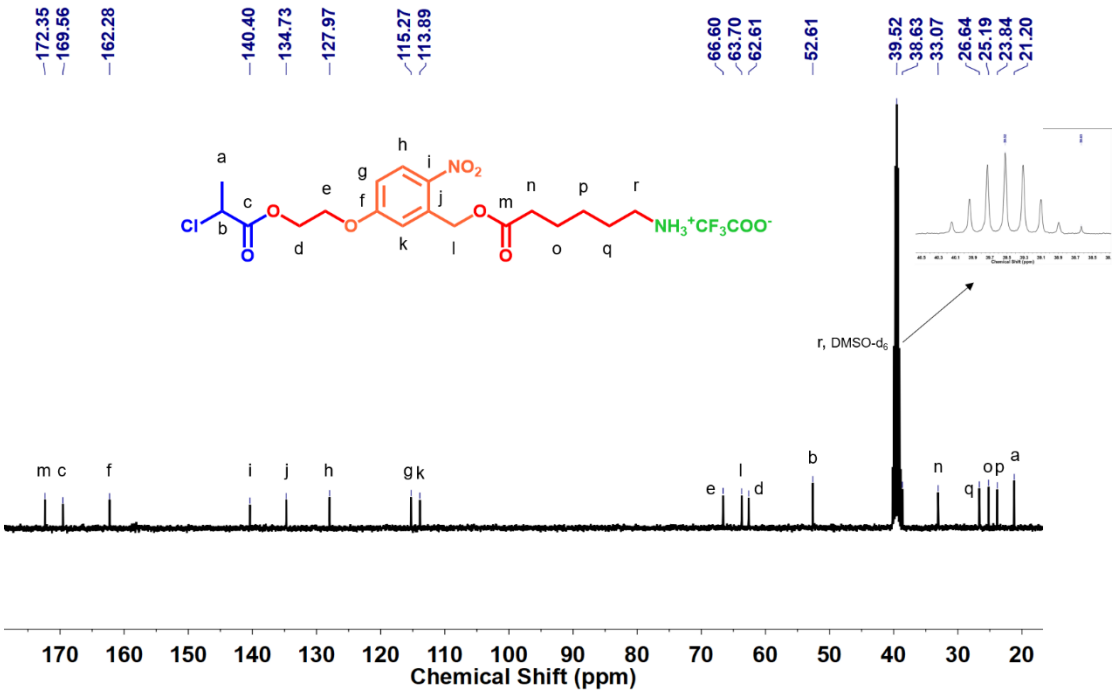

Figure 3.4.3.12. ^{13}C NMR of Cl-Ar-NH3^{+} (**7**, in DMSO-d$_6$).

Synthesis of Urea-NCO. The synthesis of Urea-NCO was adapted from the reported procedure[21]. To a 250 mL round bottom flask equipped with a magnetic stirring bar was added hexamethylene diisocyanate (16.6 mL, 103 mmol, 10.4 eq) and 100 mL of anhydrous DCM. Then, a solution of hexylamine (1 g, 9.9 mol, 1 eq) in anhydrous DCM (15 mL) was injected into the flask with a 45 mL/h rate. The precipitate formed during the injection. After 30 minutes, the solution was evaporated at ~ 20 °C to form a gel-like material followed by the addition of excess of hexane. The precipitate was formed and dissolved in DCM to do another precipitation in hexane. A colorless solid (1.25 g, 47%) was obtained after the filtration.

^{1}H NMR (400 MHz, Chloroform-d) δ 4.37 (s, 2H), 3.29 (t, 2H), 3.23 – 3.01 (m, 4H), 1.79 – 1.15 (m, 16H), 0.88 (t, 3H).

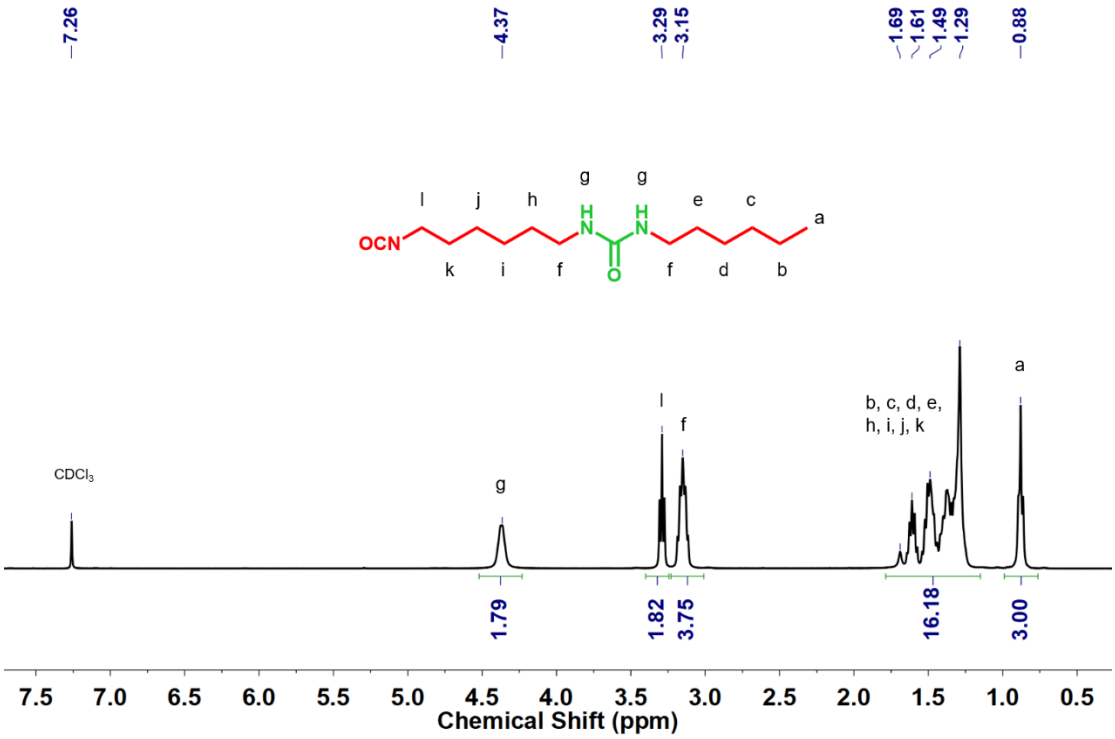

Figure 3.4.3.13. ^{1}H NMR of Urea-NCO (in $CDCl_3$).

Synthesis of ATRP initiator (Cl-Ar-2U, 8). To a solution of Urea-NCO (0.23 g, 0.86 mmol, 1 eq) and TEA (0.17 mL, 2 eq) in anhydrous DCM (34 mL) was slowly added a solution of Cl-Ar-NH_3^+ (0.5 g, 0.94 mmol, 1.1 eq) in anhydrous DCM (10 mL).

During the reaction, a colorless precipitate formed. The reaction was monitored by infrared spectroscopy. The N=C=O peak at 2270 cm^{-1} disappeared after 1 hour. The mixture was filtered and the solid was washed with $CHCl_3$ (200 mL), DE (100 mL), H_2O (200 mL), acetonitrile (100 mL) and EA (100 mL). The crude solid was recrystallized from $CHCl_3$ to afford a colorless solid (0.35 g, 60%). The synthesis was repeated and therefore 2 batches were obtained.

^1H NMR (400 MHz, DMSO-d_6, batch 1) δ 8.15 (d, 1H), 7.15 (m, 2H), 5.62 (br, 4H), 5.42 (s, 2H), 4.71 (q, 1H), 4.61 – 4.29 (m, 4H), 2.97 (m, 8H), 2.40 (t, 2H), 1.69 – 1.14 (m, 25H), 0.86 (t, 3H).

^{13}C NMR (101 MHz, DMSO-d_6, batch 1) δ 172.07, 169.18, 162.03, 157.93, 157.92, 140.40, 134.42, 127.44, 115.02, 113.89, 66.41, 63.41, 62.11, 52.30, 39.00, 33.13, 30.71, 29.70, 29.38, 25.83, 25.72, 25.58, 23.90, 21.68, 20.88, 13.44.

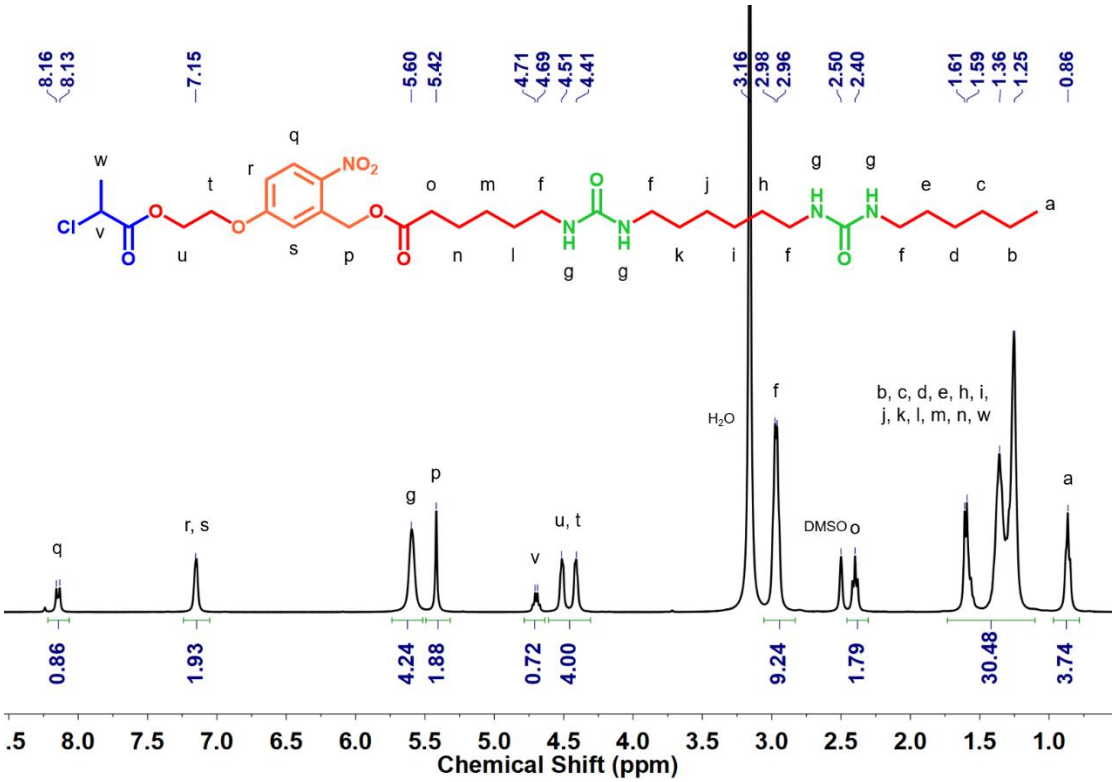

Figure 3.4.3.14. ^{1}H NMR of Cl-Ar-2U (**8**, batch 1, in DMSO-d_6, 60°C).

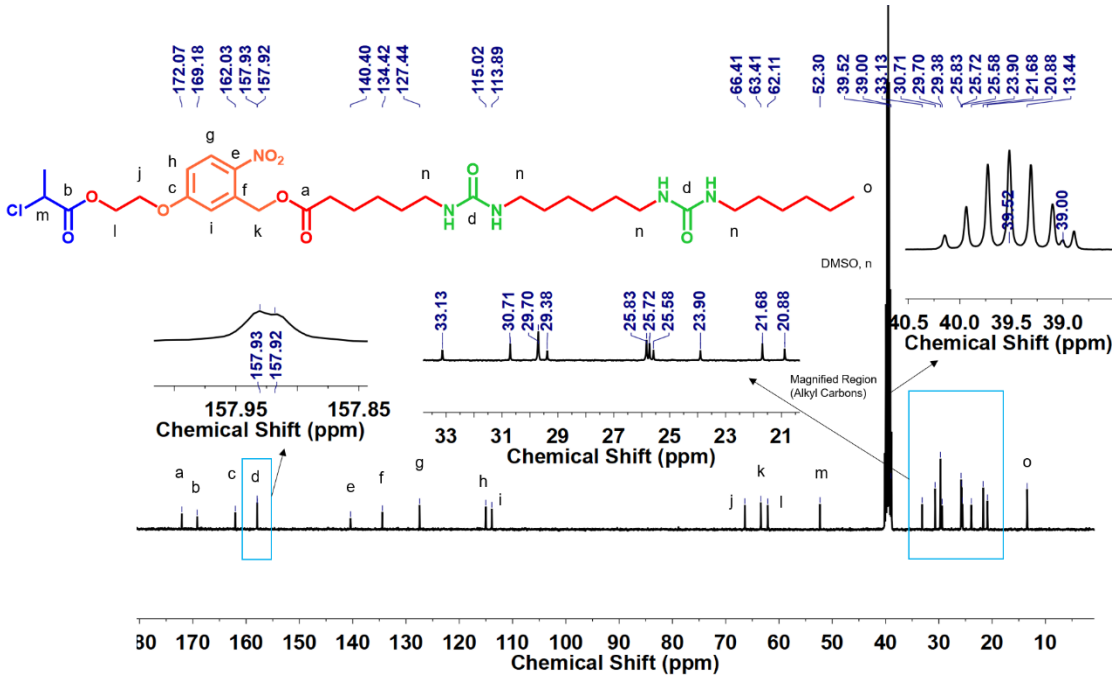

Figure 3.4.3.15. ^{13}C NMR of Cl-Ar-2U (**8**, batch 1, in DMSO-d_6, 60°C).

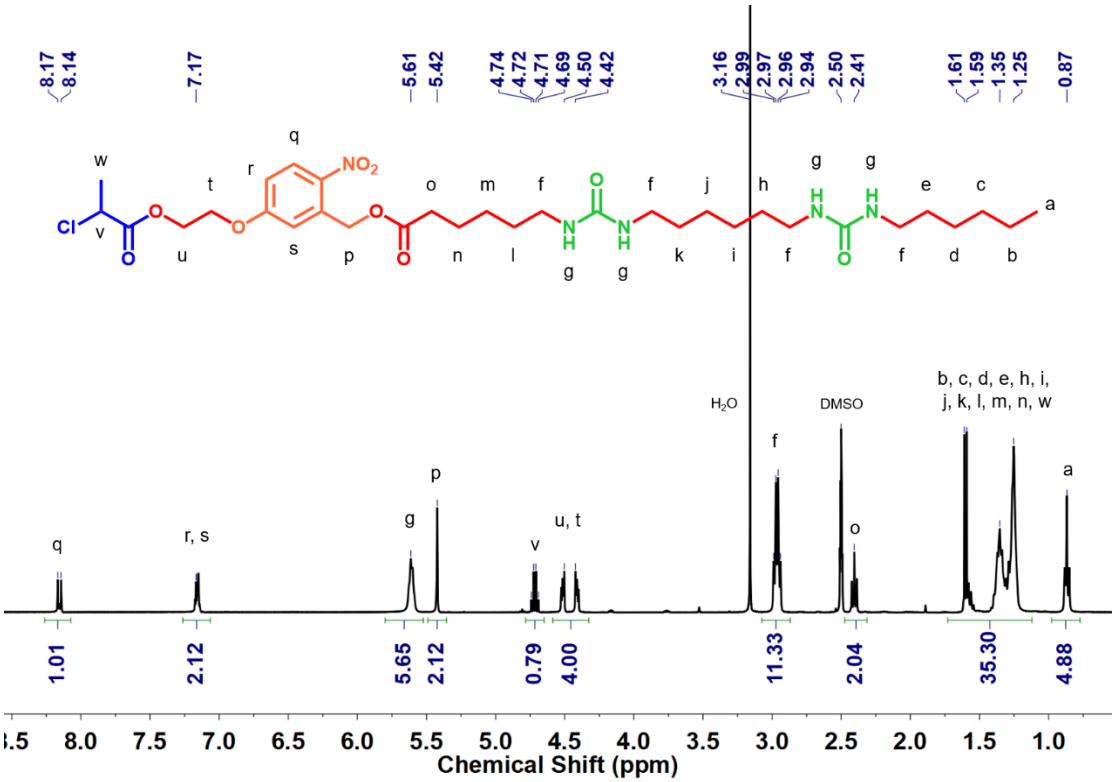

Figure 3.4.3.16. ^{1}H NMR of Cl-Ar-2U (**8**, batch 2, in DMSO-d_6, 60°C).

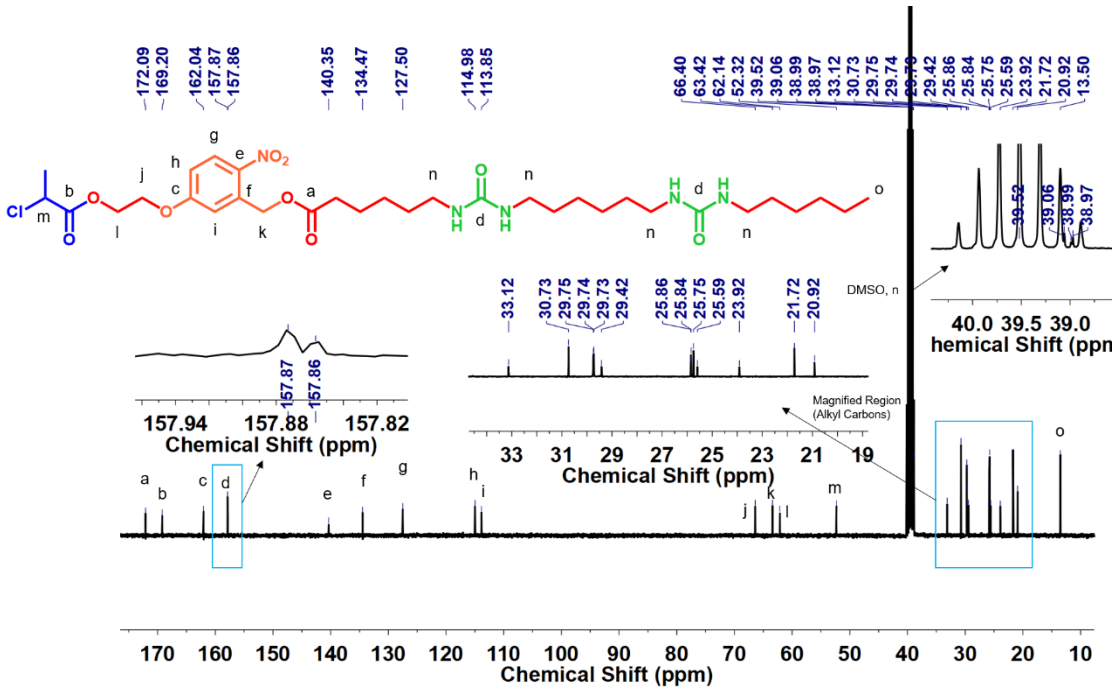

Figure 3.4.3.17. ^{13}C NMR of Cl-Ar-2U (**8**, batch 2, in DMSO-d_6, 60°C).

3.4.4 Polymerization of DMAc by ATRP

Polymerization of *N,N*-dimethylacrylamide using ATRP initiator (DP_n = 18). A 4 mL vial equipped with a magnetic stirring bar was charged with *N,N*-dimethylacrylamide (627 mg, 6.33 mmol, 83 eq), Cl-Ar-2U (52 mg, 0.076 mmol, 1 eq), Me_6TREN (17.4 mg, 0.076 mmol, 1 eq), anisole (internal standard, 40 mg, 0.37 mmol, 5 eq) and DMF (1.4 mL). The solution was bubbled with N_2 at 45 °C followed by introducing CuCl (7.5 mg, 0.076 mmol, 1 eq) under the protection of N_2. After 3 hours at 45°C, the rubber cap was open and the polymer was diluted with THF (1 mL) and DCM (2 mL). The solution was passed through a short silica column to remove metal complex before a precipitation in diethyl ether. The crude polymer was dissolved in DMF to perform dialysis (against water) to afford a colorless solid (56 mg, 33%) after freeze-drying. M_n: 2.5 kg/mol. $Đ$: 1.26. ^{1}H NMR (300 MHz, DMSO-d_6) δ 8.18 (d, 1H), 7.28 – 7.07 (m, 2H), 5.87 – 5.61 (m, 4H), 5.53 – 5.21 (m, 3H), 4.55 – 4.17 (m, 4H), 3.22 – 2.64 (m, 113H), 1.96 – 0.96 (m, 62H), 0.85 (t, 3H).

The synthesis of **PDMAc-2U with DP_n 35, 83 and 100** followed a similar procedure. After removing the metal complex by a short silica column, the solutions were directly dialyzed against methanol and afterward evaporated to remove methanol. After adding water to the products again, the colorless polymers were obtained after freeze-drying.

The syntheses of **$PDMAc_x$-2U and $PDMAc_{51}$-2U** followed a similar procedure. After removing the metal complex by a short silica column, polymers were obtained by precipitations in diethyl ether and drying.

$PDMAc_{35}$-2U. M_n: 4.5 kg/mol. $Đ$: 1.30. ^{1}H NMR (400 MHz, DMSO-d_6) δ 8.18 (d, 1H), 7.31 – 7.05 (m, 2H), 5.85 – 5.60 (m, 4H), 5.52 – 5.20 (m, 3H), 4.53 – 4.19 (m, 4H), 3.19 – 2.64 (m, 210H), 1.89 – 0.94 (m, 97H), 0.85 (t, 3H).

PDMAc$_{83}$-2U. M_n: 9.5 kg/mol. $Đ$: 1.28. ^{1}H NMR (400 MHz, DMSO-d_6) δ 8.17 (d, 1H), 7.28 – 7.05 (m, 2H), 5.86 – 5.61 (m, 4H), 5.51 – 5.19 (m, 3H), 4.55 – 4.24 (m, 4H), 3.18 – 2.66 (m, 491H), 1.92 – 0.95 (m, 192H), 0.85 (t, 3H).

PDMAc$_{100}$-2U. M_n: 9.6 kg/mol. $Đ$: 1.24. ^{1}H NMR (400 MHz, DMSO-d_6) δ 8.17 (d, 1H), 7.30 – 7.05 (m, 2H), 5.89 – 5.60 (m, 4H), 5.54 – 5.21 (m, 3H), 4.53 – 4.26 (m, 4H), 3.24 – 2.65 (m, 594H), 1.85 – 0.95 (m, 226H), 0.85 (t, 3H).

PDMAc$_{51}$-2U. M_n: 5.8 kg/mol. $Đ$: 1.29. ^{1}H NMR (300 MHz, DMSO-d_6) δ 8.17 (d, 1H), 7.27 – 7.09 (m, 2H), 5.77 – 5.67 (m, 4H), 5.54 – 5.19 (m, 3H), 4.51 – 4.23 (m, 4H), 3.23 – 2.66 (m, 321H), 1.95 – 0.98 (m, 128H), 0.85 (t, 3H).

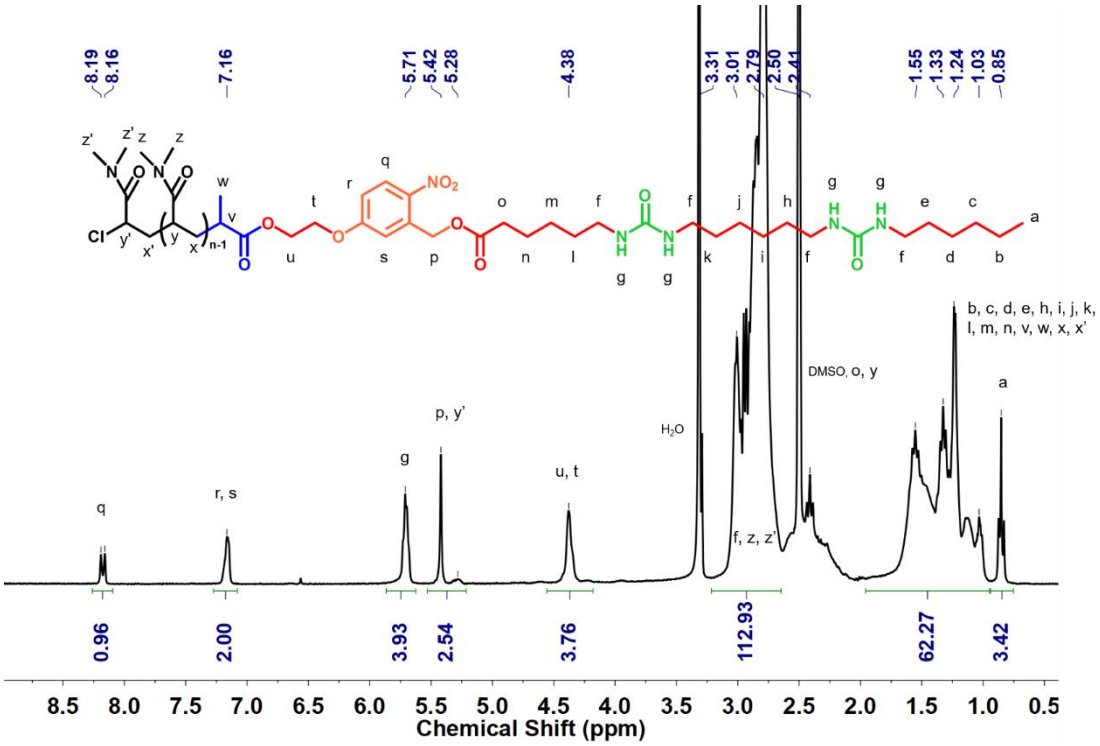

Figure 3.4.4.1. ^{1}H NMR of PDMAc$_{18}$-2U (in DMSO-d$_6$).

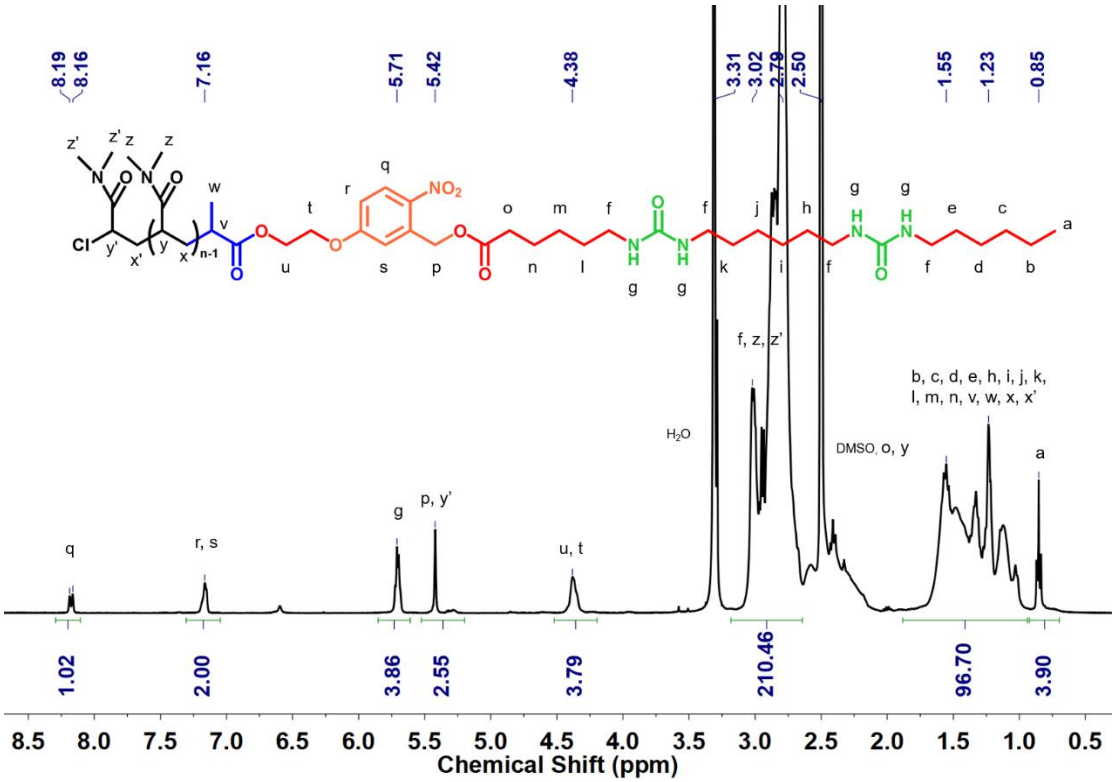

Figure 3.4.4.2. ^{1}H NMR of PDMAc$_{35}$-2U (in DMSO-d$_6$).

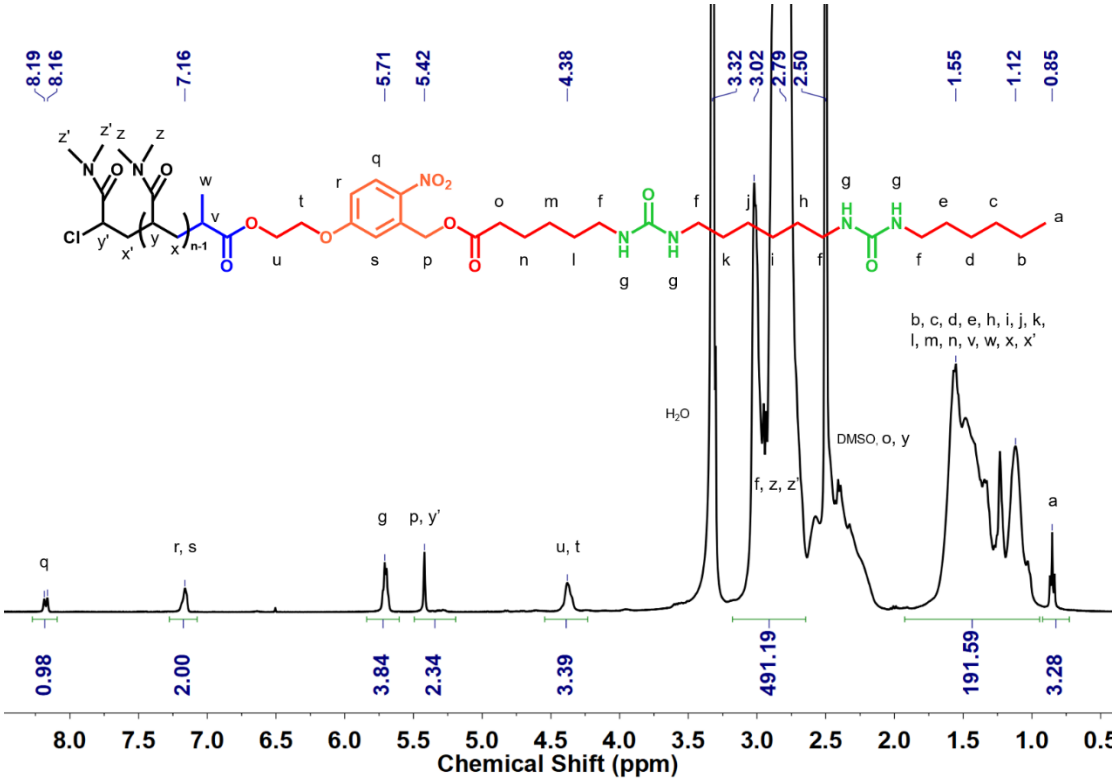

Figure 3.4.4.3. ^{1}H NMR of PDMAc$_{83}$-2U (in DMSO-d$_6$).

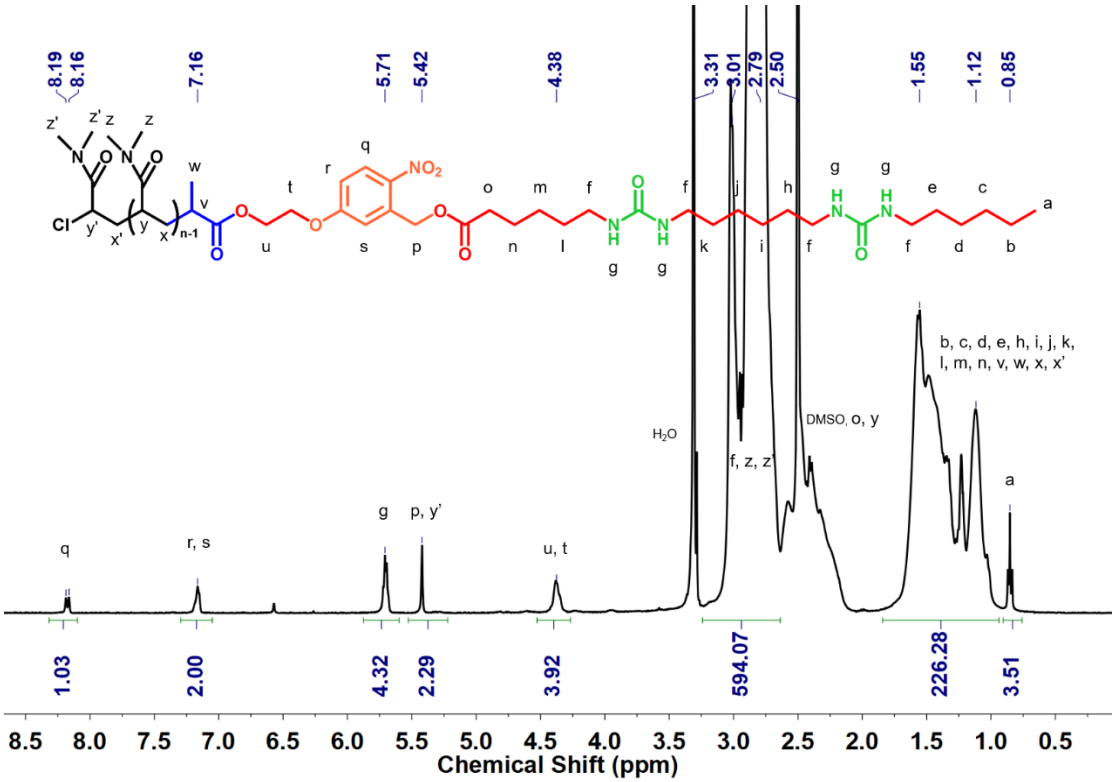

Figure 3.4.4.4. ^{1}H NMR of PDMAc$_{100}$-2U (in DMSO-d$_6$).

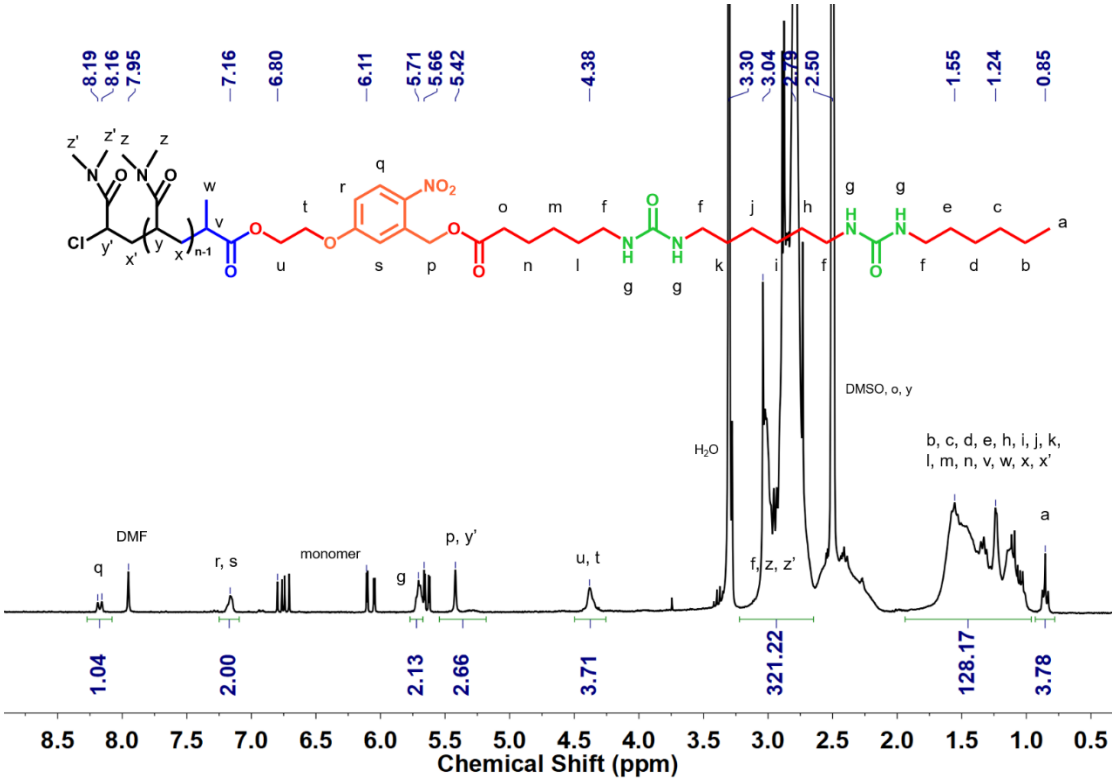

Figure 3.4.4.5. ^{1}H NMR of PDMAc$_{51}$-2U (in DMSO-d$_6$).

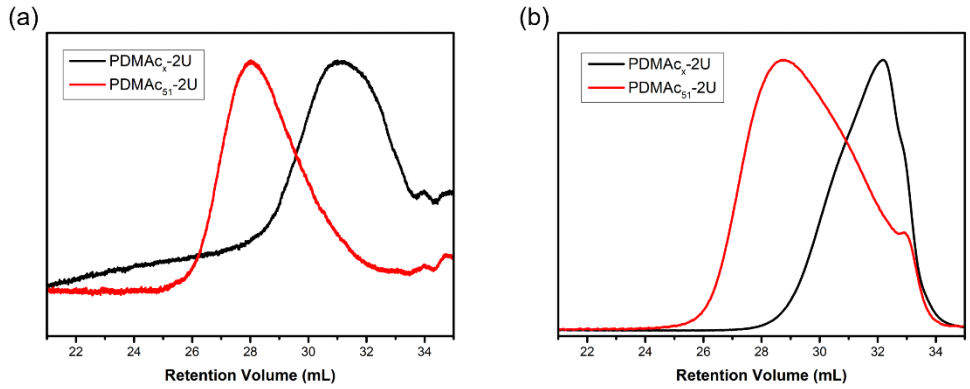

Figure 3.4.4.6. SEC figures of PDMAc$_x$-2U and PDMAc$_{51}$-2U in DMF with RI (a) and UV (311 nm) (b) signals.

3.5 References

(1) Cummins, C.; Mokarian-Tabari, P.; Holmes, J. D.; Morris, M. A. Selective etching of polylactic acid in poly(styrene)-block-poly(D,L)lactide diblock copolymer for nanoscale patterning. *J. Appl. Polym. Sci.* **2014**, *131*, 40798.

(2) Olayo-Valles, R.; Lund, M. S.; Leighton, C.; Hillmyer, M. A. Large area nanolithographic templates by selective etching of chemically stained block copolymer thin films. *J. Mater. Chem.* **2004**, *14*. 2729-2731.

(3) Hardy, C. G.; Ren, L.; Ma, S.; Tang, C. Self-assembly of well-defined ferrocene triblock copolymers and their template synthesis of ordered iron oxide nanoparticles. *Chem. Commun.* **2013**, *49*, 4373-4375.

(4) Malenfant, P. R.; Wan, J.; Taylor, S. T.; Manoharan, M. Self-assembly of an organic-inorganic block copolymer for nano-ordered ceramics. *Nat. Nanotechnol.* **2007**, *2*, 43-46.

(5) Montarnal, D.; Delbosc, N.; Chamignon, C.; Virolleaud, M. A.; Luo, Y.; Hawker, C. J.; Drockenmuller, E.; Bernard, J. Highly ordered nanoporous films from supramolecular diblock copolymers with hydrogen-bonding junctions. *Angew. Chem. Int. Ed.* **2015**, *54*, 11117-11121.

(6) Gu, W.; Zhao, H.; Wei, Q.; Coughlin, E. B.; Theato, P.; Russell, T. P. Line patterns from cylinder-forming photocleavable block copolymers. *Adv. Mater.* **2013**, *25*, 4690-4695.

(7) Zhao, H.; Gu, W.; Sterner, E.; Russell, T. P.; Coughlin, E. B.; Theato, P. Highly ordered nanoporous thin films from photocleavable block copolymers. *Macromolecules* **2011**, *44*, 6433-6440.

(8) Kang, M.; Moon, B. Synthesis of photocleavable poly(styrene-*block*-ethylene oxide) and its self-assembly into nanoporous thin films. *Macromolecules* **2008**, *42*, 455-458.

(9) Mellot, G.; Guigner, J.-M.; Jestin, J.; Bouteiller, L.; Stoffelbach, F.; Rieger, J. Bisurea-functionalized RAFT agent: a straightforward and versatile tool toward the preparation of supramolecular cylindrical nanostructures in water. *Macromolecules* **2018**, *51*, 10214-10222.

(10) Zhao, H.; Sterner, E. S.; Coughlin, E. B.; Theato, P. *o*-Nitrobenzyl alcohol derivatives: opportunities in polymer and materials science. *Macromolecules* **2012**, *45*, 1723-1736.

(11) Zeng, X.; Zhou, X.; Wu, S. Red and near-infrared light-cleavable polymers. *Macromol. Rapid. Commun.* **2018**, *39*, 1800034.

(12) Cao, J.; Huang, S.; Chen, Y.; Li, S.; Li, X.; Deng, D.; Qian, Z.; Tang, L.; Gu, Y. Near-infrared light-triggered micelles for fast controlled drug release in deep tissue. *Biomaterials* **2013**, *34*, 6272-6283.

(13) Fomina, N.; McFearin, C.; Sermsakdi, M.; Edigin, O.; Almutairi, A. UV and near-IR triggered release from polymeric nanoparticles. *J. Am. Chem. Soc.* **2010**, *132*, 9540-9542.

(14) Shen, W.; Zheng, J.; Zhou, Z.; Zhang, D. Approaches for the synthesis of *o*-nitrobenzyl and coumarin linkers for use in photocleavable biomaterials and bioconjugates and their biomedical applications. *Acta Biomater.* **2020**, *115*, 75-91.

(15) Rosales, A. M.; Vega, S. L.; DelRio, F. W.; Burdick, J. A.; Anseth, K. S. Hydrogels with reversible mechanics to probe dynamic cell microenvironments. *Angew. Chem. Int. Ed.* **2017**, *56*, 12132-12136.

(16) Griffin, D. R.; Kasko, A. M. Photodegradable macromers and hydrogels for live cell encapsulation and release. *J. Am. Chem. Soc.* **2012**, *134*, 13103-13107.

(17) Smith, Z. C.; Pawle, R. H.; Thomas III, S. W.. Photoinduced aggregation of polythiophenes. *ACS Macro Lett.* **2012**, *1*, 825-829.

(18) Abdalla, I.; Niu, Z.; Sun, B.; Jiang, X.; Zhu, M. Preparation of developing biotinylated pH-responsive glycopolymers as delivery nanocarriers for controlling release of bortezomib. *J. Pharm. Pharmacol. Res.* **2022**, *06*, 93-99.

(19) Qi, K.; Ma, Q.; Remsen, E. E.; Clark, C. G., Jr.; Wooley, K. L. Determination of the bioavailability of biotin conjugated onto shell cross-linked (SCK) nanoparticles. *J. Am. Chem. Soc.* **2004**, *126*, 6599-6607.

(20) Bontempo, D.; Li, R. C.; Ly, T.; Brubaker, C. E.; Maynard, H. D. One-step synthesis of low polydispersity, biotinylated poly(*N*-isopropylacrylamide) by ATRP. *Chem. Commun.* **2005**, 4702-4704.

(21) Mellot, G.; Guigner, J. M.; Bouteiller, L.; Stoffelbach, F.; Rieger, J. Templated PISA: driving polymerization-induced self-assembly towards fibre morphology. *Angew. Chem.* **2019**, *58*, 3173-3177.

(22) Donovan, M. S.; Lowe, A. B.; Sumerlin, B. S.; McCormick, C. L. RAFT polymerization of *N,N*-dimethylacrylamide utilizing novel chain transfer agents tailored for high reinitiation efficiency and structural control. *Macromolecules* **2002**, *35*, 4123-4132.

(23) Convertine, A. J.; Lokitz, B. S.; Lowe, A. B.; Scales, C. W.; Myrick, L. J.; McCormick, C. L. Aqueous RAFT polymerization of acrylamide and *N,N*-dimethylacrylamide at room temperature. *Macromol. Rapid Commun.* **2005**, *26*, 791-795.

(24) Yin, X.; Stöver, H. D. H. Probing the influence of polymer architecture on liquid−liquid phase transitions of aqueous poly(*N,N*-dimethylacrylamide) copolymer solutions. *Macromolecules* **2005**, *38*, 2109-2115.

(25) Teodorescu, M.; Matyjaszewski, K. Atom transfer radical polymerization of (meth)acrylamides. *Macromolecules* **1999**, *32*, 4826-4831.

(26) Rademacher, J. T.; Baum, M.; Pallack, M. E.; Brittain, W. J.; Simonsick, W. J. Atom transfer radical polymerization of *N,N*-dimethylacrylamide. *Macromolecules* **1999**, *33*, 284-288.

(27) Teodorescu, M.; Matyjaszewski, K. Controlled polymerization of (meth)acrylamides by atom transfer radical polymerization. *Macromol. Rapid Commun.* **2000**, *21*, 190-194.

(28) Xia, Y.; Yin, X.; Burke, N. A. D.; Stöver, H. D. H. Thermal response of narrow-disperse poly(*N*-isopropylacrylamide) prepared by atom transfer radical polymerization. *Macromolecules* **2005**, *38*, 5937-5943.

(29) Wan, X.; Zhang, G.; Ge, Z.; Narain, R.; Liu, S. Construction of polymer-protein bioconjugates with varying chain topologies: polymer molecular weight and steric hindrance effects. *Chem. Asian. J.* **2011**, *6*, 2835-2845.

(30) Lutz, J. F.; Neugebauer, D.; Matyjaszewski, K. Stereoblock copolymers and tacticity control in controlled/living radical polymerization. *J. Am. Chem. Soc.* **2003**, *125*, 6986-6993.

(31) Schumers, J.-M.; Gohy, J.-F.; Fustin, C.-A. A versatile strategy for the synthesis of block copolymers bearing a photocleavable junction. *Polym. Chem.* **2010**, *1*, 161-163.

(32) Yang, L.; Lei, M.; Zhao, M.; Yang, H.; Zhang, H.; Li, Y.; Zhang, K.; Lei, Z. Synthesis of the light/pH responsive polymer for immobilization of alpha-amylase. *Mater. Sci. Eng., C* **2017**, *71*, 75-83.

(33) Zong, G.; Hu, Z.; O'Keefe, S.; Tranter, D.; Iannotti, M. J.; Baron, L.; Hall, B.; Corfield, K.; Paatero, A. O.; Henderson, M. J.; Roboti, P.; Zhou, J.; Sun, X.; Govindarajan, M.; Rohde, J. M.; Blanchard, N.; Simmonds, R.; Inglese, J.; Du, Y.; Demangel, C.; High, S.; Paavilainen, V. O.; Shi, W. Q. Ipomoeassin F binds sec61α to inhibit protein translocation. *J. Am. Chem. Soc.* **2019**, *141*, 8450-8461.

(34) Hardy, C. G.; Ren, L.; Tamboue, T. C.; Tang, C. Side-chain ferrocene-containing (meth)acrylate polymers: Synthesis and properties. *J. Polym. Sci., Part A:Polym. Chem.* **2011**, *49*, 1409-1420.

Chapter IV: Assembly and characterization of pH-responsive nanocylinders

4.1 Introduction

Block copolymer solution self-assembly is particularly interesting for a range of applications in biomedicine[1, 2] and nanofabrication[3, 4], originated from the ability of self-assembling into micelles ($p \leq 1/3$), cylinders ($1/3 < p \leq 1/2$), vesicles ($1/2 < p \leq 1$) with different packing parameters (p)[5]. Based on these promising nanostructures, BCPs incorporated with responsiveness in one or two blocks under external stimuli such as physical stimuli (light[6], temperature[7], etc.), chemical stimuli (pH[8], etc.) and biological stimuli (enzyme[9], etc.), are designed for monitoring the process of stimuli-responsiveness or altering original nanostructures.

Among stimuli-responsive BCPs, pH-responsive BCPs are a class of polymers that can respond to pH variations and thus cause morphology changes (ie. disassembly and transformation), conferring them with potentials of various applications in stabilizers[10], membranes[11], drug delivery[12], etc. Often, pH-responsive polymers are polyelectrolytes since they contain weak acidic or basic groups that release or accept protons under corresponding pH environments, giving electrostatic interactions in the systems. Typical acid-terminated pH-responsive polymers include poly(acrylic acid) (PAA) [13], poly(methacrylic acid) (PMAA) [14] and poly(4-vinylbenzoic acid) (PVBA) [8], and instead, amine-terminated pH-responsive polymers cover poly((2-dimethylamino) ethyl methacrylate) (PDMA) [15], poly((2-diethylamino) ethyl methacrylate) (PDEA) [16] and poly((2-diisopropylamino) ethyl methacrylate) (PDPA) [17]. For PAA related BCPs, PAA-*b*-PS was earliest and extensively investigated system[18]. The BCP was not soluble in water but this could be realized by ionizing PAA block, forming micelle aggregates. Based on this, “star” and “crew-cut”-like micelles of PAA-*b*-PS were developed[19-21]. However, such micelles were not dynamic due to the hydrophobic PS, preventing the exchange of the unimer, unless the degree of polymerization or the interfacial tension

was decreased[22]. The dynamic characteristic was important for applications in mimicking surfactants or biological lipid membrane. Colombani et al. adopted a soft block, poly(*n*-butyl acrylate), demonstrating that PAA-*b*-P*n*BA was readily dissolved in water and, formed dynamic and kinetically controlled micelle aggregates[22, 23].

Another strategy to achieve dynamic characteristic is introducing supramolecular interactions, especially hydrogen bonding interaction, which has been proved as a powerful and convenient means to prepare micelle aggregates[24, 25]. Sijbesma's group developed various bis-ureas-based oligo ethylene glycol (OEG), achieving dynamically linear cylinders in water[26-29]. Perrier's group utilized cyclic peptides to fabricate cylindrical nanotubes[30-32] which can be potentially loaded with drug for drug delivery. Our lab proved the readily preparation of supramolecular nanofilaments in water based on quadruple hydrogen bonds[33-36]. Overall, the hydrogen bonding interaction provides a robust tool for preparing micelle aggregates with controlled dynamics.

Recently, our group has developed an efficient method to achieve Janus cylindrical micelles based on six hydrogen bonding interactions between tris-ureas[37]. The complementary hydrogen bonds in the ends of two polymers enable them to form Janus nanocylinder, with two chemically distinct sides[38, 39]. The characteristics of Janus nanocylinder endows them with dual functionality, presenting the great importance to design multi-functional materials for demands of various applications.

In this chapter, we designed and synthesized two end-functionalized polymers with complementary hydrogen bonding, _4_8_poly(acrylic acid) (_4_8_PAA) and_8_4_poly(*N*,*N*-dimethylacrylamide) (_8_4_PDMAc), as shown in Figure 4.1.1. Firstly, we hope that _4_8_PAA co-assembles with _8_4_PDMAc to form Janus nanocylinders. Secondly, after ionizing _4_8_PAA with a base, we can imagine several possibilities, depending on the strength of the electrostatic repulsions among the PAA chains. Electrostatic repulsion will induce stretching of the PAA chains, and thus swelling of the nanocylinders if the tris-urea self-assembly is strong enough (case (1) in Figure 4.1.1). If the nanocylinders are flexible enough, this swelling could lead to a

deformation of the nanocylinders such as bending (case (2)). Alternatively, if the tris-urea self-assembly is too weak, electrostatic repulsions among PAA chains could lead to the dissolution of the _4_8_PAA chains and breaking of the nanocylinders (case (3)). Therefore, our aim in this project is to probe the pH-responsiveness of self-assembled Janus nanocylinders.

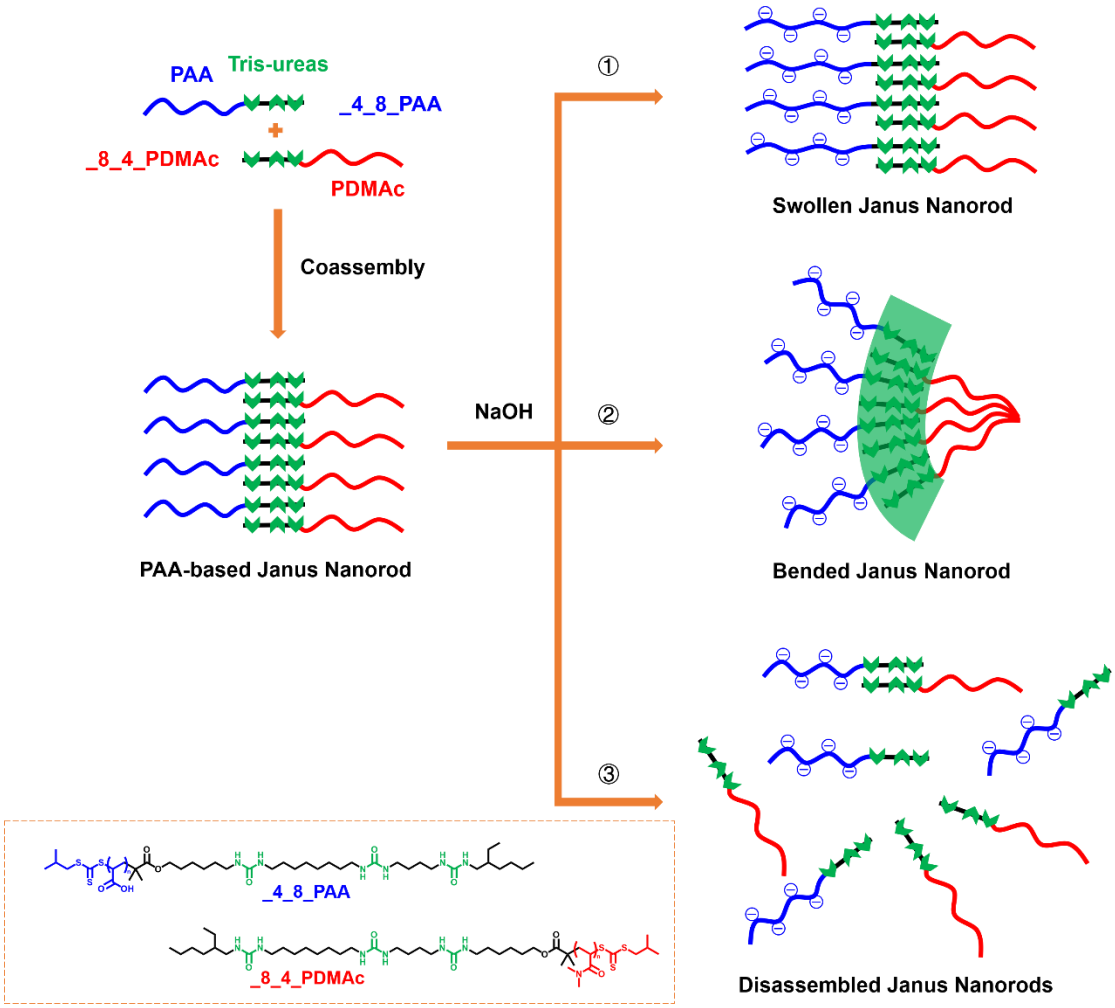

Figure 4.1.1. Illustration of co-assembly of Janus nanocylinder and its possible evolution when ionizing PAA.

4.2 Results and discussions

4.2.1 Synthesis and characterization of _4_8_PAA and _8_4_PDMAc

Several lengths of PAA and PDMAc chains were synthesized to tune the co-assembly properties.

The syntheses of _4_8_PAA$_{183}$ and _8_4_PAA$_{67}$ were adapted from Shuaiyuan Han thesis[40] using RAFT polymerization in DMSO at 65 °C from _4_8_CTA or _8_4_CTA. Polymerizations were stopped at about 70% conversion to avoid termination at high monomer conversion. The polymers were obtained by dialysis and freeze-drying. SEC of the polymers after methylation are shown in Figure 4.2.1.1a and the results are summarized in Table 4.2.1.1.

The syntheses of _8_4_PDMAc$_{35}$, _8_4_PDMAc$_{90}$ and _8_4_PDMAc$_{220}$ followed the procedure described in Chapter 2 (2.4.1 Polymerization of acrylamides using _8_4_CTA and _4_8_CTA), i.e. in DMSO. Meanwhile, to avoid the dialysis and freeze-drying steps, some polymers (_8_4_PDMAc$_{120}$ and _8_4_PDMAc$_{55}$) were synthesized in DMF and purified by precipitations. The characterization of all PDMAc is presented in Figure 4.2.1.1b and Table 4.2.1.1. Consistency between $M_{n,\,NMR}$ and $M_{n,\,th}$ was observed. All polymers were monodispersed. _8_4_PDMAc presented low dispersity even when DP_n is up to 220. However, the polymerizations in DMF lead to a slightly broader distribution.

Table 4.2.1.1. Synthesized PAA and PDMAc based on _4_8_ or _8_4_CTA.

Name	RAFT Agent	Solvent	$[M]_0/[CTA]_0/[AIBN]_0$	Monomer Concen. (M)	Temp. (°C)	Conv. (%)[a]	$DP_{n,NMR}$[b]	$M_{n,th}$ (kg/mol)[c]	$M_{n,NMR}$ (kg/mol)[d]	$M_{n,SEC}$ (kg/mol)[e]	$Đ$[e]
_4_8_PAA$_{42}$[f]	_4_8_CTA-SH	DMSO	71/1/0.1	0.7	-	72	42	3.7	3.8	5.1[g]	1.24
_4_8_PAA$_{183}$	_4_8_CTA-B1	DMSO	286/1/0.1	2	65	68	183	14.8	14.0	19.3[g]	1.25
_8_4_PAA$_{67}$	_8_4_CTA-B7	DMSO	100/1/0.1	2	65	70	67	5.8	5.6	8.0[g]	1.16
_8_4_PDMAc$_{35}$	_8_4_CTA-B7	DMSO	57/1/0.1	0.2	65	70	35	4.7	4.3	5.8	1.10
_8_4_PDMAc$_{55}$	_8_4_CTA-B7	DMF	175/1/0.1	0.2	65	34	55	5.8	6.2	5.9	1.20
_8_4_PDMAc$_{90}$	_8_4_CTA-B7	DMSO	172/1/0.1	0.2	65	50	90	9.3	9.7	11.0	1.08
_8_4_PDMAc$_{120}$	_8_4_CTA-B7	DMF	286/1/0.1	1	70	41	120	12.4	12.7	10.8	1.20
_8_4_PDMAc$_{220}$	_8_4_CTA-B7	DMSO	286/1/0.1	0.2	65	79	220	23.2	22.6	24.1	1.16

[a] Calculated by ^{1}H NMR at the time of beginning and ending.

[b, d] Calculated by ^{1}H NMR of the purified polymers.

[c] Theoretical M_n was calculated taking conversion into account.

[e] Determined by SEC in DMF (with 1 g/L LiBr) using PMMA standards and refractive index detection.

[f] Synthesized by Shuaiyuan Han[40].

[g] PAA was methylated before injections. The final molecular weights were obtained by multiplying 0.825 (the ratio of AA part in methylethacrylate unit).

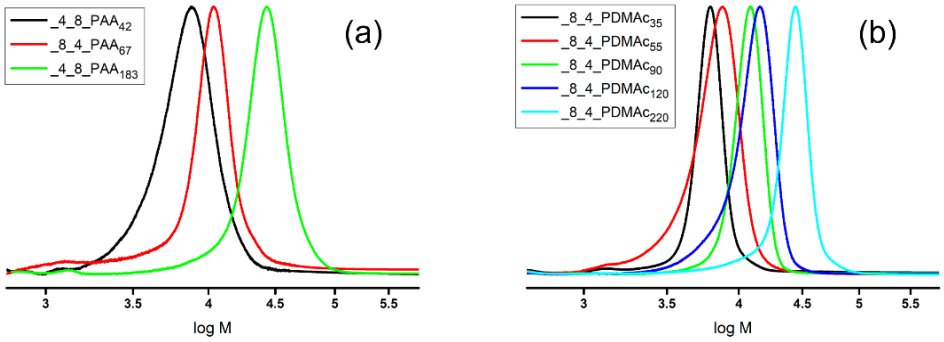

Figure 4.2.1.1. SEC figures of PAA (a) and PDMAc (b) in DMF (+ LiBr).

4.2.2 pH-responsiveness of the co-assembly of _4_8_PAA with _8_4_PDMAc

For the preparation of co-assembly solution, as shown in Figure 4.2.2.1, _4_8_PAA and _8_4_PDMAc are dissolved in DMSO separately and give 100 g/L concentrations. Then the two solutions are mixed together with a molar ratio of 1/1. Finally, with the slow adding of H_2O to the solution, the co-assembly solution with 1 g/L can be prepared for cryo-TEM.

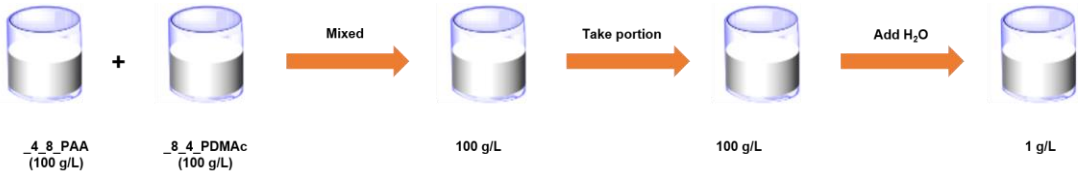

Figure 4.2.2.1. Illustration of preparation of co-assembly solution with 1 g/L.

For coassembly, we target 4 systems. To be specific, short PAA (_4_8_PAA_{42}) and long PAA (_4_8_PAA_{220}) are chosen to coassemble with the shortest PDMAc (_8_4_$PDMAc_{35}$) and the longest PDMAc (_8_4_$PDMAc_{220}$). Increasing the length of PAA should increase the repulsive electrostatic interaction in PAA/PDMAc when PAA is ionized. The visual aspect of the solutions after the coassembly process are shown in Figure 4.2.2.2. From the transparency, _4_8_PAA_{42}/_8_4_$PDMAc_{220}$ > _4_8_PAA_{183}/_8_4_$PDMAc_{220}$ > _4_8_PAA_{42}/_8_4_$PDMAc_{35}$. Precipitate was observed in _4_8_PAA_{183}/_8_4_$PDMAc_{35}$. These results are consistent with the fact

that the acidic form of PAA is poorly soluble in water while PDMAc is very soluble in water. Moreover $PDMAc_{35}$ is apparently not long enough to ensure a good colloidal stability to the nanoparticles. Considering the transparency of the samples, $\_4\_8\_PAA_{42}/\_8\_4\_PDMAc_{220}$ was firstly investigated.

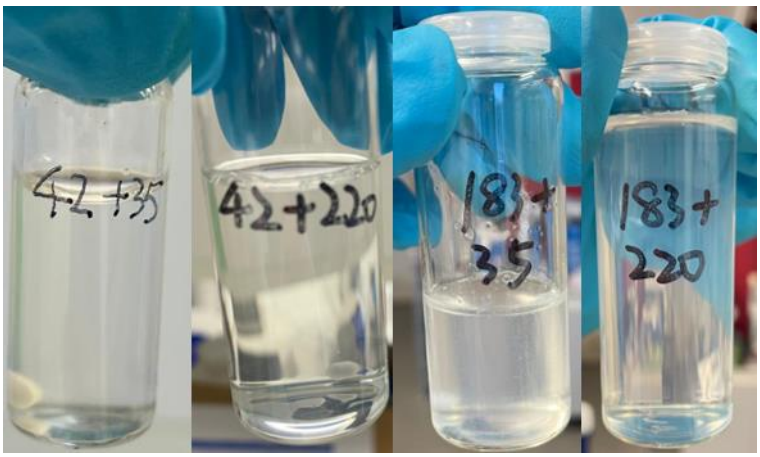

Figure 4.2.2.2. Visual aspect of solutions of $\_4\_8\_PAA_{42}/\_8\_4\_PDMAc_{35}$, $\_4\_8\_PAA_{42}/\_8\_4\_PDMAc_{220}$, $\_4\_8\_PAA_{183}/\_8\_4\_PDMAc_{35}$ and $\_4\_8\_PAA_{183}/\_8\_4\_PDMAc_{220}$ (from left to right).

4.2.2.1. $\_4\_8\_PAA_{42}/\_8\_4\_PDMAc_{220}$

When $\_4\_8\_PAA_{42}$ was coassembled with $\_8\_4\_PDMAc_{220}$, the solution had a pH of 5.4 and remained transparent. The cryo-TEM (Figure 4.2.2.1.1a) showed few nanorods which had a diameter of ~ 9 nm.

Addition of 1 equivalent of acid to the solution still yielded a transparent solution at pH 2.8. Longer nanorods (> 1μm) were observed and many of them were entangled (Figure 4.2.2.1.1f), indicating probably aggregation through interaction of PAA domains in different nanorods.

Instead of adding acid, we gradually added NaOH to the initial pH 5.4 solution: PAA was ionized at pH 7.5, 7.7 and 8.8, and similar nanorods were observed. When pH was at 10.7 (adding 1 equivalent of NaOH), nanorods were still observed, but their contrasts seemed lower at pH 10.7 (Figure 4.2.2.1.1d) compared to the solution at pH

5.4 (Figure 4.2.2.1.1a) and their diameter was smaller (~ 7 nm). The cryo-TEM figures of the solution at pH 10.7 also showed spheres. Overall, these results indicated the initial coassembly was broken or PAA may be swollen becoming invisible in cryo-TEM. Since conclusion seemed difficult on this system we decided to focus on a system with longer PAA part that should show a clearer pH sensitivity.

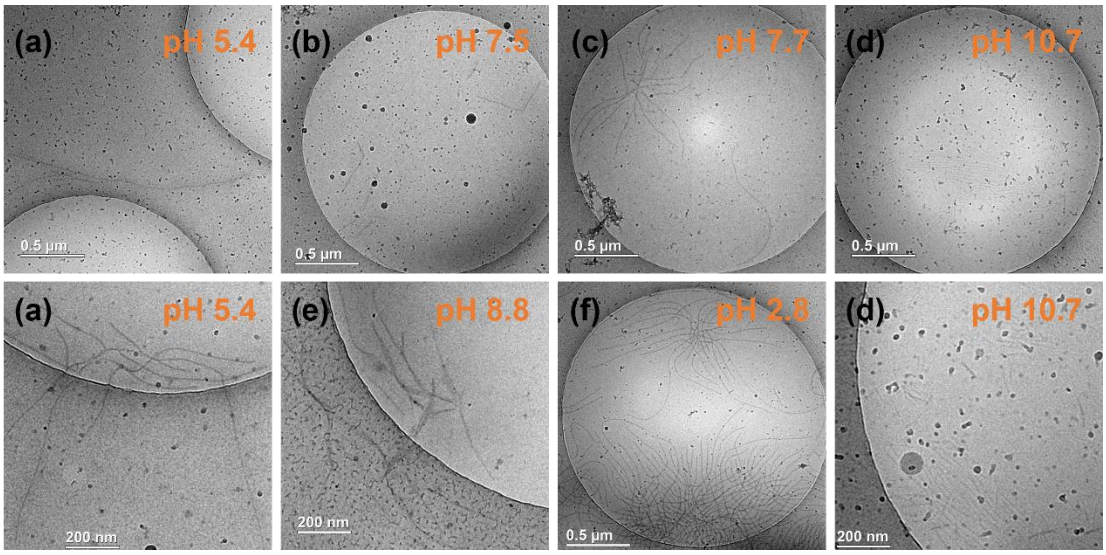

Figure 4.2.2.1.1. Cryo-TEM figures of _4_8_PAA$_{42}$/_8_4_PDMAc$_{220}$ at different pHs: (a) without adding NaOH and HCl, (b) with adding 0.1 eq. NaOH to (a), (c) with adding 0.2 eq. NaOH to (a), (d, e) with adding 1 eq. NaOH to (a) (two independent experiments) and (f) with adding 1 eq. HCl to (a).

4.2.2.2. _4_8_PAA$_{183}$/_8_4_PDMAc$_{220}$

When _4_8_PAA$_{183}$ was coassembled with _8_4_PDMAc$_{220}$, the solution had a pH of 4.7 and remained transparent. The cryo-TEM verified the existence of many nanorods (Figure 4.2.2.2.2a), which had a diameter of ~ 18 nm. The formation of nanorods was also confirmed by SANS (Figure 4.2.2.2.1) by the presence of a characteristic q^{-1} slope at small q. A fit of the SANS data was possible with the form factor of a cylinder of diameter 28 nm, in reasonable agreement with the cryo-TEM data.

When adding 0.1 eq of HCl into the solution of _4_8_PAA$_{183}$/_8_4_PDMAc$_{220}$, the solution was still transparent and some nanorods were still observed at pH 3.9, with 19 – 24 nm in diameter (Figure 4.2.2.2.2b). However, when 0.2 eq HCl was introduced to the solution of _4_8_PAA$_{183}$/_8_4_PDMAc$_{220}$, precipitates occurred.

When 1 eq of NaOD was added into the initial solution, the SANS intensity strongly decreased and the q^{-1} dependency was lost, suggesting the disassembly of Janus nanorods. From Figure 4.2.2.2.2c, e and f, cryo-TEM shows that nanorods can still be observed but their diameter is significantly reduced after adding NaOH (~ 8 nm). These results suggest that due to PAA ionization, some _4_8_PAA$_{183}$ is dissolved away from the initial nanorods and that only fragments of these nanorods are obtained. In fact, these results can be compared to the blank experiments where _4_8_PAA$_{183}$ alone or _8_4_PDMAc$_{220}$ alone are assembled by adding water to an initial DMSO solution. Figure 4.2.2.2.3. shows that _4_8_PAA$_{183}$ alone forms no identifiable objects while _8_4_PDMAc$_{220}$ alone forms few nanorods of ~ 9 nm diameter. This blank experiment confirms that if _4_8_PAA$_{183}$ is dissolved at high ionization, _8_4_PDMAc$_{220}$ that is left behind is able to form thin nanorods on its own.

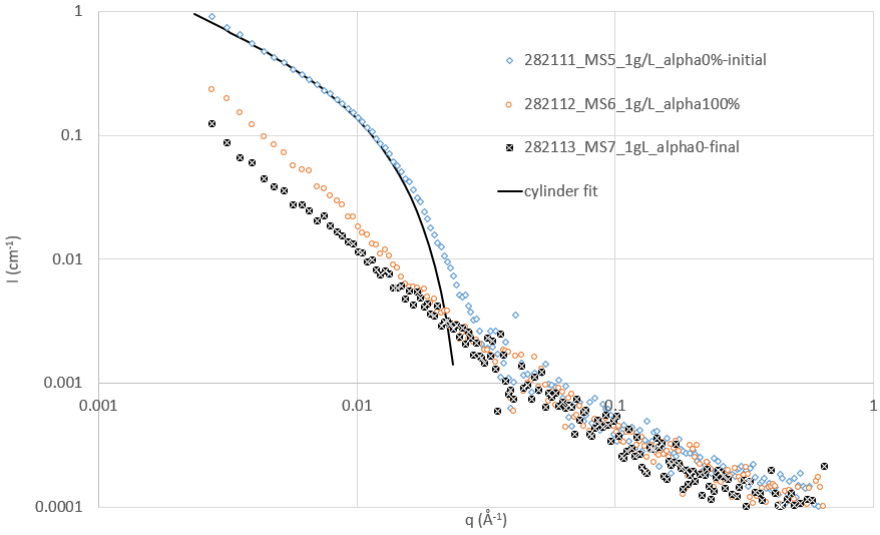

Figure 4.2.2.2.1. SANS figures of solutions of _4_8_PAA$_{183}$/_8_4_PDMAc$_{220}$ without adding NaOD and DCl (blue), with adding 1 eq of NaOD (orange), and with adding 1 eq of NaOD and DCl (black).

After ionization of PAA triggered the disassembly, we tested if addition of acid would make it possible to revert the process. We therefore added 1 equivalent of acid to the samples. Both cryo-TEM (Figure 4.2.2.2.2d) and SANS (Figure 4.2.2.2.1.) data show that the disassembly process was not reversible.

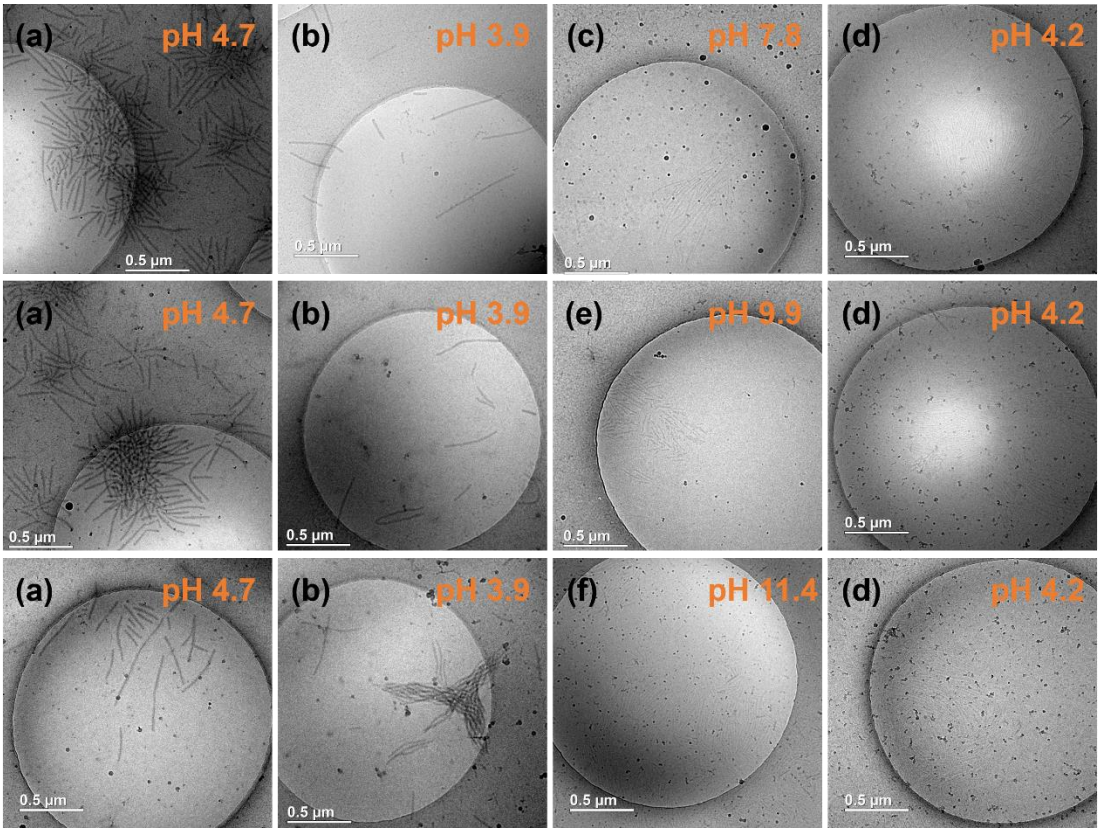

Figure 4.2.2.2.2 Cryo-TEM figures of _4_8_PAA$_{183}$/_8_4_PDMAc$_{220}$ at different pHs: (a) without adding NaOH and HCl,

(b) with adding 0.1 eq. HCl to (a),

(c, e, f) with adding 1 eq. NaOH to (a), (3 independent experiments)

and (d) with adding 1 eq. HCl to (e).

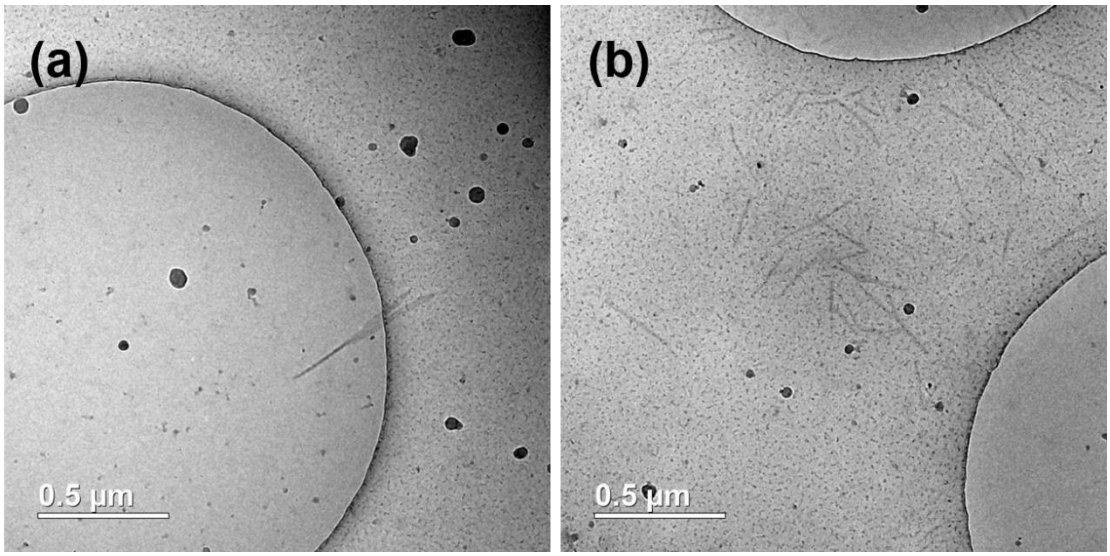

Figure 4.2.2.2.3. Cryo-TEM figures of _4_8_PAA_{183} alone (a) and_8_4_$PDMAc_{220}$ alone (b).

4.3 Conclusions

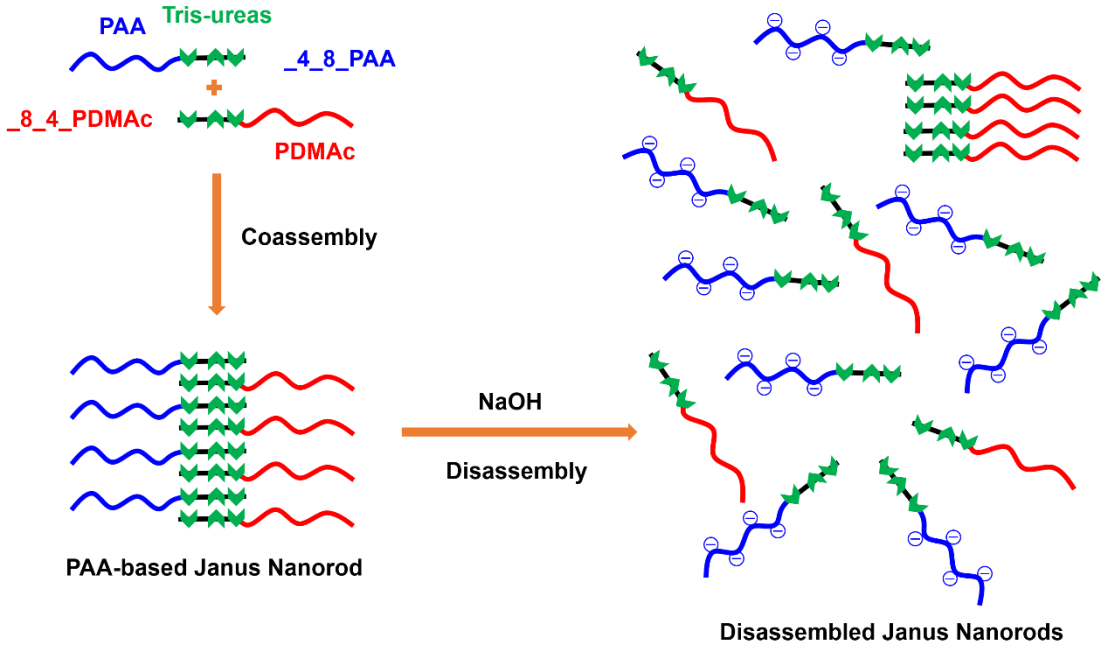

Figure 4.3.1. Illustration of the formation and the disassembly of PAA-based Janus nanorods.

In this chapter, _4_8_PAA and _8_4_PDMAc with different DP_n were synthesized by RAFT polymerization with corresponding RAFT agents. Then these polymers were characterized with ^{1}H NMR and SEC. ^{1}H NMR showed good purities of polymers and the good agreement of molecular weights between NMR and theory. SEC indicated the low dispersity even for DP_n up to 220.

Cryo-TEM confirmed the observation of nanorods of _4_8_PAA$_{42}$/_8_4_PDMAc$_{220}$ at pH 5.4 with a diameter of ~ 9 nm. When adding 1 eq of NaOH to the initial solution, nanorods with a lower contrast and with a diameter of ~7 nm at pH 10.7 were observed. Meanwhile, few spheres were found in cryo-TEM.

For _4_8_PAA$_{183}$/_8_4_PDMAc$_{220}$, SANS indicated the formation of nanocylinders at small q with a q^{-1} dependency, which was confirmed by cryo-TEM with the observation of many nanorods. When 1 eq of NaOD was added to the initial solution, SANS suggested the loss of nanocylinders due to the disappearance of q^{-1}

dependency. Few nanorods with a diameter of ~ 8 nm were found, indicating that they may originate from the assembly of _8_4_PDMAc$_{220}$ alone when comparing to a blank cryo-TEM experiment of _8_4_PDMAc$_{220}$. Finally, when HCl was added to the ionized solution, SANS and cryo-TEM results confirmed the irreversible process of the disassembly.

4.4 Supporting information

4.4.1 Materials

1, 3, 5-Trioxane (97%, Fluka), trimethylsilyldiazomethane (TMS, Acros, 2 M in hexane), hydrochloric acid (37%, Sigma-Aldrich), dimethyl sulfoxide (≥99.9%, Fisher Chemical), methanol (≥99.9%, Carlo Erba), diethyl ether, *N,N*-dimethylformamide (≥99.8%, Honeywell) and dialysis membrane (cellulose, 1000 Da or 3500 Da, Carl Roth) were used as received.

N,N-dimethylacrylamide (DMAc, 99%, Sigma-Aldrich) was purified on a basic aluminium oxide column to remove the inhibitor. Acrylic acid (Sigma-Aldrich, 99%) was distilled before the use. 2, 2'- azobis(2-methylpropionitrile) (AIBN, 98%, Sigma-Aldrich) was recrystallized from methanol.

4.4.2 Analytical techniques

Nuclear Magnetic Resonance (NMR). ^{1}H NMR spectra were obtained in deuterated solvents using Bruker 400 or 600 MHz NMR spectrometer. All ^{1}H NMR spectra were referenced to the peak at 2.5 ppm (in DMSO-d_6). For monomer consumption in polymerization, the integration of trioxane was set as reference to calculate the monomer conversion.

Size Exclusion Chromatography (SEC). Polymers with a ~ 3 mg/mL concentration were analyzed by SEC using DMF (+ 1 g/L LiBr) as eluent phase. The columns of DMF SEC were thermostated at 60 °C, and the flow rate was set at 0.8 mL/min. The injecting solution contained toluene (20 drops in 100 mL DMF) internal standard. Polymers in DMF were detected by a differential refractive index detector (RI) and a Diode Array UV Detector (309 nm). The molecular weights were calibrated with PMMA refractive index signal. For PAA, the polymers were methylated before injections. The final molecular weights were obtained by multiplying 0.825 (the ratio

of AA part in methylacrylate unit). The general preparation of methylation[41] of PAA was described as follows.

5 mg of PAA was dissolved in 2 mL of mixed solvent (V_{MeOH}/V_{THF} = 1/1) before adding one drop of concentrated HCl (37 %) to make sure acidic condition. Then, several dorps of trimethylsilyldiazomethane was dropwise added into the solution until no bubbles produced and the solution still remained light yellow. The solution was evaporated under N_2 flux for SEC analysis.

pH meter. pH was tested with DL50 Graphix from Mettler Toledo connected to an Inlab Micro electrode. After calibration, the electrode was fully immersed into the solutions to get values until total equilibrium.

Cryo-TEM. Cryo-TEM samples were flash frozen in liquid ethane and then observed at -180 °C on a JEOL JEM-2100 LaB_6 microscope operating at 200 kV under low-dose conditions (10 electrons $Å^{-2}$ s^{-1}). Digital images were recorded on a Gatan Ultrascan 1000 CCD camera.

4.4.3 Synthesis of _4_8_and _8_4_RAFT agents

The syntheses of _4_8_ and _8_4_RAFT agents were described in Chapter II, 2.6.3 section.

4.4.4 Synthesis of _4_8_and _8_4_polymers

_4_8_PAA_{42} was synthesized by Han[40]. M_n: 5.1 kg/mol, $Đ$: 1.24. ^{1}H NMR (400 MHz, DMSO-d_6) δ 12.31 (s, 40H), 5.83 – 5.66 (m, 6H), 4.76 – 4.56 (m, 1H), 3.94 (t, 2H), 3.03 – 2.83 (m, 12H), 2.42 – 2.04 (m, 40H), 2.03 – 0.93 (m, 128H), 0.91 – 0.71 (m, 6H).

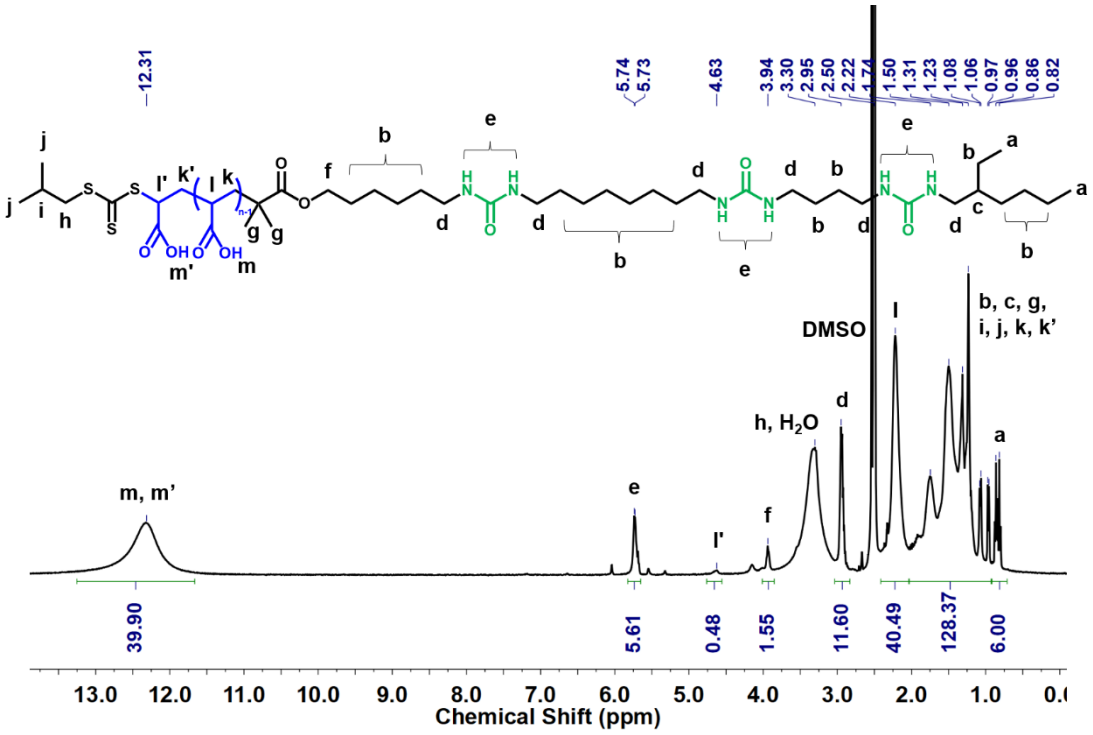

Figure 4.4.4.1. ^{1}H NMR of _4_8_PAA$_{42}$ (in DMSO-d$_6$).

Polymerization of acrylic acid using _4_8_CTA (DP_n = 183). The synthesis of _4_8_PAA$_{183}$ is described in detail as follows and _8_4_PAA$_{67}$ followed the similar way. A 50 mL round-bottom flask equipped with a magnetic stirring bar was charged with acrylic acid (1 g, 13.9 mmol, 286 eq), _4_8_CTA (38.4 mg, 0.0486 mmol, 1 eq), DMSO (6 mL) and trioxane (50 mg, 0.556 mmol, 11.4 eq). Then, the solution was bubbled with N_2 at 65 °C for 30 minutes before the injection of 1 mL of a 0.796 mg/mL stock solution of AIBN in DMSO (0.796 mg AIBN, 0.1 eq). The solution was bubbled with N_2 for another 10 minutes. After 580 minutes, the flask was plunged into an ice-water bath and the cap was opened after several minutes. 68% for the final conversion was determined by ^{1}H NMR (relative integration of the internal reference peak at 5.07 ppm and CH_2=CH peak at 6.20 ppm). The polymer solution was purified by dialysis with 3.5 kDa membrane and a further freeze-drying step to give a colorless powder (0.61 g, 85%). M_n: 19.3 kg/mol, $Đ$: 1.25.^{1}H NMR (600 MHz, DMSO-d_6) δ 12.21 (s, 190H), 5.81 – 5.61 (m, 6H), 4.75 – 4.60 (m, 1H), 3.94 (t, 2H), 3.02 – 2.83 (m, 12H), 2.36 – 2.05 (m, 179H), 2.02 – 0.91 (m, 410H), 0.90 – 0.77 (m, 6H).

_8_4_PAA$_{67}$ (M_n: 8.0 kg/mol, $Đ$: 1.16). ^{1}H NMR (400 MHz, DMSO-d_6) δ 12.26 (s, 63H), 5.84 – 5.63 (m, 6H), 4.76 – 4.58 (m, 1H), 3.94 (t, 3H), 3.01 – 2.85 (m, 12H), 2.39 – 2.04 (m, 65H), 2.01 – 0.92 (m, 178H), 0.90 – 0.75 (m, 6H).

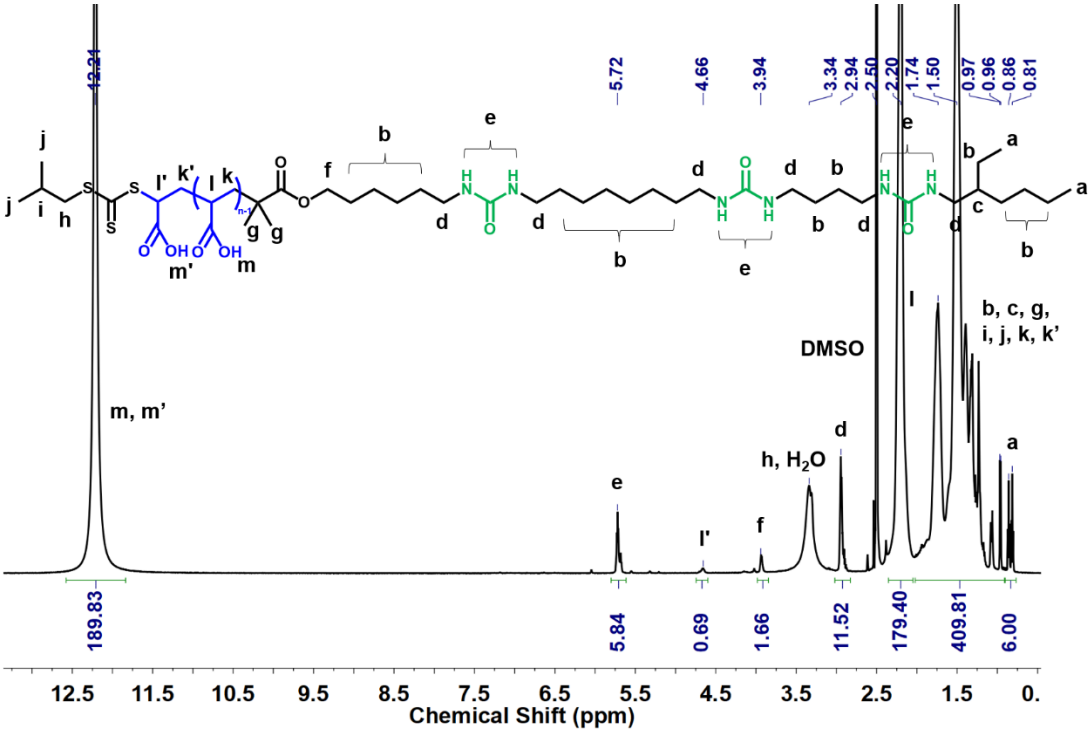

Figure 4.4.4.2. ^{1}H NMR of _4_8_PAA$_{183}$ (in DMSO-d$_6$).

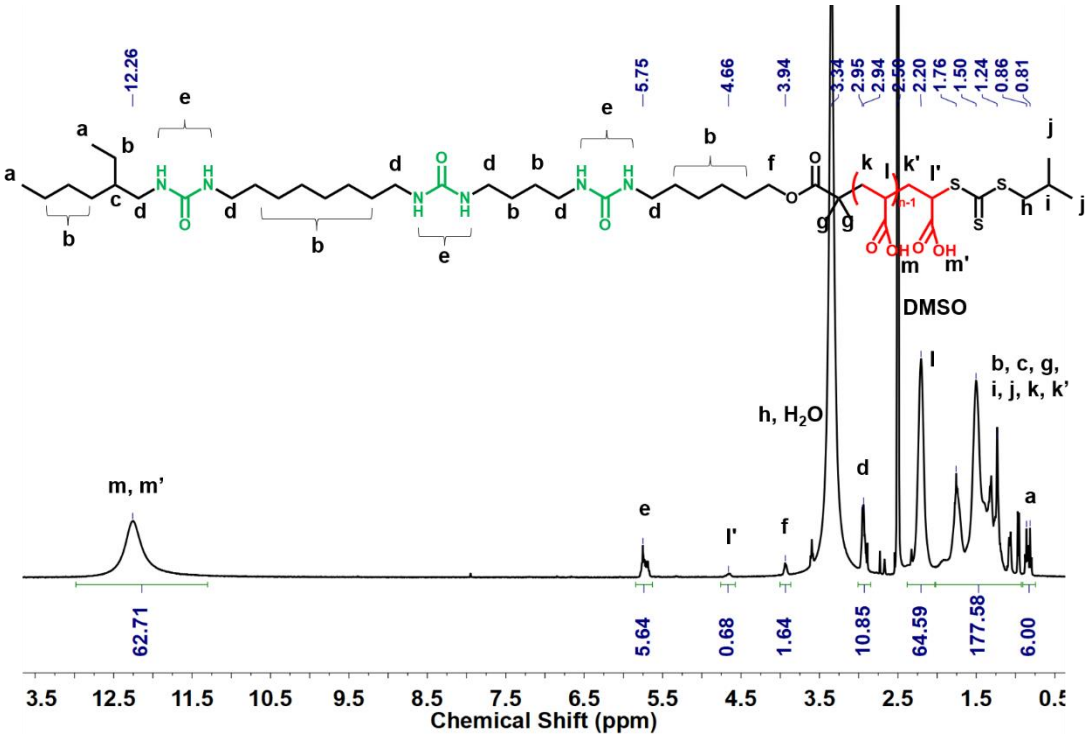

Figure 4.4.4.3. ^{1}H NMR of _8_4_PAA$_{67}$ (in DMSO-d$_6$).

Polymerization of *N,N*-dimethylacrylamide by _8_4_CTA in DMSO (DP_n = 220). The synthesis of _8_4_PDMAc$_{220}$ was described in detail as follows. **_8_4_PDMAc$_{90}$ and _8_4_PDMAc$_{35}$** followed the similar way. A 100 mL round-bottom flask equipped with a magnetic stirring bar was charged with *N,N*-dimethylacrylamide (1 g, 10.1 mmol, 286 eq), _8_4_CTA (27.9 mg, 0.0353 mmol, 1 eq), DMSO (48.5 mL) and trioxane (36 mg, 0.4 mmol, 11.3 eq). Then, the solution was bubbled with N_2 at 65 °C for 30 minutes before the injection of 1 mL of a 0.58 mg/mL stock solution of AIBN in DMSO (0.58 mg AIBN, 0.1 eq). The solution was bubbled with N_2 for another 10 minutes. After 15 hours, the flask was plunged into an ice-water bath and the cap was opened after several minutes. 79% for the final conversion was determined by ^{1}H NMR (relative integration of the internal reference peak at 5.03 ppm and CH_2=CH peak at 5.6 ppm). The polymer solution was purified by dialysis with 1 kDa membrane and a further freeze-drying step to give a yellow powder (0.76 g, 92%). M_n: 24.1 kg/mol, $Đ$: 1.16. ^{1}H NMR (400 MHz, DMSO-d_6) δ 5.80 – 5.64 (m, 6H), 5.18

– 5.02 (m, 1H), 3.94 (t, 2H), 3.23 – 2.66 (m, 1294H), 2.06 – 1.90 (m, 1H), 1.88 – 0.92 (m, 486H), 0.90 – 0.76 (m, 6H).

_8_4_PDMAc$_{35}$. M_n: 5.8 kg/mol, $Đ$: 1.10. ^{1}H NMR (400 MHz, DMSO-d_6) δ 5.82 – 5.61 (m, 6H), 5.17 – 5.02 (m, 1H), 3.94 (t, 2H), 3.18 – 2.65 (m, 227H), 2.05 – 1.90 (m, 1H), 1.78 – 0.91 (m, 116H), 0.91 – 0.75 (m, 6H).

_8_4_PDMAc$_{90}$. M_n: 11.0 kg/mol, $Đ$: 1.08. ^{1}H NMR (400 MHz, DMSO-d_6) δ 5.80 – 5.63 (m, 6H), 5.17 – 5.03 (m, 1H), 3.95 (t, 2H), 3.23 – 2.64 (m, 547H), 2.02 – 1.89 (m, 1H), 1.79 – 0.92 (m, 225H), 0.91 – 0.74 (m, 6H).

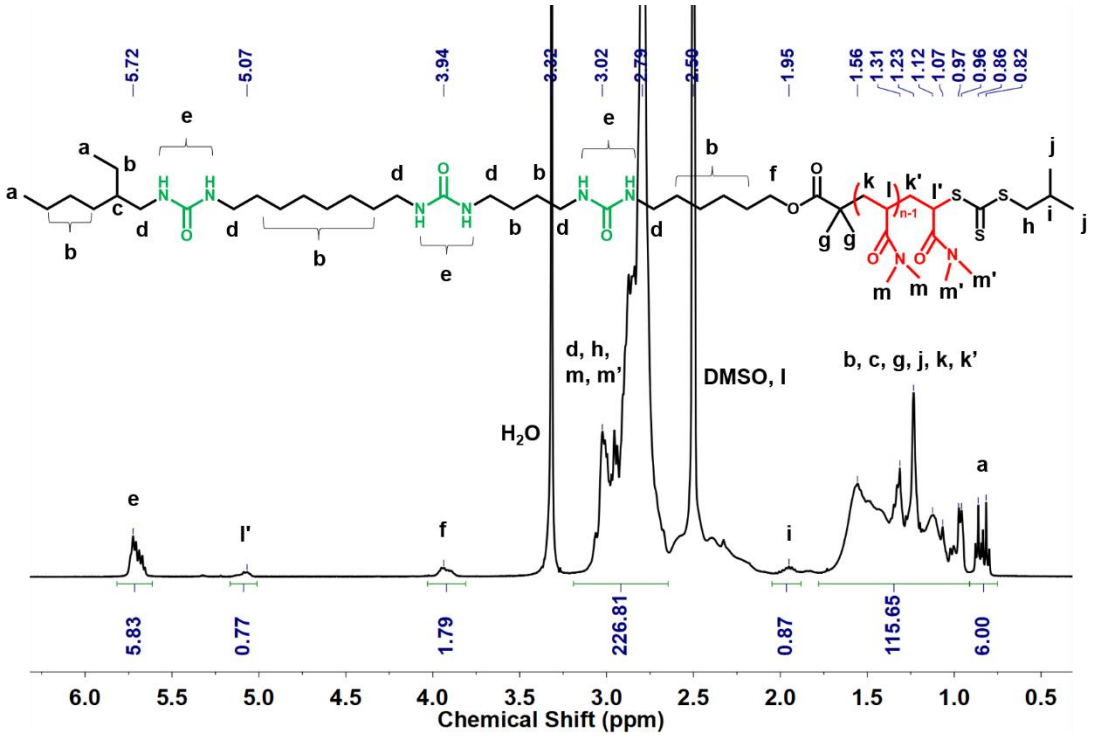

Figure 4.4.4.4. ^{1}H NMR of _8_4_PDMAc$_{35}$ (in DMSO-d$_6$).

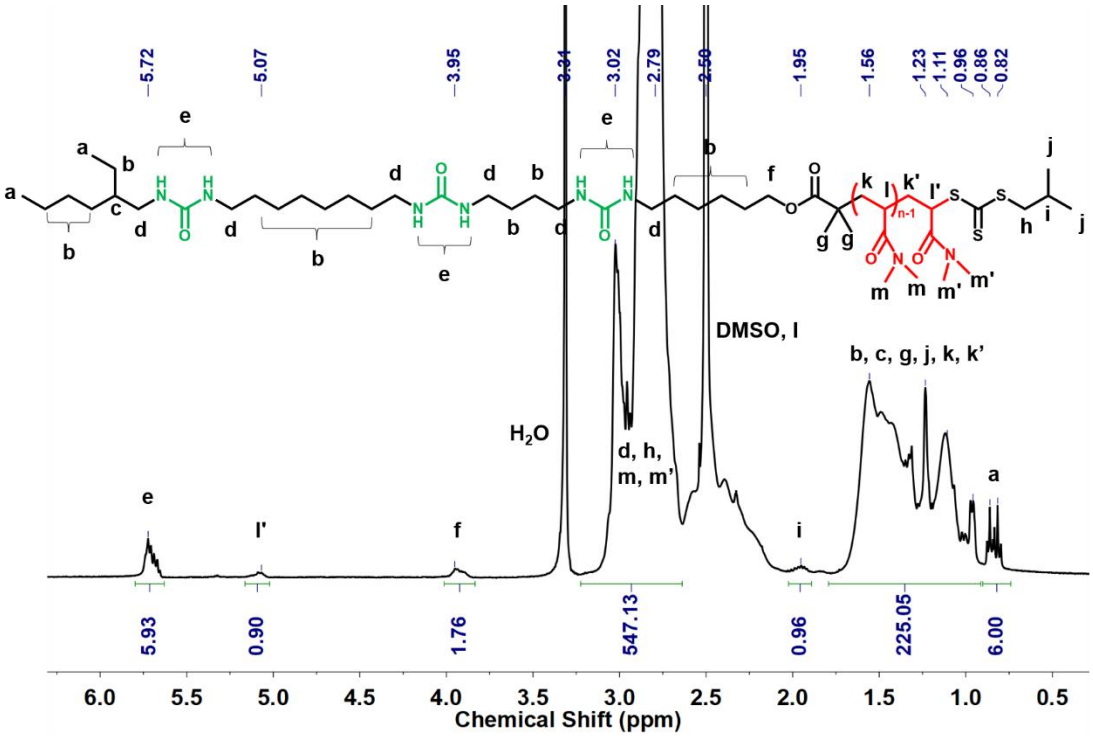

Figure 4.4.4.5. ^{1}H NMR of _8_4_PDMAc$_{90}$ (in DMSO-d$_6$).

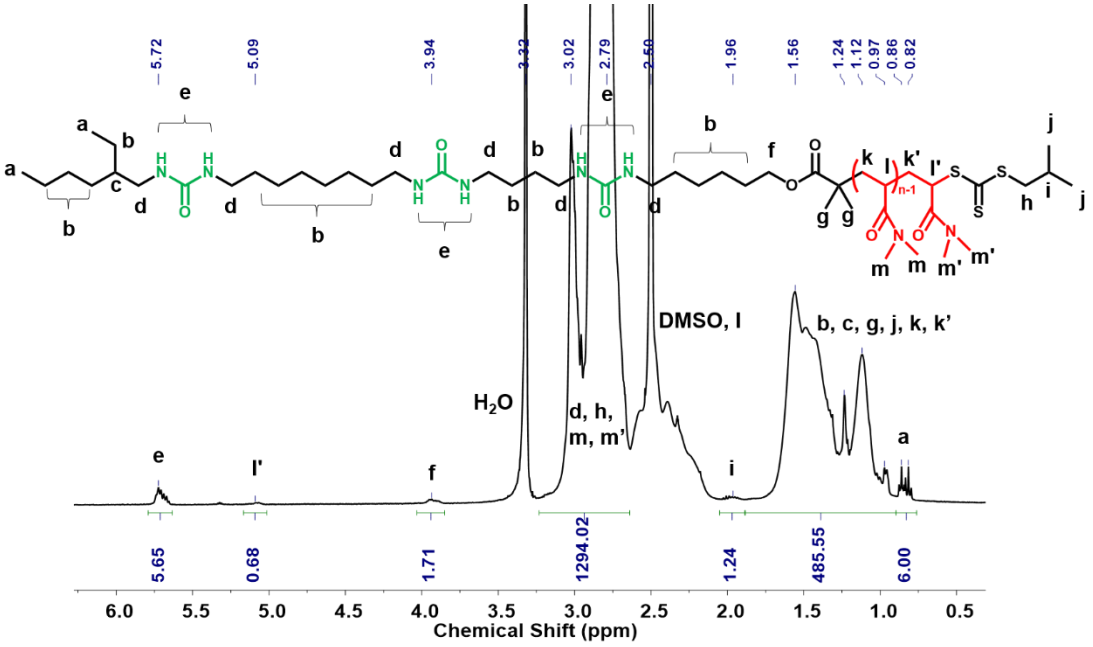

Figure 4.4.4.6. ^{1}H NMR of _8_4_PDMAc$_{220}$ (in DMSO-d$_6$).

Polymerization of *N,N*-dimethylacrylamide by _8_4_CTA in DMF (DP_n = 55). A 100 mL round-bottom flask equipped with a magnetic stirring bar was charged with *N,N*-dimethylacrylamide (0.7 g, 7.07 mmol, 175 eq), _8_4_CTA (32 mg, 0.0405 mmol, 1 eq), DMF (34 mL) and trioxane (25.5 mg, 0.283 mmol, 7.0 eq). Then, the solution was bubbled with N_2 at 65 °C for 30 minutes before the injection of 1 mL of a 0.674 mg/mL stock solution of AIBN in DMF (0.674 mg AIBN, 0.1 eq). The solution was bubbled with N_2 for another 10 minutes. After 9 hours, the flask was plunged into an ice-water bath and the cap was opened after several minutes. 34% for the final conversion was determined by ^{1}H NMR (relative integration of the internal reference peak at 5.03 ppm and CH_2=CH peak at 5.6 ppm). The light yellow polymer (0.09 g, 33%) was obtained by precipitation into cold diethyl ether, dissolution in DCM and a second precipitation into cold diethyl ether. M_n: 5.9 kg/mol, $Đ$: 1.20. ^{1}H NMR (600 MHz, DMSO-d_6) δ 5.79 – 5.64 (m, 6H), 5.19 – 5.01 (m, 1H), 3.95 (t, 2H), 3.21 – 2.65 (m, 339H), 2.05 – 1.89 (m, 1H), 1.75 – 0.93 (m, 155H), 0.91 – 0.75 (m, 6H).

_8_4_PDMAc$_{120}$ was synthesized similarly to _8_4_PDMAc$_{55}$ but in 1M monomer concentration and 70 °C. M_n: 10.8 kg/mol, $Đ$: 1.20. ^{1}H NMR (400 MHz, DMSO-d_6) δ 5.79 – 5.61 (m, 6H), 5.15 – 5.03 (m, 1H), 3.95 (t, 2H), 3.23 – 2.65 (m, 722H), 2.04 – 1.90 (m, 1H), 1.89 – 0.92 (m, 285H), 0.90 – 0.74 (m, 6H).

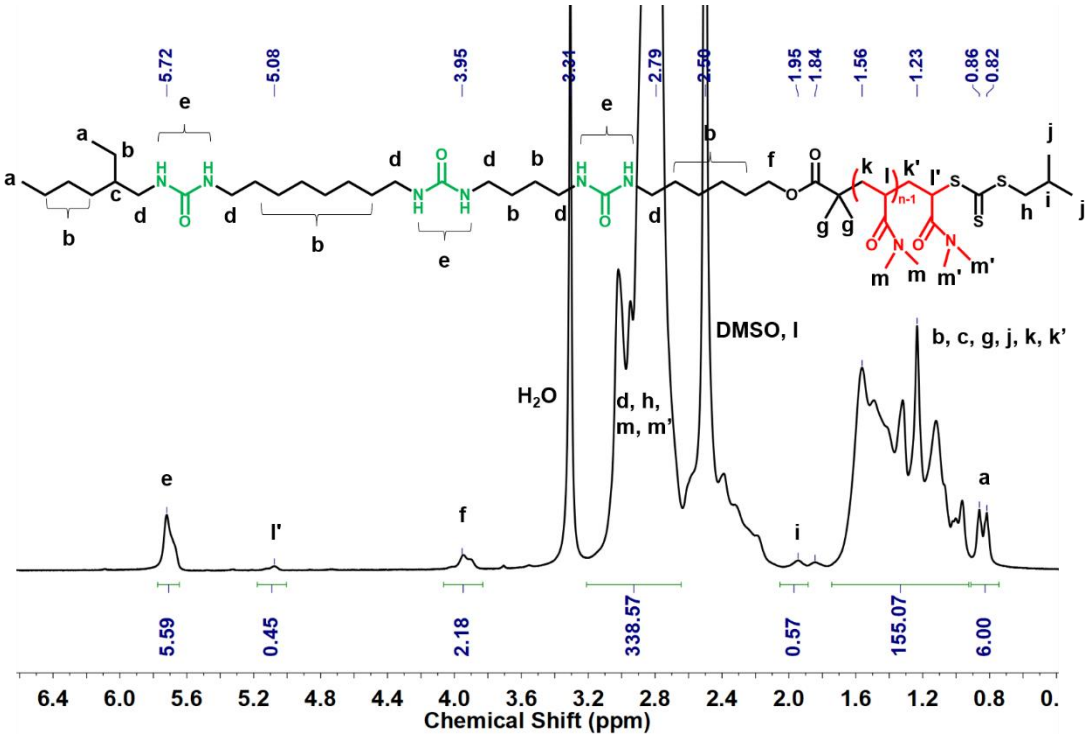

Figure 4.4.4.7. ^{1}H NMR of _8_4_PDMAc$_{55}$ (in DMSO-d$_6$).

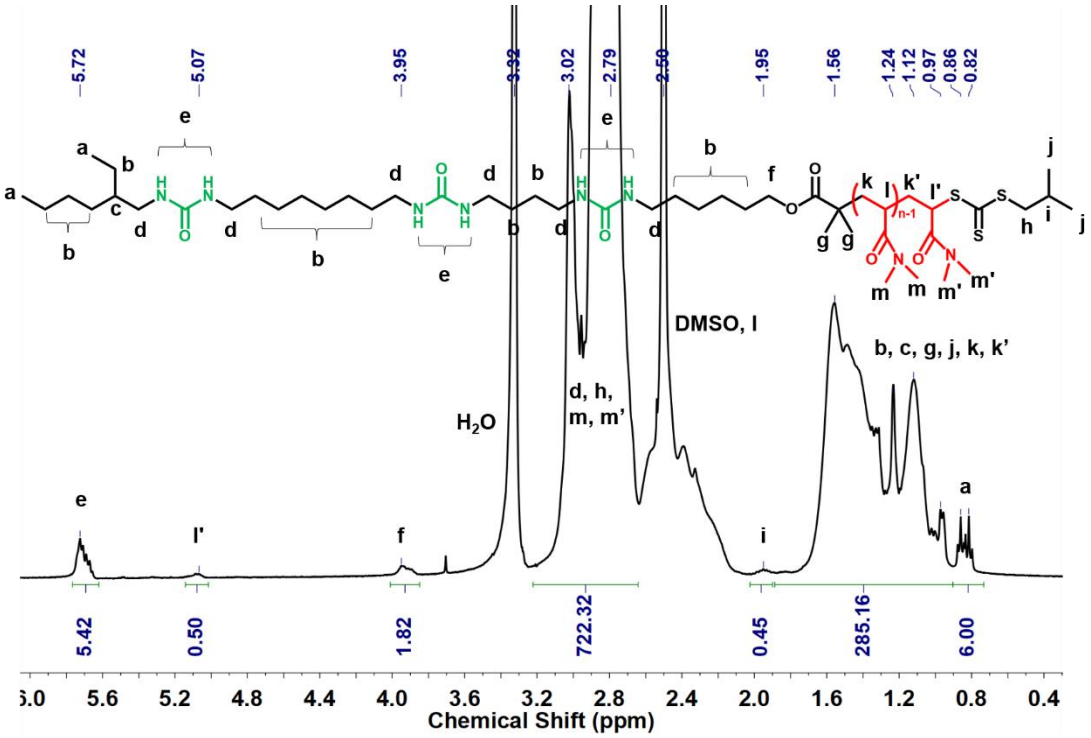

Figure 4.4.4.8. ^{1}H NMR of _8_4_PDMAc$_{120}$ (in DMSO-d$_6$).

4.5 References

(1) Zhang, C.; Liu, T.; Wang, W.; Bell, C. A.; Han, Y.; Fu, C.; Peng, H.; Tan, X.; Kral, P.; Gaus, K.; Gooding, J. J.; Whittaker, A. K. Tuning of the aggregation behavior of fluorinated polymeric nanoparticles for improved therapeutic efficacy. *ACS Nano* **2020**, *14*, 7425-7434.

(2) Ghosh, B.; Biswas, S. Polymeric micelles in cancer therapy: state of the art. *J. Controlled Release* **2021**, *332*, 127-147.

(3) Kästle, G.; Boyen, H. G.; Weigl, F.; Lengl, G.; Herzog, T.; Ziemann, P.; Riethmüller, S.; Mayer, O.; Hartmann, C.; Spatz, J. P.; Möller, M.; Ozawa, M.; Banhart, F.; Garnier, M. G.; Oelhafen, P. Micellar nanoreactors—preparation and characterization of hexagonally ordered arrays of metallic nanodots. *Adv. Funct. Mater.* **2003**, *13*, 853-861.

(4) Li, X.; Iocozzia, J.; Chen, Y.; Zhao, S.; Cui, X.; Wang, W.; Yu, H.; Lin, S.; Lin, Z. From precision synthesis of block copolymers to properties and applications of nanoparticles. *Angew. Chem. Int. Ed.* **2018**, *57*, 2046-2070.

(5) Karayianni, M.; Pispas, S. Block copolymer solution self-assembly: recent advances, emerging trends, and applications. *J Polym Sci.* **2021**, *59*, 1874-1898.

(6) Kloxin, A. M.; Kasko, A. M.; Salinas, C. N.; Anseth, K. S. Photodegradable hydrogels for dynamic tuning of physical and chemical properties. *Science* **2009**, *324*, 59-63.

(7) Yan, J.; Ji, W.; Chen, E.; Li, Z.; Liang, D. Association and aggregation behavior of poly(ethylene oxide)-*b*-poly (*N*-isopropylacrylamide) in aqueous solution. *Macromolecules* **2008**, *41*, 4908-4913.

(8) Liu, S.; Armes, S. P. Polymeric surfactants for the new millennium: a pH-responsive, zwitterionic, schizophrenic diblock copolymer. *Angew. Chem. Int. Ed.* **2002**, *41*, 1413-1416.

(9) Medintz, I. L.; Clapp, A. R.; Brunel, F. M.; Tiefenbrunn, T.; Tetsuo Uyeda, H.; Chang, E. L.; Deschamps, J. R.; Dawson, P. E.; Mattoussi, H. Proteolytic activity monitored by fluorescence resonance energy transfer through quantum-dot–peptide conjugates. *Nat. Mater.* **2006**, *5*, 581-589.

(10) Qin, S.; Yong, X. Controlling the stability of Pickering emulsions by pH-responsive nanoparticles. *Soft Matter* **2019**, *15*, 3291-3300.

(11) Musarurwa, H.; Tawanda Tavengwa, N. Recent progress in the application of pH-responsive polymers in separation science. *Microchem. J.* **2022**, *179*, 107503.

(12) Singh, J.; Nayak, P. pH-responsive polymers for drug delivery: trends and opportunities. *J Polym Sci.* **2023**, *61*, 2828-2850.

(13) Charbonneau, C.; Chassenieux, C.; Colombani, O.; Nicolai, T. Controlling the dynamics of self-assembled triblock copolymer networks via the pH. *Macromolecules* **2011**, *44*, 4487-4495.

(14) Gao, Q.; Xu, Y.; Wu, D.; Sun, Y.; Li, X. pH-Responsive drug release from polymer-coated mesoporous silica spheres. *J. Phys. Chem. C* **2009**, *113*, 12753-12758.

(15) Munoz-Bonilla, A.; Fernandez-Garcia, M.; Haddleton, D. M. Synthesis and aqueous solution properties of stimuli-responsive triblock copolymers. *Soft Matter* **2007**, *3*, 725-731.

(16) Goncalves da Silva, A. M.; Lopes, S. I.; Brogueira, P.; Prazeres, T. J.; Beija, M.; Martinho, J. M. Thermo-responsiveness of poly(*N*,*N*-diethylacrylamide) polymers at the air-water interface: The effect of a hydrophobic block. *J. Colloid Interface Sci.* **2008**, *327*, 129-137.

(17) Xu, Z.; Xue, P.; Gao, Y. E.; Liu, S.; Shi, X.; Hou, M.; Kang, Y. pH-responsive polymeric micelles based on poly(ethyleneglycol)-*b*-poly(2-(diisopropylamino) ethyl

methacrylate) block copolymer for enhanced intracellular release of anticancer drugs. *J. Colloid Interface Sci.* **2017**, *490*, 511-519.

(18) Zhang, L.; Barlow, R. J.; Eisenberg, A. Scaling relations and coronal dimensions in aqueous block polyelectrolyte micelles. *Macromolecules* **1995**, *28*, 6055-6066.

(19) Moffitt, M.; Khougaz, K.; Eisenberg, A. Micellization of ionic block copolymers. *Acc. Chem. Res.* **1996**, *29*, 95-102.

(20) Zhang, L.; Eisenberg, A. Thermodynamic vs kinetic aspects in the formation and morphological transitions of crew-cut aggregates produced by self-assembly of polystyrene-*b*-poly(acrylic acid) block copolymers in dilute solution. *Macromolecules* **1999**, *32*, 2239-2249.

(21) Dai, S.; Ravi, P.; Tam, K. C. pH-Responsive polymers: synthesis, properties and applications. *Soft Matter* **2008**, *4*, 435-449.

(22) Shedge, A.; Colombani, O.; Nicolai, T.; Chassenieux, C. Charge dependent dynamics of transient networks and hydrogels formed by self-assembled pH-sensitive triblock copolyelectrolytes. *Macromolecules* **2014**, *47*, 2439-2444.

(23) Colombani, O.; Ruppel, M.; Burkhardt, M.; Drechsler, M.; Schumacher, M.; Gradzielski, M.; Schweins, R.; Müller, A. H. E. Structure of micelles of poly(*n*-butyl acrylate)-*block*-poly(acrylic acid) diblock copolymers in aqueous solution. *Macromolecules* **2007**, *40*, 4351-4362.

(24) Brunsveld, L.; Folmer, B. J.; Meijer, E. W.; Sijbesma, R. P. Supramolecular polymers. *Chem. Rev.* **2001**, *101*, 4071-4098.

(25) De Greef, T. F.; Smulders, M. M.; Wolffs, M.; Schenning, A. P.; Sijbesma, R. P.; Meijer, E. W. Supramolecular polymerization. *Chem. Rev.* **2009**, *109*, 5687-5754.

(26) Pal, A.; Karthikeyan, S.; Sijbesma, R. P. Coexisting hydrophobic compartments through self-sorting in rod-like micelles of bisurea bolaamphiphiles. *J. Am. Chem. Soc.* **2010**, *132*, 7842-7843.

(27) Fernandez-Castano Romera, M.; Lafleur, R. P. M.; Guibert, C.; Voets, I. K.; Storm, C.; Sijbesma, R. P. Strain stiffening hydrogels through self-assembly and covalent fixation of semi-flexible fibers. *Angew. Chem. Int. Ed.* **2017**, *56*, 8771-8775.

(28) Fernandez-Castano Romera, M.; Lou, X.; Schill, J.; Ter Huurne, G.; Fransen, P. K. H.; Voets, I. K.; Storm, C.; Sijbesma, R. P. Strain-stiffening in dynamic supramolecular fiber networks. *J. Am. Chem. Soc.* **2018**, *140*, 17547-17555.

(29) Fernandez-Castano Romera, M.; Gostl, R.; Shaikh, H.; Ter Huurne, G.; Schill, J.; Voets, I. K.; Storm, C.; Sijbesma, R. P. Mimicking active biopolymer networks with a synthetic hydrogel. *J. Am. Chem. Soc.* **2019**, *141*, 1989-1997.

(30) Danial, M.; Tran, C. M.; Young, P. G.; Perrier, S.; Jolliffe, K. A. Janus cyclic peptide-polymer nanotubes. *Nat. Commun.* **2013**, *4*, 2780.

(31) Rho, J. Y.; Cox, H.; Mansfield, E. D. H.; Ellacott, S. H.; Peltier, R.; Brendel, J. C.; Hartlieb, M.; Waigh, T. A.; Perrier, S. Dual self-assembly of supramolecular peptide nanotubes to provide stabilisation in water. *Nat. Commun.* **2019**, *10*, 4708.

(32) Yang, J.; Song, J. I.; Song, Q.; Rho, J. Y.; Mansfield, E. D. H.; Hall, S. C. L.; Sambrook, M.; Huang, F.; Perrier, S. Hierarchical self-assembled photo-responsive tubisomes from a cyclic peptide-bridged amphiphilic block copolymer. *Angew. Chem. Int. Ed.* **2020**, *59*, 8860-8863.

(33) Obert, E.; Bellot, M.; Bouteiller, L.; Andrioletti, F.; Lehen-Ferrenbach, C.; Boue, F. Both water- and organo-soluble supramolecular polymer stabilized by hydrogen-bonding and hydrophobic interactions. *J. Am. Chem. Soc.* **2007**, *129*, 15601-15605.

(34) Mellot, G.; Guigner, J. M.; Bouteiller, L.; Stoffelbach, F.; Rieger, J. Templated PISA: driving polymerization-induced self-assembly towards fibre morphology. *Angew. Chem.* **2019**, *58*, 3173-3177.

(35) Mellot, G.; Guigner, J.-M.; Jestin, J.; Bouteiller, L.; Stoffelbach, F.; Rieger, J. Bisurea-functionalized RAFT agent: a straightforward and versatile tool toward the preparation of supramolecular cylindrical nanostructures in water. *Macromolecules* **2018**, *51*, 10214-10222.

(36) Mellot, G.; Guigner, J. M.; Jestin, J.; Bouteiller, L.; Stoffelbach, F.; Rieger, J. Unexpected thermo-responsiveness of bisurea-functionalized hydrophilic polymers in water. *J. Colloid Interface Sci.* **2021**, *581*, 874-883.

(37) Han, S.; Pensec, S.; Yilmaz, D.; Lorthioir, C.; Jestin, J.; Guigner, J. M.; Niepceron, F.; Rieger, J.; Stoffelbach, F.; Nicol, E.; Colombani, O.; Bouteiller, L. Straightforward preparation of supramolecular Janus nanorods by hydrogen bonding of end-functionalized polymers. *Nat. Commun.* **2020**, *11*, 4760.

(38) Walther, A.; Muller, A. H. Janus particles: synthesis, self-assembly, physical properties, and applications. *Chem. Rev.* **2013**, *113*, 5194-5261.

(39) Pang, X.; Wan, C.; Wang, M.; Lin, Z. Strictly biphasic soft and hard Janus structures: synthesis, properties, and applications. *Angew. Chem. Int. Ed.* **2014**, *53*, 5524-5538.

(40) Han, S. Supramolecular Janus nanorods formed by self-assembly of polymers in aqueous medium. Thesis. **2019**, 1-227.

(41) Couvreur, L.; Lefay, C.; Belleney, J.; Charleux, B.; Guerret, O.; Magnet, S. First nitroxide-mediated controlled free-radical polymerization of acrylic acid. *Macromolecules* **2003**, *36*, 8260-8267.

General Conclusion

In this thesis, the main objective was to design and synthesize advanced and responsive materials from self-assembled nanocylinders in order to meet various potential needs. To be specific, the syntheses of Janus nanocylinders allow investigations of supramolecular polymers in the field of photolithography. The strategy of the introduction of photo-responsive group into nanocylinders is not only to achieve small feature sizes in surface nanopatterning, but also to investigate the photo cleavable behavior in solution. With the pH-responsive property in Janus nanocylinders, the disassembly behavior is hoped for some potential applications in nanocarriers or sensors.

In the first chapter, the "bottom up" method was described as the alternative for "top down" method to achieve small features in lithography. A general introduction of block copolymers and supramolecular polymers based on lamellar and cylindrical morphologies aiming to obtain small domain sizes were highlighted.

In the second chapter, syntheses of chain transfer agents (_8_4_CTA and _4_8_CTA) were optimized and characterized. Then, in order to be able to tune various properties (solubility, glass transition temperature and etching contrast), many polymers including polyacrylamide, polyacrylate, polystyrene, and, Si- and Fe-containing polymers were synthesized and characterized by ^{1}H NMR and SEC. The synthesized polymers in this chapter were all transmitted to our collaborators. The self-assembly of these polymers in solution is currently studied at IMMM (Le Mans). In particular, based on _4_8_PDMAc and _8_4_PHEA, they have explored the influence of experimental conditions (rate of water addition, polymer concentration, temperature, DP_n of polymers) to optimize the self-assembly process. The deposition of the pre-assembled Janus nanocylinders on surfaces is currently studied at ICMN (Orléans) by drop-casting, dip-coating and Langmuir-Blodgett depositions.

In the third chapter, a photo-cleavable linker was introduced into nanocylinders

to investigate photo-responsive behaviors in solution and on surface. First, photo-cleavable PDMAc-2Us were synthesized with DP_n ranging from 18 to 100 and then characterized by ^{1}H NMR and SEC. Cryo-TEM confirmed the existence of nanocylinders, with few spheres after direct dissolution of PDMAc$_{18}$-2U in water. Mainly spheres were obtained in the case of PDMAc$_{100}$-2U due to the steric hindrance when increasing the chain length. Second, kinetic experiments monitored by UV-visible spectroscopy during irradiation of PDMAc$_{18}$-2U showed the feasibility of photocleavable strategy. The cleavage was confirmed by the polymer shift in SEC. Third, the surface behavior of nanocylinders was also investigated. When PDMAc$_{18}$-2U was transferred onto silicon substrates by drop casting, many nanocylinders were observed by AFM. Good alignment of nanocylinders in the μm range were obtained. After UV irradiation, several solvents were tested to rinse PDMAc. The removing effect is still under investigation.

In the fourth chapter, pH-responsive poly(acrylic acid) (PAA) was introduced into the nanocylinders for the investigation of pH-responsiveness. End-functionalized polymers with complementary hydrogen bonding units and various molar masses, _4_8_PAA and _8_4_PDMAc were synthesized and then characterized by ^{1}H NMR and SEC. SANS and cryo-TEM results revealed the formation of nanocylinders for the system _4_8_PAA$_{183}$ / _8_4_PDMAc$_{220}$ at neutral pH. In basic conditions, with the complete ionization of PAA, nanocylinders were broken. The initial structure could not be recovered after addition of one equivalent of acid, indicating the irreversible nature of the disassembly. This result opens the way for the design of pH responsive systems.

Résumé

L'objectif principal de cette thèse est de concevoir et de synthétiser des matériaux avancés à base de nanocylindres afin de répondre à divers besoins potentiels. Plus précisément, la synthèse de nanocylindres Janus permet l'étude des polymères supramoléculaires en nanolithographie ; les nanocylindres photosensibles donnent accès à des dimensions très faibles intéressantes pour la photolithographie; et les nanocylindres sensibles au pH présentent un intérêt potentiel comme précurseurs de capteurs magnétiques ou comme vecteurs de médicaments.

Dans le premier chapitre bibliographique, nous avons constaté l'obtention de motifs de plus en plus petits en photolithographie. Cependant, il est de plus en plus difficile d'obtenir des motifs de taille inférieure à 10 nm, voire inférieure à 5 nm par cette méthode "top-down" traditionnelle, en raison de la limite de diffraction de la lumière et du coût élevé des autres techniques avancées. Compte tenu de cette difficulté, la méthode "bottom-up" est une alternative intéressante pour obtenir des domaines de plus petite taille. Dans ce chapitre, la nanostructuration à base de copolymères à blocs est décrite, soulignant l'efficacité des morphologies lamellaires et cylindriques utilisées en nanolithographie. Cependant, pour obtenir des motifs inférieurs à 10 nm, des polymères à χ élevé sont nécessaires, ce qui limite à certains polymères contenant du fluor, du silicium ou des groupes hydroxyles. De plus, il est encore difficile d'obtenir des tailles de domaine inférieures à 5 nm, même en utilisant des copolymères à blocs à χ élevé. Une deuxième méthode « bottom-up » consiste à introduire une interaction supramoléculaire dans un polymère (ou des copolymères à blocs). Selon la position de l'interaction supramoléculaire, comme le montre la figure GC1, quatre stratégies sont généralement utilisées pour la nanostructuration de surface. Premièrement, un groupe supramoléculaire est intégré au centre des copolymères à blocs, améliorant ainsi la séparation de phase de ces derniers. Dans certains cas, l'interaction supramoléculaire domine la force motrice de la séparation de phase, indiquant la possibilité d'obtenir de petites tailles de domaine lorsque les bras des copolymères à blocs sont courts.

Deuxièmement, le groupe supramoléculaire fonctionnalisé au centre dans un polymère symétrique pourrait diriger la formation de nanocylindres, qui est entièrement pilotée par l'interaction supramoléculaire. Troisièmement, deux polymères contenant des groupes supramoléculaires complémentaires à leurs extrémités pourraient être assemblés pour former des morphologies lamellaires ou cylindriques. Comparée à la première stratégie, qui nécessite une synthèse continue pour obtenir différents copolymères à blocs, la stratégie de co-assemblage réduit considérablement les temps de synthèse si l'on cible le même nombre de copolymères. Il serait donc plus pratique de construire une bibliothèque de polymères supramoléculaires par co-assemblage. Enfin, lorsque le groupe supramoléculaire se trouve à l'extrémité d'un copolymère à blocs, l'ajout d'un groupe difonctionnalisé complémentaire pourrait guider l'assemblage des copolymères à blocs, formant ainsi des morphologies inattendues. Globalement, ce chapitre présente la nanostructuration de surface à partir de copolymères à blocs et de polymères supramoléculaires.

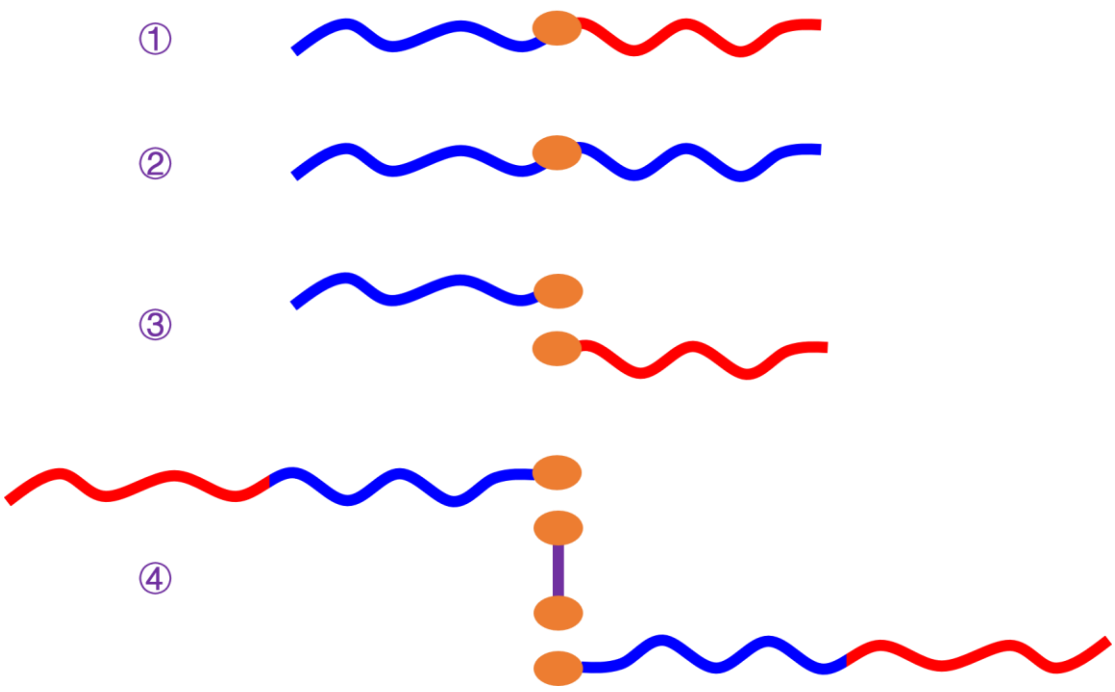

Figure GC1. Quatre stratégies d'auto-assemblage ou de co-assemblage de polymères supramoléculaires pour la nanostructuration de surface.

Dans le deuxième chapitre, la voie de synthèse d'un agent de transfert

(_8_4_CTA) a été adaptée en raison de difficultés de reproductibilité. Parallèlement, les rendements des intermédiaires ont été optimisés. Il convient de noter que la pureté du _8_4_CTA doit être vérifiée par SEC du polymère après polymérisation, car la RMN ^{1}H et la DSC ne fournissent pas d'informations suffisantes sur les impuretés. Pour le _8_4_CTA, une nouvelle voie de synthèse a été conçue car le coûteux 1,8-diisocyanatooctane n'était pas disponible commercialement. En conservant la même méthode pour le _8_4_CTA, le _4_8_CTA a montré une bonne pureté après un test de polymérisation.

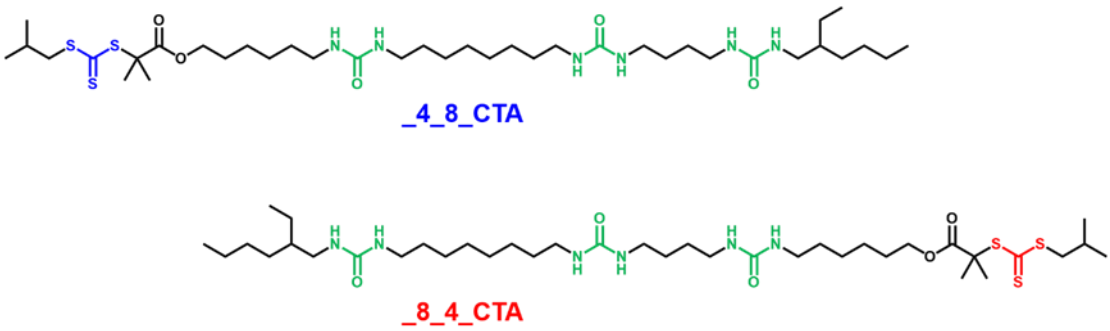

Figure GC2. Structures chimiques des agents complémentaires RAFT _4_8_ et _8_4_.

Après la synthèse des CTA _4_8_ et _8_4_, les polymères correspondants pour la nanostructuration de surface ont été synthétisés. Comme le montre la figure GC3, le polymère _4_8_ s'assemble avec le polymère _8_4_ pour former un nanocylindre Janus en solution. Les nanocylindres Janus sont ensuite transférés sur un substrat de silicium par drop-casting, dip-coating ou par la technique de Langmuir-Blodgett. Après le dépôt, un bras du nanocylindre Janus peut potentiellement être retiré sélectivement, puis le dopage ou la gravure directe peuvent être effectués.

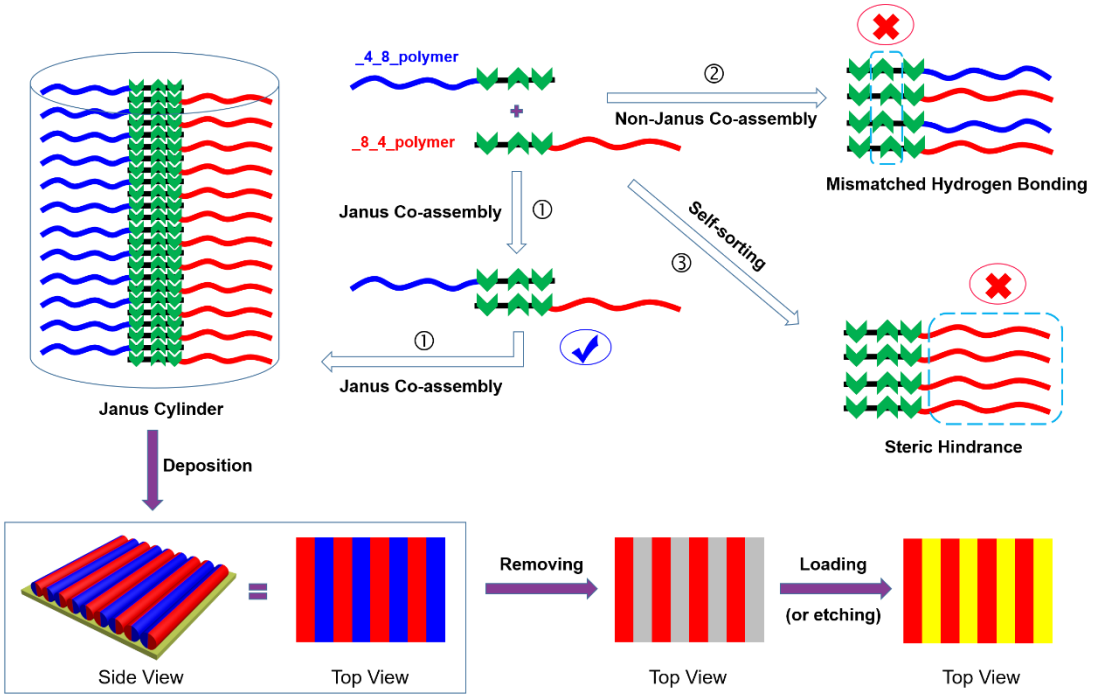

Figure GC3. Illustration du processus de co-assemblage et de nano-structuration.

Le *N,N*-diméthylacrylamide (DMAc) a été choisi comme échantillon représentatif pour étudier la cinétique. Le PDMAc monodispersé, observé en SEC à différents temps de polymérisation, indique la bonne pureté du _8_4_CTA. La relation quasi-linéaire entre $\ln(M_0/M_t)$ et le temps indique un bon contrôle pendant la polymérisation. La dispersité est toujours autour de 1,10.

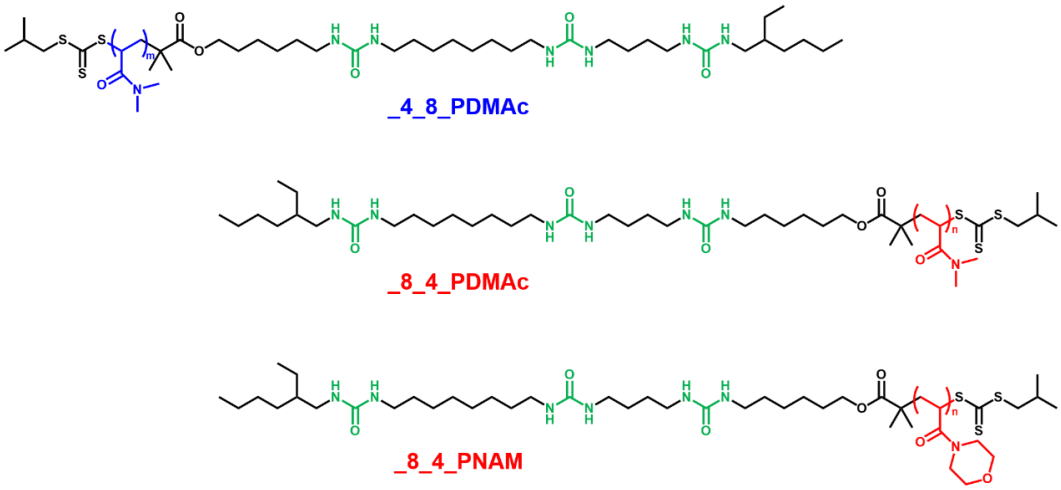

Figure GC4. Structures chimiques des polyacrylamides complémentaires _4_8_ et _8_4_.

Le polystyrène est également synthétisé ici, car il a été utilisé comme polymère classique en nanostructuration et constituera donc une référence utile. L'introduction d'un atome de silicium dans le monomère styrène améliore le contraste de gravure avec d'autres polymères. En effet, la gravure ionique réactive à l'O_2 (RIE) éliminerait le PDMAc complémentaire, tandis que le PTMSS serait oxydé à une vitesse plus faible. Les polymérisations du styrène et du TMSS sont plus longues que celles des autres monomères, car ce sont des monomères à faible constante de propagation. Cependant, les faibles dispersités (1,12 pour _8_4_$PTMSS_{61}$ et 1,09 pour _4_8_PS_{32}) indiquent que les polymérisations sont toujours contrôlées globalement.

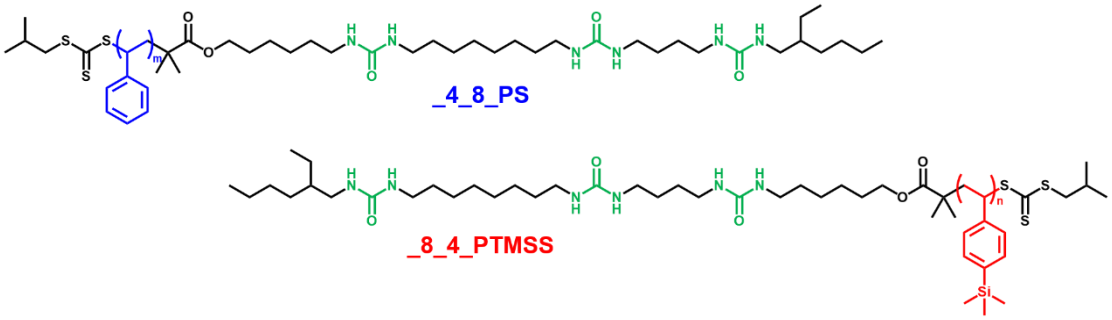

Figure GC5. Structures chimiques des _4_8_PS et _8_4_PTMSS complémentaires.

Comme le montre la figure GC6, à l'exception du PHEA, tous les autres polymères sont hydrophobes. Cependant, lorsque le _8_4_PHEA s'assemble avec un _4_8_polymère (par exemple, le _4_8_PDMAc), le _8_4_PHEA peut être réticulé lorsque le nanocylindre est soumis à des vapeurs de glutaraldéhyde après le dépôt, ce qui rend le _8_4_PHEA insoluble dans l'eau. En choisissant un solvant adapté pour l'autre bras, celui-ci peut être retiré, facilitant ainsi le dopage ou la gravure. Pour la synthèse du _8_4_PHEA, trois longueurs différentes de DP_n 47, 600 et 1300 ont été synthétisées afin d'étudier l'effet de la taille du polymère sur le coassemblage avec le _4_8_PDMAc. Idéalement, les polyacrylates _8_4 sont synthétisés pour s'assembler avec le _4_8_PDMAc, qui a démontré sa bonne capacité à former des nanocylindres Janus lorsqu'il s'assemble avec des polymères complémentaires.

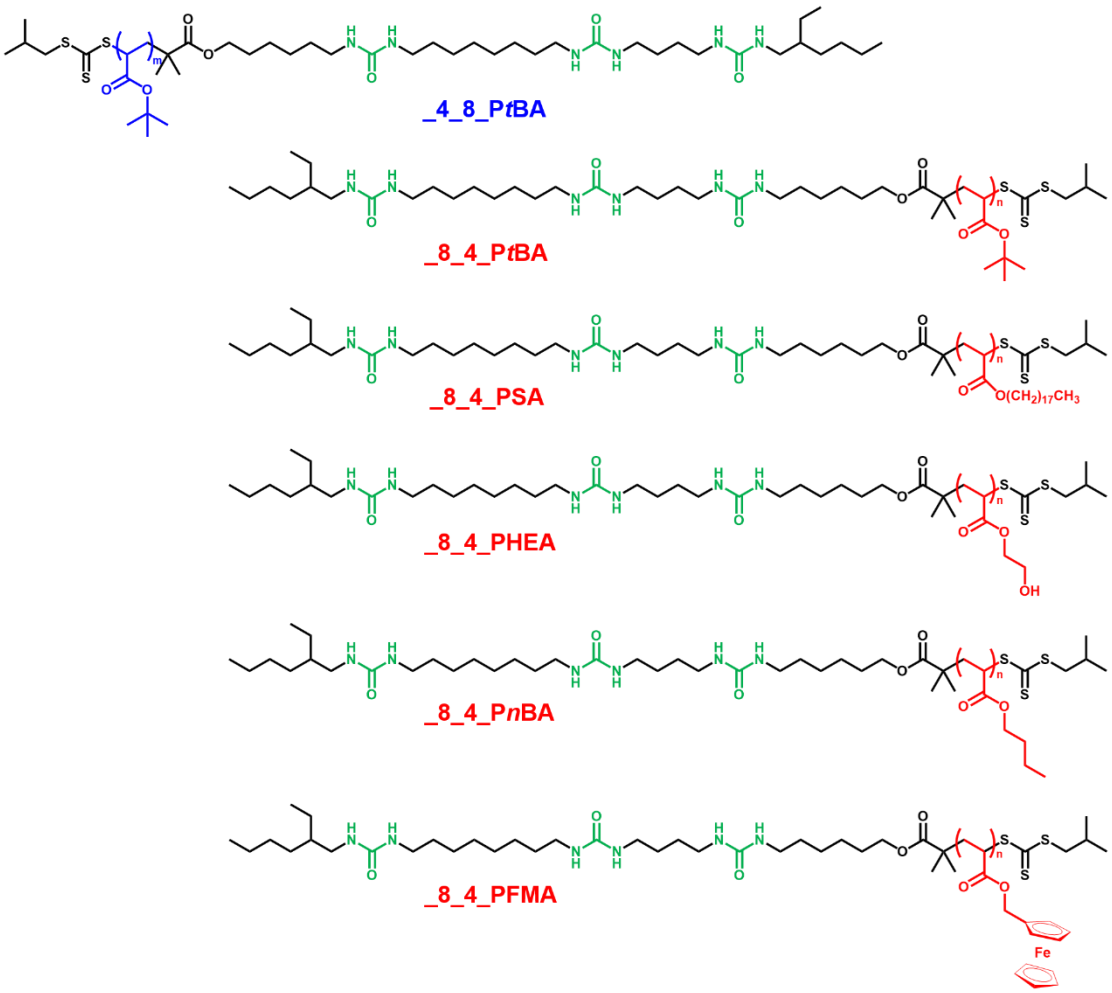

Figure GC6. Structures chimiques des polyacrylates _4_8_ et _8_4_.

Le _8_4_P*n*BA et le_8_4_P*t*BA ont été synthétisés car, lors de leur coassemblage avec le _4_8_PDMAc, le contraste de phase est bon en AFM grâce à l'écart de Tg entre le PDMAc (~ 125 °C) et le P*t*BA (~ 52 °C). De plus, le P*t*BA est moins collant que le P*n*BA. Le PtBA a montré des dispersités de 1,09 à 1,15 lorsque le DP_n est compris entre 32 et 68.

Le PSA est un polymère hydrophobe difficilement soluble dans les solvants polaires (comme le méthanol) en raison de la longue chaîne alkyle de sa chaîne latérale. Par conséquent, l'élimination sélective du PDMAc des nanomotifs PDMAc/PSA par le choix d'un solvant approprié devient possible, offrant ainsi un accès simple aux tranchées régulières sur les substrats de silicium. Pour le _8_4_PSA, des DP_n = 33 et 73 ont été synthétisés pour un test préliminaire de l'effet de co-assemblage.

Enfin, une grande quantité (1,7 g) de _8_4_PSA$_{37}$ avec une dispersité de 1,14 a été synthétisée pour une étude plus approfondie par nos collaborateurs.

Les polymères contenant du ferrocène ont suscité un vif intérêt en raison non seulement de leur réactivité redox, mais aussi de leur « contraste de gravure » lorsqu'ils sont combinés à d'autres polymères. Il est intéressant de noter que les polymères contenant du ferrocène forment de l'oxyde de fer, tandis que d'autres polymères sont pyrolysés à haute température. De cette façon, les polymères contenant du ferrocène présentent l'avantage naturel d'offrir un « contraste de gravure » lors de la nanostructuration. Afin d'étudier le co-assemblage avec le _4_8_PDMAc, un _8_4_PFMA avec le DP_n 69 a été synthétisé.

Les polymères synthétisés dans ce chapitre ont tous été caractérisés par RMN ^{1}H et SEC, et ont été transmis à nos collaborateurs. L'auto-assemblage de ces polymères en solution est actuellement étudié à l'IMMM (Le Mans). En particulier, en s'appuyant sur _4_8_PDMAc et _8_4_PHEA, ils ont exploré l'influence des conditions expérimentales (vitesse d'ajout d'eau, concentration en polymère, température, masse molaire des polymères) pour optimiser le processus d'auto-assemblage..

Le dépôt des nanocylindres Janus préassemblés sur des surfaces est actuellement étudié à l'ICMN (Orléans) par drop-casting, dip-coating et dépôts de Langmuir-Blodgett.

Dans le troisième chapitre, un amorceur ATRP contenant deux urées a été synthétisé afin de réaliser la polymérisation du *N,N*-diméthylacrylamide. Le PDMAc-2U avec un DP_n de 18 à 100 a été caractérisé par RMN ^{1}H et SEC. La cryo-TEM a confirmé l'existence de nanocylindres, avec peu de sphères dans le PDMAc$_{18}$-2U mais de nombreuses sphères dans le PDMAc$_{100}$-2U en raison de l'encombrement stérique.

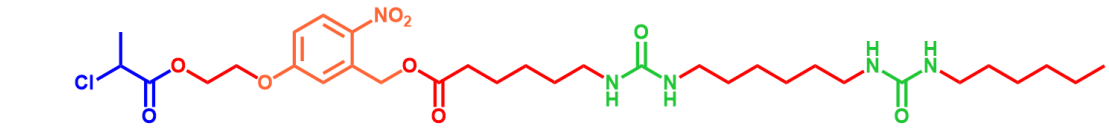

Cl-Ar-2U

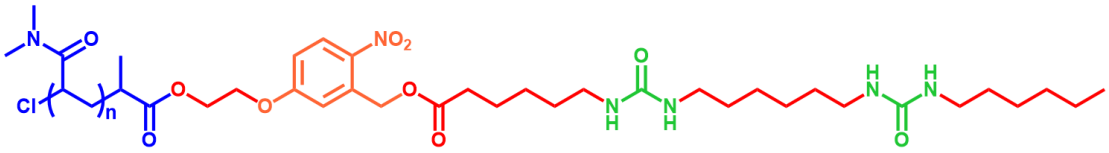

PDMAc-2U

Figure GC7. Structures chimiques de l'amorceur ATRP à base de bis-urée (Cl-Ar-2U) et de son polymère correspondant (PDMAc-2U).

En raison de la présence d'ester *o*-nitrobenzylique dans le polymère, celui-ci peut être clivé à une longueur d'onde UV de 300 ou 365 nm. L'expérience de cinétique de clivage du $PDMAc_{18}$-2U a montré la faisabilité du clivage, démontré par la diminution de l'absorbance en spectroscopie UV-visible et par le décalage du polymère en SEC. Lorsque $PDMAc_{18}$-2U a été transféré sur des substrats de silicium par cdrop-casting, de nombreux nanocylindres ont été observés par AFM avec de bons alignements à l'échelle du micron. Ensuite, du pentane, de l'eau et de l'acétate d'éthyle ont été utilisés pour rincer le PDMAc. Le pentane (mauvais solvant) n'a pas affecté le film, indiquant son inutilité pour l'élimination. Après l'utilisation d'une seule goutte d'eau, certaines couches du film ont été totalement lavées à certains endroits, suggérant que l'eau est un trop bon solvant. Après rinçage du film avec quatre gouttes d'acétate d'éthyle, une légère diminution de 18 nm de son épaisseur a été constatée, sans modification significative. L'effet de l'élimination est encore à l'étude. D'autres solvants, tels que le DCM et le chloroforme, seront testés. Par ailleurs, un mélange de solvants efficaces et de solvants moins efficaces (par exemple, acétate d'éthyle dans du pentane) pourrait constituer un bon test en immergeant le substrat dans le mélange pendant quelques minutes.

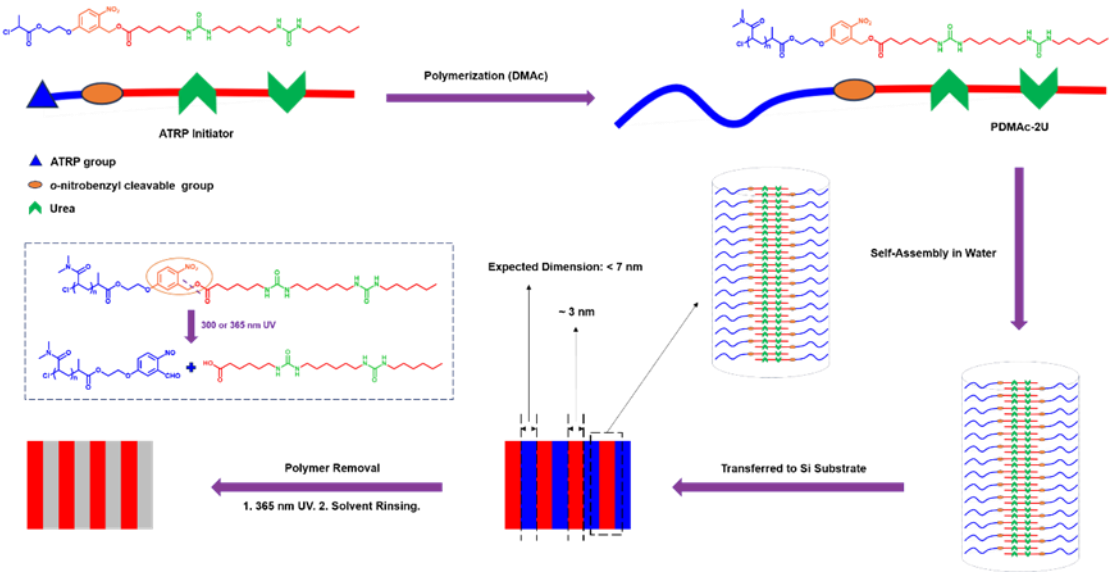

Figure GC8. Illustration du PDMAc-2U photoclivable après clivages en solution et en surface.

Dans le quatrième chapitre, certains PAA et PDMAc ont été synthétisés par polymérisation RAFT en utilisant _4_8_ ou _8_4_CTA. Parmi eux, _4_8_PAA$_{42}$, _4_8_PAA$_{183}$, _8_4_PDMAc$_{35}$ et _8_4_PDAMc$_{220}$ ont été utilisés pour étudier la dépendance au pH.

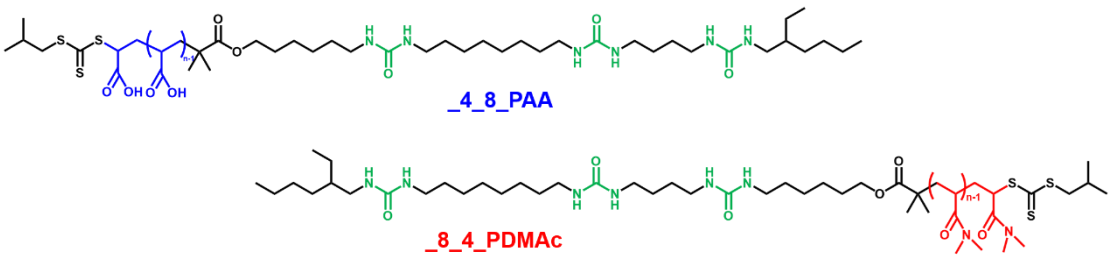

Figure GC9. Structures chimiques de _4_8_PAA et _8_4_PDMAc.

Lors du co-assemblage du _4_8_PAA$_{183}$ avec le _8_4_PDMAc$_{35}$, des précipités se sont produits. En racourcissant le PAA (_4_8_PAA$_{42}$ / _8_4_PDMAc$_{35}$) ou en allongeant le PDMAc (_4_8_PAA$_{183}$ / _8_4_PDMAc$_{220}$) la solubilité des co-assemblages est améliorée. Il est intéressant de noter que la cryo-MET du _4_8_PAA$_{183}$ / _8_4_PDMAc$_{220}$ montre la présence de nanocylindres, confirmée par SANS. Après l'ajout d'un équivalent de NaOH (Figure GC8 a, c, e et f), la plupart des nanocylindres

disparaissent. Après l'ajout d'un équivalent de HCl à la solution précédente, les chaînes polymères n'ont pas pu se réassembler pour former des nanocylindres, ce qui indique que le processus est irréversible après l'ionisation du PAA. Ces résultats préliminaires permettent d'envisager l'utilisation du pH pour contrôler la structure des nanocylindres.

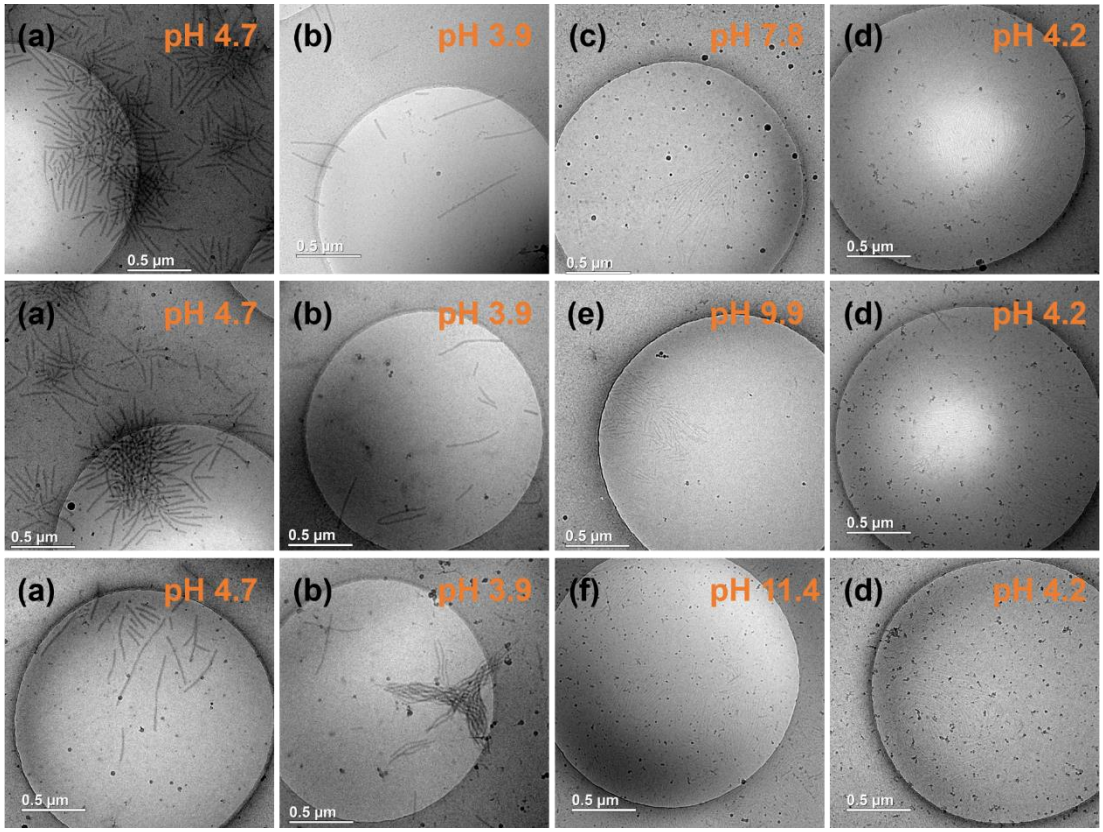

Figure GC10. Figures Cryo-TEM de _4_8_PAA$_{183}$/_8_4_PDMAc$_{220}$ à différents pH sans ajout de NaOH et de HCl (a), avec ajout de HCl (b), avec ajout de NaOH (c, e et f) et avec ajout de NaOH et de HCl (d).

Syntheses of urea-based supramolecular polymers for nanocylinders assemblies in solution and on surface

Nanocylinders are promising nanostructures for the design of advanced and responsive materials to address emerging industrial and biomedical needs. In this study, we explored supramolecular assemblies based on hydrogen bonding interactions in bis- and tris-urea moieties, both in solution and on surface, with the aim of achieving sub-10 nm features for surface nanopatterning applications. First, a series of tris-urea-based polymers with complementary hydrogen bonds were synthesized, with the consideration of different properties (solubility, glass transition temperature, etching contrast), to construct a library of supramolecular polymers and for the investigation of surface nanopatterning. Second, a photocleavable strategy was introduced into bis-urea-based supramolecular polymers to investigate the photo-responsiveness of nanocylinders and also to achieve sub-10 nm features in supramolecular systems. After a straightforward preparation of nanocylinders in water, the cleavage kinetics using UV light demonstrated the photo-responsiveness of the nanocylinders. When the degree of polymerization of the supramolecular polymer was low ($DP_n = 18$), AFM indicated the formation of well aligned nanocylinders with ~ 7 nm of diameter over areas of 2 × 2 μm^2. Finally, with the design of pH-responsive nanocylinders, we confirmed the formation of nanocylinders decorated with poly(acrylic acid) (PAA) chains and observed its disassembly upon ionization of PAA. These results pave the way for the design of sub-10 nm building blocks for nanopatterning applications or with various pH-responsive properties.

Keywords: supramolecular polymers, nanocylinders, advanced materials, responsive materials, bis-urea, tris-urea, surface nanopatterning, Janus, photo-responsive, photo-cleavage, pH-responsive

Synthèses de polymères supramoléculaires à base d'urée pour l'assemblage de nanocylindres en solution et sur surface

Les nanocylindres sont des nanostructures prometteuses pour la conception de matériaux avancés et stimulables pour diverses applications. Dans cette étude, nous avons exploré des assemblages supramoléculaires basés sur des interactions par liaisons hydrogène entre groupements bis- et tris-urées, en solution et sur surface, afin d'obtenir des motifs inférieurs à 10 nm pour des applications en nanostructuration de surface. Tout d'abord, une série de polymères à base de tris-urée formant des liaisons hydrogène complémentaires ont été synthétisés, en tenant compte de différentes propriétés (solubilité, température de transition vitreuse, contraste de gravure), afin de constituer une bibliothèque de polymères supramoléculaires permettant de nanostructurer des surfaces. Deuxièmement, une stratégie par photoclivage a été considérée avec des polymères supramoléculaires à base de bisurées afin d'étudier la photostimulation des nanocylindres et afin d'obtenir des motifs inférieurs à 10 nm. Après une préparation simple des nanocylindres dans l'eau, la cinétique de clivage à l'aide de lumière UV a démontré la photo-réactivité des nanocylindres. Lorsque le degré de polymérisation du polymère supramoléculaire était faible ($DP_n = 18$), l'AFM a indiqué la formation de nanocylindres bien alignés avec ~ 7 nm de diamètre sur des zones de 2 × 2 μm^2. Enfin, avec le design de nanocylindres sensibles au pH, nous avons confirmé la formation de nanocylindres décorés avec des chaînes de poly(acide acrylique) (PAA) et observé leur désassemblage lors de l'ionisation du PAA. Ces résultats ouvrent la voie au design d'objets cylindriques de moins de 10 nm de diamètre pour des applications en nanolithographie ou ayant des propriétés contrôlables par le pH.

Mots-clés : polymères supramoléculaires, nanocylindres, matériaux avancés, matériaux stimulables, bis-urée, tris-urée, nanostructuration de surface, Janus, photo-stimulable, photo-clivage, pH-sensible